ABSTRACT

On the Gram-positive Bacterial Cell Wall

James D. Chang, Ph.D.

Mentor: Sung Joon Kim, Ph.D.

Cell wall is the outermost part of Gram-positive bacteria. It is intricately tied to the bacteria's response to environmental stimuli and challenges, and its makeup dynamically changes as a part of bacterial adaptation. Peptidoglycan is the biopolymer that composes nearly half of the cell wall, and by studying peptidoglycan valuable insights can be gained into the structure and function of the cell wall. This dissertation examines the chemical compositional changes to the cell wall peptidoglycan in Gram-positive bacteria *Enterococcus faecalis* and *Staphylococcus aureus* through solid-state NMR and liquid chromatography-mass spectrometry. These methods analyzed the peptidoglycan without harsh chemical treatments commonly applied to the cell wall that facilitate the use of traditional biochemical methods. Bypassing these treatments allowed for studying various modifications that would have been previously overlooked, and the

studies in this dissertation provide peptidoglycan composition analysis at the level of detail where growth conditions and antibiotic challenges to the bacteria could be observed. These studies have revealed that bacteria's peptidoglycan composition is dynamic, with the bacteria readily altering its cell wall through peptidoglycan as responses to different stimuli and situations. This dissertation presents a representative sampling of experiments undertaken to study the cell wall of Gram-positive bacteria, and it is hoped that they represent different ways of analyzing the cell wall of these medically important pathogens.

On the Gram-positive Bacterial Cell Wall

by

James D. Chang, B.S., M.S.

A Dissertation

Approved by the Department of Chemistry and Biochemistry

_____

Patrick J. Farmer, Ph.D., Chairperson

Submitted to the Graduate Faculty of
Baylor University in Partial Fulfillment of the
Requirements for the Degree
of

Doctor of Philosophy

Approved by the Dissertation Committee

_____

Sung Joon Kim, Ph.D., Chairperson

_____

Bryan F. Shaw, Ph.D.

_____

Mary Lynn Trawick, Ph.D.

_____

Kevin L. Shuford, Ph.D.

_____

Cheolho Sim, Ph.D.

Accepted by the Graduate School
August 2017

_____

J. Larry Lyon, Ph.D., Dean

Page bearing signatures is kept on file in the Graduate School.

TABLE OF CONTENTS

LIST OF FIGURES

LIST OF SCHEMES

LIST OF TABLES

LIST OF ABBREVIATIONS

Ac: Acetylation

Ala: Alanine

BHI: Brain Heart Infusion Medium

CI: Confidence Interval

CP: Cross Polarization

Des-Ori: Desleucyl-oritavancin

EDM: Enterococcus Defined Medium

ESI: Electrospray Ionization

ESM: Enterococcus Standard Medium

GlcNAc / NAG: N-acetylglucosamine

Lac: Lactate

LC: Liquid Chromatography

Lys: Lysine

Glu: Glutamic Acid

MAS: Magic Angle Spinning

MIC: Minimum Inhibitory Concentration

MRSA: Methicillin-Resistant *Staphylococcus aureus*

MS: Mass Spectrometry

MurNAc / NAM: N-acetylmuramic acid

m/z: Mass Over Charge Ratio

NMR: Nuclear Magnetic Resonance

Ori: Oritavancin

PG: Peptidoglycan

REDOR: Rotational-Echo Double Resonance

SASM: *Staphylococcus aureus* Standard Medium

SILAC: Stable Isotope Labeling with Amino Acids in Cell Culture

TEM: Transmission Electron Microscope

TSB: Trypticase Soy Broth

UDP: Uridine Diphosphate

VRSA: Vancomycin-Resistant *Staphylococcus aureus*

VRE: Vancomycin-Resistant *Enterococcus faecalis*

VSE: Vancomycin-Susceptible *Enterococcus faecalis*

XIC: Extracted Ion Chromatogram

ACKNOWLEDGMENTS

First, I would like to offer heartfelt gratitude to Dr. Sung Joon Kim. He has been instrumental in not only my coming to Baylor, but to my growth as both a graduate student and a fledging scientist. His generosity, patience, and earnestness are traits I hope my future colleagues and students see in me as I learned from him. The pursuit of rigorous intellectual inquiry is another valuable lesson I learned from Dr. Kim and my dissertation committee members, Dr. Bryan Shaw, Dr. Mary Lynn Trawick, Dr. Kevin Shuford, and Dr. Cheolho Sim. It is my wish that their excellence in science can be readily seen in my own work, and I would like to thank each and every one for me becoming the scientist I am today.

Special thanks go out to Dr. Alejandro Ramirez for his training and assistance in utilizing the mass spectrometer for my research. His contribution to this dissertation has been invaluable, and I would like to thank him for being so patient and kind with me. My research into bacterial cell wall began with the project overseen by Dr. Sung Kun Kim and Dr. Mieke Lahousse, and I would like to thank them for sparking my interest in the topic. Dr. Jugeshwar Kshetrimayum and Dr. Nelson van der Velde have been a pleasure to work with on my non-bacterial projects, and I wish I had more time to collaborate with these two insightful postdocs.

Scientific discussions among intellectual peers are the sources of ideas and critiques. While I did not have the pleasure of having more time in the Kim lab with Binayak Rimal, Chengyin Liu, and Olatunde Olademehin, the desire for knowledge and

understanding these fellow lab members demonstrated during my time with them inspired me, and I learned so much simply by teaching and sharing the lab with them. I also would like to thank Alireza Abdolvahabi, Yunhua Shi, Jing Wu, Brett Harper, and Matthew Brantley for allowing me to talk frankly about my research and providing me with encouragement, insights, and humor.

The ones who contributed the most to this dissertation and my research in the years here at Baylor are the undergraduate members of the Kim lab past and present. They are the source of such joy, satisfaction, and mirth in my time spent both in and out of the lab. Witnessing them grow and mature as they finished their degrees and moved on towards bright futures was my pleasure, and I will fondly look back at their commitment to the lab, neverending thirst for learning, and brilliant insights only their unprejudiced eyes could see. In no particular order, I would like to thank David Song, Tran Nguyen, Elizabeth Hughes, Bryan Le, Angeline Nguyen, Erin Foster, Alex Guinn, Rebecca Ramirez, Ashley Wallace, Lauryn Coffman, Aanchal Thadani, Jeremy Sieker, Thanh Nguyen, Carter Lantz, and Tara Hurley. In times of success and failure, hope and apprehension, and celebration and disappointment, their constant belief in our partnerships always brought encouragement and smile to my face.

I came into this doctoral program expecting to be trained as a scientist: I leave Baylor not only as a scientist, but also a thinker. I expected to learn about life, but I learned how to live a life. Baylor has been a very nurturing environment for both my mind and soul, and I am a better person for having been a student here. I wholeheartedly thank Dr. Burt Burleson for his spiritual guidance and support through both my brightest

and darkest days here. I learned what it means to be a scholar and a man faithful to his calling.

Finally, I would like to once again thank Erin Foster. Her role in contributing to the beginning of this research was invaluable, and her encouraging attitude during all those months spent attempting to start this research was of tremendous inspiration. This dissertation is the fruit of all that labor, and I am truly grateful to her for her part in making all my ideas behind this research come true.

For my parents / 내 부모님 에게

Let us not become weary in doing good, for at the proper time we will reap a harvest if we do not give up.

Galatians 6:9

CHAPTER ONE

Introduction

Nearly 50% of the dry mass of Gram-positive bacteria is the cell wall and biopolymers associated with it.[1] Serving as the boundary between the bacteria and environment, the cell wall is intricately involved in every biological function of the bacteria, from cell division and metabolism to pathogenesis and colony-formation.[2-3] Biological advantages that arise from having a cell wall are numerous, from tolerance of osmotic pressure differential more than sufficient to disrupt any membrane to formation of biofilm that enables growth and survival of bacterial colonies in otherwise extremely hostile conditions.[4] These advantages to the bacterial survival conferred through their cell wall enable these bacteria to thrive in every condition imaginable from desiccating abiotic surfaces to internal body tissues under constant immunological surveillance. Importance of the cell wall to the degree of success these Gram-positive bacteria enjoy cannot be overstated.[5-7]

Study of these cell walls however is difficult for many reasons. Through biochemical analysis, microbiologists recognized early on that bacterial cell wall has a chemical unique to bacteria termed murein, and that it formed the majority of cell wall mass.[1-3] Thus it seemed that the cell wall could be completely understood through chemical means. However, researchers quickly ran into a problem they had not foreseen as they sought to characterize the structure of murein. While advances in biochemistry led to the development of many different techniques that can categorize and analyze

biopolymers ranging from proteins to nucleic acids, biochemical composition analysis of purified murein showed that it was exclusively made up of two sugars (N-acetylglucosamine and N-acetyl muramic acid) and just few amino acids.[1,8-9] Murein, now termed peptidoglycan for its two main components, remained an intractable subject.

Development of x-ray crystallography enormously expanded the field of structural biology, where the tremendous amount of structural variability can arise from only a limited number of amino acids. Advancements in molecular biology led to understanding genetic heritability based on only four bases. These developments gave hopes to microbiologists who looked for an equivalent breakthrough that would enable them to decipher the rules behind peptidoglycan. However, much anticipated breakthroughs that microbiologists have been eagerly waiting for did not materialize. Despite all efforts, peptidoglycan from live bacteria could not be crystallized – through biophysical studies, scientists discovered that each bacterial cell wall, large enough to be seen under microscopes, was a single macromolecule built from covalent linking of individual building blocks.[4,10-13] Enough facts about peptidoglycan still were gathered through these biochemical studies. First, there exists a subunit with both sugars and all the variety of amino acids and serves as the minimum building block.[1-4] Second, these subunits could each be covalently linked to their neighboring subunits by two different types of links: a β-1,4 glycosidic linkages between N-acetylglucosamine and N-acetylmuramic acid, and a peptide bond between D-Alanine and another amino acid, typically L-Lysine or D-aminopimelic acid.[8,14-17] Third, each individual peptidoglycan subunit may be covalently modified by addition or removal of moieties ranging in size from acetate all the way up to large biopolymers such as teichoic acids and surface

proteins.[14] All these changes seemed to occur in seemingly random and unpredictable fashion, resulting in highly irregular and aperiodic structure at the tertiary structural level of the cell wall even with the organization found at the local secondary structural level.[13, 18-19] Peptidoglycan thus is a macromolecule the size of a bacteria with amorphous nature unamenable to traditional structural biology methods.

Breakthroughs on studying peptidoglycan came from a unlikely direction. Originally used in polymer sciences, solid-state NMR proved to be surprisingly adaptable in study of the cell wall through the use of various techniques such as magic angle spinning (MAS), cross polarization (CP), and rotational-echo double-resonance (REDOR).[15-18] While the cell wall itself at large scale is disorganized, there still are rules and trends the individual subunits follow in binding to each other. Careful isotopic labeling of amino acid substituents in peptidoglycan allows for solid-state NMR experiments that can specifically pick out certain types of links in the cell wall. For example, ^{15}N labeling of ε-nitrogen in L-Lysine paired with ^{13}C of L-Alanine allows for the dipolar coupling between those two nuclei with a very specific dephasing curves in REDOR as their proximity in a peptide stem-to-stem linkage allows for REDOR experiment to be selective for that link.[20-25] Comparing the peak intensities between two different conditions directly correlates with the density of stem-to-stem links (cross-links) in the cell wall in those conditions.

These solid-state NMR studies have led to detection of the changes to peptidoglycan between different conditions and strains. These experiments confirmed the existence of variability to the peptidoglycan composition on the whole cell level, and suggested that detailed examination of peptidoglycan alterations on molecular level

would be fruitful. Mass spectrometry analyses on high performance liquid chromatography fractions of mutanolysin-digested peptidoglycan have been attempted in the past.[9, 26-30] These studies indicated that such digest is composed from vast number of peptidoglycan built from different number of peptide-bond linked subunits, with each subunit sometimes having covalent modifications. But thorough analysis of the peptidoglycan digest remained difficult. While each individual chromatographic peak could be tentatively identified through finding a representative peptidoglycan variety with that specific elution time, difficulty in identifying these fragments with combinatoric number of variations made mass spectrometric analysis of peptidoglycan arduous.

Advent of high resolution mass spectrometry offers a way to approach the problem from peptidoglycan variations by identification of these fragments with solely their m/z values.[31] Previously, liquid chromatography-mass spectrometry analysis of peptidoglycan heavily relied upon the chromatographic separation for the separation and identification of these complex mixtures of fragments. Researchers would pick a peak from the chromatogram of the cell wall digest, identify a single peptidoglycan fragment from that peak, and label that peak as being composed of that fragment.[29-30] This process would be repeated for all peaks deemed major, even though the criteria for judging what qualities define such a peak remained rather arbitrary. Furthermore, there was the inability to resolve each individual chromatographic peak into subcomponents. A quick inspection of mass spectrum from one timepoint in the chromatographic profile of peptidoglycan digest reveals a bewildering number of peaks that indicate the presence of multiple species.[32] Clearly there were many more species to be identified from one

timepoint than just a single fragment. High resolution mass spectrometry shifts the burden of separation away from chromatographic profiles to mass spectra.

High resolution mass analyzer alone did not allow the research outlined in this dissertation that sought to analyze peptidoglycan mixtures at unprecedented level of detail. Enzymatic digests of the purified cell wall contain hundreds of distinct peptidoglycan fragments. Even with the largest possible amount of the sample being injected into the instrument, proportions of distinct fragments typically were very small – values smaller than 10^{-5} were common – and thus the instrument needed to have high sensitivity in order to analyze such mixtures and quantify these minor species. Nanospray ionization, a variety of electrospray ionization at nanoliter-scale volumes, was essential for revealing the intricacies hidden in lower-abundance fragments as lower abundance fragments could be detected through improved ionization. The increase in sensitivity provided by the nanospray and ultra-high performance liquid chromatography allowed the capacity of high resolution mass analyzer to be fully utilized.[32-33]

This ability to collect data on unprecedented detail for minor peptidoglycan species through the improvements in ion identification and detection meant that the analysis of data could no longer be done using the traditional method of manually creating the library of ions to be found and searching for it at each time point. While the ability to search for a specific fragment's ion through its unique m/z value was already present in the software solution provided by the mass spectrometer manufacturer, obtaining the library of those m/z values to search for posed a problem. Without a good, diverse library of those fragments and their m/z values, advantages gained through increased sensitivity could not be fully utilized. Generating such a library necessitated a

new approach to the analysis of peptidoglycan liquid chromatography-mass spectrometry data.[32] Increased sensitivity meant that more variations resulting from structural modifications of peptidoglycan can be looked for, which required a way to generate m/z values for all the fragments too low abundances to be detected through prior methods. Fortunately, these covalent modifications to one peptidoglycan fragment can be considered combinatorically.[8, 14] As each subunit can have only one instance of any given modification (with the exception for modifications that are restricted to the terminal subunit of a fragment), all the combinations of modifications in a fragment can be described by a series of integers, with each term representing the number of a specific modification. This allowed generation of all variations through a program, and the chemical formula for a fragment with specific variations could be calculated. These calculated chemical formulas were then used to generate m/z values.

In silico generation of the peptidoglycan library led to vast number of peptidoglycan fragments to be matched with observed peaks. As the library had already been generated in the MATLAB program written in house specifically for this purpose, matching of the observed m/z values from the peaks with the calculated m/z from the library was done by modifying the same program to add the matching feature. This combining of calculated values and observed data facilitated analysis to the point where the number of peptidoglycan variations examined becomes large enough to give a unprecedented look into various modifications that occur to peptidoglycan as part of bacterial response to different conditions and situations.[32-33]

This dissertation is based on studies of the cell wall from two Gram-positive bacteria, *Staphylococcus aureus* and *Enterococcus faecalis*. These pathogens are two of

the leading causes for hospital-acquired infections and studies on them hold high clinical relevance.[34-35] Recent increase in antibiotic resistance seen in these bacteria has necessitated changes to treatment protocols in recent years, and they have required frequent use of antibiotics typically reserved for multi-drug resistant bacteria such as vancomycin and carbapenems.[6, 36-37] Antibiotic related studies on this dissertation involved the glycopeptide antibiotic vancomycin and the semi-synthetic glycopeptide antibiotic oritavancin derived from the former.[25, 31-32] The primary mode of action for both antibiotics is the sequestration of peptidoglycan precursor lipid II through the drug binding that prevents the recycling of lipid II.[38-40] But as lipid II is structurally identical to peptidoglycan except for the lipid transporter segment, if a glycopeptide can bind to lipid II it must also be able to bind to other parts of the cell wall through peptidoglycan as well.[24-25] This implies the existence of secondary mode of action, and these studies investigate the effects on the cell wall through this mode of action.

Both modes of action have far reaching consequences beyond the halting of lipid II recycling. Peptidoglycan composition of Vancomycin-resistant *Enterococcus faecalis* (VRE) and Vancomycin-resistant *Staphylococcus aureus* (VRSA) were examined in presence of vancomycin, and it was found that properties of the cell wall such as peptidoglycan polymerization through cross-linking and acetylation states changed with the induction of vancomycin resistance.[32] As the vancomycin resistance mechanism for those two bacteria do not directly involve altering these two properties of peptidoglycan, studying these indirect consequences to peptidoglycan allowed insights into peptidoglycan biosynthesis and maintenance.

Finally, the last chapter of this thesis is the development of a new analytical method to study the peptidoglycan composition by liquid chromatography-mass spectrometry through the application of Stable Isotope Labeling with Amino Acids in Cell Culture (SILAC).[41-43] While commonly used in eukaryotic systems, this approach is seldom used in bacterial systems due to the amino acid self-sufficiency of many bacteria that prevents complete labeling of peptidoglycan. Further compounding the issue is the presence of multiple isotopically labeled amino acids in some peptidoglycan fragments being analyzed, as incomplete isotopic enrichment altered the isotopic distribution and peak intensity in mass spectra.[44] These issues were overcome by exploiting the regular and periodic nature of peptidoglycan at the level of subunits. Incorporation of the label into peptidoglycan and isotopic enrichment of each atom were both treated as stochastic events with fixed probabilities of occurrence, which allowed for calculating the amount of corrections needed to compensate for these factors. Resulting SILAC of *E. faecalis* peptidoglycan demonstrated the difference in composition between free-floating planktonic and biofilm-forming sessile bacteria. Other results in this dissertation show the difference in the peptidoglycan composition of *E. faecalis* as the culture matured.[33] Thus, this thesis outlines the efforts to describe the cell wall not just at the species and strain level, but at spatial and temporal level as well, which is depth of detail previously unascertained in peptidoglycan.

All the studies in this dissertation survey the peptidoglycan composition, and they either determined the specific properties of a single peptidoglycan variety using solid-state NMR, or took a snapshot of the overall peptidoglycan composition using liquid chromatography-mass spectrometry. It is my hope that the reader finds these studies both

useful and hopeful: useful in sketching out methods to study a relatively unknown macromolecule in peptidoglycan, and hopeful in demonstrating that even inherently disordered peptidoglycan can still be studied in detail and useful insights gleaned from analyzing it.

Attributions

Chapter Two: Sung Joon Kim and Peng Tao designed the experiments. James Chang, Hongyu Zhou, and Maria Preobrazhenskaya performed experiments and analyzed the data. All authors contributed to the writing of the manuscript.

Chapter Three: Sung Joon Kim designed the experiments. James Chang, Erin Foster, and Hao Yang performed experiments and analyzed the data. All authors contributed to the writing of the manuscript.

Chapter Four: Sung Joon Kim and James Chang designed the experiment. James Chang, Erin Foster, and Ashley Wallace performed the experiment and analyzed the data. All authors contributed to the writing of the manuscript.

Chapter Five: Sung Joon Kim and James Chang designed the experiment. James Chang, Rebecca Ramirez, Alex Guinn, Binayak Rimal, Chengyin Liu, Erin Foster, Lauryn Coffman, Ashley Wallace, Aanchal Thadani performed the experiment and analyzed the data. Sung Joon Kim and James Chang contributed to the writing of the manuscript.

Chapter Six: Sung Joon Kim and James Chang designed the experiment. James Chang, Erin Foster, Aanchal Thadani, and Alejandro Ramirez performed the experiment and analyzed the data. Sung Joon Kim and James Chang contributed to the writing of the manuscript.

Chapter Seven: All authors contributed to designing of the experiment. James Chang, Erin Foster, and Ashley Wallace performed the experiment and analyzed the data. Sung Joon Kim and James Chang contributed to the writing of the manuscript.

CHAPTER TWO

The Carboxyl-Terminus of Eremomycin Facilitates Binding to the Non-D-Ala-D-Ala Segment of the Peptidoglycan Pentapeptide Stem

This chapter published as: Chang, J.; Zhou, H.; Preobrazhenskaya, M.; Tao, P.; Kim, S. J. The Carboxyl-Terminus of Eremomycin Binding to the Non-D-Ala-D-Ala Segment of the Peptidoglycan Pentapeptide Stem. *Biochemistry* **2016**, *55(24)*: 3383-3391.

Abstract

Glycopeptide antibiotics inhibit cell wall biosynthesis in Gram-positive bacteria by targeting the peptidoglycan (PG) pentapeptide stem structure (L-Ala-D-iso-Gln-L-Lys-D-Ala-D-Ala). Structures of glycopeptide complexed with PG-stem mimic have shown that the D-Ala-D-Ala is the primary drug-binding site; however, biochemical evidences suggest that the glycopeptide-PG interaction involves more than D-Ala-D-Ala binding. Glycopeptide interactions with the non-D-Ala-D-Ala segment of the PG stem were investigated using solid-state NMR. LCTA-1421, a double ^{15}N-enriched eremomycin derivative with a C-terminus ^{15}N-amide and ^{15}N-Asn amide, was complexed with whole cells of *Staphylococcus aureus* grown in a defined media containing L-[ε-^{13}C]Ala and D-[1-^{13}C]Ala in the presence of alanine racemase inhibitor alaphosphin. ^{13}C{^{15}N} and ^{15}N{^{13}C} rotational-echo double resonance (REDOR) NMR measurements determined the ^{13}C-^{15}N internuclear distances between the ^{15}N-Asn amide of LCTA-1421 and the ^{13}Cs of the bound D-[1-^{13}C]Ala-D-[1-^{13}C]Ala to 5.1 and 4.8 Å, respectively. These measurements also determined the distance from the C-terminus ^{15}N-amide of LCTA-1421 to the L-[ε-^{13}C]Ala of PG to 3.5 Å. The measured REDOR distance constraints position the glycopeptide C-terminus in proximity to the L-Ala of the PG,

suggesting that the C-terminus of glycopeptide interacts near the L-Ala segment of the PG stem. *In vivo* REDOR measurements provided structural insight into how C-terminus modified glycopeptide antibiotics operate.

Introduction

Vancomycin is a glycopeptide antibiotic exhibiting potent activities against almost all strains of Gram-positive cocci and bacilli.[45] In 1956, Eli Lilly and Company discovered vancomycin in soil samples collected from Borneo; the antibiotic was being produced by soil microbe *Amycolatopsis orientalis*. Since the discovery of vancomycin, researchers have identified about 50 different glycopeptide-antibiotic producing organisms with over one hundred different natural glycopeptides.[46-47] All glycopeptides have a heptapeptide core (aglycon) structure formed by heavily cross linked amino acids through a series of phenolic oxidative couplings. The glycopeptides are classified into four types based on their chemical structure (Supplemental Figure 2.S1).[48] Vancomycin is a Type I glycopeptide with methylated-leucine and asparagine at the first and third positions of the aglycon, respectively. In Type II glycopeptides, such as avoparcin, the first and the third residues are replaced by aromatic amino acids. Type III and IV glycopeptides also have aromatic amino acids at the first and third positions, but they are cross-linked by a phenolic-ether linkage. Ristocetin is an example of Type III, with its aglycon structured modified by six sugar adducts. Teicoplanin, a Type IV glycopeptide, has an aglycon-core structure identical to Type III, but differs by an acyl chain attached to the sugar moiety.

Glycopeptides inhibit peptidoglycan (PG) biosynthesis by binding to lipid II, a membrane-bound PG precursor. This behavior was discovered when adding vancomycin

to cell extracts of *S. aureus* inhibited the formation of the PG (Figure 2.1) and the incorporation of glycine into the lipid II.[38] When vancomycin is added to whole cells of bacteria, cytoplasmic precursors accumulate (Park's Nucleotide) and the cell wall thins. These results support the hypothesis that vancomycin inhibits transglycosylation by targeting the lipid II.[49] By binding to lipid II, vancomycin effectively sequesters the lipid transporter C_{55}, the limiting factor in PG biosynthesis, which is present only in a small number of copies per bacterium. The lipid transporter is only regenerated from lipid II during the transglycosylation step of PG biosynthesis.

Vancomycin binding to D-Ala-D-Ala was first determined when vancomycin failed to inhibit *in vitro* PG polymerization of UDP-MurNac-tetrapeptide purified from the membrane fractions of *Gaffkya homari.*[50] Since the UDP-MurNac-tetrapeptide lacked the terminal D-Ala found on the PG-pentapeptide stem (Figure 2.1), it was inferred that vancomycin operates in part by binding to the terminal D-Ala-D-Ala of PG. When adding D-Ala-D-Ala dipeptide antagonized vancomycin's activities, this finding confirmed that the D-Ala-D-Ala of PG is the vancomycin binding site. Vancomycin dissociation constant to Acyl-D-Ala-D-Ala, determined by capillary electrophoresis, is 4.3 μM.[51]

Figure 2.2 shows the x-ray crystal structure of vancomycin bound to diacetyl-L-Lys-D-Ala-D-Ala[52] and the solution-state NMR structure of chloroeremomycin complexed with PG precursor analogue L-Ala-D-iso-Glu-L-Lys-D-Ala-D-Ala.[53] Both vancomycin and chloroeremomycin share an identical heptapeptide core structure that forms the D-Ala-D-Ala binding site. Five hydrogen bonds stabilize the D-Ala-D-Ala as

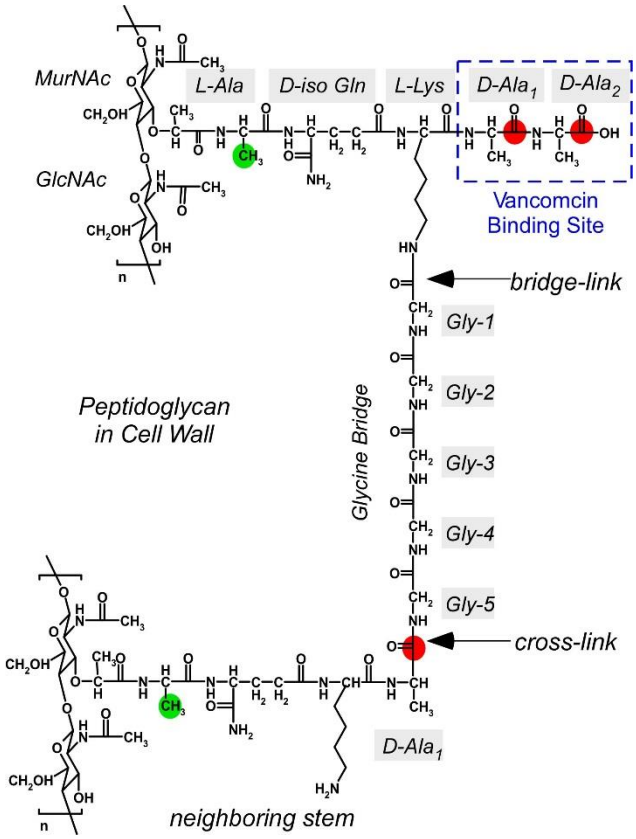

Figure 2.1: Chemical structure of *S. aureus* cell wall peptidoglycan (PG). PG has a repeat unit consisting of a disaccharide (MurNAc-GlcNAc) and a pentapeptides stem consisting of the sequence L-Ala-D-iso-Gln-L-Lys-D-Ala-D-Ala. A pentaglycine bridge is attached to the ε-nitrogen of the L-Lys. The ^{13}C-isotope enriched labels are incorporated into PG by growing *S. aureus* in the defined media containing D-[1-^{13}C]Ala and L-[ε-^{13}C]Ala, in the presence of the alanine racemase inhibitor alaphosphin (5 μg/ml). The positions of ^{13}C-isotope enriched labels for the D-[1-^{13}C]Ala are shown as red circles, and L-[ε-^{13}C]Ala as green circles. The dotted blue box indicates the D-Ala-D-Ala terminus of the PG-stem, the known vancomycin binding site.

it is attached to the aglycon structure (Figure 2.2, bottom): i) the first three H-bonds are located between the amide-protons (NH2, NH3, NH4) and the carboxyl oxygen on the C-terminus of the D-Ala-D-Ala, ii) a fourth bond is located between the carbonyl oxygen on the 4th residue of the aglycon (CO4) and an amide proton of the terminal D-Ala, and iii) a fifth bond is located between the amide proton of the 7th residue of the aglycon (NH7) and the carbonyl oxygen of the L-Lys. The hydrophobic interactions between the

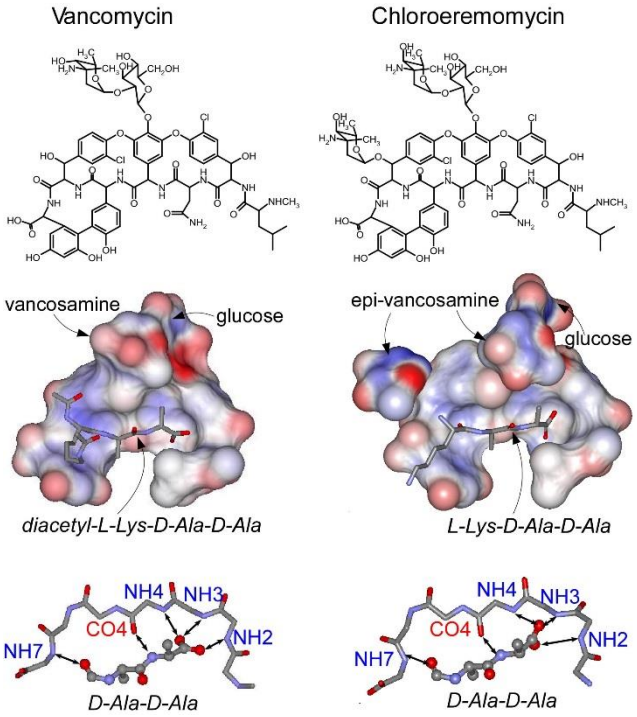

Figure 2.2: Top: Chemical structures of Type I glycopeptides, vancomycin (left) and chloroeremomycin (right). The heptapeptide core is heavily cross-linked and modified by sugars. The disaccharide of vancomycin is glucose-vancosamine, and the disaccharide of eremomycin is glucose-4-epi-vancosamine. Middle: X-ray crystal structure of vancomycin (left) complexed with the diacetyl-L-Lys-D-Ala-D-Ala (PDB identifier 1FVM).[52] A solution-state NMR structure of chloroeremomycin (right) complexed with L-Ala-D-iso-Glu-L-Lys-D-Ala-D-Ala (PDB identifier 1GAC).[53] The L-Ala-D-iso-Glu of the bound ligand is omitted from the chloroeremomycin structure for clarity. Bottom: PG-stem binding involves formation of five hydrogen bonds connecting the heptapeptide backbone structures of vancomycin (left) and chloroeremomycin (right) to the dipeptide D-Ala-D-Ala. The glycopeptide backbones are labeled by the residue numbers and the hydrogen bonds are represented as arrows. The side chains of glycopeptides and D-Ala-D-Ala are omitted for clarity.

aromatic residues of the glycopeptide core structure and the methyl group of the alanines in the dipeptide is thought to further stabilize the drug-bound structure. In both x-ray crystal and solution-state NMR structures, the disaccharides of vancomycin and chloroeremomycin do not participate in D-Ala-D-Ala binding.

Structure and activity studies of glycopeptides and biochemical evidences suggest that *in vivo* glycopeptide-PG binding is far more complex than mere D-Ala-D-Ala dipeptide binding.[46, 54] Some of the evidences are listed: 1) The strength of the

glycopeptide's binding affinity to D-Ala-D-Ala does not correlate with the drug's activity. For example, the binding affinity between chloroeremomycin and diacetyl-L-Lys-D-Ala-D-Ala is approximately 23 times less than vancomycin, but its activity is approximately 5 to 10 times greater. 2) The chlorine atom on the second amino acid of vancomycin improves the activity. The dechlorinated vancomycin (monodechlorovancomycin) is only half as active as vancomycin. 3) The removal of sugars from vancomcyin (deglycosylated vancomycin) does not affect the D-Ala-D-Ala binding, but it reduces the activity by a factor of 5. The sugars on vancomycin have been attributed to the formation of drug dimer, but *in vivo* glycopeptides are found as monomers,[20-21, 55-57] which suggests that the sugars enhance the activity by facilitating the PG binding through sugar-PG interactions.[20] 4) Methylated leucine, the first amino acid on vancomycin, is crucial for activity. The Edman degradation removal of leucine destroys the dipeptide binding affinity and its activity. 5) Asparagine, the third residue of vancomycin, does not participate in D-Ala-D-Ala binding but is required for its activity.[58] Replacing asparagine with glutamine (lengthening the side chain by 1 carbon) or replacing it with an aspartate (introducing negative charge) reduces the activity by 2 and 10 times, respectively. Asparagine substitution by isoaspartate destroys the antimicrobial activity.[46, 54] 6) Alkylation of the drug sugar by a hydrophobic side chain improves the activity.[59-62] 7) The carboxyl terminus modifications of the glycopeptide improve the activity even though it is not involved in the D-Ala-D-Ala binding.[63]

In this study, we investigate *in vivo* glycopeptide-PG binding interactions using solid-state NMR. Unlike solution-state NMR and x-ray diffraction structures based on the drug bound to PG-mimicking peptides, solid-state NMR enables direct investigation

of glycopeptide-PG complex in intact whole cells of *S. aureus*. In order to probe the glycopeptide-PG interactions, we have synthesized eremomycin derivative LCTA-1421 (Figure 2.3, top). LCTA-1421 is a bis[^{15}N]amide-carboxyeremomycin with two ^{15}N-isotope labeled probes: 1) a ^{15}N-amide at asparagine side chain of aglycon structure positioned inside the D-Ala-D-Ala binding pocket, and 2) a C-terminus ^{15}N-amide at the amino acid 7th position.

The first probe, ^{15}N-amide asparagine of LCTA-1421, was used to characterize the structure of LCTA-1421 aglycon bound to the D-Ala-D-Ala segment of PG-stem in whole cells. We anticipated that the *in situ* aglycon structure of LCTA-1421 bound to the D-Ala-D-Ala segment of PG in cell wall will be different from the solution-state NMR and x-ray diffraction structures based on drug bound to a model peptide which suffers from the artifacts of drug dimerization and crystal lattice constraints, respectively. The *in situ* aglycon structure of LCTA-1421 bound to PG was inferred from the internuclear ^{13}C-^{15}N distance measurements between the Asn ^{15}N-amide of LCTA-1421 to the ^{13}Cs in D-[1-^{13}C]Ala-D-[1-^{13}C]Ala of PG-stem using rotational-echo double resonance (REDOR) NMR.[64-65]

The second probe, the C-terminus ^{15}N-amide of LCTA-1421, was used to determine whether glycopeptide interaction with the non-D-Ala-D-Ala segment of PG-stem structure by measuring the ^{13}C-^{15}N distances between the C-terminus ^{15}N-amide of LCTA-1421 to the ^{13}C in L-[ε-^{13}C]Ala of PG-stem. LCTA-1421 exhibits improved antimicrobial activity over parent compound (Supplementary Table 2.S2) which suggests that the C-terminus ^{15}N-amide of LCTA-1421 interaction with the non-D-Ala-D-Ala segment of PG-stem is important for enhancing antimicrobial activity. Thus further

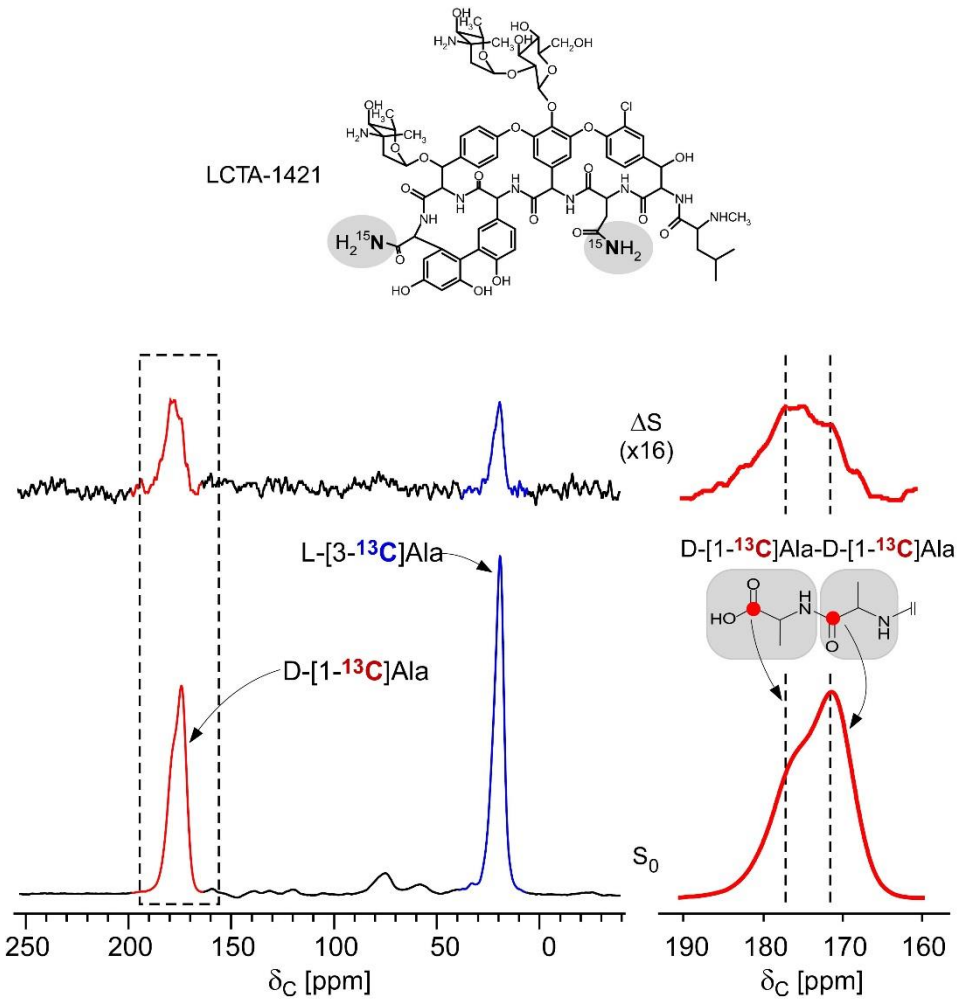

Figure 2.3: Top: Chemical structure of LCTA-1421. LCTA-1421 has two ^{15}N-isotope enriched labels (gray circles): the first is a C-terminus ^{15}N-amide and the second is a ^{15}N-amide side chain of an asparagine. LCTA-1421 shows improved antimicrobial activity. Table S2 summarizes the minimum inhibitory concentrations of vancomycin, eremomycin, and C-terminus-modified eremomycins against vancomycin sensitive and resistant strains. Bottom: ^{13}C{^{15}N} REDOR spectra during 32.4 ms dipolar evolution of whole cells of *S. aureus* grown in defined media containing D-[1-^{13}C]Ala and L-[3-^{13}C]Ala complexed to LCTA-1421. Left: The alanyl-carbonyl carbon of D-[1-^{13}C]Ala is visible at 175 ppm (red), and the alanyl-methyl carbon of L-[ε-^{13}C]Ala is visible at 30 ppm (blue) in the reference spectra (bottom). In the difference *ΔS* spectra (top), only the carbons that are in dipolar contact with the ^{15}N of LCTA-1421 are visible. Both the alanyl-carbonyl carbon of the D-[1-^{13}C]Ala at 175 ppm (red), and the alanyl-methyl carbon of the L-[ε-^{13}C]Ala at 30 ppm (blue) are dephased by the ^{15}N of LCTA-1421. Right) The carbons of D-[1-^{13}C]Ala are resolved. The spectra were the result of the accumulation of 160,000 scans.

understanding of glycopeptide interactions with non-D-Ala-D-Ala segment of PG-stem is crucial for the future for development of novel therapeutic agents, in particular against the vancomycin-resistant enterococci whose mechanism of vancomycin resistance is based on PG-stem D-Ala-D-Ala modification to D-Ala-D-Lac.

Materials and Methods

Synthesis of LCTA-1421 and LCTA-1110

The synthesis of bis[^{15}N]amide-carboxyeremomycin (LCTA-1421) is described in Solov'eva et al.[66] Briefly, eremomycin was treated with barium hydroxide at 37°C for 4 hr to yield carboxyeremomycin.[58] The [^{15}N]ammonium chloride was used to incorporate ^{15}N-enriched labels at the amino acid positions 3 and 7 of carboxyeremomycin using PyBOP and HBPyU as condensing reagents.[66] The MS-ESI calculated mass for LCTA-1421 ($C_{73}H_{90}N_9{}^{15}N_2O_{25}Cl$) $[M+H]^+$ was 1557.57, and the found $[M+2H]^{2+}$ mass was 779.80. The chemical shift of the ^{15}N-amide at the C-terminus (amino acid position 7) was 110.22 ppm, and the ^{15}N-amide side chain of asparagine (amino acid position 3) was 113.28 ppm by solution-state NMR. The synthesis of eremomycin *p*-fluorophenylpiperazinamide (LCTA-1110) is described elsewhere,[67] but briefly, LCTA-1110 was obtained by condensation of eremomycin with 4-fluorophenylpiperazine using PyBOP or HBPyU as condensing reagents.

Minimum Inhibitory Concentrations of Glycopeptide Antibiotics

As recommended by the National Committee for Clinical Laboratory Standards, the micro dilution method using Mueller-Hinton broth determined minimal inhibitory concentrations (MICs) for vancomycin, eremomycin, LCTA-1421, and LCTA-1110

against *Staphylococcus epidermidis*, *Staphylococcus haemolyticus*, vancomycin-intermediate resistant *S. aureus* (VISA), vancomycin-susceptible *Enterococcus faecium*, vancomycin-susceptible *Enterococcus faecalis*, vancomycin-resistant *E. faecium* (VanA type), and vancomycin-resistant *E. faecalis* (VanA type).

Growth of Whole Cells of S. aureus

A starter culture of *S. aureus* (ATCC 6538P) was added (1% final volume) to a one-liter flask containing 250 mL of sterile *S. aureus* Standard Medium (SASM), which is composed of L-[ε-^{13}C]Ala and D-[1-^{13}C]Ala in the presence of the alanine racemase inhibitor alaphosphin (5 mg/l). The detailed protocol for preparing SASM is described elsewhere.[16, 20-21] The cells were harvested at the optical density of 660 nm of 1.0, washed twice, and then resuspended in 10 mL of water containing 7.1 mg LCTA-1421. After 10 min on ice, the LCTA-1421-bacteria complex was frozen using liquid N_2, and then lyophilized. The lyophilized sample weight was 250 mg.

Solid-state NMR Spectrometer and REDOR NMR Parameters

REDOR NMR experiments were performed on 89-mm bore Oxford (Cambridge, England) superconducting solenoid at 4.7 T (200 MHz for 1H), using a four-frequency transmission-line probe with a Chemagnetics/Varian ceramic stator. The samples were contained in 7.5-mm outside diameter zirconia rotor spinning at 5 kHz at room temperature. Radio frequency pulses for ^{13}C and ^{15}N were produced by 1-kW ENI (Andover, MA) LPI-10 power amplifiers. Radio frequency pulses for ^{1}H were produced by a 1-kW Kalmus Engineering Int. Ltd (Valencia, CA) power amplifier, and the ^{19}F pulses by a 1-kW Dressler Hochfrequenztechnik Gmbh (Stolberg-Vicht, Germany) power

amplifier. All four amplifiers were under active control. Radio-frequency pulse lengths for π-pulse were 10 μs for ^{13}C, ^{15}N and ^{19}F. Proton-carbon and proton-nitrogen matched cross-polarization transfers were at 50 kHz for 2 ms. Proton dipolar decoupling during signal acquisition was 105 kHz. Standard XY-8 phase cycling[68] was used for all refocusing and dephasing pulses.

REDOR NMR method recouples heteronuclear dipolar interactions under magic-angle spinning (MAS)[64-65] to determine heteronuclear dipolar couplings and hence inter-nuclear distances. REDOR NMR is described elsewhere;[16, 20-21] briefly, in the full echo (S_0) spectrum, dipolar dephasing is refocused over a single rotor period by MAS. In the S spectrum, the spin part of the dipolar interaction prevented full refocusing by applying dephasing π-pulses, which reduced peak intensity for dipolar coupled spin pairs. The difference in signal intensity ($\Delta S = S_0 - S$) for the observed spin (^{13}C or ^{15}N) is directly related to the heteronuclear dipolar coupling from which the corresponding distance to the dephasing spin is determined. The normalized REDOR difference ($\Delta S/S_0$), based on the peak height measurements, is a direct measure of dipolar coupling, which was calculated using the modified Bessel function expressions given by Mueller et al.[69] and de la Caillerie and Fretigny[70] for an IS spin-$^1/_2$ pair. The error bar for each REDOR dephasing was determined based on the maximum noise peak intensity respect to the dephased peak intensity.

Molecular Dynamics Simulation of PG-LCTA-1421 Complex

Molecular dynamic simulation of LCTA-1421 bound to PG pentapeptide stem structure was carried out without water molecules to focus on the drug-target binding interactions. The initial model was generated based on the NMR structure of

chloroeremomycin complexed to the PG-stem structure (L-Ala-D-iso-Gln-L-Lys-D-Ala-D-Ala) (PDB ID: 1GAC). The CHARMM General Force Field (CGenFF)[71] for the simulating system was generated using the online server ParamChem (https://cgenff.paramchem.org/). After 20 ns molecular dynamics simulation, the following distance constraints were applied: i) 3.5 Å between L[ε-^{13}C]Ala with an ^{15}N-amide in C-terminus of LCTA-1421, ii) 5.1 Å between D[1-^{13}C]Ala with ^{15}N-amide asparagine in LCTA-1421, and iii) 4.8 Å between D[1-^{13}C]Ala with the ^{15}N-amide at the C-terminus of LCTA-1421. Additional harmonic constraints (5 kcal/mol) were added to prevent the simulation deviating from the NMR structure.

Results

^{13}C{^{15}N}REDOR NMR of PG-LCTA-1421 Complex

^{13}C{^{15}N}REDOR spectra during 32.4 ms dipolar evolution for whole cells of *S. aureus* labeled with D-[1-^{13}C]Ala and L-[ε-^{13}C]Ala complexed with LCTA-1421 are shown in Figure 2.3. For *S. aureus* when grown in the presence of alaphosphin (5 μg/ml) the provisioned D-[1-^{13}C]Ala does not scrambling to L-[1-^{13}C]Ala.[72] The ^{13}C-carbonyl carbons of D-[1-^{13}C]Ala-D-[1-^{13}C]Ala appear at 175 ppm (red), and the ^{13}C-methyl carbon of L-[ε-^{13}C]Ala at 30 ppm (blue). The chemical shift assignments for the ^{13}C-carbonyl carbons of D-[1-^{13}C]Ala-D-[1-^{13}C]Ala were determined using ^{13}C → ^{15}N transferred-echo double-resonance NMR experiment of whole cells of *S. aureus* labeled with D-[1-^{13}C]Ala and [^{15}N]Gly.[73] In the difference (*ΔS*) spectrum, both 175- and 30-ppm peaks are dephased by the ^{15}Ns of LCTA-1421. An expanded region centered around 175 ppm (Figure right) shows that the ^{13}C-carbonyl carbon of D-[1-^{13}C]Ala are

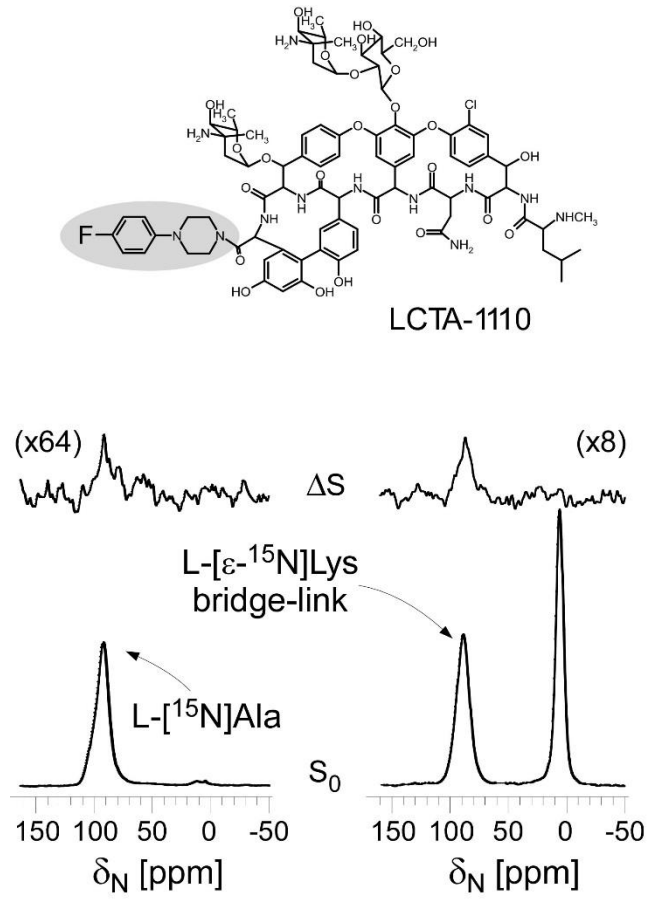

Figure 2.4: $^{15}N\{^{19}F\}$ REDOR spectra during 19.2 ms dipolar evolution of whole cells of *S. aureus* grown in defined media containing L-[^{15}N]Ala (left) and L-[ε-^{15}N]Lys (right) complexed with LCTA-1110 (top). The difference spectra (ΔS) are on the top and the full-echo spectra (S_0) are on the bottom. For the ^{15}N-^{19}F distance from the L-[^{15}N]Ala of PG to the ^{19}F of LCTA-1110 is 6.0 Å, and the distance from the L-[ε-^{15}N]Lys to the ^{19}F of LCTA-1110 is 7.9 Å. $^{15}N\{^{19}F\}$ REDOR dephasing curve is found in Kim et al.[20]

partially resolved. The 178-ppm peak is assigned to carboxyl-carbonyl carbon and 173 ppm is assigned to the peptidyl-carbonyl carbon of the D-[1-^{13}C]Ala-D-[1-^{13}C]Ala in the PG stem.[73] The ^{13}C-carbonyl carbons of D-[1-^{13}C]Ala-D-[1-^{13}C]Ala are dephased exclusively by the asparagine ^{15}N-amide of LCTA-142 due to its position found near to the bound D-Ala-D-Ala.[52] The methyl carbon of L-[ε-^{13}C]Ala, on the other hand, is exclusively dephased by the C-terminus ^{15}N-amide of LCTA-1421, based on earlier structural characterization of LCTA-1110 complexed to PG.[61] LCTA-1110 is a

fluorinated analogue of LCTA-1421 with a *p*-fluorophenylpiperazinamide at the C-terminus position (Figure 2.4, top).

Structural characterization of LCTA-1110 complexed to PG provided the first clue that the C-terminus of LCTA-1110 might be involved in binding to non-D-Ala-D-Ala segment of PG-stem structure,[20] which led to the synthesis of LCTA-1421 to investigate the interaction. Figure 2.4 shows the $^{13}N\{^{19}F\}$ REDOR spectra of whole cells of *S. aureus* grown in defined media containing L-[^{15}N]Ala (left) and L-[ε-^{15}N]Lys (right) complexed with LCTA-1110 (top) during 19.2 ms of dipolar evolution.[20] The measured ^{15}N-^{19}F distance from the ^{19}F of LCTA-1110 to the L-[^{15}N]Ala of the bound PG was 6.0 Å, and the distance to the L-[ε-^{15}N]Lys was 7.9 Å.[20] REDOR distances unambiguously position the fluorine of LCTA-1110 away from the bound dipeptide D-Ala-D-Ala but near the L-Ala of the bound PG stem. Therefore, in PG-LCTA-1421 complex the methyl carbon of L-[ε-^{13}C]Ala in PG stem is dephased exclusively by the C-terminus ^{15}N-amide of LCTA-1421, positioning the C-terminus ^{15}N-amide in close vicinity to L-[ε-^{13}C]Ala. $^{13}C\{^{15}N\}$REDOR dephasing curve and the measured distances are shown in Figure 6.

$^{15}N\{^{13}C\}$REDOR NMR of PG-LCTA-1421 Complex

The positioning of the C-terminus ^{15}N-amide of LCTA-1421 in proximity of L-[ε-^{13}C]Ala is confirmed in Figure 2.5 which shows the $^{15}N\{^{13}C\}$REDOR spectra of whole cells of *S. aureus* grown in defined media containing D-[1-^{13}C]Ala and L-[ε-^{13}C]Ala complexed to LCTA-1421 during 16.2 ms dipolar evolution. The inset shows the partially resolved amide peaks of LCTA-1421. The 85-ppm peak is assigned to the ^{15}N-amide of the asparagine side chain, and the 92 ppm to the C-terminus ^{15}N-amide of LCTA-1421. In the *ΔS* spectrum, the C-terminus ^{15}N-amide at 92 ppm is dephased by the

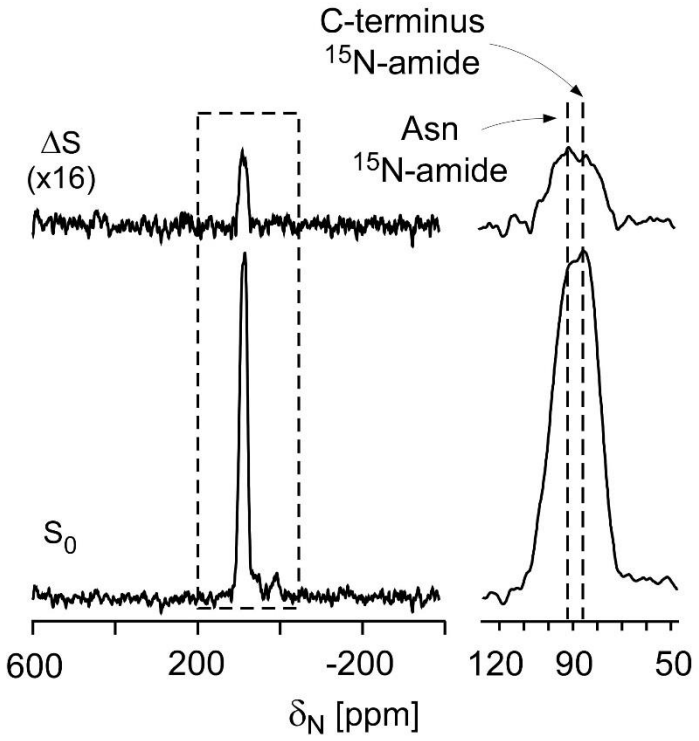

Figure 2.5: $^{15}N\{^{13}C\}$ REDOR spectra during 16.2 ms dipolar evolution of whole cells of *S. aureus* grown in defined media containing D-[1-^{13}C]Ala and L-[ε-^{13}C]Ala complexed to LCTA-1421. The full echo spectrum (S_0) is shown at the bottom of the figure and the REDOR difference (ΔS) is at the top. The amide regions of the full-echo and difference spectra are inset. The ^{15}N-amide of Asn in LCTA-1421 found at 92 ppm is resolved from the ^{15}N-amide of C-terminus amide at 85 ppm. The spectra were the result of the accumulation of 248,770 scans.

^{13}C-methyl carbon of the L-[ε-^{13}C]Ala and the 85-ppm peak by the ^{13}C-carbonyl carbons of the bound D-[1-^{13}C]Ala-D-[1-^{13}C]Ala.

^{13}C-^{15}N REDOR Distance Constraints for PG-LCTA-1421 Complex

The calculated $^{13}C\{^{15}N\}$REDOR dephasing curves for whole cells of *S. aureus* labeled with D-[1-^{13}C]Ala and L-[ε-^{13}C]Ala complexed with LCTA-1421 are shown in Figure 2.6 (left). The dephasing curve for the carboxyl D-[1-^{13}C]Ala_5 is shown in red solid line, and peptidyl-carbonyl carbon of D-[1-^{13}C]Ala_4 is shown in red dotted line. Each calculated dephasing curve includes ^{13}C-natural abundance contribution, which is fully dephased to 1% by 2 ms. The calculated ^{13}C-^{15}N distances for the Asn ^{15}N-amide

of LCTA-1421 to the carboxyl- and peptidyl-carbonyl carbons of the bound D-[1-^{13}C]Ala-D-[1-^{13}C]Ala are 4.8 and 5.1 Å, respectively. The ^{13}C-^{15}N distance from the C-terminus ^{15}N-amide of LCTA-1421 to the alanyl-methyl carbon of L-[ε-^{13}C]Ala (30 ppm) is 3.5 Å. This positions the ^{15}N-amide of the asparagine side chain in LCTA-1421 to 3.5 Å from the L-[ε-^{13}C]Ala and C-terminus ^{15}N-amide to 5.1 and 4.8 Å from the ^{13}Cs in bound dipeptide D-[1-^{13}C]Ala$_4$-D-[1-^{13}C]Ala$_5$, respectively.

Comparable ^{13}C-^{15}N distances are determined from ^{15}N{^{13}C}REDOR dephasing curves shown in Figure 2.6 (right). The red line is the calculated dephasing curve for the asparagine ^{15}N-amide dephasing (red circles) for two ^{13}C-^{15}N distances of 4.3 and 5.5 Å. The blue line is the calculated dephasing curve for the C-terminus ^{15}N-amide of LCTA-1421 dephasing (blue circles) for the ^{13}C-^{15}N distances of 3.8 Å. The ^{13}C-^{15}N distances determined by ^{15}N{^{13}C}REDOR are in reasonable agreement with ^{13}C{^{15}N}REDOR results. The measured ^{13}C-^{15}N distances are illustrated in Figure 2.6 (bottom) and are summarized in Supplementary Table 2.S1. The measured REDOR distances are used as constraints for the molecular dynamic simulation of LCTA-1421 complexed to the PG-stem structure shown in Figure 2.6.

Antimicrobial Activities of the Carboxyl-Terminus Modified Glycopeptide Antibiotics

Supplementary Table 2.S2 shows the minimal inhibitory concentrations (MICs) of vancomycin, eremomycin, LCTA-1421, and LCTA-1110 against vancomycin-susceptible and resistant strains of Gram-positive bacteria. The C-terminus modified glycopeptides, LCTA-1421 and LCTA-1110, exhibit mild improved activities across-the-board against vancomycin-susceptible Gram-positives, vancomycin-intermediate resistant *S. aureus*, and vancomycin-resistant *E. faecium* and *E. faecalis*.

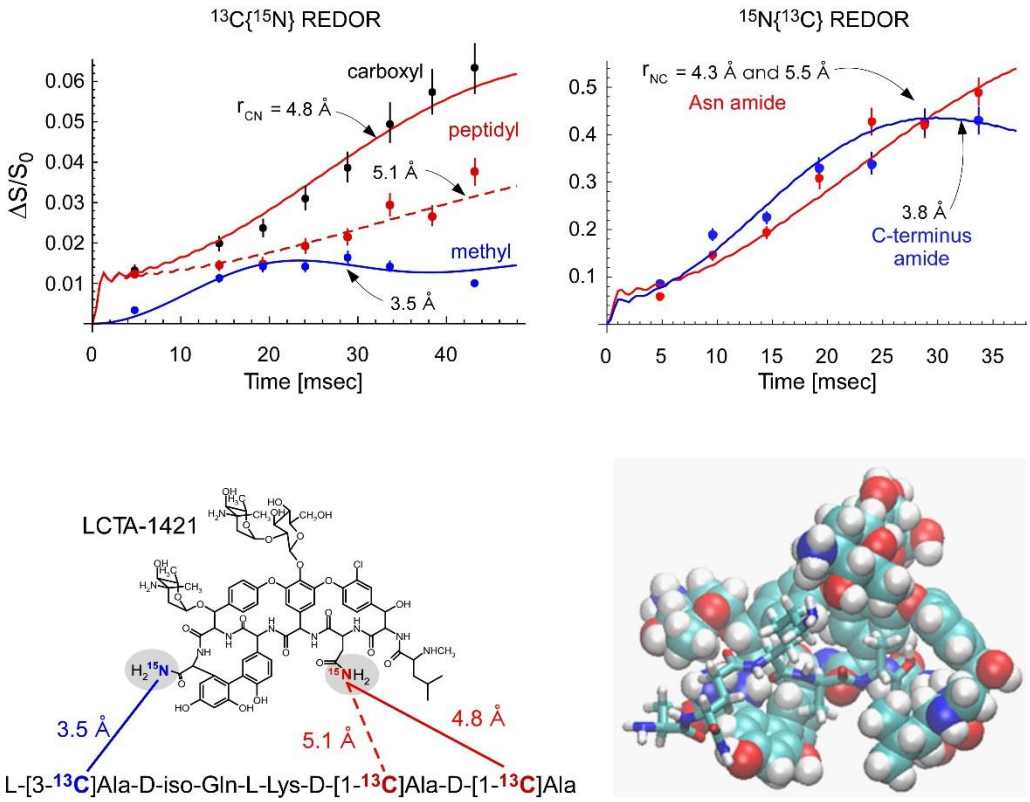

Figure 2.6: Top Left: $^{13}C\{^{15}N\}$ REDOR dephasing for whole cells of *S. aureus* grown in defined media containing D-[1-^{13}C]Ala and L-[ε-^{13}C]Ala complexed to LCTA-1421 plotted as a function of dipolar evolution. The calculated $^{13}C\{^{15}N\}$ REDOR dephasing curves for 175 ppm (solid red line), 173 ppm (dotted red line), and 30 ppm (solid blue line) correspond to the ^{13}C-^{15}N distances of 5.1 Å, 4.8 Å, and 3.5 Å, respectively. The $^{13}C\{^{15}N\}$ REDOR dephasing curve is the result of the total accumulations of 475,396 scans for each S_0 and S spectra. Top Right: $^{15}N\{^{13}C\}$ REDOR dephasing are plotted as a function of dipolar evolution. The red line represents the calculated $^{15}N\{^{13}C\}$ REDOR dephasing curve for the ^{15}N-^{13}C distances of 4.3 and 5.5 Å, and the distances between the asparagine ^{15}N-amide side chain and the ^{13}Cs of D-[1-^{13}C]Ala-D-[1-^{13}C]Ala bound to LCTA-1421. The blue line represents the dephasing curve for the ^{15}N-^{13}C distance of 3.8 Å between the C-terminus ^{15}N-amide of LCTA-1421 and the ^{13}C of L-[ε-^{13}C]Ala of PG. The $^{15}N\{^{13}C\}$ REDOR dephasing curve is result of the total accumulations of 1,036,810 scans. Bottom Left: A summary of measured REDOR distance constraints. Bottom Right: A molecular dynamic simulation model structure of LCTA-1421 bound to a pentapeptide PG-stem structure (L-Ala-D-iso-Gln-L-Lys-D-Ala-D-Ala). The simulation was carried out without water molecules with the solid-state NMR distance constraints: i) 3.5 Å between L[ε-^{13}C]Ala with an ^{15}N-amide in C-terminus of LCTA-1421, ii) 5.1 Å between D[1-^{13}C]Ala with ^{15}N-amide asparagine in LCTA-1421, and iii) 4.8 Å between D[1-^{13}C]Ala with the ^{15}N-amide at the C-terminus of LCTA-1421. REDOR NMR measurement of LCTA-1241 complex with whole cell *S. aureus* places the ^{15}N-amide side chain of asparagine approximately 5 Å from the carbonyl-carbons of the bound D-Ala-D-Ala of PG. This is contrary to the position of the asparagine side chain found outside of the D-Ala-D-Ala binding pocket in x-ray crystal structures.

Discussion

LCTA-1421 Asparagine Side Chain Functions as a "Flap"

Structure-activity studies have shown that the asparagine is essential for the activities in Type I glycopeptides.[46, 54, 63] Schäfer et al.[74] proposed that the vancomycin asparagine side chain functions as a gate to regulate the ligand access to the binding cleft. In an "open" conformation in the x-ray crystal structure of an asymmetric vancomycin dimer, the asparagine side chain swung out of the binding cleft with an acetate ion occupying the D-Ala-D-Ala binding site. In a "closed" conformation, the asparagine side chain is swung into the binding cleft.[74] A x-ray crystal structure of vancomycin bound to diacetyl-L-Lys-D-Ala-D-Ala (Figure 2.2 left) also showed that the asparagine side chain is swung out of the binding cleft to accommodate the ligand binding. Loll et al.[75] proposed that the asparagine side chain functions as a "flap" in the absence of a ligand, acting as a ligand surrogate by occupying the binding site. The "flap" prevents the hydration of the ligand binding cavity which is energetically favorable as the water molecules placed within a highly polarized binding pocket are thought to be difficult to remove in order for the ligand to bind.

It is unclear how critical the "flap" is for the glycopeptide activity. As shown in Supplemental Figure 2.S1, Types III, and IV, glycopeptides have aromatic residues at amino acids in positions 1 and 3 that are cross-linked by a phenolic-ether linkage. This ridged macrocylic ring structure is incompatible with the proposed "flap" function in vancomycin and furthermore, glycopeptide antibiotics of Types III and IV exhibit potent antimicrobial activities, even in the absence of the "flap," suggesting that asparagine's "flap" mechanism may not have a significant effect.

LCTA-1421 Asparagine Side Chain Forms a Binding Cleft

REDOR measurements position the asparagine ^{15}N-amide of LCTA-1421 at 5.1 and 4.8 Å from the ^{13}C-carbonyl carbons of D-[1-^{13}C]Ala-D-[1-^{13}C]Ala of the bound PG stem (Figure 2.6). The proximity of the asparagine ^{15}N-amide to the binding cleft is contrary to the average N-C distances of 7.9 and 6.1 Å determined by x-ray diffraction on vancomycin's hexamer-repeat unit (PDB identifier 1FVM). Each individual N-C distance in vancomycin's hexamer unit are tabulated and shown in Supplementary Table 2.S3. In the x-ray crystal structure, the asparagine side chain of vancomycin is positioned out of the D-Ala-D-Ala binding site; in contrast, solid-state NMR positions the asparagine sidechain closer to the D-Ala-D-Ala binding pocket. We believe that the crystallization of vancomycin, forming a hexamer-repeat unit, affects the conformation of the vancomycin-dipeptide bound structure. In comparison, solution-state NMR of the chloroeremomycin dimer determines that the corresponding N-C distances are 6.9 and 4.4 Å.[53] The solution-state NMR measurement agrees closely with REDOR NMR distance measurements of 5.1 and 4.8 Å (Figure 2.6). However, one caveat is that the solution NMR structure represents a chloroeremomycin bound to a model peptide mimicking PG as a dimer. We have found that glycopeptide antibiotics that readily form a dimer in a solution,[76-78] when complexed to whole cells of *S. aureus,* are found as a monomer when bound to PG.[20-21, 79] Even one of the most strongest dimer-forming glycopeptides, oritavancin, is found as a monomer when complexed to the PG in whole cells of *S. aureus*.[21] Hence, distance constraints determined by REDOR NMR represent *in vivo* glycopeptide conformation of monomeric-PG binding in the cell wall of intact

whole cells, without any effects from drug dimerization, PG-mimic binding, or crystal-lattice constraints.

We propose an alternative relationship between the asparagine side chain and the formation of the ligand-binding site. The asparagine side chain does not directly form a hydrogen bond with D-Ala-D-Ala, but its proximity to the bound dipeptide strongly suggests a possible interaction with the *N*-methyl-leucine (1st amino acid of LCTA-1421). The asparagine side chain interaction with the N-methyl-leucine can form a binding cavity that can stabilize the dipeptide binding. Either Edman degradation of the N-methyl-leucine in eremomycin (the parent compound of LCTA-1421),[80] or the replacement of asparagine with glutamine or aspartate can disrupt this action, thus diminishing antimicrobial activities. In the case of asparagine substitution by isoaspartate, the D-Ala-D-Ala binding site is destroyed by rearrangement, forming CDP-I, which is devoid of antimicrobial activities.[81] REDOR distance constraints indicate that the asparagine and leucine side chains constitute a part of a hydrophobic pocket necessary for the D-Ala-D-Ala binding. The proposed interaction between the asparagine and *N*-methyl-leucine in the presence of dipeptide will require further investigation.

Carboxyl-Terminus of LCTA-1421 Interacts with the Non-D-Ala-D-Ala Segments of PG

The solid-state NMR measurements position the L-Ala segment of the bound PG-stem near the C-terminus of the LCTA-1421 (Figure 2.6). The measured ^{13}C-^{15}N distance between the C-terminus ^{15}N-amide of LCTA-1421 and the L-[ε-^{13}C]Ala of the PG stem is 3.5 Å by ^{13}C{^{15}N} REDOR (Figure 2.3) and 3.8 Å by ^{15}N{^{13}C}REDOR (Figure 2.5). The results are in excellent agreement with the position of fluorine in LCTA-1110 (Figure 2.4) bound to PG in intact whole cells of *S. aureus* determined at 6.0

Å from the ^{15}N of L-[^{15}N]Ala of the bound PG stem.[72] These structural measurements are consistent with the C-terminus of glycopeptide interaction with the non-D-Ala-D-Ala segments of PG.

The MIC measurements (Table 2.S2) show that the C-terminus modifications enhance the antimicrobial activities of glycopeptides. The MIC values of LCTA-1421 and LCTA-1110 are more active than the parent compound eremomycin. The reason for the enhanced activities is that the C-terminus modification enhances glycopeptide-PG binding through interactions that involves more than just D-Ala-D-Ala binding. REDOR distance constraints positions the C-terminus of LCTA-1421 in vicinity of the L-Ala of the bound PG-stem structure in intact whole cells of *S. aureus*. This non-D-Ala-D-Ala interaction is critical for enabling the drug binding to the D-Ala-D-Lac terminated PG stem found in vancomycin-resistant enterococci, and thus is likely to be responsible for the small enhancement in activities of LCTA-1421 against vancomycin-resistant and intermediate resistant pathogens (Supplementary Table 2.S2).

In conclusion, glycopeptide antibiotics exhibit potent antibacterial activities by inhibiting PG biosynthesis in Gram-positive bacteria. The primary glycopeptide-PG interaction involves the aglycon structure of glycopeptide binding to the D-Ala-D-Ala of PG-stem structure. However, structure activity relationship studies of chemically modified glycopeptides suggest that drug-target interaction is complex. In the case of C-terminus modified glycopeptides, the antibiotic C-terminus interactions with the non-D-Ala-D-Ala segments of PG improves drug activity. To investigate glycopeptides interactions with non-D-Ala-D-Ala segments of PG, we complexed LCTA-1421 to intact whole cells of *S. aureus* and we characterize the PG-LCTA-1421 complex using solid-

state NMR. We have synthesized LCTA-1421 for this study with selective ^{15}N-isotope incorporations into its aglycon structure, one at the Asn sidechain and the other at the C-terminus. REDOR NMR measurements positioned the ^{15}N-amide of Asn sidechain of LCTA-1421 is in close proximity (5.1 and 4.8 Å) to the ^{13}Cs in bound D-[1-^{13}C]Ala-D-[1-^{13}C]Ala dipeptide, which indicated that the asparagine plays an important role in D-Ala-D-Ala binding. We have also found that the C-terminus ^{15}N-amide of LCTA-1421 is positioned in close proximity to the L-[1-^{13}C]Ala segment of the bound PG stem. Future experiments will be required to further investigate the glycopeptide C-terminus interactions with non-D-Ala-D-Ala segment of PG-stem structure which is crucial for enhancing antimicrobial activity against the vancomycin-resistant enterococci. Multiple REDOR distance constraints will be used to develop a detailed molecular model structure of glycopeptide-PG complex to provide structural insight for the development of novel therapeutic agents against emerging multi-drug resistant pathogens.

Acknowledgments

The authors acknowledge Southern Methodist University's Center for Scientific Computation for computing resources, and thank Ms. Svetlana E. Solovieva and Ms. Elena P. Mirchink, D.Sc., (Gause Institute of New Antibiotics, Moscow) for the antibacterial activity of LCTA compounds.

Supplemental Information

Chemical structure of classes of glycopeptide antibiotics, a summary table of ^{13}C-^{15}N REDOR distance constraints determined for LCTA-1421bound to peptidoglycan in intact whole-cells of *S. aureus*, and minimal inhibitory concentrations of C-terminus

modified glycopeptide antibiotics against vancomycin susceptible and resistant pathogens are provided.

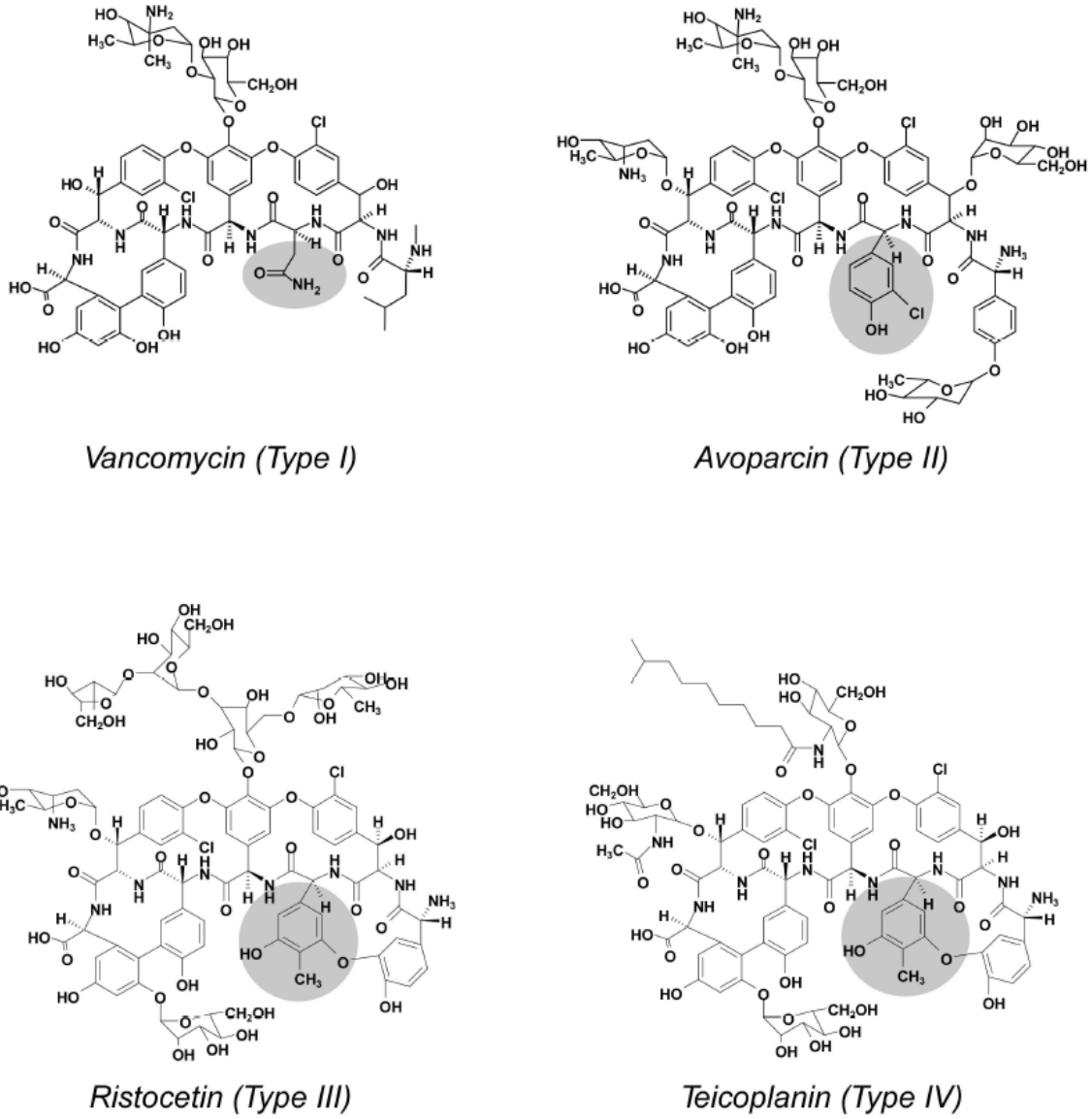

Supplementary Figure 2.S1: Classification of glycopeptides. The aglycon of vancomycin has an asparagine at the amino acid position 3 (gray circle). For glycopeptides of Types II, III, and IV, the amino acids at positions 1 and 3 are replaced by aromatic residues. In Type III and IV, these residues are cross-linked by a phenolic-ether linkage.[54]

Supplementary Table 2.S1: REDOR distance constraints.

LCTA-1421	$^{13}C\{^{15}N\}$REDOR (Å)			$^{15}N\{^{13}C\}$REDOR (Å)		
	L-[3-^{13}C]Ala (1st residue)	D-[1-^{13}C]Ala (4th residue)	D-[1-^{13}C]Ala (5th residue)	L-[3-^{13}C]Ala (1st residue)	D-[1-^{13}C]Ala (4th residue)	D-[1-^{13}C]Ala (5th residue)
^{15}N-amide Asparagine	NM	5.1	4.8	NM	5.5	4.3
^{15}N-amide C-terminus	3.5	NM	NM	3.8	NM	NM

Supplementary Table 2.S2: Minimum inhibitory concentrations (MIC, μg/mL) of C-terminus-modified eremomycins against vancomycin sensitive and resistant strains.

Compound/ Strain	533 *Staphylococcus epidermis*	602 *Staphylococcus haemolyticus*	Vancomycin-Intermediate Resistant *S. aureus* (VISA)		Vancomycin-Susceptible Enterococci (VSE)		Vancomycin-Resistant Enterococci (VRE)	
			3797 *S. aureus* [a]	3798 *S. aureus* [b]	568 *E. faecium* [c]	559 *E. faecium* [d]	569 *E. faecalis* [e]	560 *E. faecalis* [f]
Vancomycin	1	2	16	8	2	1	>128	>128
Eremomycin	0.13	0.13	8	8	0.25	0.25	>128	>128
LCTA-1421	0.06	0.13	0.25	0.5	0.13	0.25	>64	>64
LCTA-1110	0.5	1	1	1	0.5	0.5	32	32

[a]Vancomycin-intermediate resistant *S. aureus* (VISA) strain HIP-3836. [b]*S. aureus* (VISA) strain HIP-5827. [c]VSE *E. faecium* strain 568. [d]VSE *E. faecalis* strain 559. [e]VRE *E. faecium* of *VanA*-type strain 569. [f]VRE *E. faecalis* of *VanA*-type strain 560.

Supplementary Table 2.S3: Distances from the nitrogen of the asparagine-amide side chain to the alanyl-carbonyl carbons of the bound D-Ala-D-Ala dipeptide in the x-ray crystal structure of a vancomycin hexamer bound to diacetyl-Lys-D-Ala-D-Ala (PDB identified 1FVM).[52]

Vancomycin hexamer each complexed with a diacetyl-Lys-D-Ala-D-Ala	To the peptidyl-carbonyl carbon of D-Ala (Å)	To the C-terminus carbonyl carbon of D-Ala (Å)
Vancomycin 1	7.65	5.54
Vancomycin 2	8.28	6.95
Vancomycin 3	8.36	6.51
Vancomycin 4	8.37	6.65
Vancomycin 5	7.41	5.56
Vancomycin 6	7.33	5.34
Average	7.90	6.09

CHAPTER THREE

Quantification of D-Ala-D-Lac Terminated Peptidoglycan Structure in Vancomycin-Resistant *Enterococcus faecalis* Using a Combined Solid-state NMR and Mass Spectrometry Analysis

This chapter published as: Chang, J. D.; Foster, E. E.; Yang, H.; Kim, S. J. Quantification of the D-Ala-D-Lac-Terminated Peptidoglycan Structure in Vancomycin-Resistant *Enterococcus faecalis* Using a Combined Solid-State Nuclear Magnetic Resonance and Mass Spectrometry Analysis. *Biochemistry* **2017**, *56(4)*: 612-622.

Abstract

Induction of vancomycin resistance in vancomycin-resistant enterococci (VRE) involves replacement of the D-Ala-D-Ala terminus of peptidoglycan (PG) stems with D-Ala-D-Lac, dramatically reducing the binding affinity of vancomycin to lipid II. Effects from vancomycin resistance induction on *Enterococcus faecalis* (ATCC 51299) were characterized using a combined solid-state NMR and LC-MS analysis. Solid-state NMR directly measured the total amounts of D-Lac and L,D-Ala metabolized from [2-^{13}C]pyruvate, accumulated Park's nucleotide, and changes to the PG bridge-linking density during early exponential growth phase (OD_{660nm} 0.4) in intact whole cells of VRE. Large accumulation of depsipeptide substituted Park's nucleotide consistent with the inhibition of transglycosylation step of PG biosynthesis during the initial phase of vancomycin resistance was observed, while no changes to the PG bridge-linking density following the induction of vancomycin resistance was detected. This indicated that the PG bridge attachment to lipid II by the peptidyl transferases was not inhibited by the D-Ala-D-Lac substituted PG-stem structure in VRE. Compositions of mutanolysin-digested isolated cell walls of VRE grown with and without vancomycin resistance induction were

determined by LC-MS. Muropeptides with PG stems terminating in D-Ala-D-Lac were found only in VRE grown in presence of vancomycin. Percentages of muropeptides with a pentapeptide stem terminating in D-Ala-D-Lac for VRE grown in presence of vancomycin were 26% for mid-exponential (OD_{660nm} 0.6) and 57% for stationary growth phase (OD_{660nm} 1.0). These high percentages indicate that D-Ala-D-Lac substituted lipid II was efficiently utilized for PG biosynthesis in VRE.

Introduction

Vancomycin-resistant enterococci (VRE) are opportunistic pathogens commonly found in the gastrointestinal tract. They can translocate across the intestinal lining into bloodstream and cause bacteremia, sepsis, endocarditis, and other potentially fatal infections. With increased vancomycin usage, various enterococcal infections have become common in nosocomial settings.[82] Historically, *Enterococcus faecalis* alone has been responsible for 80-90% of all enterococcal infections.[83] *E. faecalis* is one of the leading nosocomial agents for catheter-associated infections due to its ease of transmission through surface contacts. One of many factors that contribute to persistence of *E. faecalis* in healthcare settings is its robust cell wall approximately 30 nm in thickness. The primary component of this cell wall is peptidoglycan (PG), which is assembled from repeating subunits to form the lattice structure.[17, 84]

Biosynthesis of these PG subunits is carried out in three stages. The first stage, which takes place in the cytoplasm, is the sequential addition of amino acids to UDP-MurNAc for the synthesis of Park's nucleotide (Scheme 3.1a). Resulting Park's nucleotide is the cytoplasmic monosaccharide precursor of PG with the amino acid PG-stem structure (L-Ala-D-iso-Glu-L-Lys-D-Ala-D-Ala) attached to MurNAc. The second

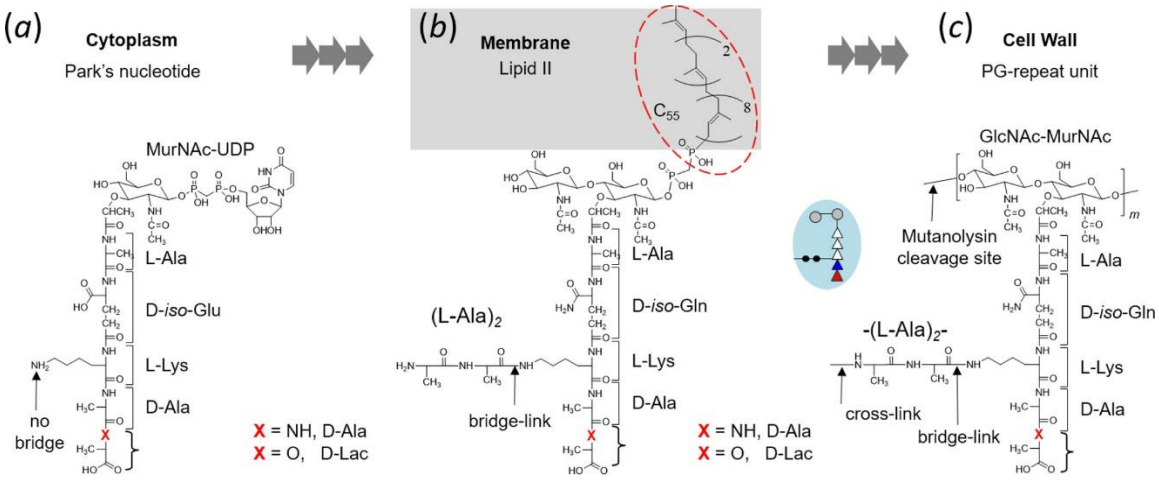

Scheme 3.1: Peptidoglycan biosynthesis in *Enterococcus faecalis*. (a) The first stage of PG biosynthesis takes place in the cytoplasm with Park's nucleotide (UDP-MurNAc-L-Ala-D-iso-Glu-L-Lys-D-Ala-D-Ala) as the end product. In vancomycin-resistant *E. faecalis*, the terminal D-Ala of Park's nucleotide is replaced by D-Lac. (b) The second stage of PG biosynthesis occurs on the interior side of bacterial cytoplasmic membrane, where UDP-MurNAc-stem from Park's nucleotide is transported by the lipid transporter C_{55} to form lipid II (*N*-acetylglucosamine-*N*-acetyl-muramyl-pentapeptide-pyrophosphoryl-undecaprenol). Attachment of L-Ala-L-Ala bridge to the PG-stem is carried out by peptidyl transferases BppA1 and BppA2. D-iso-Glu is amidated to D-iso-Gln. (c) The final stage of PG biosynthesis is carried out on the external side of cytoplasmic membrane with incorporation of the PG-repeat unit into the cell wall.

stage of PG biosynthesis is carried out on the interior side of cytoplasmic membrane with the transfer of Park's nucleotide to the membrane transporter C_{55} (undecaprenyl phosphate). During this stage, PG disaccharide (GlcNAc-MurNAc) is first assembled by the addition of *N*-acetylglucosamine (GlcNAc), then two L-Ala of the crosslinking bridge are sequentially added by peptidyl transferases BppA1 and BppA2[85] to the ε-nitrogen side chain of L-Lys of the PG stem to form lipid II (Scheme 3.1b). The final stage of PG assembly is carried out by translocating lipid II to the exterior side of cytoplasmic membrane. Transglycosylase polymerizes PG disaccharides of lipid II to extend the glycan chain, and transpeptidase interconnects neighboring glycan chains through cross-links.[86] A cross-link is the peptide bond between the *N*-terminus of L-Ala from the bridge in one PG unit to the *C*-terminus of penultimate D-Ala from the stem on a neighboring

glycan chain. The terminal D-Ala (5^{th} amino acid) from the acceptor stem is cleaved upon cross-link formation.

Vancomycin resistance is conferred upon VRE by substitution of the D-Ala-D-Ala terminus of the PG stem, the vancomycin binding site, with a depsipeptide D-Ala-D-Lac.[87-88] The substitution replaces the amide of final D-Ala with an oxygen from D-Lac, which introduces an electrostatic repulsion between oxygen in the ester bond of D-Ala-D-Lac to carbonyl from the fourth residue of vancomycin, and this reduces vancomycin's binding affinity to the altered stem by a thousand fold.[89-90] VRE with the D-Ala-D-Lac PG-stem modification exhibit high-levels of vancomycin resistance with minimal inhibitory concentrations (MIC) that often exceed 100 μg/mL.[91]

E. faecalis strain ATCC 51299 used for this study is VRE of *VanB* type[92] with the plasmid that includes *$vanR_B$, $vanS_B$, $vanH_B$, vanB, $vanX_B$, $vanY_B$,* and *vanW*.[93] $VanS_B$ and $VanR_B$ are part of a two-component regulatory system, where $VanS_B$ is a membrane-bound sensor kinase that as a response to vancomycin phosphorylates the response-regulator protein $VanR_B$,[94] which is a transcription factor that activates downstream elements *$vanH_B$, vanB, $vanX_B$,* and *$vanY_B$*.[93] $VanH_B$ and VanB are involved in biosynthesis of D-Ala-D-Lac, where $VanH_B$ is a dehydrogenase that catalyzes production of D-Lac from pyruvate,[95] and VanB is a ligase that joins D-Lac and D-Ala together to form a depsipeptide.[96] Biosynthesis of D-Ala-D-Lac is accompanied by breaking down of D-Ala-D-Ala by $VanX_B$ and $VanY_B$. $VanX_B$ is a D,D-dipeptidase that cleaves the dipeptide D-Ala-D-Ala,[97] while $VanY_B$ is a D,D-carboxypeptidase that removes terminal D-Ala from the PG stem of Park's nucleotide.[98-99] The effect of both peptidases is rapid degradation

of D-Ala-D-Ala in the PG stem of Park's nucleotide, which is replaced by the depsipeptide D-Ala-D-Lac.

Although D-Ala-D-Lac substituted Park's nucleotide has been identified from cytoplasmic fractions of vancomycin-resistant *E. faecalis*[100] and *E. faecium*,[101] D-Ala-D-Lac terminated PG stems have not yet been observed from isolated cell walls of *E. faecalis*[102] and *E. faecium.*[103] Their absence suggested that D-Ala-D-Lac substituted lipid II is not readily utilized for the cell wall biosynthesis and/or D-Lac is cleaved from PG stems in the cell wall by highly active D,D-carboxypeptidases.[102-103] D-Ala-D-Lac substituted PG stem is also thought to interfere with the attachment of bridge structure to lipid II, as treatment of vancomycin-resistant *Staphylococcus aureus* of *VanA* type (strain COLVA) with vancomycin resulted in increased concentrations of muropeptide species missing the bridge structure.[104] *In vitro* assay has shown that addition of D-Ala-D-Lac substituted lipid II strongly inhibits FemX activity,[105] where FemX is the peptidyl transferase that catalyzes the first committed step in the attachment of pentaglycine bridge to lipid II in *S. aureus*. In *E. faecalis*, L-Ala-L-Ala bridge attachment is carried out by peptidyl transferases BppA1 and BppA2[85] which belong to the same family of Fem proteins found in *S. aureus*.[85, 106] Hence, D-Ala-D-Lac terminated lipid II is likely to be a poor substrate for peptidyl transferases in *E. faecalis*.

In this study, we characterized changes in the PG composition of vancomycin-resistant *E. faecalis* (ATCC 51299) grown with and without vancomycin using solid-state NMR and liquid chromatography-mass spectrometry (LC-MS). Solid-state NMR was used to directly measure in intact cells the PG bridge-link density and Park's nucleotide accumulation in *E. faecalis* using L-[1-^{13}C]Ala and L-[ε-^{15}N]Lys, and characterize [2-

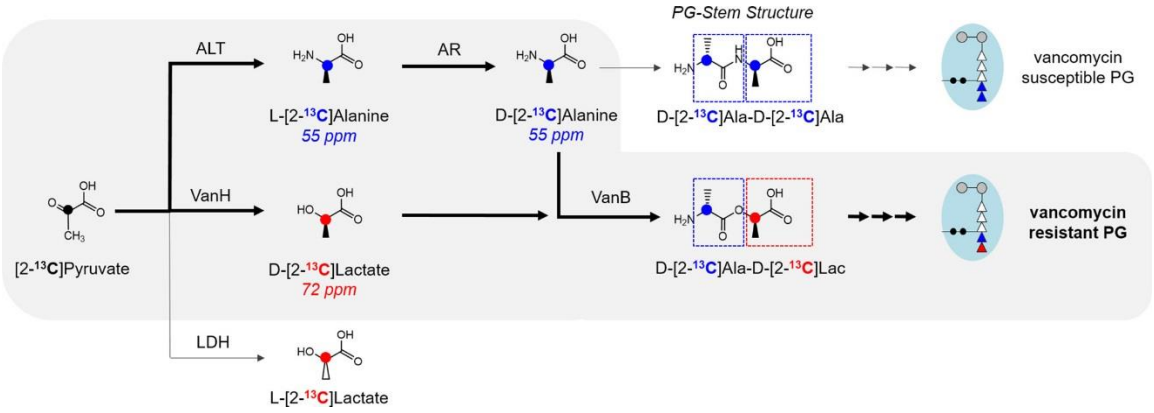

Scheme 3.2: [2-^{13}C]Pyruvate metabolism in vancomycin-resistant *E. faecalis*. In absence of vancomycin, [2-^{13}C]pyruvate is utilized for the biosynthesis of L-[2-^{13}C]Ala by alanine transaminase (ALT), then to D-[2-^{13}C]Ala by alanine racemase (AR). [2-^{13}C]pyruvate metabolism to L-[2-^{13}C]Lac by lactate dehydrogenase (LDH) does not occur in VRE under aerobic growth. Following the induction of vancomycin resistance, $VanH_B$ catalyzes the biosynthesis of D-[2-^{13}C]Lac.

^{13}C]pyruvate utilization for the biosynthesis of D-[2-^{13}C]Lac (Scheme 3.2). LC-MS analysis was performed on mutanolysin digested isolated cell walls of VRE. Mutanolysin is an *N*-acetylmuramidase which cleaves the MurNAc $\beta_{1\text{-}4}$ glycosidic linkage in PG (Scheme 3.1), and resulting muropeptide fragments were analyzed by LC-MS to determine the incorporation efficiency of D-Ala-D-Lac substituted lipid II in the cell wall of VRE.

Experimental Methods

Bacterial Growth and Isotope Labeling

From overnight starter culture of vancomycin-resistant *E. faecalis* (ATCC 51299), 1% inoculum of the starter culture was added to one-liter flasks containing 330 mL of sterile Enhanced Standard Medium (ESM). ESM was modified from SASM[21] to enable both staphylococcal and enterococcal bacteria to grow.[57] PG bridge-links in intact *E. faecalis* were ^{13}C-^{15}N pair labeled by growing them in ESM where natural abundance L-Ala and L-Lys were replaced by L-[1-^{13}C]Ala and L-[ε-^{15}N]Lys. Alanine racemase

inhibitor alaphosphin (5 μg/mL) and D-Ala (0.1 g/L) were added to prevent racemic scrambling of L-[1-^{13}C]Ala and provide the source of D-Ala. To determine $VanH_B$ activity in VRE, *E. faecalis* were grown in ESM supplemented with Na-[2-^{13}C]pyruvate (0.1 g/L). Vancomycin resistance was induced during the exponential growth (OD_{660nm} 0.3) by addition of vancomycin to final concentration of 10 μg/mL. Cells were harvested after 1 hour of growth by centrifugation at 10,000 g for 10 minutes at 4 °C in Sorvall GS-3 rotor. Resulting pellets were washed twice with 100 mL of cold deionized water, then resuspended in approximately 25 mL of deionized water, followed by rapid freezing and lyophilization.

Rotational-Echo Double Resonance (REDOR) NMR

REDOR is a solid-state NMR method used to recouple dipolar interactions under magic-angle spinning (MAS).[64-65] REDOR experiment consists of two parts. In the first part, polarization transfer from the protons prepares ^{13}C magnetization, and the spectrum is collected after *N* rotor periods without dipolar evolution; this observed ^{13}C spectrum is referred to as the S_0 spectrum. In the second part of REDOR experiment, ^{13}C-^{15}N dipolar coupling is reintroduced by applying rotor-synchronized dephasing π pulses to ^{15}N nuclei. ^{15}N pulses invert the sign of dipolar coupling and interfere with the MAS spatial refocusing, which result in net dipolar phase accumulation and reduced ^{13}C signal intensity; this ^{13}C spectrum with the dephasing pulses is referred to as the dephased spectrum with *N* rotor cycles of dipolar evolution. From these two spectra, the difference spectrum ($\Delta S = S - S_0$) with intensities only from ^{13}C dipolar coupled to ^{15}N is derived. Normalized REDOR difference ($\Delta S / S_0$) is the direct measure of dipolar coupling, and

this quantity was calculated using modified Bessel function expressions given by Mueller et al.[69] and de la Caillerie and Fretigny[70] for an IS spin-1/2 pair.

Solid-state NMR Spectrometer

Solid-state NMR analyses were performed on lyophilized intact cells of *E. faecalis* packed into Chemagnetics/Varian 7-mm zirconia rotors. REDOR was performed at 4.7-T field (proton radio frequency of 200 MHz) provided by 89-mm bore Oxford (Cambridge, England) superconducting solenoids utilizing a four-frequency transmission-line probe with 17-mm long, 8.6-mm inside-diameter analytical coil and Chemagnetics/Varian ceramic stator. Rotors were spun at 5000 Hz with speed under active control to within ±2 Hz. π pulse lengths were 10 μs for both ^{13}C and ^{15}N. Matched proton-carbon cross-polarization transfers were made in 2 ms at 50 kHz. Proton dipolar decoupling was 98 kHz during data acquisition. Standard XY-8 phase cycling was used for all refocusing and dephasing pulses.[68] All measurements were carried out at ambient room temperature.

Cell Wall Isolation

Overnight cultures of *E. faecalis* were used to inoculate brain-heart infusion (BHI) media containing vancomycin (6 μg/mL). Cultures were grown for 24 hours at 37°C with 180 RPM shaking. Cells were harvested at exponential (OD_{600nm} ~0.6) and stationary growth (OD_{600nm} 1.0) phases by centrifugation (Beckman Coulter Allegra X-15R, SX4750 rotor) at 4750 rpm for 12 min at 4°C. Autolysins were inactivated by immersing pellets in boiling water baths for 30 minutes. Collected samples were divided equally into multiple microcentrifuge tubes with each containing approximately 400 μL

(0.65 g) of 0.5 mm glass beads. Cells were agitated (Disruptor Genie, Scientific Industries) with beads for 15 minutes in alternating cycles of 1 minute of bead-beating and 1 minute of rest, giving a total of 8 cycles of 1-minute bead-beating and 7 cycles of 1-minute rest. Following the bead-beating, disrupted cells were resuspended in phosphate buffered saline (PBS) containing 8 mg/mL NaCl, 0.2 mg/mL KCl, 1.44 mg/mL Na_2HPO_4, and 0.24 mg/mL KH_2PO_4. Beads were filtered out from the cells using Steriflip 20 μm nylon net vacuum filter unit (EMD Millipore). Disrupted cells were washed once in PBS, boiled in 2% sodium dodecyl sulfate solution for 30 minutes, and washed 5 times with autoclaved deionized water. Resulting isolated cell walls were suspended in 20 mM Tris pH 8.0 buffer. To the samples, 200 μg of DNase (Sigma-Aldrich) was added and the mixture incubated for 24 hours at 37°C and 180 RPM. Trypsin (300 μg) (Sigma-Aldrich) was then added to the digest, and the sample incubated for additional 24 hours at 37°C and 180 RPM. Following the digestions, samples were centrifuged to spin down the isolated cell wall. Resulting pellets were resuspended in 20 mM Tris buffer, frozen, and lyophilized.

Mutanolysin Digestion of Isolated Cell Wall

Lyophilized cell walls suspended in 2 mL of 20 mM Tris pH 8.0 buffer were first digested with 100 units of mutanolysin (Sigma-Aldrich) for 24 hours at room temperature, then additional 100 units were added for 24 more hours of digestion. Digested cell wall fragments were centrifuge filtered through 30 kDa molecular weight cutoff filters at 14800 RPM. Filtered muropeptides were reduced using sodium borohydride (10 mg/mL) in 1 mL 0.5 M borate pH 9.0 at room temperature for 30

minutes. Reduction was quenched by addition of 120 µL of 85% phosphoric acid, and the samples were frozen and lyophilized.

LC-MS Analysis

Mutanolysin-digested cell wall (20-40 mg) in 500 µL of 20 mM Tris pH 8.0 buffer was diluted 1:10 in methanol with 0.1% formic acid. Waters Synapt G2 High Definition Mass Spectrometer (HDMS) Time-of-Flight (TOF) mass analyzer and Waters C18 ACUITY Ultra Performance Liquid Chromatography (UPLC) were used to analyze mutanolysin digested fragments of peptidoglycan. Chromatographic separation of mutanolysin-digested peptidoglycan was carried out by injecting 1 µL of the sample from a 5 µL sample loop to the column under isocratic condition of 99% buffer A (99.8% anhydrous methanol with 0.1% formic acid) and 1 % buffer B (100% acetonitrile) for 5 minutes. Waters nanoACQUITY C18 reverse-phase column (75 µm X 100 mm, 1.7 µm beads with 130 Å pore size) with nanoACQUITY C18 trap column (180 µm X 20 mm, 5 µm beads with 100 Å pore size) was used for chromatographic separation. First, a linear gradient to 50% buffer B was applied for 60 minutes. The column was subsequently regenerated under isocratic condition with 85% buffer B for 5 minutes, a linear gradient to 98% buffer A for 1 minute, then isocratic at 98% buffer A for 23 minutes. The flow rate was kept constant (0.6 µL/min) throughout the analysis.

Resulting eluents were analyzed by Waters Synapt G2 HDMS-TOF mass analyzer operating in positive ion mode with the fragments ionized through electrospray ionization (ESI) with spray voltage of 35 V and capillary voltage of 3.5 kV. The mass analyzer was optimized for m/z range of 100-2000, with Fibrinopeptide B (Glu-Fib) as the lock mass for calibration. MS/MS fragmentation was accomplished through collision-induced

dissociation with nitrogen gas at 120°C and 2.00 Bar. Transfer collision energy was 5 V, and trap collision energy was 30 V. MassLynx Mass Spectrometry Software (Waters) was used for data analysis. Values for calculating the exact mass for mutanolysin-digested PG fragments were obtained from the Molecular Mass Calculator on the Biological Magnetic Resonance Data Bank (www.bmrb.wisc.edu). The difference between observed and calculated masses needed to be less than 10 ppm for ions to be identified as positive matches.

Results and Discussion

Park's Nucleotide Accumulation in Vancomycin-treated VRE

Growth curves of VRE (ATCC 51299) grown in ESM in presence of vancomycin as monitored by measuring the optical density at 660 nm ($OD660_{nm}$) are shown in Figure 3.1a. ESM was supplemented with natural abundance D-Ala (0.1 g/L) and alaphosphin (5 μg/mL). Alaphosphin (L-alanyl-L-1-aminoethylphosphonic acid) is an alanine racemase inhibitor that prevents racemic scrambling between L-Ala and D-Ala. The MIC of alsphosphin against *E. faecalis* in the absence of supplemental D-Ala was < 5 μg/mL. Stock solutions of vancomycin were added during mid-growth (OD_{600nm} 0.3) to final concentrations of 0, 5, 10 and 20 μg/mL. A dose-dependent growth delay immediately following the vancomycin addition was observed, but even high concentration of vancomycin (20 μg/mL) did not fully inhibit VRE growth.

To determine the effects of vancomycin on PG biosynthesis, ^{15}N-cross polarization at magic-angle spinning (CPMAS) NMR measurements were performed on intact cells of VRE grown in ESM containing L-[1-^{13}C]Ala and L-[ε-^{15}N]Lys. ESM was

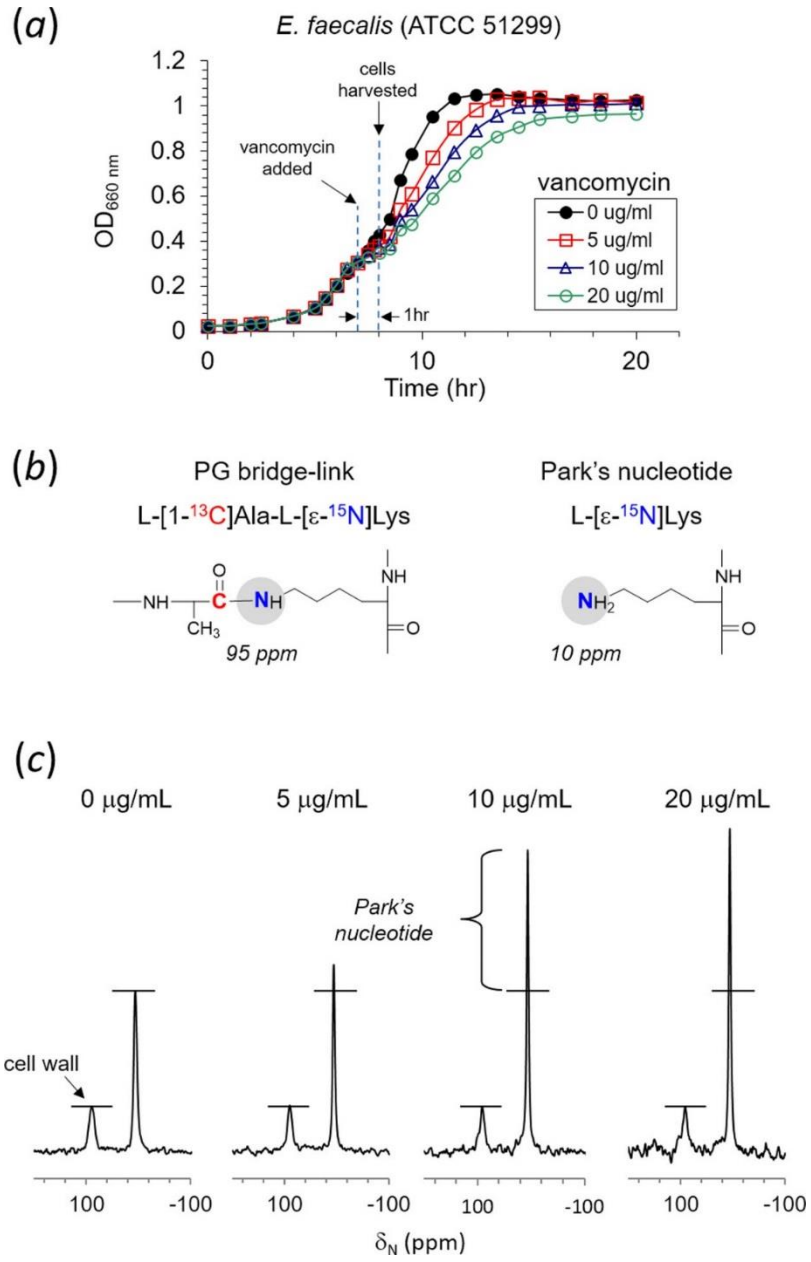

Figure 3.1: (a) Growth curves of vancomycin resistant *E. faecalis* (ATCC 51299) in ESM containing L-[1-^{13}C]Ala and L-[ε-^{15}N]Lys. Growth was monitored by measuring optical density at 660 nm (OD_{660nm}). Vancomycin was added to final concentrations of 0, 5, 10, and 20 μg/mL during growth at $OD660_{nm}$ 0.3. Cells were harvested at $OD660_{nm}$ 0.4 for ^{15}N-CPMAS NMR analysis. (b) Incorporation of L-[ε-^{15}N]Lys into the PG bridge-link is visible as a lysyl-amide at 95 ppm, and into Park's nucleotide as a lysyl-amine at 10 ppm in ^{15}N-CPMAS spectra. (c) ^{15}N-CPMAS spectra of *E. faecalis* labeled with L-[1-^{13}C]Ala and L-[ε-^{15}N]Lys. Spectra are normalized to 95-ppm intensity. L-[ε-^{15}N]Lys incorporated into PG bridge-linked resonates at 95 ppm, and L-[ε-^{15}N]Lys into proteins and Park's nucleotide at 10 ppm. VRE grown in presence of vancomycin show Park's nucleotide accumulation, indicating that vancomycin inhibited the transglycosylation step of PG biosynthesis. ^{15}N-CPMAS spectra of VRE grown in vancomycin concentrations of 0, 5, 10, and 20 μg/mL are results of 74092, 80000, 70512, and 80000 accumulated scans, respectively. The magic angle spinning was at 5000 Hz. All measurements were carried out at ambient room temperature.

supplemented with alaphosphin (5 μg/mL), to prevent racemic scrambling of L-[1-^{13}C]Ala to D-[1-^{13}C]Ala, and provided with natural abundance D-Ala (0.1 g/L) to prevent inhibition of *E. faecalis* growth by alaphosphin.[107] Vancomycin was added during growth at OD_{600nm} 0.3, and the culture harvested for analysis approximately one hour following addition of vancomycin at OD_{660nm} 0.4. Exogenous L-[ε-^{15}N]Lys provided in ESM was readily taken up by *E. faecalis* and found incorporated into PG without scrambling. The L-[ε-^{15}N]Lys incorporation efficiency into PG determined by mass spectrometry was 90%. In ^{15}N-CPMAS echo spectra (Fig. 3.1c), L-[ε-^{15}N]Lys incorporation to Park's nucleotide as a lysyl-amine was observed at 10 ppm, and incorporation to PG-repeat units in the cell wall as a lysyl-amide was at 95 ppm.[107] The ^{15}N-natural abundance contribution to lysyl-amide and amine intensities are minor.[49] Since the ^{15}N lysyl-amide peak is unique to crosslinked PG, its intensity is directly proportional to the total number of PG-repeat units found in the cell wall.

^{15}N-CPMAS echo spectrum of VRE treated with vancomycin (10 μg/mL) showed near doubling of the lysyl-amine peak intensity at 10 ppm from accumulation of Park's nucleotide (Fig. 3.1c). The amount of Park's nucleotide was estimated by back-extrapolating lysyl-amide and amine peak integrals to zero-contact time in order to account for differences in relaxation in rotating frame and cross-polarization transfer rates.[107-108] The extrapolated lysyl-amine to lysyl-amide peak integral ratio for VRE grown in absence of vancomycin was 3.2 to 1.0, and for VRE grown in presence of vancomycin (10 μg/mL) it was 4.8 to 1.0. Thus the relative amount of Park's nucleotide accumulation in the cytoplasm of VRE following induction of vancomycin resistance is 1.6 (4.8 - 3.2) times the total number of PG-repeat units in the cell wall of VRE. The

degree of Park's nucleotide accumulation in VRE is comparable to those observed for vancomycin-susceptible *Staphylococcus aureus* when treated with vancomycin[49] or oritavancin.[109] The buildup of Park's nucleotide in VRE is consistent with vancomycin inhibition of the transglycosylation step of PG biosynthesis.

Increased D-Lac Biosynthesis in VRE

Pyruvate metabolism in VRE was investigated by growing *E. faecalis* in ESM containing natural abundance D-glucose (10 g/L) supplemented with sodium-[2-^{13}C]pyruvate (0.1 g/L). At OD_{660nm} 0.3, the culture was divided into two aliquots of 500 mL. Vancomycin was added to final concentration of 10 μg/mL to one aliquot, and cells were grown for 1 hour and harvested. ^{13}C-CPMAS NMR was used to monitor the [2-^{13}C]pyruvate utilization for [2-^{13}C]Ala and [2-^{13}C]Lac biosynthesis in intact cells. ^{13}C-chemical shift assignments for [2-^{13}C]pyruvate (206 ppm), [2-^{13}C]Ala (55 ppm), and [2-^{13}C]Lac (72 ppm) were determined based on the [2-^{13}C]pyruvate metabolism in *Propionibacterium freudenreichii*.[110] Absence of 206-ppm peak in the ^{13}C-CPMAS spectrum (Fig. 3.2a, top) shows that [2-^{13}C]pyruvate is readily taken up and metabolized by VRE.

Multiple metabolic pathways for [2-^{13}C]pyruvate exist in VRE. In absence of vancomycin, as *E. faecalis* lack the tricarboxylic cycle,[111] [2-^{13}C]pyruvate is readily routed for the biosynthesis of L-[2-^{13}C]Ala by alanine transaminase, which in turn is converted into D-[2-^{13}C]Ala by alanine racemase. This preferential utilization of pyruvate for alanine biosynthesis was evident by large 55-ppm peak in the ^{13}C-CPMAS spectrum (Fig. 3.2a, top). Another metabolic pathway for [2-^{13}C]pyruvate is the biosynthesis of MurNAc, where [2-^{13}C]pyruvate is phosphorylated to phosphoenol-[2-^{13}C]pyruvate,

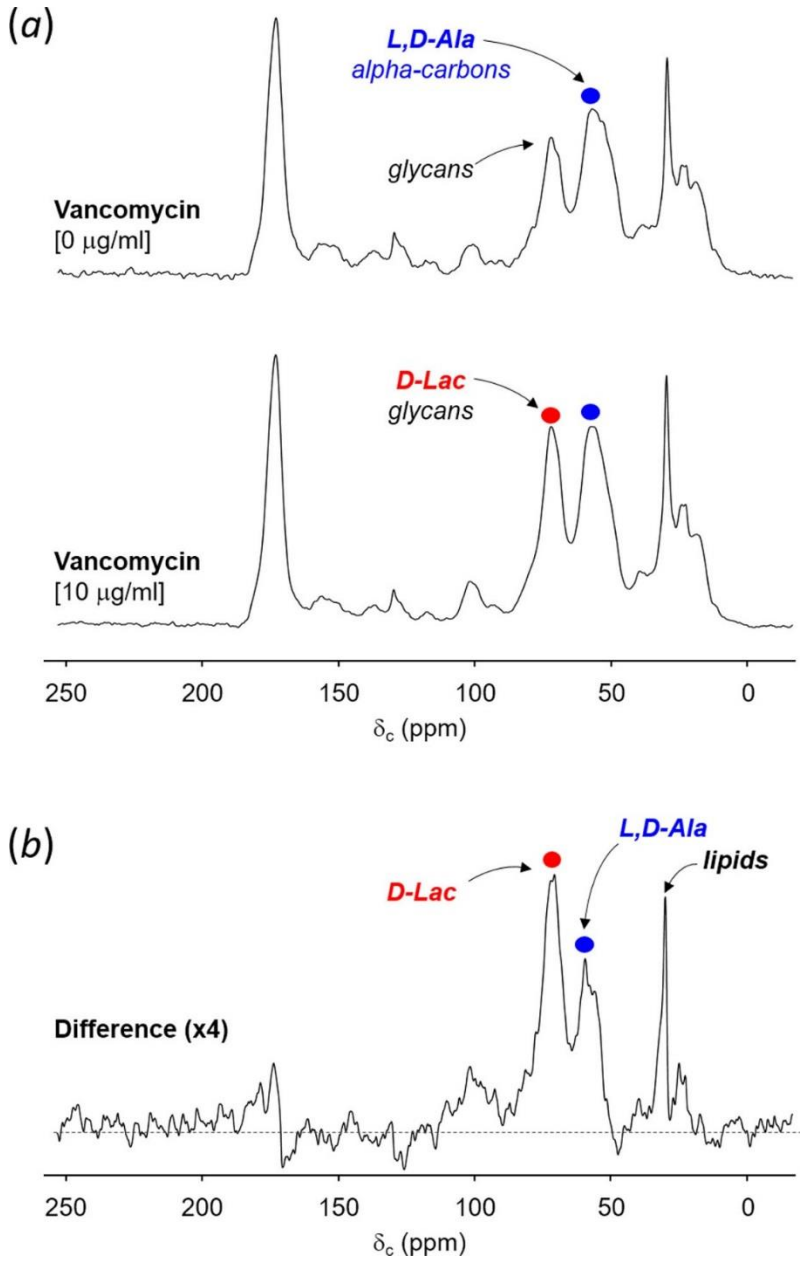

Figure 3.2: (a) ^{13}C-CPMAS spectra of whole cells of *E. faecalis* grown in ESM supplemented with sodium-[2-^{13}C]pyruvate (0.1 g/L). Vancomycin was added to final concentration of 10 μg/mL to one aliquot, and cells were grown for 1 hour and harvested. The 206-ppm peak assigned to [2-^{13}C]pyruvate is absent from the ^{13}C-CPMAS spectrum of VRE grown without vancomycin, due to [2-^{13}C]pyruvate being fully utilized for the biosynthesis of [2-^{13}C]Ala visible at 55 ppm (blue circle) and MurNAc at 72 ppm, which overlaps with the natural abundance ^{13}C from glycans in PG. ^{13}C-CPMAS spectra of VRE grown with and without vancomycin are results of 40000 and 80000 accumulated scans respectively. The magic angle spinning was at 5000 Hz. (b) The difference spectrum was obtained by subtracting ^{13}C-CPMAS spectrum of VRE grown without vancomycin from the spectrum of VRE grown with vancomycin, and it shows increased D-[2-^{13}C]Lac biosynthesis in VRE consistent with $VanH_B$ activity.

transferred to UDP-GlcNAc by MurA[112-113] as carboxyvinyl, then reduced to form UDP-MurNAc. UDP-MurNAc is the precursor for Park's nucleotide and [2-^{13}C]pyruvate is incorporated into MurNAc as lactate that appears as a 72 ppm peak in the ^{13}C-CPMAS spectrum (Fig. 3.2a, top).

Finally, lactate dehydrogenase can convert [2-^{13}C]pyruvate to L-[2-^{13}C]Lac; however, this conversion only occurs during anaerobic growth and is not observed under aerated growth conditions.[111] Therefore, the 72-ppm peak in the ^{13}C-CPMAS spectrum of VRE grown in absence of vancomycin (Fig. 3.2a, top) is from the ^{13}C-labeled lactate moiety in MurNAc and contribution from ^{13}C-natural abundance. The source of ^{13}C-natural abundance is D-glucose (10 g/L) found in ESM, which is one hundred times the amount of ^{13}C-labeled Na-[2-^{13}C]pyruvate (0.1 g/L).

^{13}C-CPMAS spectrum of VRE treated with vancomycin is shown in Fig. 3.2a (bottom). The increase in 72-ppm peak intensity correlates with the induction of *vanH$_B$* in VRE, which is a dehydrogenase that converts [2-^{13}C]pyruvate to D-[2-^{13}C]Lac. Metabolic changes associated with pyruvate utilization in VRE following induction of vancomycin resistance are clearly visible in the difference spectrum (Fig. 3.2b). The difference spectrum was obtained by subtracting the ^{13}C-CPMAS spectrum of VRE grown without vancomycin (Fig. 3.2a, top) from the spectrum of VRE grown with vancomycin (Fig. 3.2a, bottom). The spectral subtraction removes contributions from natural abundance ^{13}C and basal [2-^{13}C]pyruvate metabolism prior to the induction of vancomycin resistance. In the difference spectrum, 72-ppm intensity for D-[2-^{13}C]Lac is approximately twice that of 55 ppm assigned for D,L-[2-^{13}C]Ala. This ratio indicates that VanH$_B$ activity highly

increases during vancomycin-resistance induction, and suggests increase in the amount of depsipeptide-substituted Park's nucleotide in VRE.

PG Bridge-link Density in VRE

To determine the inhibitory effect of D-Ala-D-Lac on the attachment of PG bridge to lipid II,[104-105] the density of PG bridge-link in intact cells of VRE was measured using solid-state NMR. Figure 3.5 shows $^{13}C\{^{15}N\}$ rotational-echo double resonance (REDOR) NMR spectra at 4.8 ms dipolar evolution for whole cells of *E. faecalis* grown in ESM (Fig. 3.3a, left) and with vancomycin added to 10 μg/mL concentration (Fig. 3.3a, right). ESM contained isotope labels L-[1-^{13}C]Ala and L-[ε-^{15}N]Lys, and was supplemented with alaphosphin (5 μg/mL) and D-Ala (0.1 g/L). Growth in isotopically enriched ESM pair labeled ^{13}C-^{15}N of PG bridge-links (Fig. 3.3a, inset) in the cell wall of VRE. Full-echo (S_0) spectra are shown at the bottom, and difference (ΔS) spectra are at the top. S_0 spectra are normalized to the intensity of alanyl-carbonyl carbon from L-[1-^{13}C]Ala at 174 ppm. Overlaid and enlarged S_0 spectra centered at 174 ppm (Fig. 3.3b) show change in the lineshape for VRE grown in presence of vancomycin with the appearance of a 177-ppm shoulder. The shoulder is due to increased contribution from the alanyl-carboxyl carbon as result of $VanX_B$ (D,D-dipeptidase) and $VanY_B$ (D,D-carboxypeptidase) activities.

In $^{13}C\{^{15}N\}$ REDOR ΔS spectra at 4.8 ms dipolar evolution (Fig. 3.3a), only ^{13}Cs from L-[1-^{13}C]Ala-L-[1-^{13}C]Ala bridge dipolar coupled to the ε-^{15}N sidechain in L-[ε-^{15}N]Lys within 4 Å are detected. Figure 3.5c shows $^{13}C\{^{15}N\}$REDOR dephasing of 174 ppm plotted as a function of dipolar evolution time for VRE grown in absence (solid circle) and presence of vancomycin (open circle). Observed dephasings fit to a calculated REDOR dephasing curve for two distances of 1.3 and 3.3 Å (black solid line), but not to

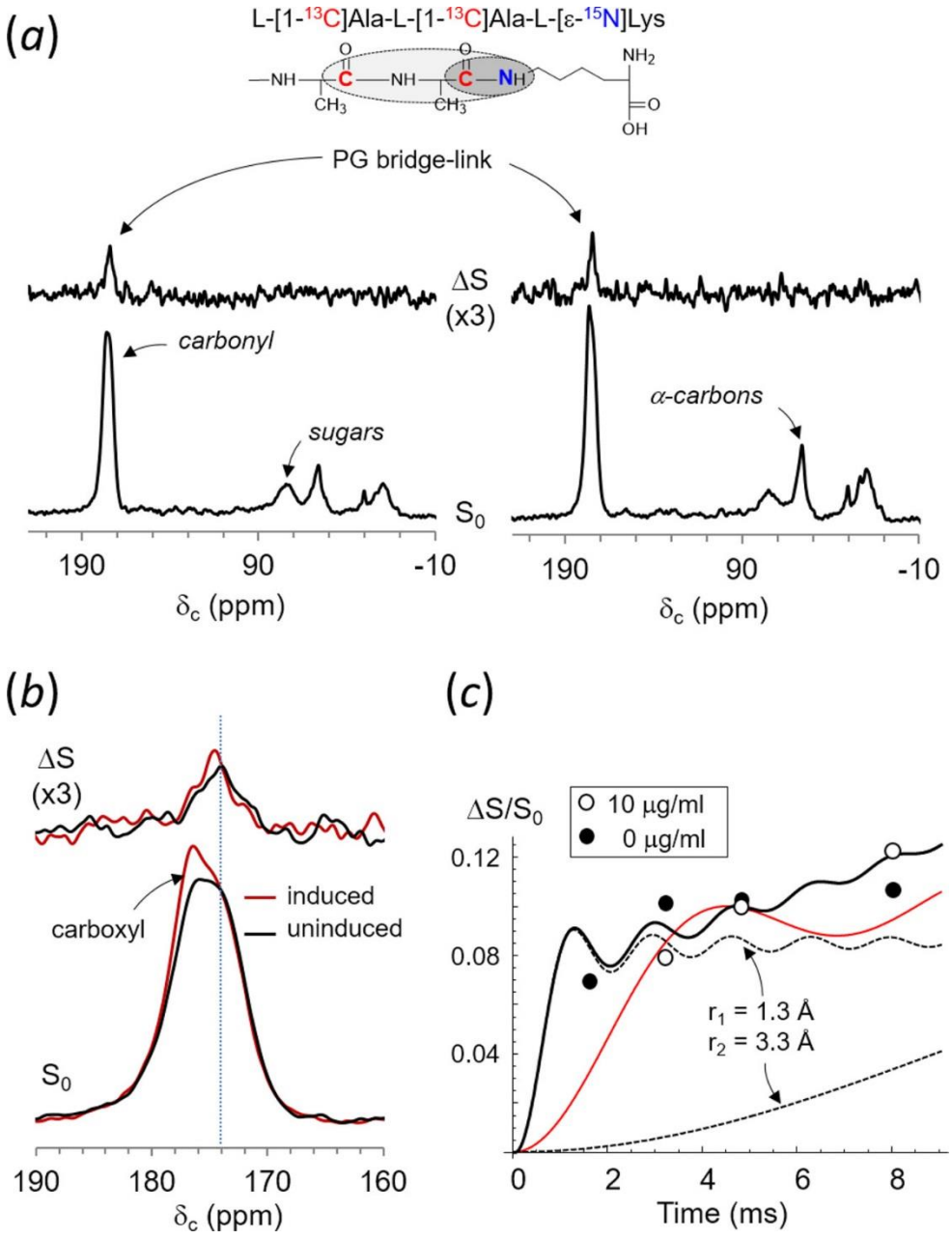

Figure 3.3: (a) $^{13}C\{^{15}N\}$REDOR of whole cells of *E. faecalis* labeled with L-[1-^{13}C]Ala and L-[ε-^{15}N]Lys at 4.8 ms dipolar evolution grown in absence (left) and presence of vancomycin at 10 μg/mL (right). $^{13}C\{^{15}N\}$REDOR spectra of VRE grown in vancomycin concentrations of 0 and 20 μg/mL are results of 75248 and 320000 accumulated scans respectively. The magic angle spinning was at 5000 Hz. (b) Enlarged overlaid S_0 and ΔS spectra centered at 174 ppm for VRE grown with vancomycin (red), and without (black). ΔS 174-ppm peak intensity, which was directly proportional to the bridge-link density, was independent of induction of vancomycin resistance in VRE. (c) $^{13}C\{^{15}N\}$REDOR dephasings ($\Delta S/S_0$) of alanyl-carboxyl carbon at 174 ppm. Solid line is the calculated REDOR dephasing curve for two ^{13}Cs in L-[1-^{13}C]Ala-L-[1-^{13}C]Ala bridge that are dephased by the ^{15}N of L-[ε-^{15}N]Lys with ^{13}C-^{15}N distances of 1.3 and 3.3 Å (dotted lines). $^{13}C\{^{15}N\}$REDOR dephasing is highly selective for the PG-bridge structure, as demonstrated by the calculated dephasing curve for ^{13}C-^{15}N distances corresponding to 2.0 and 4.0 Å (red curve), which does not fit observed dephasings.

a single ^{13}C-^{15}N distance (not shown). Calculated dephasing curves for ^{13}C-^{15}N distances of 1.3 and 3.3 Å are shown as dotted black lines. These measured distances correspond to intra-molecular distances between ^{13}Cs in (L-[1-^{13}C]Ala)$_2$-bridge structure to ^{15}N of L-[ε-^{15}N]Lys on the same PG-repeat unit. As inter-molecular ^{13}C-^{15}N couplings that exceed 4 Å distance do not contribute to the observed dephasing, $^{13}C\{^{15}N\}$ REDOR dephasings are highly specific for the PG bridge-link. A calculated REDOR dephasing curve for ^{13}C-^{15}N distances of 2.0 and 4.0 Å, shown as a red solid line, does not fit observed dephasings. Thus, the *ΔS* 174-ppm intensity at 4.8 ms is directly proportional to the total number of PG bridge-links in intact whole cells of VRE. Since the *ΔS* 174-ppm intensity does not change with the addition of vancomycin to VRE, induction of vancomycin resistance does not affect the PG bridge-link density. Therefore, the D-Ala-D-Lac substituted PG stem in lipid II did not inhibit sequential additions of L-Ala-L-Ala bridge structure by peptidyl transferases BppA1 and BppA2 in vancomycin-resistant *E. faecalis*.

Quantification of D-Ala-D-Lac Terminated Muropeptides in VRE Cell Walls by LC-MS

Although D-Ala-D-Lac terminated PG precursors have been routinely observed in the cytoplasm fraction of VRE grown in presence of vancomycin, depsipeptide terminated PG-stem structures have never been observed from isolated cell walls of vancomycin-resistant *E. faecalis*[102] and *E. faecium.*[103] This absence has led to suggestions that lipid II with a D-Ala-D-Lac stem is not readily incorporated into the cell wall or that D-Lac is cleaved from lipid II during PG biosynthesis.[103] To determine incorporation of D-Ala-D-Lac terminated PG-stem structures into VRE's cell wall, LC-MS analysis was performed on mutanolysin-digested cell walls of vancomycin-resistant *E. faecalis* (ATCC 51299). Figure 3.4 shows mass spectra for doubly-charged PG dimer from VRE at

stationary growth phase (a) and with vancomycin added (b). The m/z of 1066.0632 in Fig. 3.4a corresponds to the chemical formula $C_{87}H_{153}N_{21}O_{40}^{2+}$, which is a PG dimer with pentapeptide stem terminating in D-Ala-D-Ala, while the m/z of 1066.5479 in Fig. 3.4b corresponds to the chemical formula $C_{87}H_{152}N_{20}O_{41}^{2+}$ for a PG dimer with pentapeptide stem terminating in D-Ala-D-Lac. The difference in mass for a PG dimer with the depsipeptide substitution is an increase of 1 Da, which shifts the m/z by 0.50 (Fig. 3.4b). The D-Ala-D-Lac modified PG dimer is chromatographically well resolved from its unmodified counterpart, as shown in the select ion chromatogram (Fig. 3.4b insets) by retention time increase of 2 minutes. In general, all D-Ala-D-Lac substituted muropeptide species were clearly resolved by the increase in retention time from unmodified muropeptides through chromatographic separation. Co-elution of mixed muropeptide species was not observed, and the deconvolution of mixed isotopic distributions for analysis was not needed as the observed distributions indicated presence of only a single muropeptide ion. Chemical structures and calculated exact masses for these PG dimers are provided in Supplementary Fig. 3.S1.

LC-MS provided direct evidence for the incorporation of D-Ala-D-Lac substituted PG-stem structures into cell walls of VRE. The incorporation efficiency of D-Ala-D-Lac terminated PG stem was determined by a quantitative PG compositional analysis on 88 of most abundant muropeptide-derived ions selected from 270 total ions identified through LC-MS. Each muropeptide species was quantified by integrating the ion-current chromatogram of selected ion. While this method of determining the abundance is an approximation due to possible differences in the ionization efficiency between muropeptides species, it nevertheless is a good approximation as such PG composition

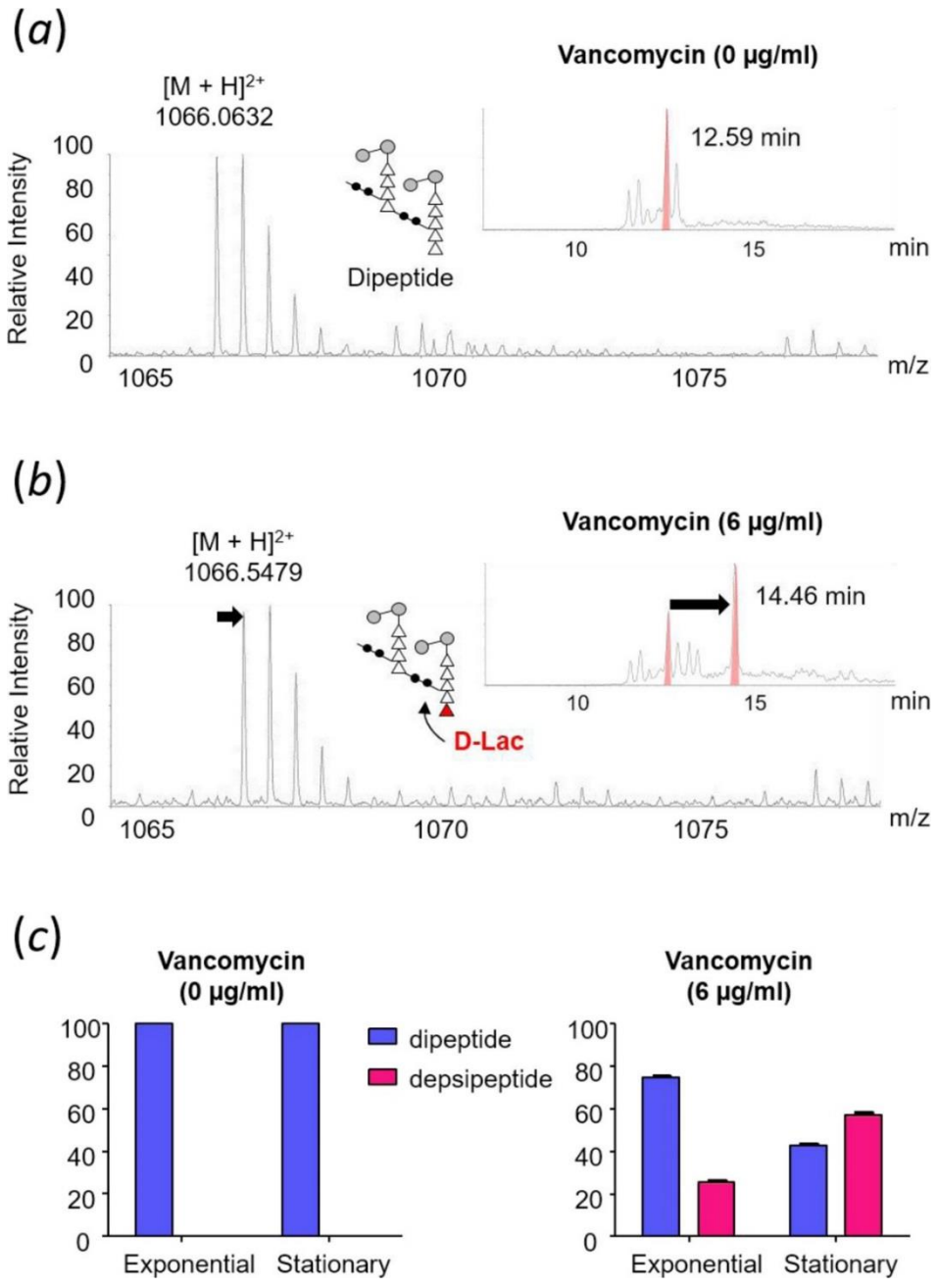

Figure 3.4: Mass spectra of doubly-charged PG dimers identified from mutanolysin-digested isolated cell wall of vancomycin-resistant *E. faecalis* grown in absence (a) and presence of vancomycin (b) at stationary growth phase. The chemical structure, formula, and exact mass for PG dimers are provided in Supplementary Table. 3.S1-S4. Select ion chromatograms (inset) show that D-Ala-D-Lac substituted PG dimer has a longer retention time that resolves it from the unmodified dimer. (c) Changes in the PG composition of dipeptide and depsipeptide terminated PG stems in the cell wall of *E. faecalis* grown in absence (left) and presence of vancomycin (right) during exponential and stationary growth phases. Muropeptides with PG stems terminating in D-Ala-D-Lac are only found in the cell wall of VRE grown in presence of vancomycin. Error bars represent 95% confidence interval.

analysis on *E. faecium* by LC-MS using integration of ion current has yielded results that are in good agreement with solid-state NMR measurements.[26] Chemical structure, calculated m/z, observed m/z, and the scaled integral for all identified muropeptide species are provided in Supplementary Table 3.S1-S4.

Bar graphs shown in Figure 3.4c represent total sum normalized integrals of ion chromatograms from muropeptide species that have a pentapeptide stem structure. Integrals for muropeptide species with a PG-stem structure terminating in D-Ala-D-Ala are shown in blue and D-Ala-D-Lac in red. Muropeptides with D-Ala-D-Lac terminated PG-stem structures are found only from cell walls of VRE grown in presence of vancomycin. Percentages of pentapeptide fragments with a D-Ala-D-Lac terminated PG-stem structure to all pentapeptide fragments at exponential growth phase and stationary growth phase are 25.37 ± 1.94% and 57.33 ± 1.84 % respectively, while percentages of muropeptides with a PG stem terminating in D-Ala-D-Ala at exponential and stationary are 73.63% and 42.67%. Relatively high abundances of depsipeptide-terminated muropeptides confirmed that the depsipeptide-terminated lipid II is efficiently incorporated into the cell wall in VRE.

Conclusion

Addition of vancomycin to vancomycin resistant *E. faecalis* (ATCC 51299) during mid-exponential growth resulted in concentration-dependent perturbed growth (Fig. 3.1a). Large Park's nucleotide accumulation in vancomycin-treated VRE (Fig. 3.1c) indicated that vancomycin inhibited the transglycosylation step of PG biosynthesis by targeting lipid II, suggesting that VRE grown with vancomycin continued to biosynthesize lipid II with a PG stem terminating in D-Ala-D-Ala. The amount of

unutilized Park's nucleotide in the cytoplasm was commensurate with the concentration of vancomycin present in the media for culturing VRE. The estimated amount of accumulated Park's nucleotide for VRE grown with vancomycin (10 μg/mL) was approximately 1.6 times the total number of PG-repeat units found in the cell wall (Fig. 3.1c).

VRE grown in presence of vancomycin showed increased $VanH_B$ activity, as confirmed by the increased metabolic conversion of [2-^{13}C]pyruvate to D-[2-^{13}C]Lac (Fig. 3.2b), and $VanX_B$ and $VanY_B$ activities (Fig 3.4b) for the biosynthesis of D-Ala-D-Lac substituted lipid II. D-Ala-D-Lac substituted PG stem structure has been thought to interfere with the attachment of L-Ala-L-Ala bridge to lipid II that may result in reduced incorporation of lipid II with D-Ala-D-Lac substituted PG stem into the cell wall, but ^{13}C{^{15}N}REDOR NMR (Fig. 3.1) demonstrated that the bridge-link density in VRE was not affected by induction of vancomycin resistance. Thus, L-Ala-L-Ala bridge attachment to lipid II was not inhibited by the D-Ala-D-Lac substituted PG stem structure in VRE. LC-MS directly confirmed the presence of D-Ala-D-Lac terminated PG-stems in the cell wall of VRE (Fig. 3.4). Quantitative PG composition analysis determined that muropeptides with a D-Ala-D-Lac terminated PG stem constituted approximately 26% of all muropeptides with a pentapeptide stem at exponential and 57% at stationary growth phase. Thus, VRE continue to biosynthesize two variants of lipid II even after the induction of vancomycin resistance: one with a PG stem that terminates in D-Ala-D-Ala and the other in D-Ala-D-Lac. Both types of lipid II are efficiently utilized for incorporation into the cell wall of vancomycin resistant *E. faecalis* following the induction of vancomycin resistance.

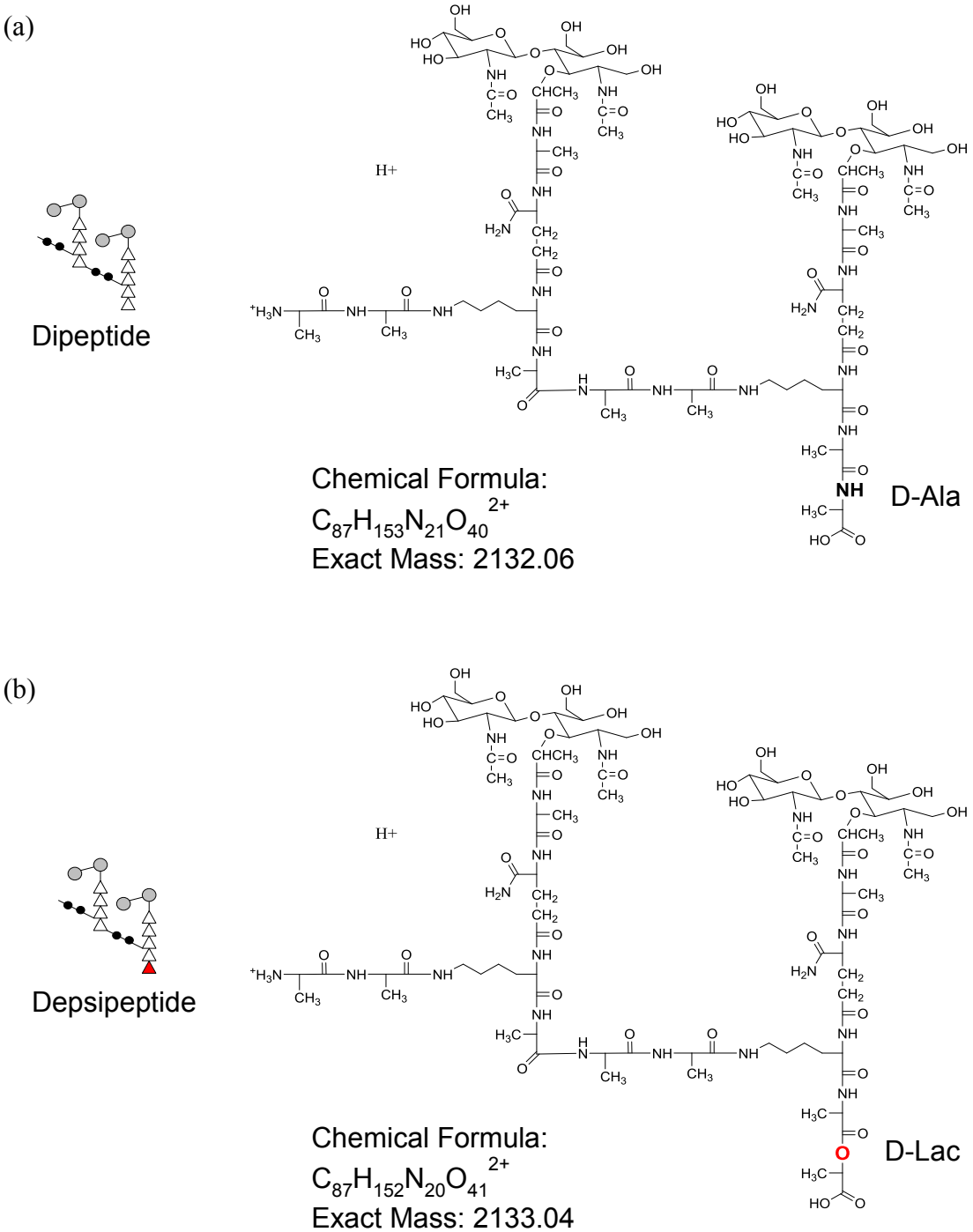

Supplementary Figure 3.S1: (a) Chemical structure of a PG dimer with a pentapeptide stem terminating in D-Ala-D-Ala from vancomycin-resistant E. faecalis (ATCC 51299) grown in absence of vancomycin. (b) Chemical structure of a PG dimer with a pentapeptide stem terminating in D-Ala-D-Lac from vancomycin-resistant *E. faecalis* grown in presence of vancomycin (6 µg/mL).

Supplementary Table 3.S1: List of peptidoglycan fragments observed by LC-MS for vancomycin-resistant *E. faecalis* (ATCC 51299) grown in absence of vancomycin during the exponential growth phase (OD_{600} 0.6). Chemical formula shown are for non-ionized peptidoglycan fragments.

Chemical Formula	Charge Obs.	Calculated (m/z)	Observed[1] (m/z)	Scaled integral[1]	Observed[2] m/z	Scaled integral[2]	Observed[3] m/z	Scaled integral[3]
C41H71N9O20	2	463.7375	463.7178	447	463.7178	676	463.7178	579
C39H70N9O19	2	484.7428	484.7287	6634	484.7287	5819	484.7287	5241
C42H75N10O20	2	520.2613	520.2299	9960	520.2200	9268	520.2200	10324
C47H81N11O22	2	534.7746	534.7697	21398	534.7697	19110	534.7697	18118
C44H77N10O21	2	541.2666	541.2915	39512	541.2915	46283	541.2915	38861
C45H80N11O21	2	555.7799	555.7808	6400	555.7705	6553	555.7705	6319
C47H82N11O22	2	576.7852	576.8089	30515	576.7984	27483	576.7984	24854
C83H143N19O39	3	649.6599	649.6593	241794	649.6593	288311	649.6593	264532
C83H143N19O39	2	973.9862	973.9894	136465	973.9894	147705	973.9894	110714
C81H142N19O38	3	663.6634	663.6667	2873710	663.6667	3271206	663.6667	2885170
C81H142N19O38	2	994.9915	995.0037	3517480	995.0037	3589885	995.0037	3321445
C81H142N19O38	1	1988.9758	1988.9984	11906	1988.9984	14281	1988.9984	12878
C86H148N20O40	3	673.3390	673.3409	63263	673.3409	59571	673.3409	77303
C86H148N20O40	2	1009.5048	1009.5031	28309	1009.5031	39483	1009.5031	32686
C83H144N19O39	3	677.6670	677.6758	362929	677.6758	389742	677.6758	365868
C83H144N19O39	2	1015.9968	1016.0197	446557	1016.0197	494266	1016.0197	404279
C84H147N20O39	3	687.3425	687.3481	806433	687.3481	892086	687.3481	731617
C84H147N20O39	2	1030.5101	1030.5168	607893	1030.5168	615535	1030.5168	528643
C89H153N21O41	3	697.0180	697.0199	533224	697.0199	593223	697.0199	564200
C89H153N21O41	2	1045.0234	1045.0317	137847	1045.0317	146790	1045.0175	134022
C86H149N20O40	3	701.3460	701.3607	180926	701.3607	162305	701.3607	222672
C87H152N21O40	3	711.0215	711.0255	6588213	711.0255	6844143	711.0255	6299936
C87H152N21O40	2	1066.0286	1066.0393	4289477	1066.0393	4568330	1066.0393	3540535
C89H154N21O41	3	725.0250	725.0293	193347	725.0293	231622	725.0293	184973
C89H154N21O41	2	1087.0339	1087.0400	91320	1087.0400	90624	1087.0400	80893
C125H215N29O58	4	742.6211	742.6517	140831	742.6279	144291	742.6279	140831

C125H215N29O58	3	989.8258	989.8596	336790	989.8322	491136	989.8184	295785
C123H214N29O57	4	753.1238	753.1351	905646	753.1231	930088	753.1231	859448
C123H214N29O57	3	1003.8293	1003.8375	3393731	1003.8375	3701847	1003.8375	3393823
C123H214N29O57	2	1505.2403	1505.2425	204061	1505.2425	210740	1505.2425	197147
C128H220N30O59	4	760.3804	760.4135	83700	760.3895	76629	760.3775	76359
C128H220N30O59	3	1013.5048	1013.5441	81477	1013.5024	59489	1013.5024	81261
C125H216N29O58	4	763.6264	763.6437	222873	763.6437	272307	763.6316	285042
C125H216N29O58	3	1017.8328	1017.8436	456649	1017.8436	459953	1017.8436	425309
C125H216N29O58	2	1526.2456	1526.2691	45150	1526.2691	35775	1526.2691	48069
C126H219N30O58	4	770.8831	770.8877	244108	770.8877	244158	770.8877	201911
C126H219N30O58	3	1027.5083	1027.5055	805735	1027.5055	692226	1027.5055	1122453
C126H219N30O58	2	1540.7588	1540.7507	41517	1540.7507	51975	1540.7507	63011
C131H225N31O60	4	778.1397	778.1418	327079	778.1539	283500	778.1418	272770
C131H225N31O60	3	1037.1838	1037.2271	421811	1037.1989	398875	1037.1848	407398
C129H224N31O59	4	788.6423	788.6511	1157533	788.6511	1247761	788.6388	1120764
C129H224N31O59	3	1051.1874	1051.1945	4701929	1051.1945	4843200	1051.1945	5171673
C129H224N31O59	2	1576.2774	1576.2742	289585	1576.2742	305282	1576.2742	289260
C131H226N31O60	3	1065.1909	1065.2269	76806	1065.2126	79128	1065.2269	59425
C167H287N39O77	4	997.7455	997.7877	74974	997.7601	75153	997.7463	68375
C167H287N39O77	3	1329.9916	1330.0541	68177	1329.9904	57197	1329.9904	70747
C165H286N39O76	4	1008.2482	1008.2550	1330279	1008.2550	1239789	1008.2550	1249994
C165H286N39O76	3	1343.9951	1343.9912	582757	1343.9912	648261	1343.9912	640974
C170H292N40O78	4	1015.5048	1015.5466	156051	1015.5048	82037	1015.5048	98394
C170H292N40O78	3	1353.6706	1353.7245	32922	1353.6602	26541	1353.6602	28884
C167H288N39O77	4	1018.7508	1018.7492	193790	1018.7632	234437	1018.7632	220166
C167H288N39O77	3	1357.9986	1358.0170	160069	1358.0170	131095	1358.0170	123630
C168H291N40O77	4	1026.0074	1026.0085	418962	1026.0085	391427	1026.0085	368087
C168H291N40O77	3	1367.6742	1367.6717	145388	1367.6556	163152	1367.6717	131164
C173H297N41O79	4	1033.2641	1033.3077	330082	1033.2796	305294	1033.2656	344194
C173H297N41O79	3	1377.3497	1377.4092	66677	1377.3606	63408	1377.3444	46727
C171H296N41O78	4	1043.7667	1043.7619	1447687	1043.7619	1929308	1043.7619	1412777
C171H296N41O78	3	1391.3532	1391.3635	516607	1391.3473	548238	1391.3473	511333

C173H298N41O79	4	1054.2694	1054.2686	143438	1054.2686	110148	1054.2686	91491

[1,2,3] Observed peaks (m/z) and their corresponding integrals in three independent measurements.

Supplementary Table 3.S2: List of peptidoglycan fragments observed by LC-MS for vancomycin-resistant *E. faecalis* (ATCC 51299) grown in absence of vancomycin during the stationary growth phase (OD_{600} > 1.0). Chemical formula shown are for non-ionized peptidoglycan fragments.

Chemical Formula	Charge Obs.	Calculated (m/z)	Observed[1] (m/z)	Scaled integral[1]	Observed[2] m/z	Scaled integral[2]	Observed[3] m/z	Scaled integral[3]
C39H70N9O19	2	484.7428	484.7328	3825	484.7136	3794	484.7136	3261
C44H76N10O21	2	499.2560	499.2390	12526	499.2195	11112	499.2195	12123
C41H72N9O20	2	505.7480	505.7472	17777	505.7374	15951	505.7276	15962
C42H75N10O20	2	520.2613	520.2137	6147	520.2038	8567	520.2038	5948
C47H81N11O22	2	534.7746	534.7630	6628	534.7530	7054	534.7428	6949
C44H77N10O21	2	541.2666	541.2645	4407	541.2543	4400	541.2441	5516
C45H80N11O21	2	555.7799	555.7738	5033	555.7635	5041	555.7532	4157
C47H82N11O22	2	576.7852	576.7490	18718	576.7385	34097	576.7280	27531
C83H143N19O39	3	649.6599	649.6613	69068	649.6502	83796	649.6390	78303
C83H143N19O39	2	973.9862	973.9999	52259	973.9726	49851	973.9590	56795
C81H142N19O38	3	663.6634	663.6685	905565	663.6685	954386	663.6685	898929
C81H142N19O38	2	994.9915	995.0002	1618058	995.0002	1631511	995.0002	1676440
C81H142N19O38	1	1988.9758	1988.9947	3187	1988.9947	3704	1988.9947	4495
C86H148N20O40	3	673.3390	673.3425	33084	673.3312	33055	673.3199	30331
C86H148N20O40	2	1009.5048	1009.5133	35230	1009.4855	32814	1009.4716	39402
C83H144N19O39	3	677.6670	677.6773	204501	677.6773	286480	677.6773	218086
C83H144N19O39	2	1015.9968	1016.0019	420071	1016.0019	346105	1016.0019	386513
C84H147N20O39	3	687.3425	687.3496	512511	687.3496	526170	687.3496	541000
C84H147N20O39	2	1030.5101	1030.5266	578959	1030.5266	607029	1030.5266	592330
C89H153N21O41	3	697.0180	697.0212	212483	697.0096	210566	696.9981	210171
C89H153N21O41	2	1045.0234	1044.9850	72461	1044.9992	71087	1044.9850	72461
C86H149N20O40	3	701.3460	701.3504	107657	701.3504	111273	701.3504	99164
C87H152N21O40	3	711.0215	711.0266	3072508	711.0266	3083289	711.0266	2826401
C87H152N21O40	2	1066.0286	1066.0346	2552988	1066.0346	2576393	1066.0346	2609712
C89H154N21O41	3	725.0250	725.0302	187538	725.0302	211078	725.0302	253437
C89H154N21O41	2	1087.0339	1087.0493	149278	1087.0493	149192	1087.0493	151790

C125H215N29O58	4	742.6211	742.6286	26214	742.6048	33292	742.6048	25983
C125H215N29O58	3	989.8258	989.8287	171323	989.8013	170646	989.7875	160370
C123H214N29O57	4	753.1238	753.1356	196401	753.1116	197456	753.0996	207928
C123H214N29O57	3	1003.8293	1003.8338	2155397	1003.8062	2279513	1003.7923	2197304
C123H214N29O57	2	1505.2403	1505.2462	102483	1505.2124	121434	1505.1956	121968
C128H220N30O59	4	760.3804	760.3898	20902	760.3658	20523	760.3538	17784
C128H220N30O59	3	1013.5048	1013.5125	43648	1013.4708	43081	1013.4708	39139
C125H216N29O58	3	1017.8328	1017.8397	690630	1017.8119	722741	1017.8180	695179
C125H216N29O58	2	1526.2456	1526.2557	36666	1526.2044	28262	1526.2044	51941
C126H219N30O58	4	770.8831	770.8880	85893	770.8758	100360	770.8637	86822
C126H219N30O58	3	1027.5083	1027.5154	965190	1027.4874	928349	1027.4734	1005702
C126H219N30O58	2	1540.7588	1540.7713	47666	1540.7199	50000	1540.7027	55500
C127H218N29O59	3	1031.8363	1031.8445	140192	1031.8164	139087	1031.8024	72684
C131H225N31O60	4	778.1397	778.1175	73898	778.1296	87003	778.1175	80707
C131H225N31O60	3	1037.1838	1037.1948	293623	1037.1666	304181	1037.1525	316007
C128H221N30O59	3	1041.5118	1041.4736	142918	1041.4878	134224	1041.4736	149221
C128H221N30O59	2	1561.7641	1561.7847	3009	1561.7157	6392	1561.7157	8073
C129H224N31O59	4	788.6423	788.6510	500224	788.6265	469973	788.6142	489812
C129H224N31O59	3	1051.1874	1051.2041	4660766	1051.1617	4834726	1051.1475	5016835
C129H224N31O59	2	1576.2774	1576.2944	209182	1576.2442	233681	1576.2251	248433
C131H226N31O60	3	1065.1909	1065.1937	434055	1065.1652	442245	1065.1509	451662
C131H226N31O60	2	1597.2827	1597.3036	17345	1597.2513	27976	1597.2338	18210
C133H228N31O61	3	1079.1944	1079.2039	67928	1079.1752	91979	1079.1608	39435
C167H287N39O77	4	997.7455	997.7566	64081	997.7290	59870	997.7152	58818
C167H287N39O77	3	1329.9916	1330.0127	29667	1329.9490	39006	1329.9490	23406
C165H286N39O76	4	1008.2482	1008.2513	793986	1008.2236	804403	1008.2097	635153
C165H286N39O76	3	1343.9951	1344.0133	410496	1343.9653	586172	1343.9493	403651
C170H292N40O78	4	1015.5048	1015.5149	38079	1015.4731	30502	1015.4731	50379
C170H292N40O78	3	1353.6706	1353.6823	16174	1353.6180	26154	1353.6180	21961
C167H288N39O77	4	1018.7508	1018.7592	161973	1018.7174	174808	1018.7174	142061
C167H288N39O77	3	1357.9986	1358.0230	114344	1357.9585	104432	1357.9425	96472
C168H291N40O77	4	1026.0074	1026.0185	333957	1025.9765	371712	1025.9765	509946

C168H291N40O77	3	1367.6742	1367.6775	163616	1367.6453	144828	1367.6291	169231
C169H290N39O78	4	1029.2534	1029.2656	43908	1029.2376	84253	1029.2236	67623
C169H290N39O78	3	1372.0022	1372.0082	47034	1371.9597	18355	1371.9597	19488
C173H297N41O79	4	1033.2641	1033.2754	210812	1033.2473	295431	1033.2333	214325
C173H297N41O79	3	1377.3497	1377.3663	53793	1377.3177	49636	1377.3015	58011
C170H293N40O78	4	1036.5101	1036.5200	31790	1036.4919	19288	1036.4637	35209
C170H293N40O78	3	1381.6777	1381.6777	0	1381.6311	21360	1381.6346	0
C171H296N41O78	4	1043.7667	1043.7715	1697590	1043.7433	1597997	1043.7293	1567770
C171H296N41O78	3	1391.3532	1391.3691	568098	1391.3202	657280	1391.3040	633849
C173H298N41O79	4	1054.2694	1054.2783	252507	1054.2498	252555	1054.2357	163122
C173H298N41O79	3	1405.3567	1405.3609	95321	1405.3117	72738	1405.2953	45125
C175H300N41O80	4	1064.7720	1064.7662	20137	1064.7519	35368	1064.7378	28409

[1,2,3] Observed peaks (m/z) and their corresponding integrals in three independent measurements.

Supplementary Table 3.S3: List of peptidoglycan fragments observed by LC-MS for vancomycin-resistant *E. faecalis* (ATCC 51299) grown in presence of vancomycin (6 μg/mL) during the exponential growth phase (OD_{600} 0.6). Chemical formula shown are for non-ionized peptidoglycan fragments.

Chemical Formula	Charge Obs.	Calculated (m/z)	Observed[1] (m/z)	Scaled integral[1]	Observed[2] m/z	Scaled integral[2]	Observed[3] m/z	Scaled integral[3]
C41H71N9O20	2	463.7375	463.7106	671	463.7012	1081	463.7012	747
C39H70N9O19	2	484.7428	484.7211	27966	484.7307	28976	484.7307	14348
C44H76N10O21	2	499.2560	499.2175	3438	499.2175	3084	499.2175	1943
C42H75N10O20	2	520.2613	520.2617	55362	520.2617	50957	520.2716	43916
C47H81N11O22	2	534.7746	534.8016	3560	534.8016	8151	534.8016	7501
C47H80N10O23	2	535.2666	535.2561	2013	535.2359	3602	535.2359	3145
C44H77N10O21	2	541.2666	541.2831	18540	541.2831	18057	541.2932	17237
C45H80N11O21	2	555.7799	555.7516	1692	555.7516	1448	555.7516	1395
C45H79N10O22	2	556.2719	556.2559	4254	556.2559	4914	556.2559	4884
C47H82N11O22	2	576.7852	576.7579	1631	576.7579	1771	576.7579	1833
C47H81N10O23	2	577.2772	577.2613	3093	577.2718	4264	577.2718	2688
C83H143N19O39	3	649.6599	649.6603	171032	649.6603	164780	694.6580	137087
C83H143N19O39	2	973.9862	973.9877	97972	973.9877	91597	973.9877	82206
C81H142N19O38	3	663.6634	663.6676	1477601	663.6676	1501173	663.6676	1301409
C81H142N19O38	2	994.9915	994.9881	1735321	994.9881	1814267	994.9881	1955810
C86H148N20O40	3	673.3390	673.3417	201959	673.3417	163178	673.3417	176763
C86H148N20O40	2	1009.5048	1009.5012	66646	1009.5151	64195	1009.5151	49003
C83H144N19O39	3	677.6670	677.6652	117166	677.6652	169580	677.6652	144424
C83H144N19O39	2	1015.9968	1016.0038	317272	1016.0038	266705	1016.0038	220349
C84H147N20O39	3	687.3425	687.3488	2375431	687.3488	2245791	687.3488	2088858
C84H147N20O39	2	1030.5101	1030.5145	2463621	1030.5145	2492171	1030.5145	1801819
C89H153N21O41	3	697.0180	697.0205	26910	697.0205	27493	697.0205	30761
C89H153N21O41	2	1045.0234	1045.0296	13922	1045.0296	17671	1045.0296	9403
C89H152N20O42	3	697.3460	697.3433	39355	697.3548	27778	697.3548	34868
C89H152N20O42	2	1045.5154	1045.5094	3514	1045.5094	2705	1045.5375	0
C86H149N20O40	2	1051.5154	1051.5178	225492	1051.5178	231409	1051.5178	173406

C87H152N21O40	3	711.0215	711.0260	278888	711.0260	296145	711.0260	271687
C87H152N21O40	2	1066.0286	1066.0369	167783	1066.0369	193689	1066.0369	162886
C87H151N20O41	3	711.3495	711.3519	135823	711.3519	90245	711.3519	95479
C87H151N20O41	2	1066.5206	1066.5216	95967	1066.5216	112004	1066.5216	96908
C89H154N21O41	3	725.0250	725.0297	51550	725.0297	43064	725.0297	46018
C89H154N21O41	2	1087.0339	1087.0518	26374	1087.0518	25687	1087.0518	31277
C89H153N20O42	3	725.3530	725.3417	0	725.3417	0	725.3417	2241
C125H215N29O58	4	742.6211	742.6282	52023	742.6282	61668	742.6282	48454
C125H215N29O58	3	989.8258	989.8304	228495	989.8304	213964	989.8304	234433
C123H214N29O57	4	753.1238	753.1233	480556	753.1233	468579	753.1233	422016
C123H214N29O57	3	1003.8293	1003.8355	1885033	1003.8355	1900721	1003.8355	1626272
C123H214N29O57	2	1505.2403	1505.2358	95798	1505.2528	96309	1505.2528	56325
C128H220N30O59	4	760.3804	760.3776	117901	760.3776	99038	760.3896	89601
C128H220N30O59	3	1013.5048	1013.5003	200311	1013.5003	179509	1013.5142	170992
C125H216N29O58	4	763.6264	763.6317	68883	763.6317	43135	763.6317	59284
C125H216N29O58	3	1017.8328	1017.8277	314070	1017.8277	334968	1017.8416	281297
C125H216N29O58	2	1526.2456	1526.2452	7350	1526.2281	14579	1526.2623	4629
C126H219N30O58	4	770.8831	770.8878	459857	770.8878	419544	770.8878	456507
C126H219N30O58	3	1027.5083	1027.5174	2320544	1027.5174	2191730	1027.5174	2149093
C126H219N30O58	2	1540.7588	1540.7609	126052	1540.7609	122412	1540.7609	63599
C131H225N31O60	4	778.1397	778.1417	23061	778.1417	23845	778.1417	16441
C131H225N31O60	3	1037.1838	1037.1686	64026	1037.1827	45019	1037.1968	27496
C131H224N30O61	4	778.3857	778.3854	19159	778.3854	16414	773.3856	14987
C131H224N30O61	3	1037.5118	1037.5063	0	1037.5063	0	1037.5203	8351
C128H221N30O59	3	1041.5118	1041.5040	197187	1041.5040	292900	1041.5180	241437
C128H221N30O59	2	1561.7641	1561.7743	12159	1561.7743	11710	1561.7743	4694
C129H224N31O59	4	788.6423	788.6388	40613	788.6510	78225	788.6510	53685
C129H224N31O59	3	1051.1874	1051.1922	334431	1051.1924	290749	1051.1922	330972
C129H224N31O59	2	1576.2774	1576.2669	16428	1576.2842	13837	1576.2842	4513
C129H223N30O60	3	1051.5154	1051.5178	141179	1051.5178	152626	1051.5178	129992
C130H223N30O60	3	1055.5154	1055.5141	120888	1055.5141	163031	1055.5283	82233
C131H226N31O60	3	1065.1909	1065.1959	76806	1065.2102	79128	1065.2102	59425

C167H287N39O77	4	997.7455	997.7445	115478	997.7445	129187	997.7445	100998
C167H287N39O77	3	1329.9916	1329.9854	26171	1330.0014	25683	1330.0014	25039
C165H286N39O76	4	1008.2482	1008.2393	893695	1008.2532	892054	1008.2532	710345
C165H286N39O76	3	1343.9951	1343.9862	463306	1344.0022	294207	1344.0022	374707
C170H292N40O78	4	1015.5048	1015.5029	120491	1015.4889	98821	1015.5029	57445
C170H292N40O78	3	1353.6706	1353.6551	49279	1353.6712	34261	1353.6872	23547
C167H288N39O77	4	1018.7508	1018.4963	52623	1018.7472	44491	1018.7472	41006
C167H288N39O77	3	1357.9986	1357.9796	49390	1357.9958	43717	1357.9958	0
C168H291N40O77	4	1026.0074	1026.0065	787829	1026.0065	701257	1026.0065	931282
C168H291N40O77	3	1367.6742	1367.6665	288917	1367.6665	275457	1367.6826	239057
C173H297N41O79	4	1033.2641	1033.2915	16889	1033.2775	25552	1033.2775	25928
C173H297N41O79	3	1377.3497	1377.3229	4081	1377.3391	6742	1377.3552	8283
C173H296N40O80	4	1033.5101	1033.5021	5694	1033.5021	0	1033.5161	10936
C173H296N40O80	3	1377.6777	1377.6631	280	1377.6793	5858	1377.6793	1552
C170H293N40O78	4	1036.5101	1036.5080	137564	1036.5080	143837	1036.5080	90992
C170H293N40O78	3	1381.6777	1381.6687	17969	1381.6687	33934	1381.6687	17416
C171H296N41O78	4	1043.7667	1043.7595	114556	1043.7595	131193	1043.7595	61187
C171H296N41O78	3	1391.3532	1391.3418	15617	1391.3582	10732	1391.3582	4869
C173H298N41O79	4	1054.2694	1054.2694	0	1054.2694	0	1054.2804	4691

[1,2,3] Observed peaks (m/z) and their corresponding integrals in three independent measurements.

Supplementary Table 3.S4: List of peptidoglycan fragments observed by LC-MS for vancomycin-resistant *E. faecalis* (ATCC 51299) grown in presence of vancomycin (6 μg/mL) during the stationary growth phase (OD_{600} > 1.0). Chemical formula shown are for non-ionized peptidoglycan fragments.

Chemical Formula	Charge Obs.	Calculated (m/z)	Observed[1] (m/z)	Scaled integral[1]	Observed[2] m/z	Scaled integral[2]	Observed[3] m/z	Scaled integral[3]
C41H71N9O20	2	463.7375	463.6990	11045	463.6990	11742	463.7084	10627
C39H70N9O19	2	484.7428	484.7191	22461	484.7191	20683	484.7287	21090
C44H76N10O21	2	499.2560	499.2253	5278	499.2253	6270	499.2253	3781
C41H72N9O20	2	505.7480	505.7237	20271	505.7237	18022	505.7335	16204
C42H75N10O20	2	520.2613	520.2399	160426	520.2399	144727	520.2498	152752
C47H81N11O22	2	534.7746	534.7697	61034	534.7697	61111	534.7797	54205
C47H80N10O23	2	535.2666	535.2645	37547	535.2544	35925	535.2746	34159
C44H77N10O21	2	541.2666	541.3016	188023	541.3016	185352	541.3118	182454
C45H80N11O21	2	555.7799	555.7911	41204	555.7911	45365	555.8014	43690
C45H79N10O22	2	556.2719	556.2750	39334	556.2750	46949	556.2853	49855
C47H82N11O22	2	576.7852	576.7774	18328	576.7774	15609	576.7879	17319
C47H81N10O23	2	577.2772	577.2704	32087	577.2704	32331	577.2809	31355
C83H143N19O39	3	649.6599	649.6593	43292	649.6593	43766	649.6705	58182
C83H143N19O39	2	973.9862	973.9758	35787	973.9758	41972	974.0030	40457
C81H142N19O38	3	663.6634	663.6667	403892	663.6667	352004	663.6667	378640
C81H142N19O38	2	994.9915	994.9899	1016054	994.9899	1107781	994.9899	973420
C86H148N20O40	3	673.3390	673.3409	61976	673.3409	60310	673.3522	58463
C86H148N20O40	2	1009.5048	1009.5031	38340	1009.5031	43796	1009.5170	37385
C83H144N19O39	3	677.6670	677.6643	210227	677.6643	92763	677.6643	81013
C83H144N19O39	2	1015.9968	1015.9919	207871	1015.9919	216118	1015.9919	168872
C84H147N20O39	3	687.3425	687.3481	698214	687.3481	682818	687.3481	650380
C84H147N20O39	2	1030.5101	1030.5028	1066519	1030.5028	1279767	1030.5028	1228354
C89H153N21O41	3	697.0180	697.0199	11692	697.0199	12387	697.0314	13495
C89H153N21O41	2	1045.0234	1045.0175	4927	1045.0175	6313	1045.0459	5625
C89H152N20O42	2	1045.5154	1045.4975	560	1045.5116	299	1045.5257	399
C86H149N20O40	2	1051.5154	1051.5201	126543	1051.5201	146556	1051.5201	120885

C87H152N21O40	3	711.0215	711.0255	95613	711.0255	85890	711.0255	93832
C87H152N21O40	2	1066.0286	1066.0251	71088	1066.0251	74886	1066.0251	70315
C87H151N20O41	3	711.3495	711.3515	68886	711.3515	36393	711.3515	36860
C87H151N20O41	2	1066.5206	1066.5240	81339	1066.5240	78136	1066.5240	78263
C88H151N20O41	2	1072.5206	1072.5209	27005	1072.5209	35935	1072.5209	19899
C89H154N21O41	3	725.0250	725.0411	40551	725.0411	29508	725.0411	28167
C89H154N21O41	2	1087.0339	1087.0544	11356	1087.0544	15723	1087.0544	14658
C89H153N20O42	3	725.3530	725.3531	207738	725.3531	164034	725.3531	161808
C89H153N20O42	2	1087.5259	1087.5439	123355	1087.5439	119805	1087.5439	119086
C125H215N29O58	4	742.6211	742.6160	16529	742.6160	11110	742.6279	10036
C125H215N29O58	3	989.8258	989.8184	91157	989.8184	88515	989.8322	92124
C123H214N29O57	4	753.1238	753.1231	52641	753.1231	42036	753.1351	50084
C123H214N29O57	3	1003.8293	1003.8236	872072	1003.8236	925506	1003.8512	877802
C123H214N29O57	2	1505.2403	1505.2425	50141	1505.2425	46334	1505.2594	55901
C128H220N30O59	4	760.3804	760.3775	15215	760.3775	11226	760.3895	15508
C128H220N30O59	3	1013.5048	1013.5024	102146	1013.5024	96269	1013.5162	104676
C125H216N29O58	3	1017.8328	1017.8297	229148	1017.8297	226122	1017.8436	217742
C125H216N29O58	2	1526.2456	1526.2351	11918	1526.2351	10998	1526.2691	14235
C126H219N30O58	4	770.8831	770.8877	89550	770.8756	81161	770.8998	75994
C126H219N30O58	3	1027.5083	1027.5055	1126725	1027.5055	1097979	1027.5195	1088561
C126H219N30O58	2	1540.7588	1540.7507	65560	1540.7507	66674	1540.7850	68382
C127H218N29O59	3	1031.8363	1031.8363	0	1031.8205	24372	1031.7994	0
C131H225N31O60	4	778.1397	778.1418	8861	778.1418	7739	778.1539	8408
C131H225N31O60	3	1037.1838	1037.1708	4074	1037.1848	5818	1037.1989	11505
C128H221N30O59	3	1041.5118	1041.5061	190734	1041.5203	158653	1041.5343	174629
C128H221N30O59	2	1561.7641	1561.7644	8236	1561.7644	9656	1561.7816	11748
C129H224N31O59	4	788.6423	788.6388	7671	788.6388	3650	788.6511	3619
C129H224N31O59	3	1051.1874	1051.1803	76275	1051.1803	75975	1051.2086	65467
C129H224N31O59	2	1576.2774	1576.2568	2407	1576.2742	2864	1576.2915	2878
C129H223N30O60	3	1051.5154	1051.5060	65347	1051.5060	66485	1051.5343	69445
C130H223N30O60	3	1055.5154	1055.5165	35225	1055.5165	22391	1055.5307	22981
C131H226N31O60	3	1065.1909	1065.1841	71383	1065.1984	20873	1065.2126	49031

C131H225N30O61	3	1065.5189	1065.5261	58616	1065.5261	102532	1065.5404	81662
C131H225N30O61	2	1597.7747	1597.7722	4578	1597.7722	0	1597.8246	3804
C132H225N30O61	3	1069.5189	1069.4777	10914	1069.5205	16277	1069.5205	9091
C133H227N30O62	3	1079.5224	1079.5244	19510	1079.5244	15145	1079.5531	12821
C167H287N39O77	4	997.7455	997.7325	22421	997.7325	20347	997.7739	18087
C167H287N39O77	3	1329.9916	1329.9904	11286	1329.9585	14754	1330.0062	12486
C165H286N39O76	4	1008.2482	1008.2411	241404	1008.2411	232314	1008.2689	193818
C165H286N39O76	3	1343.9951	1343.9912	157703	1343.9912	161446	1344.0072	167857
C170H292N40O78	4	1015.5048	1015.4909	9625	1015.4909	18099	1015.5188	26947
C170H292N40O78	3	1353.6706	1353.6602	16062	1353.6442	20969	1353.6763	14540
C167H288N39O77	4	1018.7508	1018.7492	58472	1018.7492	51226	1018.7632	50899
C167H288N39O77	3	1357.9986	1358.0008	37753	1357.9848	27509	1358.0170	25174
C168H291N40O77	4	1026.0074	1026.0085	298029	1025.9946	288150	1026.0225	299408
C168H291N40O77	3	1367.6742	1367.6717	169462	1367.6717	175897	1367.6879	153137
C169H290N39O78	4	1029.2534	1029.2416	12398	1029.2557	12334	1029.2557	10801
C169H290N39O78	3	1372.0022	1372.0024	7810	1371.9862	11225	1372.0348	8547
C173H296N40O80	4	1033.5101	1033.5041	12312	1033.5041	3037	1033.5182	8231
C173H296N40O80	3	1377.6777	1377.6685	748	1377.6685	3729	1337.6861	1569
C170H293N40O78	4	1036.5101	1036.5101	30467	1036.5101	29998	1036.5242	30731
C170H293N40O78	3	1381.6777	1381.6742	25801	1381.6580	28851	1381.6903	35309
C171H296N41O78	4	1043.7667	1043.7619	20269	1043.7619	24828	1043.7759	35480
C171H296N41O78	3	1391.3532	1391.3473	11098	1391.3473	15220	1391.3635	17371
C171H295N40O79	4	1044.0127	1044.0016	5336	1044.0298	6591	1044.0298	8384
C171H295N40O79	3	1391.6812	1391.6730	7681	1391.6730	5675	1391.6892	11435
C172H295N40O79	4	1047.0127	1047.0087	18412	1047.0087	8854	1047.0369	12574
C172H295N40O79	3	1395.6812	1395.6664	2972	1395.6664	4033	1395.6826	7664
C173H298N41O79	4	1054.2694	1054.2686	16808	1054.2686	12278	1054.2827	18620
C173H298N41O79	3	1405.3567	1405.3882	6193	1405.2738	6971	1405.3555	6644
C173H297N40O80	4	1054.5154	1054.5238	7815	1054.5095	12174	1054.5380	5903
C173H297N40O80	3	1405.6847	1405.6829	4108	1405.6665	4335	1405.6992	9314

[1,2,3] Observed peaks (m/z) and their corresponding integrals in three independent measurements.

CHAPTER FOUR

Peptidoglycan O-acetylation Increases in Response to Vancomycin Treatment in Vancomycin-Resistant *Enterococcus faecalis*

This chapter published as: Chang, J. D.; Foster, E. E.; Wallace, A. G.; Kim, S. J. Peptidoglycan O-acetylation Increases in Response to Vancomycin Treatment in Vancomycin-Resistant *Enterococcus faecalis. Sci. Rep.* **2017**, *7:* 46500.

Abstract

Vancomycin resistance is conferred upon vancomycin-resistant enterococci (VRE) through the replacement of peptidoglycan (PG) stem terminal D-Ala-D-Ala with D-Ala-D-Lac. The D-Ala-D-Lac incorporation can affect both the fitness and virulence of VRE. Here we comprehensively investigate the changes to PG composition in vancomycin-resistant *Enterococcus faecalis* following the growth in presence of vancomycin using liquid chromatography-mass spectrometry. Using high-resolution mass spectrometry, 104 unique muropeptides fragments were identified and the relative abundance of each fragment was accurately quantified by integrating the ion current of a selected ion using extracted-ion chromatogram. The analysis indicates reduced PG cross-linking, increased carboxypeptidase activities, increased N-deacetylation, and increased *O*-acetylation in VRE when grown in the presence of vancomycin. We found that *O*-acetylation preferentially occurred on muropeptides fragments with reduced cross-linking with a pentapeptide stem that terminated in D-Ala-D-Lac. These findings show that *O*-acetylation preferentially occurred in regions of the cell wall with reduced PG cross-linking on PG units that have stems terminating in D-Ala-D-Lac, serving as markers to prevent both the PG-stem modification by carboxypeptidases and the cell wall

degradation by autolysins. Accurate quantitative PG composition analysis provided compositional insights into altered cell wall biosynthesis and modification processes in VRE that contribute to lysozyme resistance and enhanced virulence for VRE grown in the presence of vancomycin.

Introduction

The cell wall in Gram-positive bacteria, instead of being merely a static barrier, is a dynamic organelle that changes its structure and composition in response to the external stimuli,[114-115], including exposure to antibiotics[116]. An example of well-known cell wall modification is the mechanism of vancomycin resistance in vancomycin-resistant enterococci (VRE). Vancomycin is a glycopeptide antibiotic that binds to the D-Ala-D-Ala terminus of lipid II to inhibit the transglycosylation step of peptidoglycan (PG) biosynthesis, and it is considered one of the most effective therapeutic agents against serious infections by methicillin-resistant *Staphylococcus aureus* (MRSA). However, the emergence of VRE poses a serious threat to public health[35] as the use of vancomycin against MRSA infections frequently leads to the selection of VRE as an alternative pathogen, with VRE as result becoming one of the leading nosocomial agents.[117] In VRE, high-level vancomycin resistance is conferred by either transposable elements *vanA* or *vanB,* where both encode for a number of proteins that alter the terminal D-Ala-D-Ala of PG stem to D-Ala-D-Lac (Fig. 4.1a).[87, 118] This depsipeptide substitution reduces vancomycin's binding affinity to the PG-stem structure by a 1000-fold,[119] rendering vancomycin ineffective against VRE with minimal inhibition concentrations that often exceed 1024 μg/mL.[120]

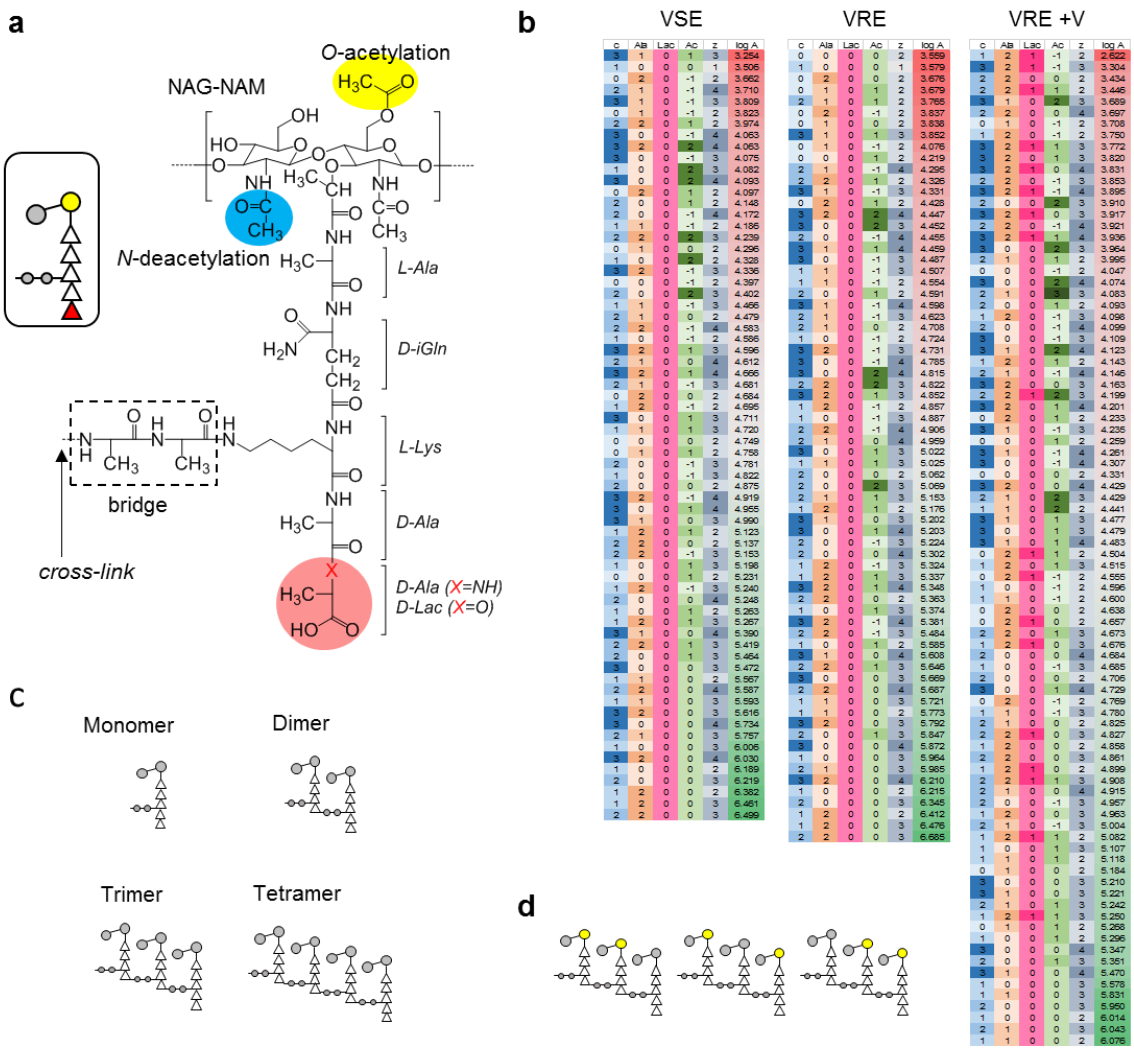

Figure 4.1: Structure of a peptidoglycan subunit and observed muropeptide fragments. a) Chemical structure of a PG subunit is shown with modifications examined in this study highlighted. Disaccharide backbone and peptide stem are modified by O-acetylation of MurNAc (yellow), N-deacetylation of GlcNAc (blue), substitution and/or removal of terminal D-Ala-D-Ala (pink), and cross-linking to the adjacent PG stem (green). Schematic figure representing a subunit is shown in inset. Mutanolysin used to generates the fragments cleaves the GlcNAc-MurNAc $\beta_{1\text{-}4}$ glycosidic linkage in PG. b) Every identified muropeptide ion is described by its cross-linking ("c"), number of terminal D-Ala ("Ala"), depsipeptide substitution to D-Lac ("Lac"), acetylation state ("Ac"), charge state ("z"), and abundance ("logA"). The abundances are calculated by taking Log_{10} of averaged area under curve from extracted ion chromatograms (n = 3). Darker shades under ion descriptions indicate higher values, while abundances are colored green to red for increasing values. c) Muropeptide oligomers with increasing number of cross-links (0 to 3) are schematically depicted. d) Figures of trimers with different possible combinations of O-acetylation that give arise to the acetylation number of +2 are shown.

Although the incorporation of D-Ala-D-Lac into cytoplasmic and membrane bound PG precursors Park's nucleotide and lipid II is essential for vancomycin resistance, depsipeptide containing PG itself has never been identified from isolated cell walls of VRE. It is unknown how much of depsipeptide substituted PGs are incorporated into the cell wall and how they are modified following the induction of vancomycin resistance in VRE. These cell wall modifications are likely to play an essential role in bacterial fitness, persistence, virulence, and resistance to other antimicrobial agents. In this report we investigate the changes to PG composition of vancomycin-resistant *Enterococcus faecalis* (ATCC 51299), VRE of *vanB* type, using liquid chromatography-mass spectrometry (LC-MS) to provide insights into altered cell wall biosynthesis and PG modifications following the induction of vancomycin resistance.

Results and Discussion

Accurate Quantification of Muropeptides by LC-MS

Isolated cell walls of VRE or vancomycin-susceptible *E. faecalis* (VSE) are digested with mutanolysin, which is a *N*-acetylmuramidase that cleaves the $\beta_{1,4}$ glycosidic bond between *N*-acetylmuramic acid (MurNAc) and *N*-acetylglucosamine (GlcNAc) of PG. Mutanolysin digestion of cell walls results in a complex mixture of muropeptide fragments not amenable to conventional spectral absorption measurements required for accurate quantification through traditional means. This difficulty arises from multiple muropeptide species that co-elute during the chromatographic separation, obfuscating identification and quantification of muropeptide peaks solely based on the absorption integral of the elutants. To circumvent this complexity, earlier studies have relied on

treatment of cell walls with hydrofluoric acid to remove PG modifications prior to the LC-MS analysis. While this step significantly enhanced chromatographic resolution and separation required for the traditional analysis by reducing the variation in muropeptide species, rich muropeptide diversity that encoded for PG modifications were lost during the treatment.

Our approach differs by i) preserving the PG modifications by forgoing the acid treatment, ii) use of high resolution mass spectrometry (HRMS) for improved detection and identification of muropeptides, and iii) direct quantification of muropeptides by integrating extracted-ion chromatogram (XIC) of the selected ions. Detection and identification of such complex mixture is nonetheless still challenging and time consuming due to the possibility of each PG subunit undergoing multiple modifications (Fig. 4.1a).[8, 14] Hence the number of all possible chemical structures for muropeptides grows combinatorially with increase in the size of PG fragment (Fig. 4.1c). In order to facilitate the identification of complex muropeptide fragments, observed accurate mass by HRMS was screened against calculated muropeptide mass library for all possible combinatorial modifications generated *in silico* using MATLAB (MathWorks). From the library of 5328 possible ions, 104 unique muropeptide fragment ions were identified and selected for the quantitative analysis. Figure 1b shows the list of selected muropeptide fragments where each row represents multiple isomers that share a common PG modification. For example, a row is used to represent a pentapeptide-stem containing PG trimer with two *O*-acetylations. Based on the positions of *O*-acetylation (Fig. 4.1d), this sub group is comprised of 3 isomers.

For the accurate quantification of muropeptides, XICs of the selected ions were integrated and the relative abundance of each ion in respect to the sum of all selected ions calculated. The advantage of this approach is that even with multiple muropeptides co-eluting during the chromatographic separation, each muropeptide species is clearly resolved in the mass-charge dimension by XIC of unique m/z value. Although there may be differences in ionization efficiencies among muropeptide species, this was not considered critical as the analysis relied on the relative compositional changes associated with the induction of vancomycin resistance. Another key implementation crucial for the accurate quantification of 104 unique muropeptides was the integration of isotopic distribution for each selected ion, as the isotopic distribution varies significantly based on the chemical composition of muropeptides. Larger muropeptides with more dispersed isotopic distributions would otherwise have been underestimated, as XICs are derived from the abundance of a single peak from the distribution. The isotopic distribution and necessary correction of abundance for each identified ion were calculated using in-house MATLAB program utilizing the built-in mass spectrometry functions.

PG Acetylation and Cross-linking

One of more striking changes to the cell wall composition that occurs in VRE following the induction of vancomycin resistance is the increase in both PG *O*-acetylation and *N*-deacetylation (Fig. 4.2a). Acetylation states of -1, 0, +1, and +2 were considered for the analysis. For example, on a dimer acetylation state of -1 represents a dimer with one *N*-deacetylated GlcNAc, 0 represents unmodified PG dimer, +1 represents *O*-acetylation of one MurNac, and +2 for *O*-acetylation of both MurNAc. Each step-wise increment in acetylation state is accompanied with the mass increase of 42 Da. Sample

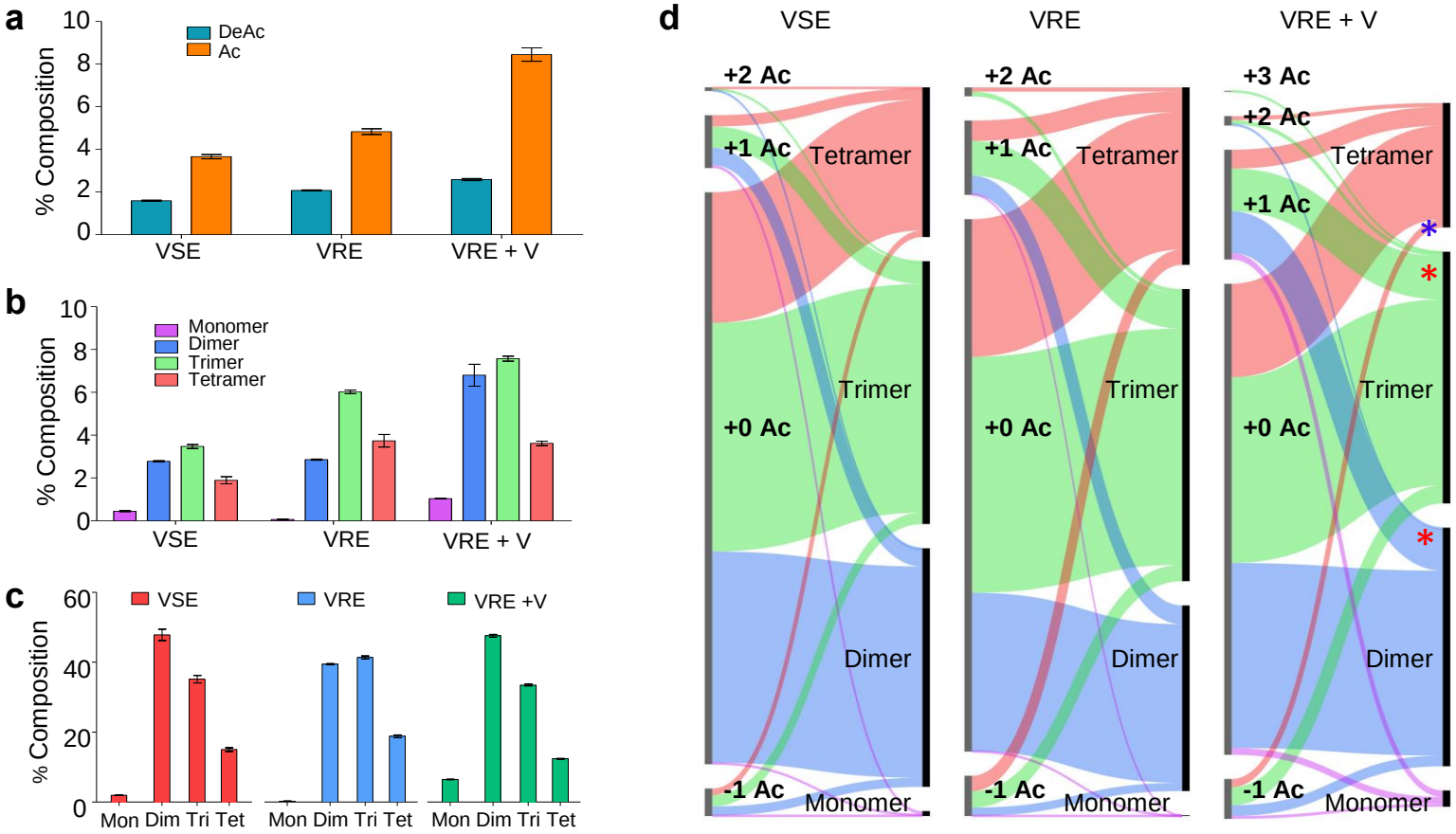

Figure 4.2: Acetylation state and crosslinking. a) Schematic drawing corresponding to PG monomer, dimer, trimer, and tetramer without any modifications are shown. b) Proportions of total PG subunits with both net positive (orange) and negative (blue) acetylation states increase when VRE is grown with vancomycin. c) Proportion of subunits with at least one O-acetylation increases for all fragments in presence of vancomycin. d) Breakdown of each acetylation state to the acetylation state and cross-linking shows an increase in overall acetylation for all degrees of crosslinking. All error bars represent 95% confidence interval (n = 3).

mass spectra of PG dimers with acetylation states of 0 and +1, identified from VRE grown with vancomycin, are shown in supplementary Fig. 4.S1. Mass spectrum of collision-induced dissociation product ions from a parent ion, +1 acetylated PG dimer with a tripeptide stem is shown in Fig. 4.S2. Percent composition for all muropeptides that have one or higher acetylation state for VRE grown with vancomycin is 19.811% ± 2.363%. This is approximately 60% increase from acetylated muropeptides in VRE (12.361% ± 0.794%) and 120% increase from VSE grown without vancomycin (9.135% ± 0.941%). Increased PG *O*-acetylation and *N*-deacetylation represent significant modifications to VRE cell wall in response to vancomycin treatment.[121-123]

Acetylated muropeptides were classified based on their number of cross-links and shown as a bar graph in Fig. 4.2b with monomers shown in purple, dimers in blue, trimers in green, and tetramers in orange. For VRE grown with vancomycin, while the monomers show the largest relative increase in *O*-acetylation with more than 16-fold increase (from 0.063% ± 0.014% to 1.036% ± 0.025%), *O*-acetylated dimers and trimers remain the most abundant species. Preferential *O*-acetylation of PG dimers and trimers are clearly noticeable, but the tetramers show a slight reduction in PG *O*-acetylation. These trends suggest that the cell wall modification through acetylation state change is neither random nor uniform, but is a selective process.

To further investigate the relationship between PG acetylation and cross-linking, PG cross-linking efficiency (ρ_{CL}) was determined for VRE as a function of presence of vancomycin. The ρ_{CL} was calculated through summations of integrated ion current XICs from selected muropeptide species (Fig. 4.1b) by dividing the total number of cross-links present with the total number of PG subunits. ρ_{CL} for VRE grown with vancomycin

(0.603 ± 0.002) shows 6% decrease in comparison to ρ_{CL} of VRE grown without vancomycin (0.641 ± 0.002), indicating a small reduction in PG cross-linking to the level comparable for VSE grown without vancomycin as measured by ρ_{CL} (0.620 ± 0.010). The effect of vancomycin resistance induction on VRE cell wall cross-linking is visible by altered oligomeric muropeptide profiles shown in Fig. 4.2c as increases in abundances of monomeric and dimeric muropeptide species and decrease in larger oligomers. Thus, the increase in PG *O*-acetylation is accompanied by reduced PG cross-linking for VRE grown in presence of vancomycin.

The correlation between PG acetylation and cross-linking is visualized by plotting simultaneously changes to the both on a flow-bar graph (Fig. 4.2d). The left axis consists of bar segments organized in an ascending order of acetylation states (Ac) from -1 to +3 with bar lengths proportional to the relative abundance as quantified through normalized summed integrals from XIC ion current of muropeptides for the corresponding acetylation state. The right axis shows bars with lengths proportional to the fraction of muropeptides with increasing cross-link. The width of interconnecting bars, which "flow" between two vertical axes, represents the fraction of muropeptides with shared modifications. While the flow-bar graph profiles of VRE and VSE grown in absence of vancomycin are similar, the profile of VRE grown in presence of vancomycin displays the following pronounced changes: i) large increase in *O*-acetylation of dimers and trimers (red stars), ii) decrease in *N*-deacetylation (-1) of tetramers (blue star), and iii) hyperacetylated trimers with the acetylation state of +3 where every MurNAc is *O*-acetylated. Preferential *O*-acetylation of dimers suggests that *O*-acetylation occurred in the region of cell wall with low PG cross-linking.

PG Acetylation and Stem Length

Another major change to the PG composition observed in VRE grown with vancomycin is the PG-stem modification by L,D- and D,D-carboxypeptidases (Fig. 4.3a).[124] The distribution of muropeptides with the cross-link acceptor-stem structure terminating with pentapeptide, tetrapeptide, and tripeptide is shown in Fig. 4.3b. For VRE grown with vancomycin, the majority of muropeptides are found with tetrapeptide-stem structure indicative of high D,D-carboxypeptidase activity, and accumulation of muropeptides with tripeptide stem eventually follows. The distribution of muropeptides with at least one *O*-acetylation as a function of PG-stem length is shown in Fig. 4.3c. Although the fraction of muropeptides containing pentapeptide stem decreases in VRE from increased carboxypeptidases activities (Fig. 4.3b), the abundance of *O*-acetylated pentapeptide-stem muropeptides increases by approximately 5-fold following the induction of vancomycin resistance (from 7.993% ± 0.694% to 44.441% ± 2.244%). These two trends imply that either *O*-acetylation prevented modification of PG stems by D,D-carboxypeptidases or the pentapeptide PG-stem motif is recognized as the site of *O*-acetylation.

To characterize the correlation between PG acetylation and stem modification, PG compositions as sorted by these two modifications are simultaneously visualized on flow-bar graphs (Fig. 4.3d). The left axis represents the fraction of muropeptides with increasing acetylation state, and the right axis muropeptides with increasing stem lengths. For VSE and VRE grown without vancomycin, PG with +1 acetylation state are composed from approximately equal proportions of pentapeptide- and tripeptide-stem muropeptides. With addition of vancomycin, the composition of +1 acetylation state PG

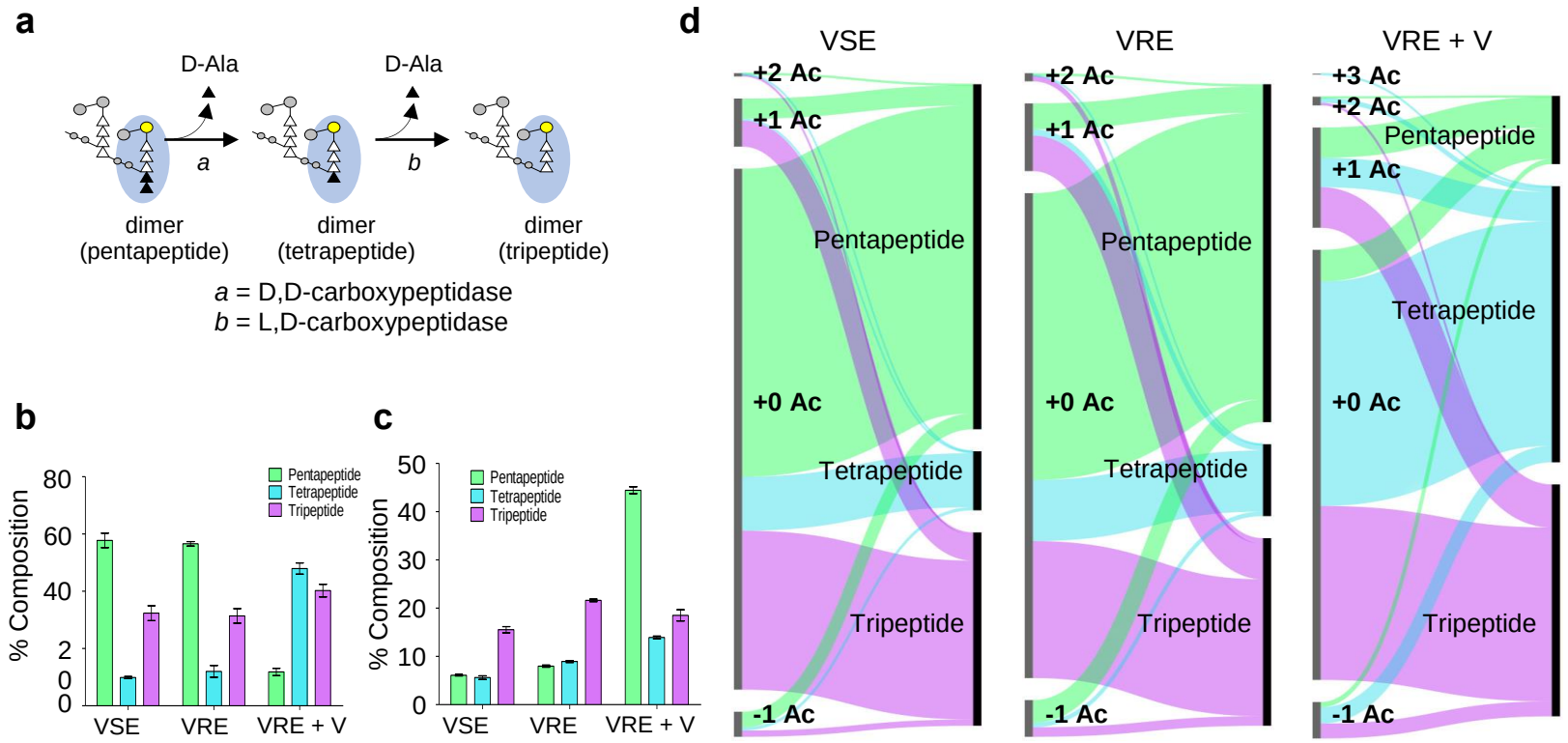

Figure 4.3: PG acetylation and peptide stem length. a) Schematic drawing of monomer pentapeptide, tetrapeptide, and tripeptide and their associated stem length modifications are shown as reference. No modifications other than the PG stem terminal editing is shown. b) Overall PG composition by peptide-stem length shows simultaneous increase in tetrapeptide and decrease in pentapeptide with addition of vancomycin. c) Proportion of subunits with one or more O-acetylation markedly increase for pentapeptides in presence of vancomycin. d) Breakdown of fragments by the acetylation state and peptide-stem length shows that upon addition of vancomycin, fragments of all peptide stem lengths are equally acetylated. +0 Ac fragments are composed of mostly penta- and tripeptides, but with addition of vancomycin tetra- and tripeptides become the majority. All error bars represent 95% confidence interval (n = 3).

for VRE changes with a significant increase in tetrapeptide-stem muropeptides to the point where muropeptides with tripeptide stem (36.033% ± 4.585%), tetrapeptide stem (33.793% ± 3.154%), and pentapeptide stem (30.174% ± 2.117%) all contribute in approximately equal proportions (Figure 4.3d, right). Of particular note is that the proportion of +1 acetylated muropeptides with a pentapeptide stem in VRE does not change with the induction of vancomycin resistance, suggesting that *O*-acetylation of muropeptides with pentapeptide stem prevents PG-stem modification by D,D-carboxypeptidase. Furthermore, accumulation of *O*-acetylated muropeptides with tetrapeptide stem is consistent with *O*-acetylation also inhibiting L,D-carboxypeptidase activity in VRE.

PG Cross-link and Stem Length

The correlation between PG cross-link and stem length in VRE is visualized using a flow-bar graph (Fig. 4.4a). The left axis consists of bars with lengths proportional to the fraction of muropeptides with increasing number of cross-links, and bars on the right axis represent fraction of muropeptides with increasing stem lengths, of which schematic representations of tetramers with (i) pentapeptide, (ii) tetrapeptide, and (iii) tripeptide PG-stem structure are shown as an example in Figure 4.4b. The flow-bar graph makes it apparent that PG compositions of VSE and VRE grown in absence of vancomycin are similar to each other, with the majority of muropeptides having pentapeptide-stem structure, tripeptide- and tetrapeptide-stem muropeptide species subsequently following in abundance. This profile changes in VRE upon addition of vancomycin with the reduction in proportion of pentapeptide-stem structured muropeptides, which is consistent with high D,D-carboxypeptidase activity. Simultaneously, the proportion of tetrapeptide-

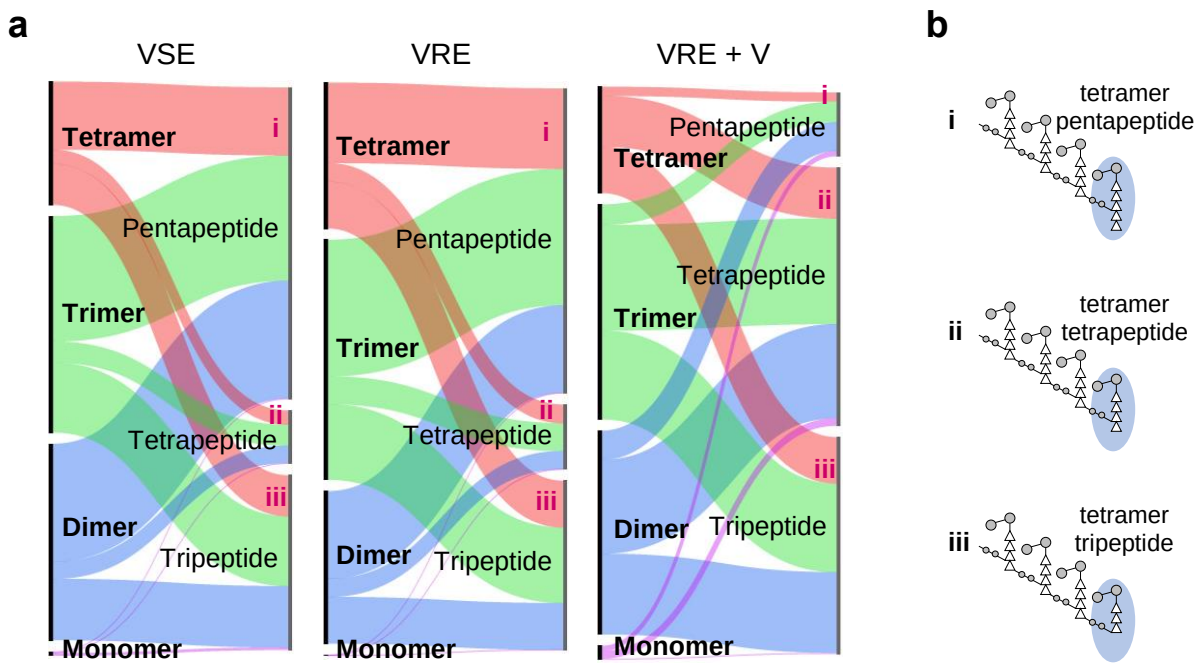

Figure 4.4: PG cross-linking and peptide-stem length. a) Breakdown of fragments by cross-linking and peptide-stem length shows the distinct shift of peptide-stem population towards tetrapeptides with vancomycin addition. b) Schematic drawing of tetramers with various lengths of peptide-stem highlights the fact that the final subunit of every oligomer is where the cross-linking occurs.

stem muropeptides increases by more than five-fold, indicating the inhibition of L,D-carboxypeptidase activity. As muropeptides with tetrapeptide-stem structure in VRE are found to be preferentially *O*-acetylated (Fig 4.3d), this also implies that L,D-carboxypeptidase activity was inhibited by the *O*-acetylation.

PG Acetylation and Depsipeptide Substitution

The incorporation of depsipeptides into PG-stem structure is the hallmark of vancomycin resistance in VRE. Muropeptides with a depsipeptide stem exhibit lengthened chromatographic retention time and an increase of 1 mass unit compared to the dipeptide containing muropeptides (Figure 4.5a). Quantitative analysis has determined that 57.328% ± 1.840% of muropeptides with a pentapeptide stem from VRE grown with vancomycin have D-Ala-D-Lac substitution. Furthermore, more than half of

muropeptides with a D-Ala-D-Lac substituted stem (57.584% ± 2.827%) have one or more *O*-acetylation (Fig 4.5b). In contrast, a large fraction of muropeptides with D-Ala-D-Ala stem are found without any acetylation (77.907% ± 2.133%). The relative ratio of muropeptides in +0 acetylation state with dipeptide to depsipeptide is 1.0:0.8, but for +1 acetylation state the ratio increases to 1.0:3.4. Therefore, muropeptides with the D-Ala-D-Lac stem structure are preferentially *O*-acetylated, and this preference is clearly visible in the flow-bar diagram as shown in Fig. 4.5c. The majority of D-Ala-D-Lac containing muropeptides have +1 and 2 acetylation state, but for muropeptides containing D-Ala-D-Ala stem structure +0 acetylation state composes the majority. Interestingly, *N*-deacetylated (-1 Ac) muropeptides display the opposite trend by primarily having D-Ala-D-Ala stem structure.

PG *O*-acetylation has been shown to inhibit the autolysin activity.[125] Thus preferential *O*-acetylation of muropeptides with D-Ala-D-Lac stem (Fig. 4.5c) suggests that the newly synthesized nascent PG in VRE containing D-Ala-D-Lac stem is marked with *O*-acetylation to prevent autolysin degradation and PG-stem modification by carboxypeptidases (Fig. 4.5b). In contrast, the old cell wall containing D-Ala-D-Ala stem structure is preferentially *N*-deacetylated. Since both *O*-acetylation and *N*-deacetylation of PG contribute to increased lysozyme resistance, we speculate that these cell wall modifications can potentially contribute to evasion of host's innate immune response.[125-126] Therefore, vancomycin therapy against VRE may indirectly cause increased virulence and transmittance in both the patient undergoing antibiotic therapy and the healthcare setting where the therapy is being administered.

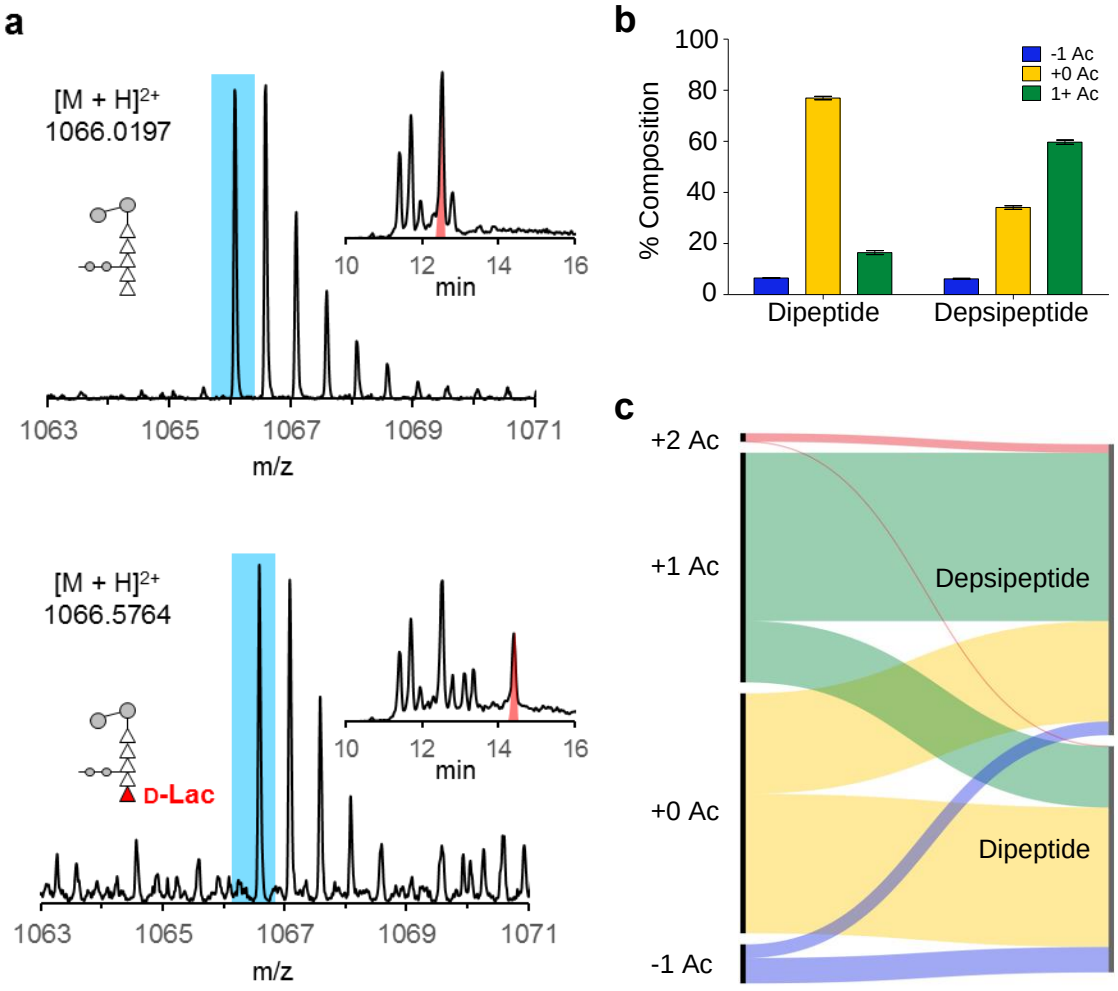

Figure 4.5: PG acetylation and depsipeptide substitution. a) Mass spectra and extracted ion chromatograms (XIC) for the unmodified dimer pentapeptide and its D-Ala-D-Lac substituted counterpart are shown. The substitution manifests itself as mass increase of 1 Da, or ½ m/z value for doubly charged ion (blue dotted line), and with different retention time (red). b) Composition of PG pentapeptides shifts towards +1 or higher acetylation state in VRE upon the induction of vancomycin resistance. c) Breakdown of each acetylation state according to the PG stem terminal displays a preference for depsipeptide to have one or more acetylated subunits. All error bars represent 95% confidence interval (n = 3).

Materials and Methods

Cell Wall Isolation and Digestion for LC-MS

Overnight cultures of VRE (ATCC 51299) and VSE (ATCC 29212) grown in brain-heart infusion media at 37°C with 180 RPM orbital shaking were used to inoculate

flasks containing 100 mL of tryptic soy broth (TSB) (1% v/v). Vancomycin resistance was induced by addition of vancomycin at the time of inoculation (6 μg/mL). Bacteria were harvested at stationary phase (OD_{600} > 0.8) by centrifugation at 4°C at 4750 RPM (Allegra X-15R with SX4750 rotor, Beckman Coulter) for 12 min. Pellets were resuspended in phosphate buffered saline (PBS) and sterilized by immersing in a boiling water bath for 30 min. Samples were bead beat (Disruptor Genie, Scientific Industries) with 0.5 mm diameter glass beads for 8 one-min cycles with 1 min of rest in between agitation. Beads and other contaminants were removed using Steriflip 20 μm nylon vacuum filter (EMD Millipore). Crude cell wall pellets were resuspended in 2 mL PBS, to which 8 mL of 2% sodium dodecyl sulfate (SDS) solution was added, then placed in a boiling water bath for 30 min. Boiled cell wall pellets had SDS removed from them by dividing the pellets into microcentrifuge tubes and washing with five 1 mL deionized water through centrifiguation. Isolated crude cell walls were resuspended in 2 mL of 50 mM Tris pH 8.0 buffer. DNase (200 μg) was added to the cell wall suspension and it was incubated at 37°C for 24 hr at 80 rpm, which was followed by addition of trypsin (200 μg) for additional 24 hr of incubation. Cell walls were washed once and resuspended in 1 mL of Tris buffer.

To generate PG fragments for the LC-MS compositional analysis, 0.66 KU of mutanolysin (Sigma-Aldrich) to hydrolyze $\beta_{1,4}$ glycosidic bonds in PG was added to the cell wall suspension at room temperature and the sample incubated for 24 hr. Additional 0.66 KU of mutanolysin was added to the mixture after the initial period, and it was further incubated for 24 hr, then the sample frozen and lyophilized (Labconco). Lyophilized mutanolysin-digested cell walls were dissolved in 1 mL of 0.375 M sodium

borate buffer (pH 9.0) prepared with HPLC-grade water, and samples were reduced by addition of 10 mg of sodium borohydride (Fisher Scientific) in 960 µL borate buffer at room temperature for 30 min. The reduction was quenched by addition of 125 µL of 85% phosphoric acid. Reduced samples were frozen at -80°C, and lyophilized. Prior to LC-MS analysis, lyophilized samples were resuspended in 1 mL of sample preparation buffer (1% trifluroacetic acid), centrifuge filtered, and cleaned up for LC-MS using 100 µL Pierce C18 tips (Thermo Scientific).

Liquid Chromatography-Mass Spectrometry

Mutanolysin-digested muropeptide fragments were chromatographically separated using NanoACQUITY Ultra Performance Liquid Chromatography System (Waters). Reverse phase BEH C18 column (length of 100 mm and diameter of 75 µm) had bead size of 1.7 µm and pore size of 130 Å. Chromatographic separation of mutanolysin-digested PG was carried out by injecting 1 µL of the sample from a 5 µL sample loop to the column under isocratic condition of 99% buffer A (99.8% anhydrous methanol with 0.1% formic acid) and 1 % buffer B (100% acetonitrile) for 5 min, then a linear gradient to 50% buffer B was applied for 30 min for the separation. The column was regenerated under isocratic condition with 85% buffer B for 5 min, a linear gradient to 98% buffer A for 1 min, then isocratic at 98% buffer A for 23 min. The flow rate was kept constant (0.6 µL/min) throughout the analysis.

The sample was ionized by nanoflow electrospray ionization (ESI) with spray voltage of 35 V and capillary voltage of 3.5 kV. Synapt G2 High Definition Mass Spectrometer (HDMS) with Time-of-Flight (TOF) mass analyzer (Waters) was run in positive ion mode. Fibrinopeptide B (Glu-Fib) was used as an internal standard to correct

for drift of the instrument. Data were analyzed using MassLynx (Waters) and MATLAB (MathWorks).

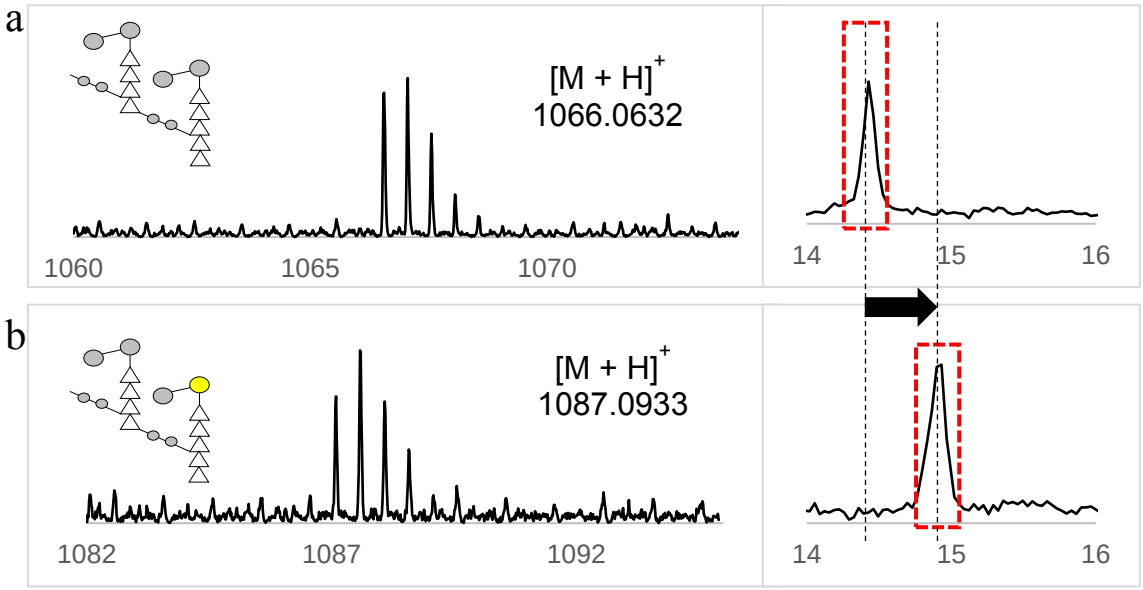

Supplementary Figure 4.S1: Example spectra and XIC of identified fragments. a) Schematic drawing of the muropeptide fragment ion, mass spectrum, and XIC for dimer pentapeptide at 0 Ac with +2 charge are shown. b) Singly O-acetylated counterpart of the same muropeptide has different m/z value and retention time as indicated by the red box in XICs. O-acetylation is denoted by a yellow circle.

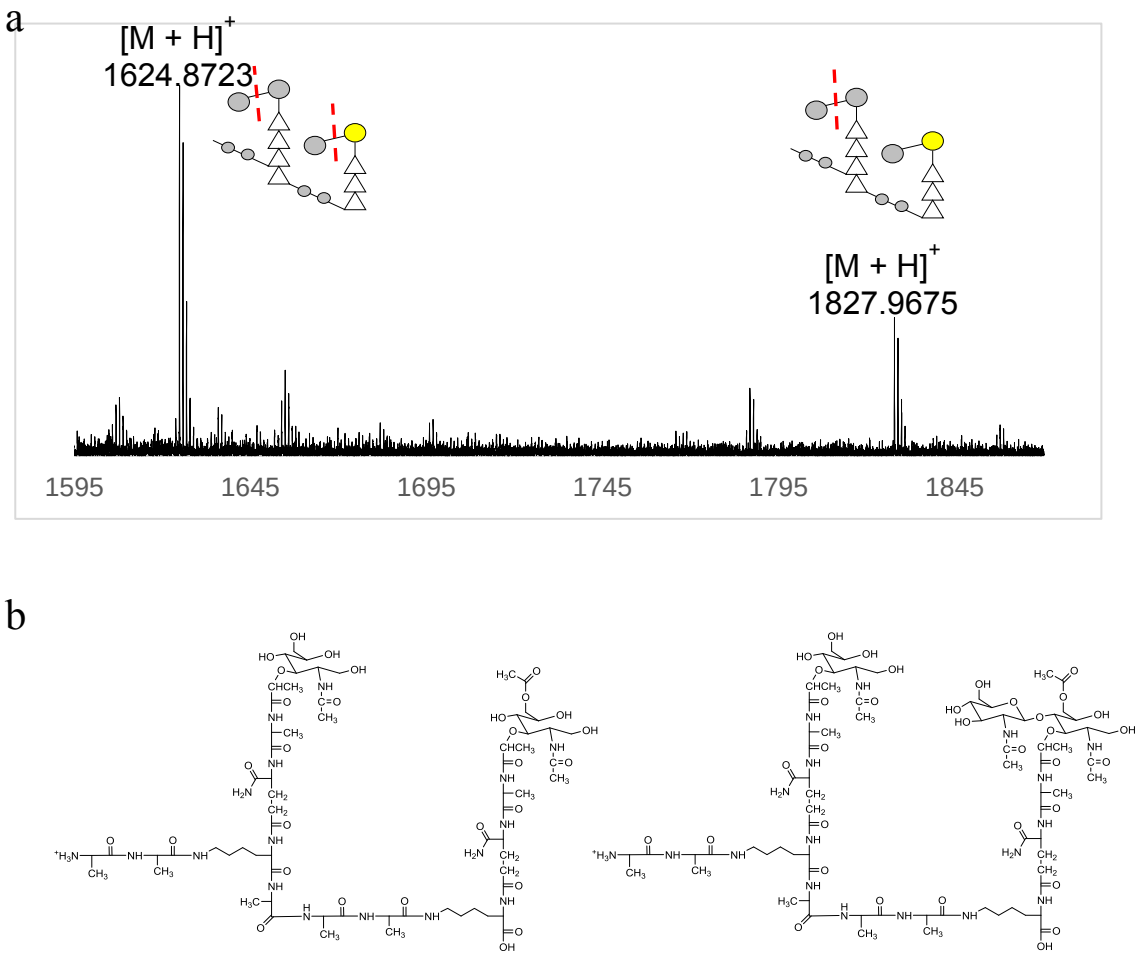

Supplementary Figure 4.S2: MS/MS spectrum of a sample peptidoglycan. a) MS/MS spectrum from a dimer pentapeptide muropeptide with +1 acetylation state shows the CID product ions with two and one GlcNAc's fragmented away. Red lines indicate the location of CID fragmentation. m/z values shown above the peaks are for (b^+) ion products of fragmentation. b) Chemical structures for product ions of dimer pentapeptide at +1 acetylation state with two and one GlcNAc fragmented away.

CHAPTER FIVE

Characterization of the Cell Wall Peptidoglycan in Vancomycin-Resistant *Staphylococcus aureus* 4 After Induction of Vancomycin Resistance

Abstract

Strains of Vancomycin-resistant *Staphylococcus aureus* (VRSA), first isolated in 2002, have the potential to cause major public health issues due to their ability to resist vancomycin, the antibiotic most commonly used for the treatment of drug resistant *S. aureus*. Given the threat already posed by multi-drug resistant *S. aureus* (MRSA) in nosocomial environments, spread of VRSA would impose a severe burden on the healthcare system. Therefore, biochemical examination of VRSA and their cell walls, potential targets for future antimicrobial compounds, would contribute towards characterizing this problematic pathogen and aid in developing novel treatments. In this study, we utilize liquid chromatography-mass spectrometry (LC-MS) to analyze the peptidoglycan (PG) composition of the cell wall from VRSA4 and the changes to it that occurs during the induction of vancomycin resistance. While the PG fragments with D-Ala-D-Lac terminated peptide stems (2.705% ± 0.332%) associated with the vancomycin resistance were observed as expected, the cell wall of VRSA4 also displayed a significant reduction in cross-linking efficiency (decrease of 7.467% ± 2.463%). Associated with this lowered cross-linking was the abundance of PG fragments without the cross-linking bridge, with nearly quarter of all PG subunits (26.181% ± 2.859%) belonging to these defective fragments. These results indicate that VRSA4, while still resistant to

vancomycin, experiences issues in the PG metabolism and supports the notion that VRSAs incur a fitness cost to become resistant to vancomycin.

Introduction

Antibiotic resistance in *Staphylococcus aureus* has been an increasing threat to the public health for number of years.[6, 34] Due to their ubiquitous distribution in general population, any type of resistance to antibiotics in *S. aureus* confers bacteria the potential to rapidly spread and cause difficulties in the treatment of life-threatening infections cause by them. Facilitated by widespread misuse of antibiotics, emergence of multi-drug resistant *Staphylococcus aureus* (MRSA) already presents a serious problem to patients in the nosocomial settings.[7, 36, 127-128] Vancomycin has historically been the drug of last resort in treating these infections by MRSA, and judicious use of vancomycin had prevented the drug resistance from arising initially. But in the 1980's, *S. aureus* with intermediate levels of resistance to vancomycin began to appear, and in 2002 first clinical cases from fully vancomycin resistant *S. aureus* (VRSA) were encountered in Michigan and Pennsylvania.[129-131] To this date 13 different strains of VRSA have been isolated, and cases of VRSA are reported to the Centers for Disease Control (CDC) as instances of particularly hazardous pathogen that could cause public health crisis.[132] Due to their broad antibiotic resistance profile, fundamental changes to the protocols for *S. aureus* infection treatment would become necessary were VRSA infections to become prevalent in the clinical setting.[133] While there has been several antibiotics that recently entered the market in response to MRSA and other multi-drug resistant Gram-positive pathogens, rapidly evolving bacterial genome in response to the selection pressure from these

antibiotics calls for continued studies of these pathogens and the ways antibiotic resistance alters their survival fitness.

In spite their broad antibiotic resistance profiles and the shared lineage from already pathogenic progenitor strain, VRSA's epidemiological progression through the general population has been unexpectedly slow so far. There have been only five cases of VRSA reported to the CDC during last five calendar years.[134] Even with the rigorous antimicrobial measures being taken in the healthcare settings, this rarity of cases by VRSA is perplexing especially given the extent of MRSA's prevalence. Twelve out of thirteen VRSA strains originate from the clonal complex CC5, a widespread MRSA strain already frequently encountered in nosocomial settings.[37, 135] Given this common presence of CC5, it is surprising that these VRSA strains identical to CC5 in almost every aspect save vancomycin resistance have not found equal level of success in becoming endemic in the general population and spreading throughout the healthcare settings. Further confounding the issue is the fact that vancomycin resistance in VRSA is conferred through the transposon *Tn1546* that comes from vancomycin-resistant *Enterococcus faecalis* through horizontal transfer of genetic material.[136-138] Gene products from this transposable element enable VRSA to substitute the D-Ala-D-Ala dipeptide that terminates the peptide stem of peptidoglycan (PG) with the depsipeptide D-Ala-D-Lac upon the induction of vancomycin resistance, and this process has been well elucidated in both *E. faecalis* and *E. faecium* (18,19,20,21,22).[20, 87, 139-141] Given how these vancomycin-resistant Enterococci (VRE) have found success even under antimicrobial stewardship programs that are becoming common, the question remains on how the same transposable element affects the overall survival fitness and pathogenicity

of VRSA.[142] Suggesting the role cell wall plays in the fitness change to VRSA are previous studies that show a synergistic effect of β-lactam antibiotics and vancomycin against Vancomycin-Intermediate *Staphylococcus aureus* (VISA) and VRSA that can tolerate both antibiotics when encountered separately.[29, 143-145] These studies point toward the idea that the cell wall biosynthesis and maintenance pathways of *S. aureus* undergoes changes upon the induction of vancomycin resistance that cost VRSA the survival fitness of utilizing the vancomycin resistance. As previously seen in VRE, such changes that decrease the fitness of VRSA would manifest themselves as changes to the composition of PG, which would make apparent the adverse impact the resistance causes.[32-33]

The cell wall of *S. aureus* is built by PG subunits that are connected to each other through two distinct ways: PG peptide stems can be cross-linked to other stems through peptide bonds between the pentaglycine bridge of the donating PG and the stem of the receiving PG, and the disaccharides formed from N-acetylglucosamine (NAG) and N-acetylmuramic acid (NAM) at the head of each PG subunit can be polymerized with other disaccharides through 1-4-β-glycosidic linkages as sugar-links (Figure 5.1b).[18] PG subunits that compose the cell wall can also be varied in their chemical structures. After their incorporation into the cell wall, PG subunits can either be O-acetylated at N-acetylmuramic acid (NAM) or N-deacetylated at N-acetylglucosamine (NAG).[14, 146] They can also have up to two of their peptide stem terminal residues removed.[147] As result of these variations in both individual PG subunits and the way they are interconnected to each other, the cell wall is heterogeneous in both composition and structure. Through the enzymatic digestion using mutanolysin, sugar-links irrespective of

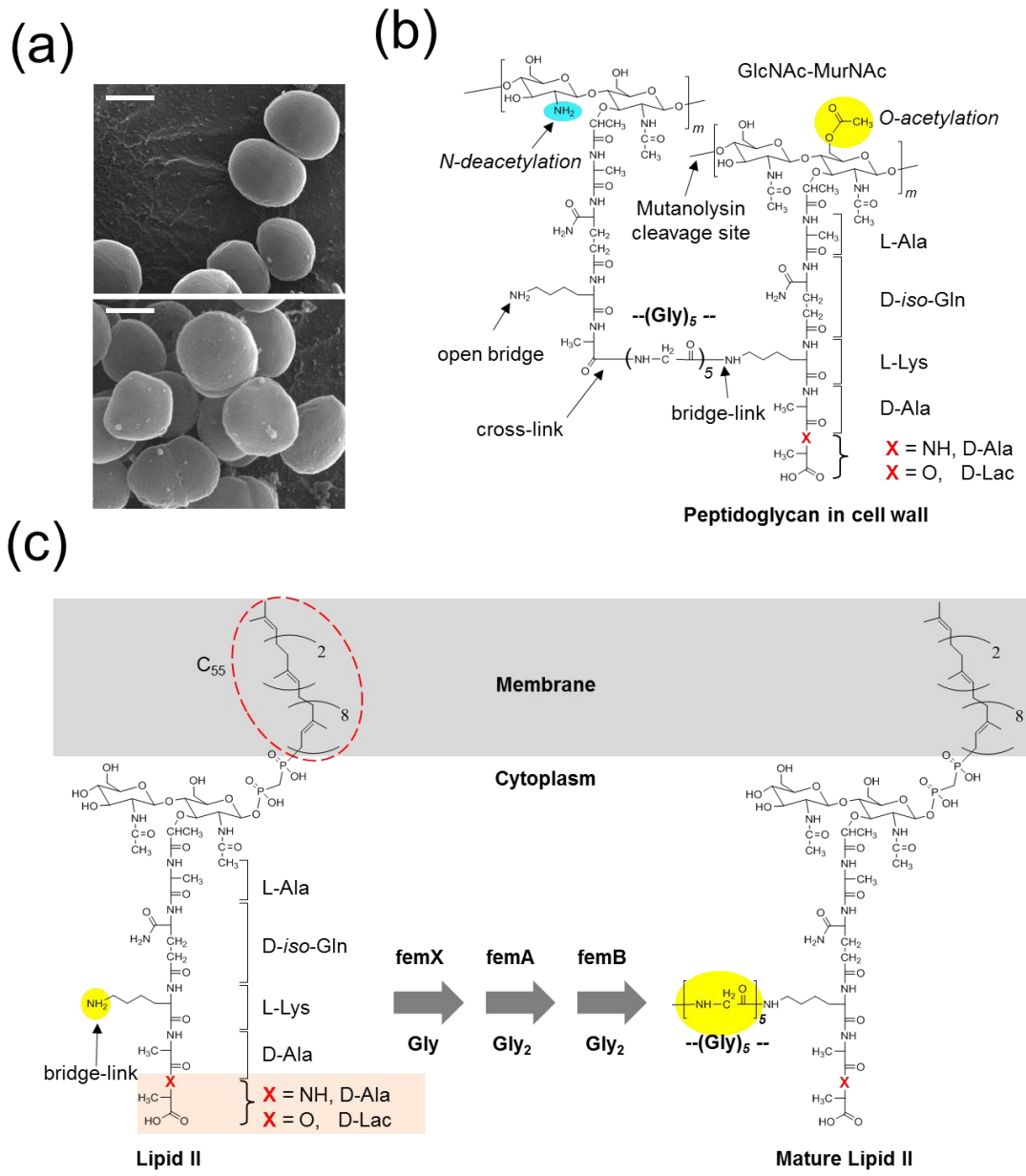

Figure 5.1: Cell Wall of Vancomycin-Resistant *Staphylococcus aureus*. (a) Scanning electron microscope images of VRSA4. Bacteria from stationary growth phase under normal conditions (top) and with the vancomycin concentration of 6 mg/mL (bottom) are shown. Bars represent 500 nm in length. (b) Chemical structure of the peptidoglycan (PG)-repeat unit of *S. aureus*. The PG-stem structure is L-Ala-D-iso-Gln-L-Lys-D-Ala-D-Ala with a pentaglycine bridge attached to the ε-nitrogen of L-Lys. In vancomycin-resistant *S. aureus*, the terminal D-Ala is replaced by D-Lac. (c) Maturation of lipid II into PG subunit. Lipid II with the disaccharide-peptide stem structure anchored to the cell membrane via C_{55}-bactoprenol transporter receives glycine residues sequentially by fem enzymes. Resulting mature lipid II is transported to the exterior for incorporation into the cell wall.

PG subunit variations can be cleaved to generate PG fragments that reflect the heterogeneous composition of the cell wall.[148] These fragments can then be analyzed through liquid-chromatography mass spectrometry (LC-MS) to shed light into the compositional changes to the VRSA's cell wall upon the induction of vancomycin resistance.[28, 32, 36] This analysis of PG composition will offer insights into changes to cross-linking and structural modifications to the PG subunits themselves, such as changes to the acetylation state and peptide stem lengths.

In this study, we survey the consequences of vancomycin-resistance induction to the cell wall composition in Vancomycin-resistant *S. aureus* strain 4 (VRSA4) using LC-MS. While VRSA4 grows even in presence of vancomycin (Figure 5.1a), previous studies on Vancomycin-resistant *E. faecalis* showed that there were significant alterations to the PG composition when the vancomycin resistance was induced, suggesting that VRSA4 too may experience such changes. Such changes to the PG composition would have ramifications on the structure of the bacterial cell wall and may cost bacteria in terms of survival fitness, as these features to the cell wall may only offer suboptimal ability for bacteria to interact with the environment.

Results

Induction of Vancomycin Resistance and PG Cross-linking

The extent vancomycin has on the PG cross-linking in VRSA4 was examined by identifying and quantifying PG fragments observed in LC-MS data. This required searching for possible PG fragment variations and categorizing positive matches by their cross-linking number. By adapting the in-house MATLAB program previously written,

the library of 512 PG fragment ions with various modifications was generated for matching against ions observed in the mass spectra.[32] Positive matches were made against this library from spectra, and the abundance of each ion was determined through integrating its associated extracted ion chromatogram (XIC). Abundance of each fragment was expressed as the proportion of that fragment ion over the sum of all identified and quantified fragment ions. The list of all identified PG fragment ions and the average values of their XIC integrals are provided in Supplementary Table 5.S1 and S2 (n = 3). The degree of cross-linking for each identified fragment ion was determined through the unique mass of a fragment arising from structural variations. Sample spectra and XICs for the fragments with varying degrees of cross-linking are shown in Figure 5.2a. Assigning the identity of each PG fragment and all modifications to that fragment allowed tabulating these fragments according to number of cross-links. Proportions of PG subunits found in fragments as grouped by different cross-linking numbers show that while VRSA4 under the normal condition tends toward having greater proportion of subunits that belong to fragments with higher degree of cross-linking, the induction of vancomycin resistance reversed this trend with the highest cross-linked fragments having the fewest subunits (Figure 5.2b). These trends hint that the cross-linking change in the cell wall is due to the overall decrease in the probability of a given subunit undergoing cross-linking. This decrease in the overall cross-linking can be clearly illustrated through calculating the cross-linking efficiency, which is ratio of the number of cross-links to all subunits. For the VRSA4 sample from normal growth condition, cross-linking efficiency of the PG was 0.625 ± 0.010 (± values indicate the 95% confidence interval), and for VRSA4 grown in the presence of 6 μg/mL vancomycin this ratio decreased to 0.581 ±

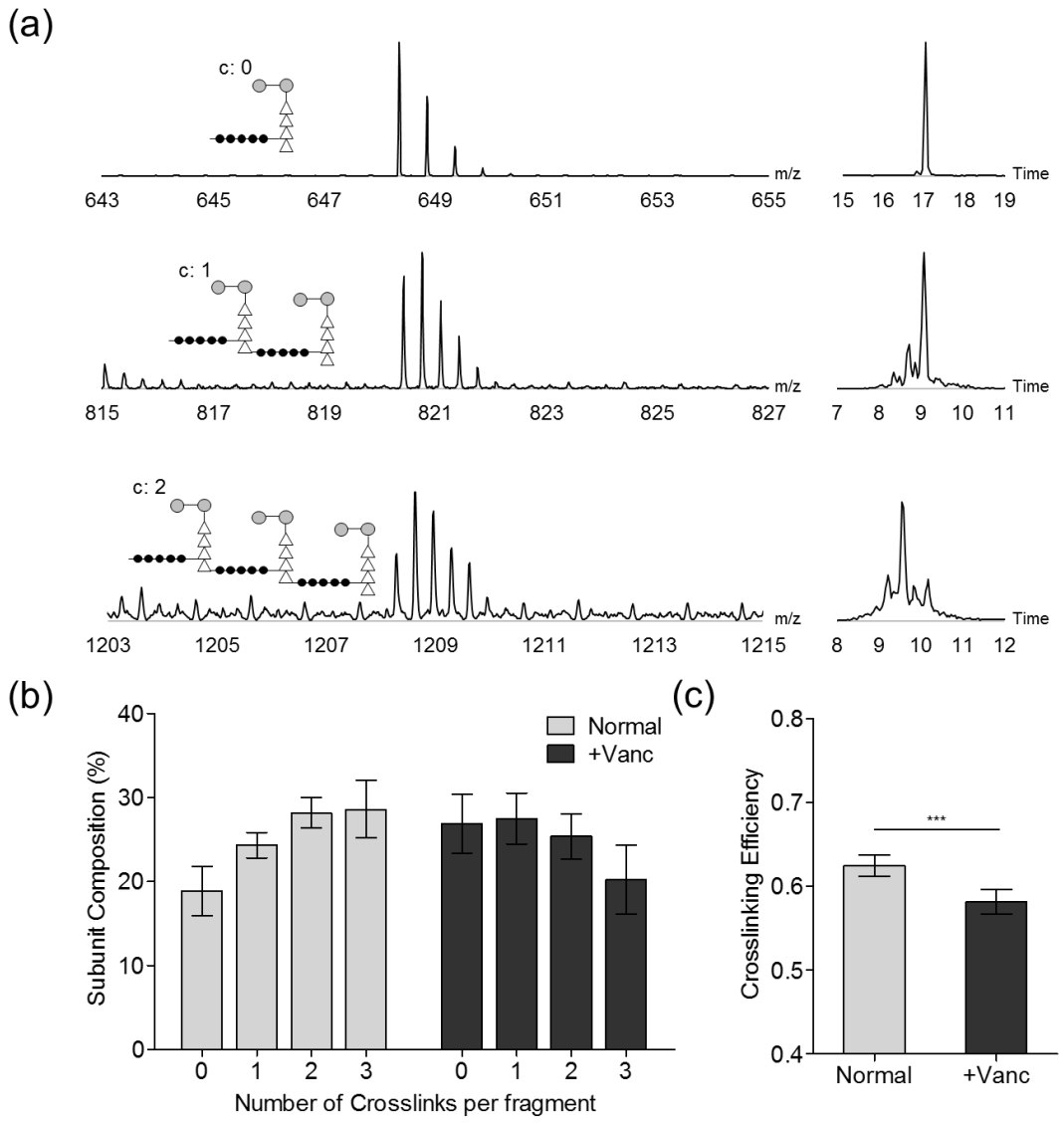

Figure 5.2: PG Cross-linking and Vancomycin-Resistance. (a) Mass spectra and XICs of PG fragments with different numbers of cross-links. Increased cross-linking results in larger fragments identifiable through specific and unique m/z values. (b) Proportion of subunits in fragments of different cross-linking numbers. VRSA4 grown in the presence of vancomycin shows a reverse in the trend towards more subunits being found in higher cross-linked fragments that is found under the normal condition. (c) Cross-linking efficiency. Cell wall synthesized by VRSA 4 during vancomycin-resistance induction has lower cross-linking efficiency (0.581 ± 0.011) than the cell wall under the normal condition (0.625 ± 0.010, $p < 0.001$). p-values were calculated using Student's t-test (*<0.05, **<0.01, ***<0.001). All error bars represent 95% confidence interval (n = 3).

0.011 (Figure 2c). This reduction indicated that the PG cross-linking decreases in the cell wall of VRSA4 in presence of vancomycin without overtly affecting the overall morphology of the bacteria (Figure 5.1a).

Pentaglycine Bridge-link and Vancomycin

The pentaglycine bridge attached to Lysine of the PG peptide stem is necessary for the cross-linking to occur between two stems. The fragments missing the bridge were identified through their characteristic mass decrease associated with five Glycine, and change to the hydrophobicity from the missing bridge also changed the retention times of these fragments (Figure 5.3a). This missing bridge would be in the position of the normally unlinked bridge in the fragment, as no further cross-linking can take place on the peptide stem without the bridge and the absence of bridge would terminate the cross-linking at that subunit. While such cross-links between PG stems without a bridge has been observed in other bacteria, they typically have PG stems with either the bridge that is single amino acid long or no bridge at all. The inhomogeneity between the bridge that is the normal five amino acid residues long or not having one would place spatial constraints on the PG lattice structure of *S. aureus* under normal PG biosynthesis, and such lack of bridge would preclude the fragment without a bridge from cross-linking. The maximum number of missing bridges per PG fragment consequently would be restricted to 1 for VRSA4. The proportion of subunits found in fragments lacking the bridge significantly increased in the presence of vancomycin (13.807% ± 1.947% to 26.181% ± 2.859%, $p < 0.001$, $n = 3$) (Figure 5.3b). This suggests that the decrease in the cross-linking efficiency could be attributed to increased frequency of PG stems that

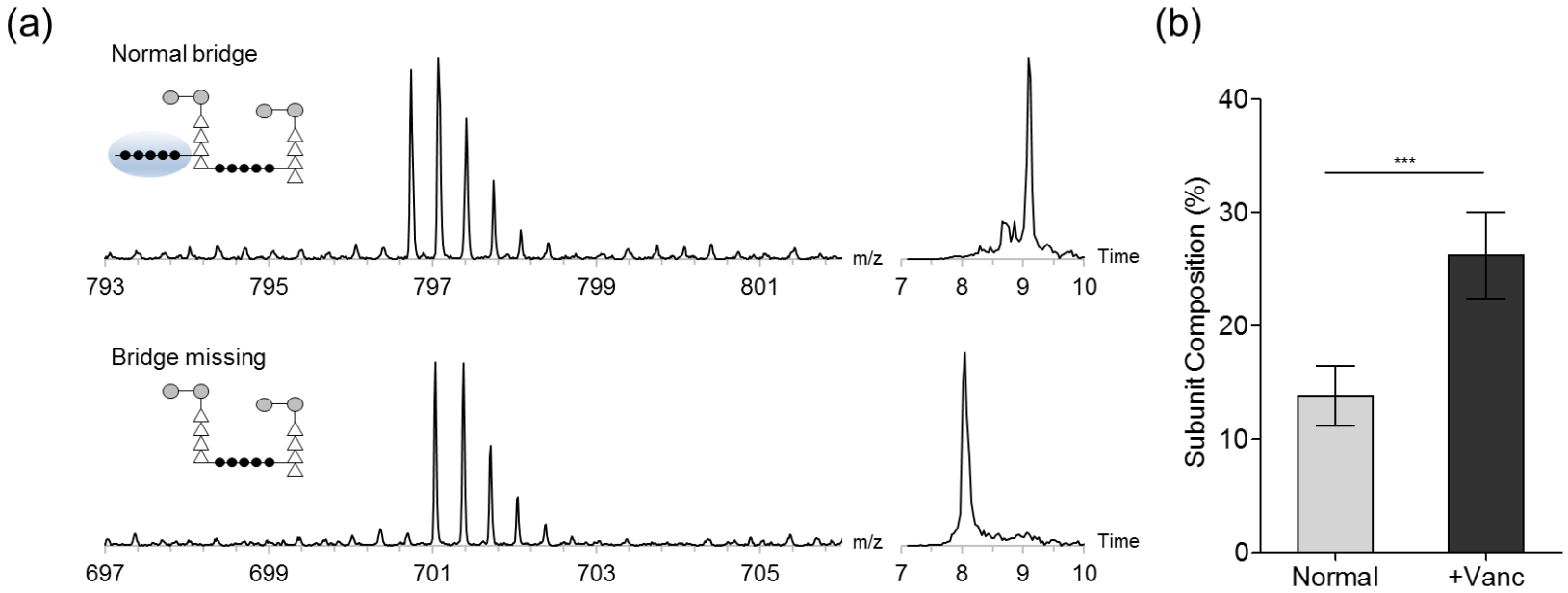

Figure 5.3: Absence of Bridge-link on PG Fragments. (a) Mass spectra and XICs of the standard dimer with the peptide stem length of 4 residues (top) and the equivalent dimer missing the pentaglycine bridge (bottom). Absence of the bridge manifests as decrease in mass of the fragment and chromatographic retention time. (b) Prevalence of missing bridges. With vancomycin, higher proportion of PG subunits are found in fragments without a bridge (26.181% ± 2.859%) compared to the normal condition without vancomycin (13.870% ± 1.947%, $p < 0.001$). p-values were calculated using Student's t-test (*<0.05, **<0.01, ***<0.001). All error bars represent 95% confidence interval (n = 3).

lack the pentaglycine bridge. Relatively high amount of PG subunits that belong to these defective fragments even in the absence of vancomycin hints that vancomycin amplifies an already present issue in the cell wall biosynthesis inherent to VRSA4.

Depsipeptide Substitution and PG Stem

The hallmark of vancomycin resistance conferred through the transposable element *Tn1546* is the presence of D-Ala-D-Lac depsipeptide in place of D-Ala-D-Ala dipeptide on the PG stem, which decreases the binding affinity of vancomycin.[136] This substitution presents itself as a mass increase of one Da arising from the change of a peptide bond to an ester bond between two terminal residues. Through LC-MS, PG fragments with D-Ala-D-Lac substitution can be identified and quantified, as this change leads to a fragment ion that has its peaks shifted by one mass unit equivalent (Figure 5.4a). Substituted fragments also have retention time sufficiently different from unchanged fragments, and this allowed clear quantification of their abundance through integrating their XICs. Overall proportion of depsipeptide substituted PG stems in VRSA 4's cell wall, while low, was nonzero and this proportion increased upon the induction of vancomycin resistance but still remained low (1.146% ± 0.228% to 2.705% ± 0.332%, $p < 0.001$, $n = 3$) (Figure 4b). However, if only the fragments with the terminal PG subunit having the full-length peptide stems that can have the substitution are considered, over quarter of the subunits are part of fragments with the depsipeptide substitution when the vancomycin resistance is induced, a significant increased from the normal condition (2.808% ± 0.448% to 25.917% ± 2.097%, $p < 0.001$, $n = 3$). This high proportion of substituted PG fragments and low overall abundance of these fragments in general may be understood when the change to the peptide stem lengths are considered. In presence

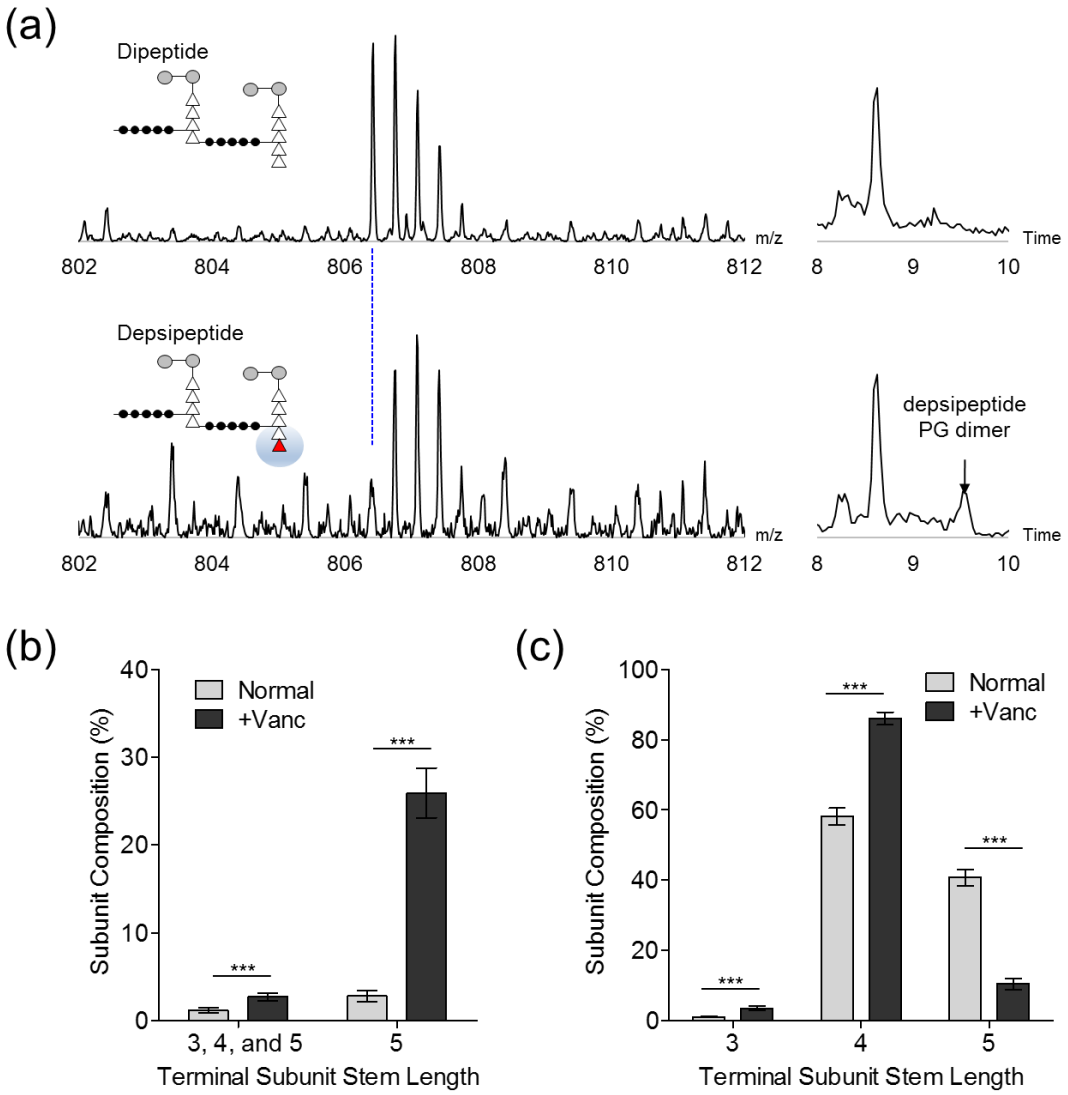

Figure 5.4: D-Ala-D-Lac Substitution and PG Stem Length. (a) Mass spectra and XICs of dimers that have full length terminal PG stems with the normal dipeptide stem ending (top) and depsipeptide substitute ending (bottom). The substitution of D-Ala-D-Ala with D-Ala-D-Lac results in the increase of one Da mass that is apparent as a shift in the isotopic distribution and chromatographic retention time. (b) Depsipeptide substitution frequency. While the overall proportion of PG subunits in fragments with the depsipeptide stem substitution increase only slightly (1.146% ± 0.228% to 2.705% ± 0.332%, $p < 0.001$), overall decrease in the proportion of full length peptide stems results in a significant increase to the proportion of subunits with the substitution (2.808% ± 0.498% to 25.917% ± 2.097%, $p < 0.001$). (c) Terminal PG peptide stem length. Induction of vancomycin resistance decreases the proportion of PG subunits from the fragments with unedited terminal PG peptide stem (40.759% ± 1.725% to 10.442% ± 1.188%). p-values were calculated using Student's t-test (*<0.05, **<0.01, ***<0.001). All error bars represent 95% confidence interval (n = 3).

of vancomycin, the proportion of all subunits from fragments with the terminal PG subunit having stem length of 4 increases (58.164% ± 1.803% to 86.070% ± 1.311%), while those with the stem length of 5 decreases nearly four-fold (40.755% ± 1.752% to 10.442% ± 1.188%) (Figure 5.4c). Thus, in VRSA4 the induction of vancomycin resistance increases the editing of terminal residue from the peptide stem, but remaining full-length stems have much greater chance of having the substitution.

Acetylation State of PG and D-Ala-D-Lac Substitution

One of the more common covalent modifications to the PG of *S. aureus* is a change to the acetylation state of a fragment through O-acetylation of NAM or N-deacetylation of NAG. These alterations to the acetylation state shift to the mass by 42 Da along with the associated hydrophobicity change to the fragment, and modified fragments are thus visible as peaks separated by 42 mass unit equivalent with XICs that show shifted retention times (Figure 5.5a). Of note are the decrease in the proportion of subunits from fragments with acetylation state of +1 (34.458% ± 2.350% to 25.050% ± 3.077%, $p = 0.002$, $n = 3$) and the corresponding increase for those from the acetylation states of 0 and -1 (35.934% ± 1.098% to 42.391% ± 2.490%, $p = 0.002$, $n = 3$, and 11.530% ± 0.038% to 18.802% ± 0.616%, $p < 0.001$, $n = 3$) (Figure 5.5b). These changes results in the average acetylation number per fragment decrease upon induction of vancomycin resistance (0.576 ± 0.010 to 0.305 ± 0.035, $p < 0.001$, $n = 3$). These trends indicate that addition of acetyl groups to PG via O-acetylation either remains constant or decreases upon the activation of vancomycin resistance. At the same time, removal of acetyl groups through N-deacetylation occurs more frequently as seen by

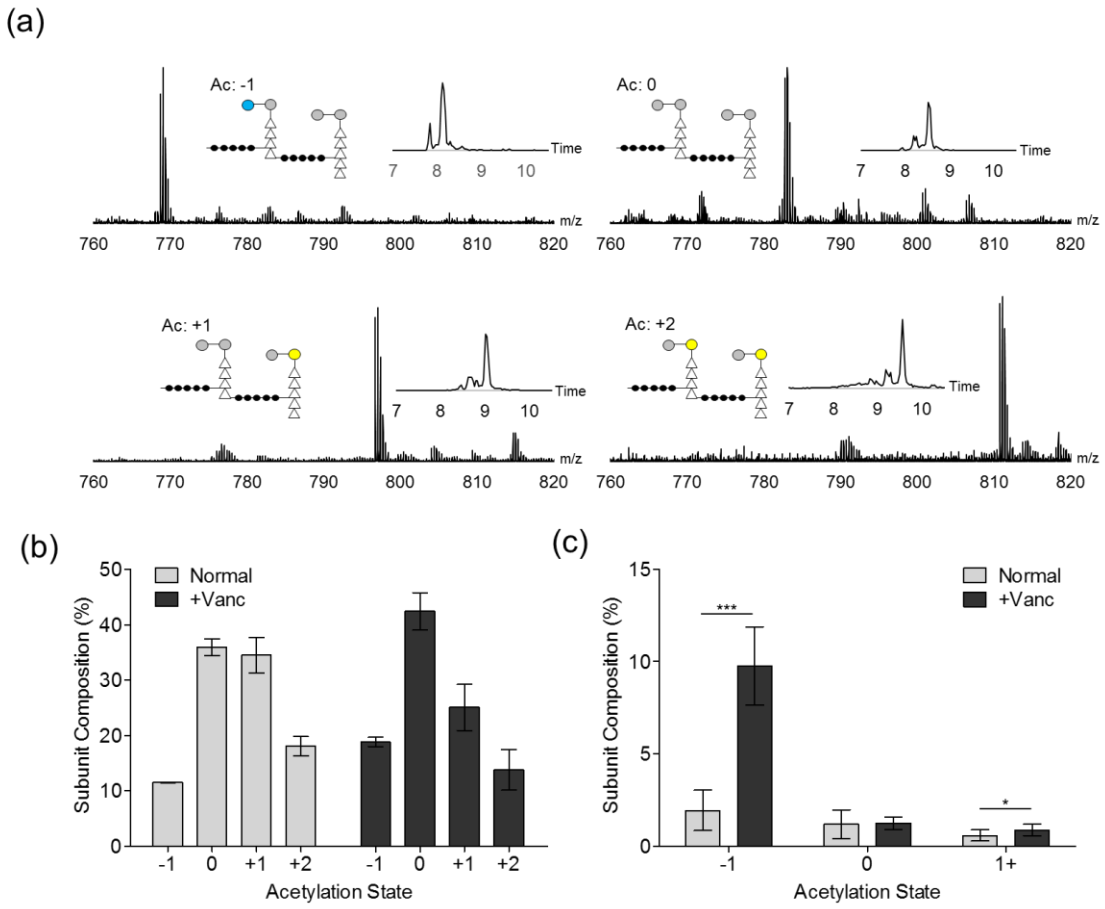

Figure 5.5: Acetylation State of PG and Depsipeptide Substitution. (a) Mass spectra and XICs of dimers with the peptide stem length of 4 residues and different acetylation states. Each increase of the acetylation number adds to mass equivalent of an acetyl group (42 Da) and lengthens the retention time. (b) Distribution of PG with different acetylation states. Addition of vancomycin shifts the distribution towards the lower acetylation state. (c) Proportion of PG with depsipeptide stems. Addition of vancomycin significantly increases the proportion of subunits from depsipeptide substituted PG fragments (1.935% ± 0.808% to 9.771% ± 1.566%, $p < 0.001$). p-values were calculated using Student's t-test (*<0.05, **<0.01, ***<0.001). All error bars represent 95% confidence interval (n = 3).

increase in the proportion of subunits from fragments with acetylation state of -1. Examination of the D-Ala-D-Lac substitution with the acetylation state reveals that N-deacetylation of fragments containing the substitution increases significantly in the presence of vancomycin (1.935% ± 0.808% to 9.771% ± 1.566%, $p < 0.001$, $n = 3$), while proportions of fragments for other acetylation states remain low (Figure 5.5c). This

selective N-deacetylation of the PG fragments with D-Ala-D-Lac ending suggests a link between the acetylation state and vancomycin resistance.

Discussion

Given the ability of VRSA4 to resist the effects of vancomycin at the organism level, it is surprising that the antibiotic nonetheless can still exert influences on the PG composition of the cell wall. The degree of PG cross-linking in *S. aureus* has been determined to be on the higher side, and this may allow VRSA4 to overcome the interference to the cross-linking process from vancomycin and retain its overall cell morphology. But as seen by the increase of defective PG subunits that cannot cross-link due to the lack of pentaglycine bridge, the cell wall of VRSA after the induction of vancomycin resistance most likely has structural differences that may manifest themselves through lower survival fitness under adverse conditions due to changes in the peptidoglycan structure and surface protein attachment.[15, 149] It has been previously demonstrated that vancomycin and β-lactam antibiotics exert synergistic antimicrobial activity even against VRSA.[144-145] Results of this experiment shows that vancomycin's modes of action other than the sequestration of lipid II contributes to its activity, as abolishment of this interaction still allows it to interfere with the PG metabolism. Considering that nearly one eighths of all PG subunits belong to fragments that cannot be further cross-linked even without the induction of vancomycin resistance, addition of vancomycin only exacerbates the problem VRSA4 has in its ability to increase the cross-linking in response to other adverse stimuli. This may leave the cell wall in a potentially vulnerable state against additional antibiotics.

Another factor that may cost VRSA4 in terms of survival fitness may be the partial activity of D-Ala-D-Lac substitution pathway even without the induction of vancomycin resistance. Biosynthesis of D-Ala-D-Lac depsipeptide involves D,D-carboxypeptidase mediated degradation of the D-Ala-D-Ala dipeptide intended for the completion of Park's nucleotide, the PG precursor to which Fem enzymes attach the bridge. Leaky expression of D,D-carboxypeptidase would lead to the bacteria to needlessly synthesize and degrade the dipeptide simultaneously and incur a metabolic cost. Presence of defective PG subunits without the bridge could also be caused by the depsipeptide substitution if the activity of fen enzymes is negatively affected *in vivo* due to Park's nucleotide now having a different chemical structure. Thus, incomplete control over the transposable element responsible for vancomycin resistance may be costing VRSA4 both in terms of metabolism and PG structure. These would reduce VRSA4's survival fitness even before the induction of vancomycin resistance, and further studies of them may help towards determining full consequences of having these antibiotic resistance elements.

Materials and Methods

S. aureus Cell Wall Isolation

Procedure for the cell wall isolation is described elsewhere.[32] An overnight culture of Vancomycin-resistant *Staphylococcus aureus* 4 were first prepared from the frozen stock in trypticase soy broth (TSB), and this culture was used to inoculate 30 mL of TSB with vancomycin added to the final concentration of 6 μg/mL as needed. The cells were grown for 24 hours at 37 degrees with 180 rpm orbital shaking. Grown cells

were harvested through centrifugation at 4750 rpm for 5 minutes (Allegra X-15R, rotor SX4750, Beckman Coulter), resuspended in 2 mL of phosphate buffered saline, and disrupted using a bead-beater (Disruptor Genie, Scientific Industries) with 0.5 mm diameter glass beads at 24°C. Eight cycles of 1 minute disruption separated by 1 minute of rest to prevent overheating of the sample were used. Disrupted cells were separated from glass beads using Steriflip 20 μm nylon net vacuum filtration system (EMD Millipore), followed by centrifugation at 25,000 x g for 3 min at 24°C. The remains of cells were boiled in 2% sodium dodecyl sulfate suspension for 30 minutes, then washed five times with deionized water through centrifugation at 25,000 x g for 3 minutes. The pellet was resuspended in 2 mL of 20 mM Tris buffer, pH 8.0. Two hundred μg of DNase was added to the suspension and the sample incubated for 24 hours at 37°C. Three hundred μg of trypsin was added to the mixture and it was incubated for additional 24 hours at 37°C. The isolated cell wall was pelleted by centrifugation at 100,000 x g for 5 minutes at 24°C and washed with 20 mM Tris pH 8.0 buffer.

Mutanolysin Digestion of S. aureus Cell Wall

The cell wall isolate of *S. aureus* suspended in 2 mL of 20 mM Tris buffer pH 8.0 was first digested using 500 U of mutanolysin (Sigma-Aldrich) at room temperature for 24 hours. 500 U of mutanolysin was then added to the mixture for additional 24 hours of incubation to ensure thorough digestion of the cell wall. Following the mutanolysin digestion, insoluble cell wall fragments were removed by 0.45 μm centrifuge filter (Amicon), and the solubilized PG fraction was collected by filtration through 30 kDa MWCO (Amicon) filter by centrifugation at 14,800 RPM (Thermo Scientific) for 5 minutes. Glycans in mutanolysin-digested muropeptides were reduced by adding sodium

borohydride to the final concentration of 10 mg/mL in 1 mL of borate buffer at pH 9.0. The reduction was carried out at 24°C for 30 minutes and quenched by the addition of 120 µL of 85% phosphoric acid. Cell wall digest was frozen and lyophilized. Lyophilized peptidoglycan samples were cleaned up for mass spectrometry analysis using 100 µL Pierce C18 tips (Thermo Scientific).

Ultra Performance Liquid Chromatography

Waters C18 nanoACUITY Ultra Performance Liquid Chromatography (UPLC) and Waters Synapt G2 High Definition Mass Spectrometer (HDMS) Time-of-Flight (TOF) mass analyzer were used to analyze the mutanolysin-digested peptidoglycan of *S. aureus*. For the UPLC separation, 1 µL of the sample in 50% acetonitrile, 0.1% formic acid was injected to a 5 µL sample loop and loaded onto the column under isocratic condition of 99% buffer A (0.1% formic acid in methanol) and 1 % buffer B (100% acetonitrile) for 1 minute. The separation was carried out by Waters nanoACQUITY reverse-phase C18 BEH column (75 µm X 100 mm, packed with 1.7 µm beads with 130 Å pore size) with C18 nanoACQUITY Symmetry C18 trap column (180 µm X 20 mm, 5 µm beads with 100 Å pore size) by applying a linear gradient to 50% buffer B for 60 min. After each separation, the column was regenerated under isocratic condition with 85% buffer B for 5 minutes, followed by a linear gradient to 98% buffer A for 1 minute, then equilibrated at 98% buffer A for 23 minutes. The flow rate was kept constant at 0.450 µL/min throughout the analysis.

Mass Spectrometry

Eluents were analyzed by Waters Synapt G2 HDMS-TOF mass analyzer operating under positive ion mode. Electrospray ionization (ESI) was performed on the sample with spray voltage of 35 V, and capillary voltage of 3.5 kV. The mass analyzer was optimized for m/z range of 100-2000. Fibrinopeptide B (Glu-Fib) was used as the calibration lock mass for the mass analyzer. MS/MS fragmentation was accomplished through collision-induced dissociation with nitrogen gas at 120°C and 2.00 Bar. The transfer collision and the trap collision energies were 5 V and 30 V, respectively.

LC-MS Data Analysis

Data analysis was carried out using MassLynx (Waters). MATLAB (MathWorks) was used for the calculation of exact masses and isotopic distributions.

Focused Ion Beam SEM

Approximately 100 μL of the bacterial culture were dropped on a microscope coverslip and air dried for 48 hours. The cells were fixed in 2.5% glutaraldehyde solution for 90 minutes, then the solution washed from the cells by submerging the coverslip in 0.06 M sodium phosphate buffer three times for 30 total minutes. The samples were dehydrated through submerging the coverslip in increasing concentrations of 50, 70, 90, and 100% (v/v) ethanol:water mixture for 10 minutes four times at each concentration. The cells were dried using a critical point dryer (EM CPD300, Leica Microsystems, Wetzlar, Germany) by first placing them at 23 degrees and 1 bar carbon dioxide, then vacuum drying for 110 minutes. The coverslip was sputter coated with iridium to the thickness of 20 nm under argon (EM ACE600, Leica Microsystems,

Wetzlar, Germany). The samples were observed using focused ion beam (FIB) scanning electron microscope (Versa 3D, FEI, Hillsboro, OR) with 30 kV electrons at the working distance of 5.0 mm and the spot size of 5.0.

Supplementary Table 5.S1: PG fragment ion matches for VRSA4. c stands for the number of cross-links, Ala for the number of D-Ala and/or D-Lac in the terminal subunit peptide stem, Ac for the acetylation state, Lac for the absence (0) or presence (1) of the depsipeptide substitution, Br for the presence (1) or absence (-1) of the cross-linking bridge, and z for the charge of the ion. mass column shows the calculated mass of each ion at pH 7. Mean Log_{10} area is the average of XIC integrals (n = 3).

c	Ala	Ac	Lac	Br	z	mass	Mean Log_{10} Area
0	0	0	0	-1	1	824.3884	4.3140
0	0	1	0	-1	1	866.3989	4.1839
0	2	0	0	-1	1	966.4626	3.9041
0	2	0	1	-1	1	967.4466	3.6920
0	2	1	0	-1	1	1008.4732	3.8802
0	0	-1	0	0	2	1070.5081	4.3465
0	0	0	0	0	1	1111.5113	3.8935
0	0	1	0	0	1	1153.5219	2.8459
0	0	1	0	0	1	1153.5219	2.8459
0	1	0	0	0	2	1182.5485	3.4154
0	2	-1	0	0	2	1212.5823	3.7724
0	2	-1	1	0	2	1213.5663	4.4567
0	1	1	0	0	2	1224.5590	4.0410
0	2	1	0	0	1	1295.5961	3.7821
0	2	1	0	0	2	1295.5961	4.8113
0	2	1	0	0	2	1295.5961	5.4971
1	1	1	0	-1	2	2100.9667	4.2697
1	1	1	0	-1	3	2100.9667	4.1735
1	2	1	0	-1	2	2172.0038	3.9224
1	2	1	0	-1	3	2172.0038	3.9700
1	1	-1	0	0	2	2305.0758	4.0482
1	1	-1	0	0	3	2305.0758	4.8688
1	1	0	0	0	2	2346.0791	4.9362
1	1	0	0	0	3	2346.0791	5.5339
1	2	-1	0	0	2	2376.1129	3.5342
1	2	-1	0	0	3	2376.1129	4.5548
1	2	-1	1	0	2	2377.0969	3.2732
1	1	1	0	0	3	2388.0896	5.3645
1	1	1	0	0	2	2388.0896	4.9409
1	2	0	0	0	2	2417.1162	4.3895
1	2	0	0	0	3	2417.1162	5.2245
1	2	0	1	0	2	2418.1002	4.0594
1	2	0	1	0	3	2418.1002	4.1849
1	1	2	0	0	3	2430.1002	4.6089
1	2	1	0	0	2	2459.1267	4.3862
1	2	1	0	0	3	2459.1267	4.9824
1	2	1	1	0	2	2460.1108	4.1619
1	2	1	1	0	3	2460.1108	3.9144
1	2	2	0	0	3	2501.1373	4.2470
2	1	0	0	-1	3	3222.4867	4.0487

2	1	1	0	-1	3	3264.4973	4.7039
2	1	2	0	-1	3	3306.5078	4.9700
2	2	1	0	-1	3	3335.5344	4.5291
2	2	2	0	-1	3	3377.5449	5.0607
2	1	-1	0	0	3	3468.6064	5.1843
2	1	-1	0	0	4	3468.6064	4.6562
2	1	0	0	0	3	3509.6097	5.6848
2	1	0	0	0	4	3509.6097	5.0185
2	2	-1	0	0	4	3539.6435	4.5574
2	1	1	0	0	3	3551.6202	5.5503
2	1	1	0	0	4	3551.6202	4.7846
2	2	0	0	0	4	3580.6468	4.7908
2	2	0	0	0	3	3580.6468	5.4847
2	1	2	0	0	3	3593.6308	4.8734
2	1	2	0	0	4	3593.6308	4.4253
2	2	1	0	0	4	3622.6574	4.6724
2	2	1	0	0	3	3622.6574	5.3336
2	2	2	0	0	4	3664.6679	3.9426
2	2	2	0	0	3	3664.6679	4.7571
3	1	2	0	-1	4	4470.0384	5.4881
3	2	1	0	-1	4	4499.0650	4.7255
3	2	2	0	-1	4	4541.0756	5.3981
3	0	0	0	0	4	4602.1032	4.0898
3	1	-1	0	0	4	4632.1370	5.2839
3	1	0	0	0	4	4673.1403	5.7479
3	1	0	0	0	3	4673.1403	4.7292
3	2	-1	0	0	4	4703.1741	5.0483
3	2	-1	0	0	4	4703.1741	5.1102
3	1	1	0	0	4	4715.1509	5.6513
3	1	1	0	0	3	4715.1509	4.7851
3	2	0	0	0	4	4744.1774	5.5648
3	1	2	0	0	4	4757.1614	5.4529
3	2	1	0	0	4	4786.1880	5.4474
3	2	2	0	0	4	4828.1985	4.7698

Supplementary Table 5.S2: PG fragment ion matches for VRSA4 with vancomycin added. c stands for the number of cross-links, Ala for the number of D-Ala and/or D-Lac in the terminal subunit peptide stem, Ac for the acetylation state, Lac for the absence (0) or presence (1) of the depsipeptide substitution, Br for the presence (1) or absence (-1) of the cross-linking bridge, and z for the charge of the ion. mass column shows the calculated mass of each ion at pH 7. Mean Log_{10} area is the average of XIC integrals (n = 3).

c	Ala	Ac	Lac	Br	z	mass	Mean Log_{10} Area
0	0	0	0	-1	1	824.3884	4.5464
0	0	1	0	-1	1	866.3989	4.6465
0	1	0	0	-1	1	895.4255	4.0298
0	2	0	1	-1	1	967.4466	3.7895
0	0	0	0	0	1	1111.5113	4.4567
0	0	1	0	0	1	1153.5219	2.4778
0	2	-1	0	0	2	1212.5823	4.4979
0	2	-1	1	0	2	1213.5663	4.7594
0	1	1	0	0	1	1224.5590	4.2224
0	1	1	0	0	2	1224.5590	4.5023
0	2	1	0	0	1	1295.5961	3.0917
0	2	1	0	0	2	1295.5961	4.8715
0	2	1	0	0	2	1295.5961	4.0503
0	2	1	1	0	2	1296.5801	3.1749
1	1	0	0	-1	2	2058.9561	3.6643
1	1	0	0	-1	3	2058.9561	3.8175
1	1	1	0	-1	2	2100.9667	4.5516
1	1	1	0	-1	3	2100.9667	4.4829
1	2	0	0	-1	3	2129.9932	3.3211
1	2	0	1	-1	3	2130.9772	3.4675
1	2	1	0	-1	2	2172.0038	3.4846
1	2	1	0	-1	3	2172.0038	3.6065
1	2	1	1	-1	3	2172.9878	3.5225
1	1	-1	0	0	3	2305.0758	4.8923
1	1	0	0	0	3	2346.0791	5.4532
1	1	0	0	0	2	2346.0791	4.8574
1	2	-1	0	0	3	2376.1129	3.8860
1	1	1	0	0	3	2388.0896	4.8028
1	1	1	0	0	2	2388.0896	4.7479
1	2	0	0	0	2	2417.1162	3.9029
1	2	0	0	0	3	2417.1162	4.3149
1	2	0	1	0	3	2418.1002	3.8590
1	1	2	0	0	3	2430.1002	3.5205
1	2	1	0	0	3	2459.1267	4.2437
1	2	1	1	0	3	2460.1108	3.7615
2	1	0	0	-1	3	3222.4867	4.6088
2	1	1	0	-1	3	3264.4973	4.9314
2	1	2	0	-1	3	3306.5078	5.2876
2	1	-1	0	0	4	3468.6064	4.5480
2	1	-1	0	0	3	3468.6064	5.1453

2	1	0	0	0	3	3509.6097	5.5069
2	1	0	0	0	4	3509.6097	4.8072
2	2	-1	0	0	3	3539.6435	4.3204
2	1	1	0	0	3	3551.6202	4.9070
2	1	1	0	0	4	3551.6202	4.0024
3	1	1	0	-1	4	4428.0279	4.8742
3	1	2	0	-1	4	4470.0384	5.3646
3	1	-1	0	0	4	4632.1370	5.2474
3	1	0	0	0	4	4673.1403	5.5795
3	1	0	0	0	3	4673.1403	4.4366
3	2	-1	0	0	4	4703.1741	4.5874
3	1	1	0	0	4	4715.1509	5.1045

CHAPTER SIX

Inhibition of *Staphylococcus aureus* Cell Wall Biosynthesis by Desleucyl-oritavancin: a Quantitative Peptidoglycan Composition Analysis by Mass Spectrometry

Abstract

Oritavancin is a lipoglycopeptide antibiotic that exhibits potent activities against vancomycin-resistant Gram-positive pathogens. The chemical structure of oritavancin is similar to that of vancomycin, but differs by a hydrophobic side chain attached to the drug disaccharide. This hydrophobic side chain of oritavancin forms a secondary-binding site that enables the drug binding to the cross-linked peptidoglycan-bridge structures in cell wall. Oritavancin's mode of action from its secondary-binding site was investigated using liquid chromatography-mass spectrometry (LC-MS) by measuring the changes in the peptidoglycan composition of mutanolysin-digested isolated cell walls from *Staphylococcus aureus* grown in presence of desleucyl-oritavancin. Desleucyl-oritavancin is an Edman degradation product of oritavancin with a damaged D-Ala-D-Ala binding site. Unlike the Edman degradation product of vancomycin, which is devoid of any activity, desleucyl-oritavancin retains potent antibacterial activities due to its secondary-binding site. Accurate quantitative peptidoglycan composition analysis based on 83 muropeptide ions by LC-MS provided new insight into the potent mechanism of action mediated by the secondary-binding site in oritavancin, where desleucyl-oritavancin treated *S. aureus* exhibit peptidoglycan with reduced cross-linking, altered stem modifications, decreased *O*-acetylation, and increased *N*-deacetylation. These changes

suggest that desleucyl-oritavancin targeted peptidoglycan templates and induced disorder in the cell wall to prevent cross-linking and to interfere with PG maturation.

Importance

Oritavancin, a lipoglycopeptide antibiotic, has a secondary-binding site for peptidoglycan in addition to its primary D-Ala-D-Ala binding site. Even after the loss of its primary-binding site through Edman degradation, the resulting antibiotic desleucyl-oritavancin exhibits potent antimicrobial activities through its still functioning secondary-binding site that targets the cross-linked peptidoglycan bridge structure in the cell wall. In this study, we characterize the mode of action for desleucyl-oritavancin's secondary-binding site using LC-MS. Quantitative peptidoglycan composition analysis of desleucyl-oritavancin treated *S. aureus* was performed by determining the relative abundances of 83 muropeptide ions matched from pre-calculated library through integrating extracted ion chromatograms. Our work highlights the use of quantitative peptidoglycan composition analysis by LC-MS to provide insights into changes to the cell wall peptidoglycan in *S. aureus* as a result of antibiotic treatment.

Introduction

Oritavancin is a potent lipoglycopeptide antibiotic with activity against multi-drug resistant Gram-positive pathogens such as vancomycin-resistant enterococci (VRE), methicillin-resistant *Staphylococcus aureus*, vancomycin-intermediate resistant *S. aureus*, and vancomycin-resistant *S. aureus* (VRSA).[150-152] Like vancomycin, oritavancin binds to the D-Ala-D-Ala of the peptidoglycan (PG) stem (Fig. 6.1a) in lipid II to inhibit the transglycosylation step of PG biosynthesis (Fig. 6.1b). By binding to lipid II, oritavancin

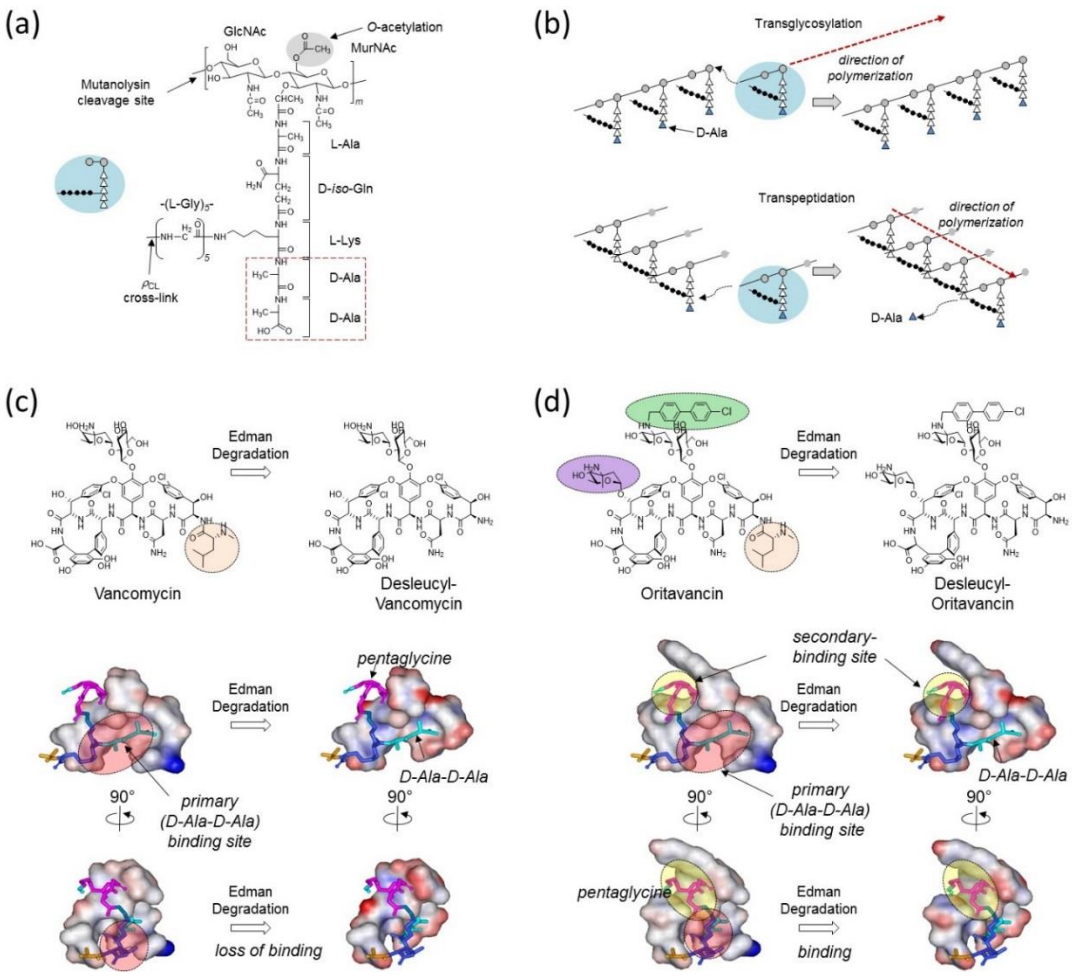

Figure 6.1: Peptidoglycan structure and biosynthesis. (a) Chemical structure of a *S. aureus* peptidoglycan (PG) repeat unit. A single repeat unit consists of a disaccharide (GlcNAc and MurNAc), pentapeptide stem (L-Ala-D-iso-Gln-L-Lys-D-Ala-D-Ala), and pentaglycine-bridge structure. Mutanolysin cleaves the $\beta_{1\text{-}4}$ glycosidic linkage between MurNAc and GlcNAc. D-Ala-D-Ala terminus of the PG-repeat unit (red box) is the primary binding site for vancomycin. The figure inset shows a schematic representation of a PG-repeat unit, with the disaccharide as gray-filled circles, amino acids in the pentapeptide stem as open triangles, and the pentaglycine bridge as filled circles. (b) PG polymerization through two distinct steps with different enzymes. First, transglycosylase elongates the disaccharide glycan chain. Transpeptidase then interconnects resulting glycan chains by forming cross-links between the N-terminus of pentaglycine bridge from one PG-unit to the penultimate D-Ala of PG stem from a neighboring glycan chain. The terminal D-Ala (blue triangle) is removed by the transpeptidase during cross-linking. (c) Chemical structures and space-filling models of vancomycin (left) and desleucyl-vancomycin (right) bound to PG. In space-filling models, D-Ala-D-Ala dipeptide is shown as a stick colored in light blue, D-iso-Gln and L-Lys in dark blue, and pentaglycine in magenta. Edman degradation of vancomycin cleaves the *N*-methylleucine (highlighted circle) and results in desleucyl-vancomycin with the damaged D-Ala-D-Ala binding site, which abolishes the antibacterial activity. (d) Chemical structures and space-filling models of oritavancin (left) and desleucyl-oritavancin (des-Ori) (right) bound to PG. Edman degradation of oritavancin results in des-Ori, which still exhibits potent antibacterial activity despite the damaged D-Ala-D-Ala binding site (red circle) due to its secondary-binding site (yellow circle). Secondary-binding site targeting the PG pentaglycine bridge structure is formed by the hydrophobic side chain of oritavancin and the aglycon structure.

prevents the transfer of PG-repeat units from lipid II to the growing nascent PG, which results in cytoplasmic accumulation of a PG precursor Park's nucleotide.[74, 109] In VRE and VRSA, the D-Ala-D-Ala terminus of PG stem is replaced by a depsipeptide D-Ala-D-Lac. This depsipeptide substitution reduces the vancomycin-binding affinity by replacing one of the five hydrogen bonds with an electrostatic repulsion.[49] While this change renders vancomycin ineffective against VRE and VRSA[49, 89], oritavancin retains its potent bactericidal activities against these vancomycin-resistant pathogens.[150-152]

The chemical structure of oritavancin differs from that of vancomycin (Fig. 6.1c-d) by an alkylation of a chlorobenzylphenyl side chain (green) to the 4-*epi*-vancomsamine on the fourth amino acid, and an additional 4-*epi*-vancomsamine (purple) at the sixth amino acid of the aglycon. Since oritavancin readily forms dimer in solution and binds to membrane vesicles,[57] drug dimerization and membrane anchoring mediated by the hydrophobic side chain of oritavancin is thought to increase its binding to the D-Ala-D-Lac terminated PG-stem structure to overcome the vancomycin resistance in VRE.[153] However, *in situ* characterizations of oritavancin's[154] and oritavancin-like glycopeptides'[21, 74, 79] binding sites in intact cells of *S. aureus* by solid-state NMR have shown that lipoglycopeptides do not bind to PG as dimers nor partition to bacterial membrane. The only instance of oritavancin's hydrophobic side chain found anchored to the lipid bilayer occurs when it is complexed to an isolated protoplast membrane of *S. aureus*. In isolated protoplast membrane, nascent PG strands that surround the cytoplasmic membrane are disrupted and extend away from the membrane. This perturbed PG arrangement exposes the lipid bilayer and permits oritavancin binding to the membrane.[20]

A model structure of oritavancin bound to a PG-repeat unit based on solid-state NMR distance constraints[55, 74] is shown in Fig. 6.1d. The model provides structural insights into the role of oritavancin's hydrophobic side chain. Two distinct binding sites are visible in the model: i) the primary-binding site, which is the aglycon structure identical to that of vancomycin for the binding of D-Ala-D-Ala,[155] and ii) the secondary-binding site which is a cleft formed between the hydrophobic side chain and the aglycon structure that targets the cross-linked PG bridge structure in the cell wall.[74] To only investigate the mode of action from the secondary-binding site, the primary-binding site was removed through Edman degradation by cleaving *N*-methlylleucine from the aglycon structure. Unlike the Edman degradation product of vancomycin des-*N*-methylleucyl-vancomycin (Fig. 6.1c), which is devoid of any antimicrobial activities, des-*N*-methylleucyl-oritavancin (referred to as des-Ori hereafter) still retains potent antimicrobial activities against both vancomycin-susceptible and resistant pathogens.[74] Thus the secondary-binding site in des-Ori is responsible for enhanced activities against vancomycin-resistant pathogens by compensating for the damaged D-Ala-D-Ala binding site, and it enables des-Ori to bind to the PG in intact whole cells of *S. aureus*.[74, 109] In this report, we investigate mode of action of the secondary-binding site in des-Ori by analyzing changes to the PG composition of *S. aureus* grown in presence of des-Ori at subminimal inhibitory concentration (sub-MIC) using liquid chromatography-mass spectrometry (LC-MS).

Results

Inhibition of S. aureus Growth by Desleucyl-oritavancin

Des-Ori was added to *S. aureus* (ATCC 6538P) during the mid-exponential growth (optical density of 600 nm at 0.6) to final drug concentrations of 0, 1, 5, 10, 15, and 20 μg/mL (Fig. 6.2a, dotted line). Despite the damaged D-Ala-D-Ala binding site, des-Ori inhibited the growth of *S. aureus* cultures. Concentration dependent inhibition of *S. aureus* growth is shown in Fig. 6.2b by plotting the amount of growth as measured by OD_{600} of cultures 100 min post des-Ori addition as a function of increasing des-Ori concentrations. Growth recovery is shown in Fig. 6.2c by plotting the time required for the resumption of growth by measuring the interval between des-Ori addition and the inflection point of the growth curve indicative of growth recovery, as a function of des-Ori concentration.

Identification and Quantification of Muropeptide Species

LC-MS analysis was performed on muropeptide fragments from isolated cell walls of *S. aureus* grown for 100 min in the presence of des-Ori at 10 μg/mL (Fig. 6.2, arrow). Muropeptide fragments were generated by digesting isolated cell walls with mutanolysin, a *N*-acetylmuramidase that cleaves the β(1-4) glycosidic bond between MurNAc and GlcNAc of PG. Resulting fragments were analyzed using LC-MS, where identification of PG fragments were made by matching the observed m/z values of each muropeptide fragments against the library of calculated m/z values generated *in silico* based on chemical formulas of all expected muropeptide fragments.[52] Quantification of each muropeptide species' relative abundance was carried out through integrating the

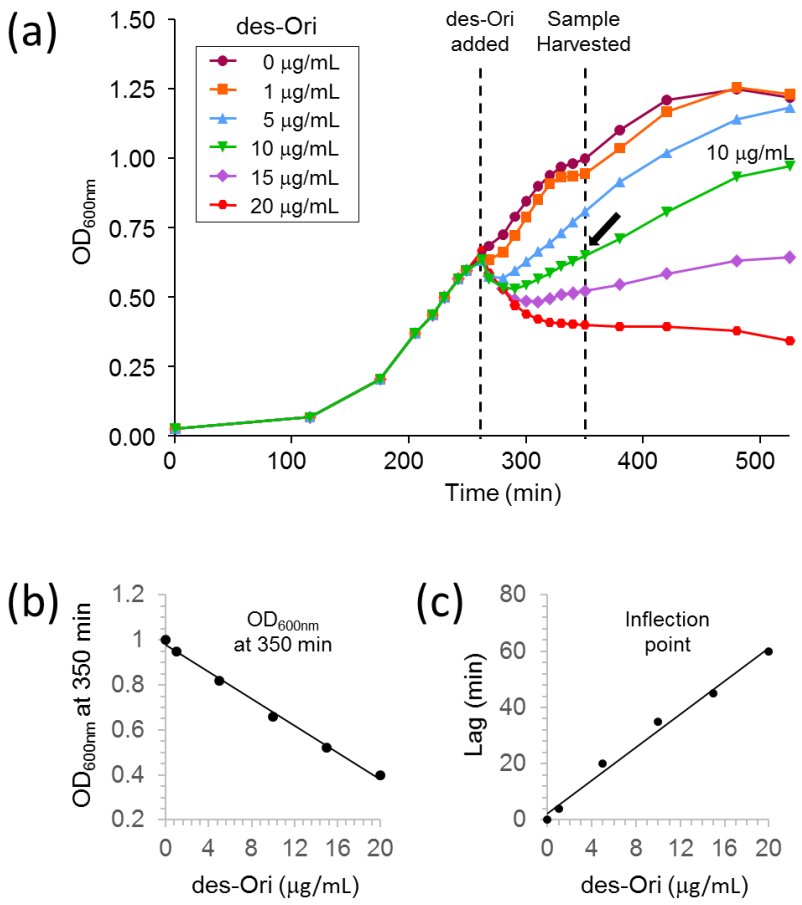

Figure 6.2: *S. aureus* growth in the presence of desleucyl-oritavancin. (a) The growth curve of *S. aureus* (ATCC 6538P) in the presence of des-Ori monitored by measuring the optical density at 600 nm (OD_{600}). Des-Ori was added to *S. aureus* at OD_{600} 0.6, and the cells were harvested after 100 min of growth in presence of des-Ori. The cell walls of *S. aureus* were synthesized in presence of des-Ori at concentrations of 0, 1, 5, 10, 15, and 20 µg/mL during mid-exponential growth (Fig. 6.2a, dotted line). Following the des-Ori addition, *S. aureus* exhibited concentration dependent growth inhibition as determined by i) the OD_{600} measurements after 100 min of growth in presence of des-Ori (Fig. 6.2b), and ii) the time delay to the point of inflection that indicate the recovery of growth (Fig. 6.2c).

extracted ion chromatogram (XIC) for selected ion species and calculating the proportion of each ion species in respect to the sum of all ion species. This approach differs from earlier approaches based on the integration of the UV absorption of chromatographically resolved peaks, where the assumption that each peak consists of a single muropeptide type is necessary. However, every elution peak during the chromatographic separation contained multiple muropeptide species due to the extraordinary chemical diversity that

resulted from various modifications to PG. This limitation was overcome through the use of XIC, which allowed extracting the integral of single ions from the total ion chromatogram and provided accurate quantification of muropeptide species with overlapping elution times. Of 960 unique muropeptide-derived ions generated for the *in silico* library, 83 muropeptide ions with masses ranging from 937 Da (monomer) to 4,870 Da (tetramer) were identified. Figure 3a provides all identified muropeptide species with the associated PG modifications and their relative abundance as measured in percent composition in isolated cell walls of *S. aureus* grown in absence or presence of des-Ori (10 μg/mL). PG modifications on the muropeptide fragments considered varying numbers of cross-links (Fig. 6.3c), *O*-acetylation and *N*-deacetylation (Fig. 6.3d), PG-stem alanylation (Fig. 6.3e), and PG cross-linker bridge attachment (Fig. 6.3f).

Des-Ori's Effects on PG Cross-link

The PG cross-linking efficiency (ρ_{CL}) and average cross-linking per muropeptide ($\overline{\rho_{CL}}$) for mutanolysin digested isolated cell walls of *S. aureus* were calculated based on equations shown in Fig. 6.3b. The cross-linking efficiency is the percent of cross-links per PG-subunit, while the average cross-linking per muropeptide is the average number of cross-links found per muropeptide fragment. The summation element $k_{i,j,l,m,n,}$ in equations shown in Fig. 6.3b represents the corrected integral of an ion's abundance for the muropeptide it was derived from with selected modifications as listed in Fig. 6.3a. First index of summation "*i*" is defined as the number of PG-repeat units found per muropeptide fragment (Fig. 6.3c). The summation was truncated after $i = 4$ due to the low abundance of oligomeric species greater than tetramers. Index of summation "*j*"

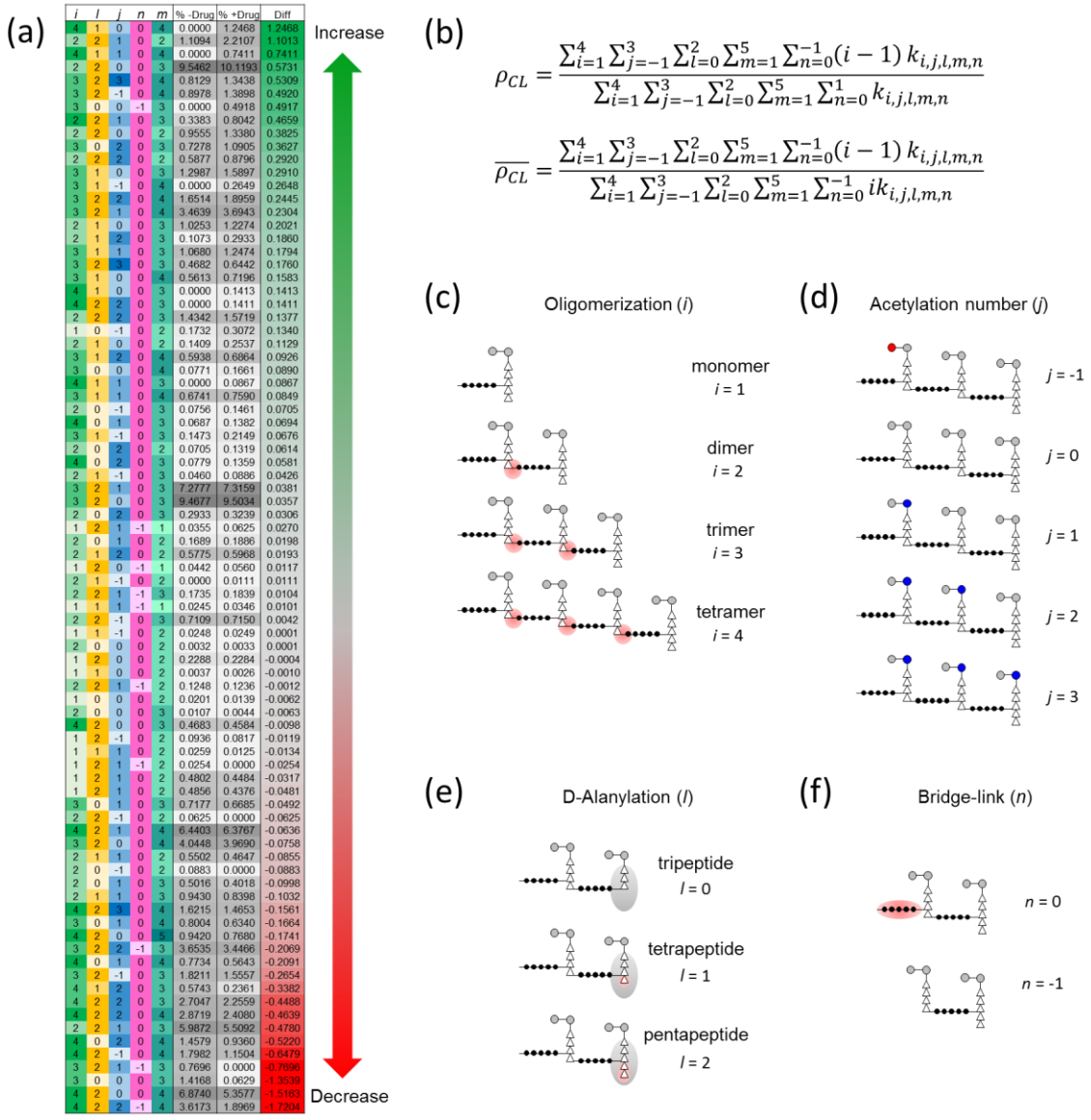

i	*l*	*j*	*n*	*m*	% -Drug	% +Drug	Diff
4	1	0	0	4	0.0000	1.2468	1.2468
2	2	1	0	2	1.1094	2.2107	1.1013
4	1	1	0	4	0.0000	0.7411	0.7411
2	2	0	0	3	9.5462	10.1193	0.5731
3	2	3	0	4	0.8129	1.3438	0.5309
3	2	-1	0	4	0.8978	1.3898	0.4920
3	0	0	-1	3	0.0000	0.4918	0.4917
2	2	1	0	3	0.3383	0.8042	0.4659
2	2	0	0	2	0.9555	1.3380	0.3825
3	0	2	0	3	0.7278	1.0905	0.3627
2	2	2	0	2	0.5877	0.8796	0.2920
3	1	0	0	3	1.2987	1.5897	0.2910
3	1	-1	0	4	0.0000	0.2649	0.2648
3	2	2	0	4	1.6514	1.8959	0.2445
3	2	1	0	4	3.4639	3.6943	0.2304
2	1	0	0	3	1.0253	1.2274	0.2021
2	1	2	0	3	0.1073	0.2933	0.1860
3	1	1	0	3	1.0680	1.2474	0.1794
3	2	3	0	3	0.4682	0.6442	0.1760
3	1	0	0	4	0.5613	0.7196	0.1583
4	1	0	0	3	0.0000	0.1413	0.1413
4	2	2	0	3	0.0000	0.1411	0.1411
2	2	2	0	3	1.4342	1.5719	0.1377
1	0	-1	0	2	0.1732	0.3072	0.1340
2	1	0	0	2	0.1409	0.2537	0.1129
3	1	2	0	4	0.5938	0.6864	0.0926
3	0	0	0	4	0.0771	0.1661	0.0890
4	1	1	0	3	0.0000	0.0867	0.0867
3	1	1	0	4	0.6741	0.7590	0.0849
2	0	-1	0	3	0.0756	0.1461	0.0705
4	0	1	0	3	0.0687	0.1382	0.0694
3	1	-1	0	3	0.1473	0.2149	0.0676
2	0	2	0	2	0.0705	0.1319	0.0614
4	0	2	0	3	0.0779	0.1359	0.0581
2	1	-1	0	3	0.0460	0.0886	0.0426
3	2	1	0	3	7.2777	7.3159	0.0381
3	2	0	0	3	9.4677	9.5034	0.0357
2	0	2	0	3	0.2933	0.3239	0.0306
1	2	1	-1	1	0.0355	0.0625	0.0270
2	0	1	0	2	0.1689	0.1886	0.0198
2	1	2	0	2	0.5775	0.5968	0.0193
1	2	0	-1	1	0.0442	0.0560	0.0117
2	1	-1	0	2	0.0000	0.0111	0.0111
2	2	1	-1	3	0.1735	0.1839	0.0104
1	1	1	-1	1	0.0245	0.0346	0.0101
2	2	-1	0	3	0.7109	0.7150	0.0042
1	1	-1	0	2	0.0248	0.0249	0.0001
2	0	0	0	2	0.0032	0.0033	0.0001
1	2	0	0	2	0.2288	0.2284	-0.0004
1	1	0	0	2	0.0037	0.0026	-0.0010
2	2	1	-1	2	0.1248	0.1236	-0.0012
1	0	0	0	2	0.0201	0.0139	-0.0062
2	0	0	0	3	0.0107	0.0044	-0.0063
4	2	0	0	3	0.4683	0.4584	-0.0098
1	2	-1	0	2	0.0936	0.0817	-0.0119
1	1	1	0	2	0.0259	0.0125	-0.0134
1	2	1	-1	2	0.0254	0.0000	-0.0254
1	2	1	0	2	0.4802	0.4484	-0.0317
1	2	1	0	2	0.4856	0.4376	-0.0481
3	0	1	0	3	0.7177	0.6685	-0.0492
2	2	-1	0	2	0.0625	0.0000	-0.0625
4	2	1	0	4	6.4403	6.3767	-0.0636
3	2	0	0	4	4.0448	3.9690	-0.0758
2	1	1	0	2	0.5502	0.4647	-0.0855
2	0	-1	0	2	0.0883	0.0000	-0.0883
2	0	1	0	3	0.5016	0.4018	-0.0998
2	1	1	0	3	0.9430	0.8398	-0.1032
4	2	3	0	4	1.6215	1.4653	-0.1561
3	0	1	0	4	0.8004	0.6340	-0.1664
4	2	0	0	5	0.9420	0.7680	-0.1741
3	2	2	-1	3	3.6535	3.4466	-0.2069
4	0	1	0	4	0.7734	0.5643	-0.2091
3	2	-1	0	3	1.8211	1.5557	-0.2654
4	1	2	0	3	0.5743	0.2361	-0.3382
4	2	2	0	3	2.7047	2.2559	-0.4488
4	2	2	0	4	2.8719	2.4080	-0.4639
2	2	1	0	3	5.9872	5.5092	-0.4780
4	0	2	0	4	1.4579	0.9360	-0.5220
4	2	-1	0	4	1.7982	1.1504	-0.6479
3	2	1	-1	3	0.7696	0.0000	-0.7696
3	0	0	0	3	1.4168	0.0629	-1.3539
4	2	0	0	4	6.8740	5.3577	-1.5163
4	2	2	-1	4	3.6173	1.8969	-1.7204

Figure 6.3: *S. aureus* peptidoglycan fragment ions examined and their relative abundances. (a) Each row shows a unique ion and its properties by column: "*i*" (green) for the number of PG-repeat unit in the muropeptide, "*l*" (yellow) for the number of D-Ala in the terminal peptide stem, "*j*" (blue) for the acetylation state of the fragment, "*n*" (pink) for the presence of cross-linking pentaglycine bridge at the terminal subunit, and "*m*" (teal) for the charge state of the ion. The columns "*% -Drug*" and "*% +Drug*" list the average relative abundances of each ion in percentages to all the ions being examined for *S. aureus* in absence and presence of des-Ori (n = 3). The column "*Diff*" shows the difference between average relative abundances for with and without the antibiotic. (b) Calculated PG cross-linking efficiency (ρ_{CL}) and average cross-linking per muropeptide ($\overline{\rho_{CL}}$). The summation element $k_{i,j,l,m,n,}$ represents the integrals of ion's abundance for a muropeptide as listed in Fig. 6.3a. Schematic representations of muropeptide fragments based on the number of PG-repeat unit (c), acetylation (d), D-alanylation (e), and bridge-link attachment (f). Index of summation "*i*" is the number of PG-repeat unit found in a muropeptide (d), "*j*" the PG acetylation state (d), "*l*" the D-alanylation of the PG stem (e), "*m*" the charge state of muropeptide ions, and "*n*" the a pentaglycine bridge attachment (f).

represents the PG acetylation ranging from -1 to 3 (Fig. 6.3d). Index of summation "*l*" is the number of D-Ala remaining in the PG stem ranging from 0 (tripeptide stem) to 2 (pentapeptide stem) (Fig. 6.3e). Index of summation "*m*" is the charge state of muropeptide ions from +1 to +5. Index of summation "*n*" represents muropeptides with (0) or without (-1) a pentaglycine bridge structure on the terminal PG subunit (Fig. 6.3f).

Figure 6.4a shows the mass spectra of unmodified PG monomer, dimer, trimer and tetramer, and their associated extracted ion chromatograms (figure inset) from the mutanolysin digested cell walls of untreated *S. aureus*. Calculated cross-linking efficiency (ρ_{CL}) for *S. aureus* grown in the absence of antibiotic was 63.32 ± 0.51%, which was reduced to 62.99 ± 0.23% when grown in the presence of des-Ori at sub-MIC (Fig. 6.4b). Calculated average cross-linking per muropeptide ($\overline{\rho_{CL}}$) for *S. aureus* grown in the absence of antibiotic of 1.987 ± 0.031 was reduced to 1.938 ± 0.005 (±: 95% confidence interval, p = 0.078) for the culture grown in the presence of des-Ori.

The concentration of added des-Ori at 10 μg/mL during mid-exponential growth is at sub-MIC as shown in Fig. 6.2, as des-Orit treatment at that concentration allowed *S. aureus* to recover growth. Although the overal change in the cross-linking efficiency of des-Orit treated *S. arueus* is relatively small, des-Ori still significantly altered the PG composition. The full extent of this effect to the cross-linking efficiency at sub-MIC is revealed by detailed quantitative peptidoglycan composition analysis, where selective increases in peptidoglycan monomers and dimers are accompanied by simultaneous decreases in trimers and tetramers (Supplementary Fig. 6.S1), which is consistent with the inhibition of transpeptidase activity by des-Orit.

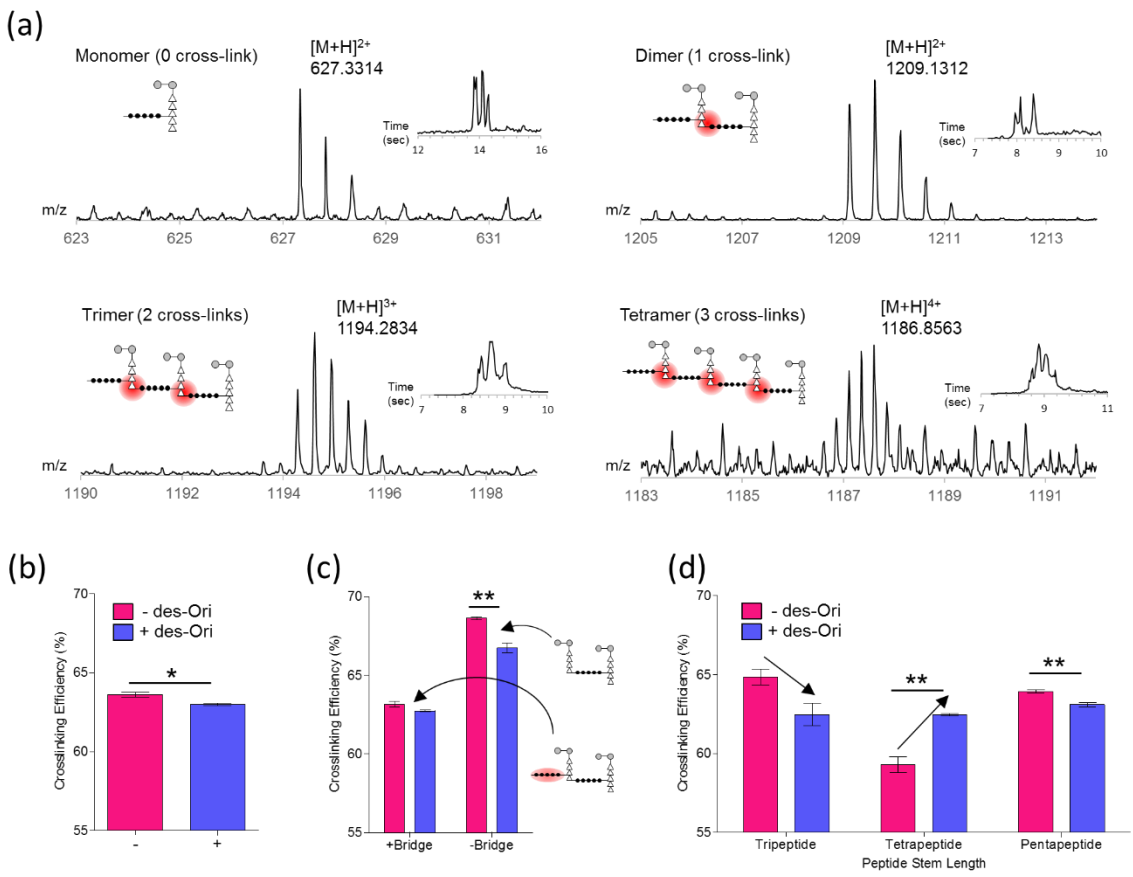

Figure 6.4: Inhibition of the transpeptidation step of peptidoglycan biosynthesis in *S. aureus* from desleucyl-oritavancin. (a) Mass spectra of PG monomer, dimer, trimer and tetramer from mutanolysin digested cell walls of untreated *S. aureus*. Corresponding extracted ion chromatograms and schematic representations of the muropeptide structure are shown as figure insets. Cross-links are highlighted by red circles. (b) Calculated PG cross-linking efficiencies (ρ_{CL}) for *S. aureus* grown in absence (-) and presence (+) of desleucyl-oritavancin at 10 μg/mL (* p = 0.0238). (c) Cross-linking efficiencies and absence of pentaglycine cross-linking bridge. (d) Terminal PG stem lengths and cross-linking efficiency. All error bars represent standard errors of mean (n = 3). Unpaired Student's t-test was used to calculate p-values (* $p < 0.05$, ** $p < 0.01$).

Des-Ori's Effects on PG Bridge-link

More pronounced transpeptidase inhibition activity by des-Ori is observed when cross-linking efficiencies are calculated for the muropeptide fragments based on the bridge-link attachment at the donor PG-stem. Figure 6.4c shows the calculated cross-linking efficiencies for muropeptides with or without the terminal pentaglycine-bridge structure from isolated cell walls of *S. arueus* grown in the absence (red) or in the

presence of des-Ori (blue), with schematic representations of PG dimers shown as figure inset. For *S. arueus* grown in the absence of des-Ori, the cross-linking efficiency for muropeptides without the terminal bridge structure (69%) is higher than that of muropetides with the bridge (63%). Higher degree of cross-linking for the muropeptides without the bridge indicates that these muropeptides are associated with highly cross-linked regions of the cell wall. With the addition of des-Ori, cross-linking efficiencies are reduced for both muropeptides with and without the terminal pentaglycine-bridge structure. However, greater degree of reduction in cross-linking is observed for the muropeptides without the bridge, which is reduced from 69% to 67% when bacteria are grown in presence of des-Ori.

Des-Ori's Effects on PG-stem Length

The change in cross-linking efficiency was further characterized in relation to the PG-stem length (Supplementary Table 6.S1). The PG stems in cell wall are modified by sequential cleaveage of D-Ala-D-Ala by D,D-, and L,D-carboxypeptidases. For untreated *S. aureus*, the cross-linking efficiency for muropeptides with a tripeptide stem was 65%, which is higher than that of muropeptides with a tetrapeptide stem (59%) (Fig. 6.4d). This indicates high L,D-carboxypeptidase activity associated with the cross-linked PG in matured cell wall.[156] But when *S. arueus* are grown in the presence of des-Ori, the cross-linking efficiency for the muropeptides with a tripeptide stem decreases while the efficiency increases for the muropeptides with a tetrapeptide PG-stem. This results suggest that des-Ori interfered with D,D-, and L,D-carboxypeptidase activities, thereby causing the accumulation of immature cell wall in des-Ori treated *S. arueus*.

Des-Ori's Effects on PG Acetylation

O-acetylation of MurNAc and *N*-deacetylation of GlcNAc are two major PG modifications that confer lysozyme resistance to facilitate the evasion of host innate immunity (Fig. 6.5a).[25] Figure 6.5b shows the mass spectra and their corresponding extracted ion chromatograms of PG dimers (figure inset) for the net acetylation states of -1, 0, 1, and 2 from mutanolysin digested cell walls of untreated *S. aureus*. Acetylation state of -1 represents *N*-deacetylation of a GlcNAc (Fig. 6.5b, red circle), 0 represents unmodified PG dimer, +1 represents *O*-acetylation of one MurNAc, and +2 represents *O*-acetylation of two MurNAc (blue circles). Since each *O*-acetylation and *N*-deacetylation changes the muropeptide mass by 42 Da, the effects of des-Ori on PG acetylation state were determined by characterizing the mass shifts in muropeptide fragments. The calculated cross-linking efficiencies for muropeptides with the acetylation states of -1, 0, and +1 are provided in Table 6.S2 and shown as a bar graph in Fig. 6.5c. The calculated ρ_{CL} for untreated *S. aureus* are similar to one another for all acetylation states, except for slightly higher cross-linking observed for the muropeptides with an acetylation state of +1 (64%). The addition of des-Ori to *S. aureus* reduced the cross-linking efficiencies in all acetylated muropeptide species, but we observe that the cross-linking efficiency of the *N*-deacetylated muropeptides was disproportionally affected by des-Ori (grey arrow). The specific role of PG *N*-deacetylation in *S. arueus* remains yet unclear, although *N*-deacetylation has been shown to be associated with increased pathogenicity and evasion of host innate immune response by *E. faecalis*, *S. pneumoniae*, and *L. monocytogenes*.[157] As *O*-acetylation is shown to increase in cultures that enter stationary growth phase,[33]

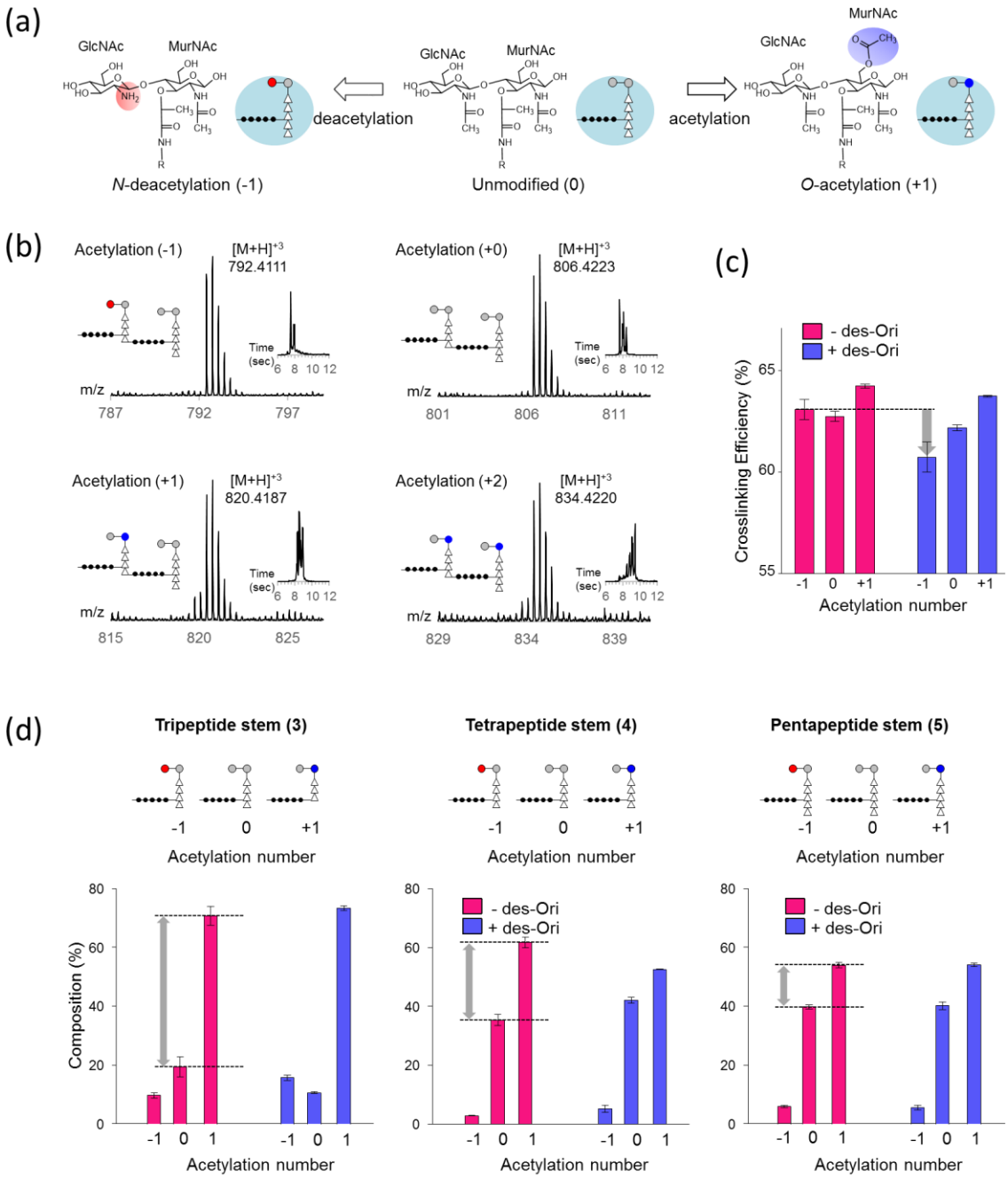

Figure 6.5: Acetylation of *S. aureus* peptidoglycan. (a) The disaccharide of PG-repeat unit, MurNAc-GlcNAc, is chemically modified by *O*-acetylation of MurNAc (+1 Ac) or *N*-deacetylation of GlcNAc (-1). (b) Mass spectra and extracted ion chromatograms of PG dimers terminating with a pentapeptide stem with acetylation states of -1, 0, 1, and 2 from mutanolysin digested cell walls of untreated *S. aureus*. A schematic representation of the proposed muropeptide structure for each acetylation state is shown as an inset. (c) Acetylation number and cross-linking efficiency. (d) Normalized percent composition by acetylation number based on terminal PG-stem lengths. All error bars represent standard error of mean (n = 3).

decreased cross-linking effiiciencies for *N*-deacetylated and *O*-acetylated muropeptides suggest that des-Ori interfered with the cell wall maturation process.

PG Acetylation and Stem Modifications

The muropeptide composition was broken down into PG-stem lengths and glycan acetylation state, and the normalized percentile compositions of muropeptides found in isolated cell walls of *S. aureus* are provided in Supplementary Table 6.S3. Fig. 6.5d shows the bar graphs of percentile muropeptide composition by the PG-stem structures, with tripeptide (left), tetrapeptide (middle), and pentapeptide (right) colored according to presence (blue) and absence (red) of des-Ori. The muropeptides with tripeptide PG-stem are found heavily *O*-acetylated (+1): approximately four times the abundance of unmodified muropeptides (0) and seven times the *N*-deacetylated muropeptides (-1). The difference in abundance between *O*-acetylated and unmodified muropeptides, shown as a gray arrow (Fig. 6.5d) lessens as the PG-stem length increases from tripeptide to pentapeptide. This result is consistent with preferential *O*-acetylation of the muropeptides with a tripeptide PG-stem, which is also found with a high degree of cross-linking (Fig. 6.4d). Hence, our findings suggest that the cell wall in *S. aureus* grown in the absence of des-Ori is composed of highly cross-linked PG that are *O*-acetylated with tripeptide-stem structure. In contrast, addition of des-Ori to *S. aureus* resulted in the cell wall with reduced PG cross-linking, reduced *O*-acetylation and *N*-deacetylation of disaccharides, and increased proportion of PG with a tetrapeptide stem structure (Fig. 6.4d).

Discussion

The glycopeptide antibiotic's interaction with the cell wall *in vivo* is complex and involves different modes of action than the primary D-Ala-D-Ala binding mode.[158] For disaccharide modified lipoglycopeptides, the drug's hydrophobic side chain forms a secondary-binding site that enables targeting of the cross-linked bridge structure of PG (Fig. 6.1d).[15, 17, 21] The secondary-binding site becomes crucial for the drug activity in des-Ori with the damaged primary-binding site that lacks the *N*-methylleucine from Edman degradation. Despite the damaged D-Ala-D-Ala binding site, this secondary-binding site allows des-Ori to retain potent antimicrobial activities against both vancomycin susceptible and resistant pathogens[18, 84], enhances the drug binding to PG in the cell wall[89, 109], and increases the binding affinity to lipid II with a pentaglycine-bridge attached by three-fold.[125] Previous solid-state NMR studies have confirmed that des-Ori binds to PG in intact whole cells of *S. aureus*.[89, 109] In contrast, binding enhancement to the PG precursor is absent for vancomycin, and its Edman degradation product is devoid of any activity.

PG composition analysis by LC-MS has confirmed that the presence of des-Ori at sub-MIC for *S. aureus* result in the reduction of PG cross-linking, which is consistent with the transpeptidase inhibition.[22] In addition, in this study we find that des-Ori preferentially reduced the cross-linking efficiencies for muropeptides without a PG-bridge (Fig. 6.4c) and with a tripeptide-stem structure (Fig. 6.4d). Des-Ori also reduced the cross-linking efficiencies for *O*-acetylated and *N*-deacetylated muropeptides species (Fig. 6.5c). Interestingly, while des-Ori treated *S. aureus* show an overall increase in *N*-deacetylated muropeptides (Fig. 6.5d), but the cross-linking efficiency for these

muropeptides was significantly reduced (Supplementary Table 6.S2). Thus, nascent PG synthesized in the presence of des-Ori shows i) increased *N*-deacetylation, ii) increased *O*-acetylation, iii) reduced PG-stem modifications, and iv) reduced cross-linking. We attribute these changes to des-Ori binding to the PG template at the inner layer of matured cell wall close to the cell membrane where the nascent PG is incorporated. This interaction with the PG-template interferes with both the alignment and orientation of nascent PG stem and bridge structures, which are necessary for efficient incorporation of these new PG into mature cell wall as mediated by the transpeptidase.[25, 56, 67] Thus, subsequent PG biosynthesis based on these defective templates results in the ensuing disorder of the cell wall with reduced PG cross-linking, altered PG acetylation, and immature PG (improper PG-stem modifications), which leaves bacteria highly susceptible to lysis.

Materials and Methods

S. aureus Cell Wall Isolation

Procedure for the cell wall isolation is described elsewhere.[32] Des-Ori was added to the final concentration of 10 μg/mL to *S. aureus* (ATCC 6538P) grown in 200 mL of TSB at OD_{600} 0.6. After 100 minutes of further growth, the cells were harvested, resuspended in 2 mL of phosphate buffered saline, and disrupted using a bead-beater (Disruptor Genie, Scientific Industries) with 0.5 mm diameter glass beads at 24°C. Eight cycles of 1 minute disruption separated by 1 minute of rest to prevent overheating of the sample were used. Disrupted cells were separated from glass beads using Steriflip 20 μm nylon net vacuum filtration system (EMD Millipore), followed by centrifugation at

25,000 x g for 3 min at 24°C. The remains of cells were boiled in 2% sodium dodecyl sulfate solution for 30 minutes, and then washed five times with deionized water through centrifugation at 25,000 x g for 3 minutes. The pellet was resuspended in 2 mL of 20 mM Tris buffer, pH 8.0, and two hundred μg of DNase was added to the suspension and the sample incubated for 24 hours at 37°C. Three hundred μg of trypsin was added to the mixture and it was incubated for additional 24 hours at 37°C. The isolated cell walls were pelleted by centrifugation at 100,000 x g for 5 minutes at 24°C and washed with 20 mM Tris pH 8.0 buffer.

Mutanolysin Digestion of S. aureus Cell Wall

The cell wall isolate of *S. aureus* suspended in 2 mL of 20 mM Tris buffer pH 8.0 was first digested using 500 U of mutanolysin (Sigma-Aldrich) at room temperature for 24 hours. 500 U of mutanolysin was then added to the mixture for additional 24 hours of incubation to ensure thorough digestion of the cell walls. Following the mutanolysin digestion, insoluble cell wall fragments were removed by 0.45 μm centrifuge filter (Amicon), and the solubilized PG fraction was collected through 30 kDa MWCO (Amicon) filter by centrifugation at 14,800 RPM (Thermo Scientific) for 5 minutes. Glycans in mutanolysin-digested muropeptides were reduced by adding sodium borohydride stock solution to final concentration of 10 mg/mL in 1 mL of borate buffer at pH 9.0. The reduction was carried out at 24°C for 30 minutes and quenched by addition of 120 μL of 85% phosphoric acid. Cell wall digest was frozen and lyophilized. Lyophilized peptidoglycan samples were cleaned up for mass spectrometry analysis using 100 μL Pierce C18 tips (Thermo Scientific).

Ultra-performance Liquid Chromatography

Waters C18 nanoACQUITY Ultra Performance Liquid Chromatography (UPLC) and Waters Synapt G2 High Definition Mass Spectrometer (HDMS) Time-of-Flight (TOF) mass analyzer were used to analyze the mutanolysin-digested peptidoglycan of *S. aureus*. For the UPLC separation, 1 μL of the sample in 50% acetonitrile, 0.1% formic acid was injected into a 5 μL sample loop and loaded onto the column under isocratic condition of 99% buffer A (0.1% formic acid in methanol) and 1 % buffer B (100% acetonitrile) for 1 minute. The separation was carried out on Waters nanoACQUITY reverse-phase C18 BEH column (75 μm X 100 mm, packed with 1.7 μm beads with 130 Å pore size) with C18 nanoACQUITY Symmetry C18 trap column (180 μm X 20 mm, 5 μm beads with 100 Å pore size) by applying a linear gradient to 50% buffer B for 60 min. After each separation, the column was regenerated under isocratic condition with 85% buffer B for 5 minutes, followed by a linear gradient to 98% buffer A for 1 minute, and then equilibrated at 98% buffer A for 23 minutes. The flow rate was kept constant at 0.450 μL/min throughout the analysis.

Mass Spectrometry

Eluents were analyzed by Waters Synapt G2 HDMS-TOF mass analyzer operating under positive ion mode. Electrospray ionization (ESI) was performed on the sample with spray voltage of 35 V, and capillary voltage of 3.5 kV. The mass analyzer was optimized for m/z range of 100-2000. Fibrinopeptide B (Glu-Fib) was used as the calibration lock mass for the mass analyzer. MS/MS fragmentation was accomplished through collision-induced dissociation with nitrogen gas at 120°C and 2.00 Bar. The transfer collision and the trap collision energies were 5 V and 30 V, respectively.

LC-MS Data Analysis

Data analysis was carried out using MassLynx (Waters). MATLAB (MathWorks) was used for the calculation of exact masses and isotopic distributions.

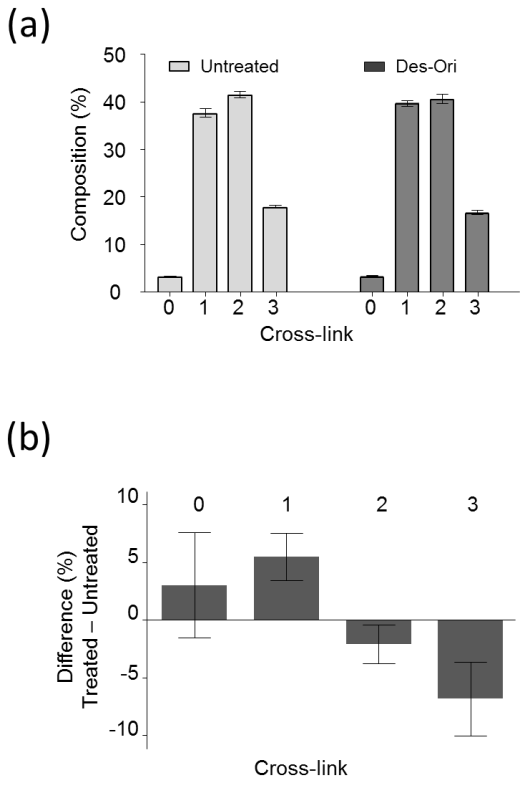

Supplementary Figure 6.S1: . Inhibition of the transpeptidation step of peptidoglycan biosynthesis in *S. aureus* from desleucyl-oritavancin. (a) Normalized integral sum of ion chromatograms of muropeptide species listed in Fig. 3a classified according to the number of cross-links. (b) Percent difference in normalized integral sums of ion chromatograms of cross-linked muropeptide species by subtracting "*Untreated*" from "*Des-Ori*" shown in (a). All error bars represent 95% confidence interval. *S. aureus* grown in the presence of desleucyl-oritavancin show an increase in PG monomers and dimers while a decrease in trimers and tetramers.

Supplementary Figure 6.S2: Muropeptide crosslinking efficiencies and the stem structure.

Muropeptides	Cross-linking efficiency (ρ_{CL}) †		P value**
	des-Ori (0 µg/mL)*	des-Ori (10 µg/mL)*	
All muropeptides	0.636 ± 0.005	0.630 ± 0.002	0.024
With a terminal pentaglycine bridge structure	0.632 ± 0.006	0.6274 ± 0.002	0.092
Without a pentaglycine terminal bridge	0.686 ± 0.003	0.667 ± 0.010	0.004
Tripeptide stem structure	0.649 ± 0.016	0.625 ± 0.023	0.053
Tetrapeptide stem structure	0.593 ± 0.016	0.625 ± 0.002	0.003
Pentapeptide stem structure	0.639 ± 0.003	0.631 ± 0.004	0.008

Supplementary Table 6.S3: Muropeptide acetylation states and cross-linking efficiency.

Muropeptide Acetylation states	Cross-linking efficiency (ρ_{CL}) †		P value**
	des-Ori (0 µg/mL)*	des-Ori (10 µg/mL)*	
-1	0.631 ± 0.015	0.607 ± 0.023	0.056
0	0.628 ± 0.008	0.622 ± 0.005	0.117
1 (or higher)	0.642 ± 0.003	0.638 ± 0.001	0.011

Supplementary Table 6.S4: Muropeptide composition by PG-stem length and acetylation state.

Muropeptides		Composition (%)[†]		P value[**]
PG-stem length	Acetylation state	des-Ori (0 µg/mL)[*]	des-Ori (10 µg/mL)[*]	
3	-1	9.764 ± 2.964	15.863 ±2.964	0.010
	0	19.450 ± 10.808	10.733 ± 0.808	0.063
	1	70.787 ± 10.121	73.405 ± 2.443	0.469
4	-1	2.838 ± 0.356	5.227 ± 3.638	0.106
	0	35.386 ± 6.176	42.133 ± 3.375	0.038
	1	61.776 ± 5.895	52.641 ± 0.295	0.008
5	-1	6.063 ± 1.487	5.674 ± 2.598	0.700
	0	39.892 ± 2.287	40.235 ± 3.910	0.821
	1	54.045 ± 2.869	54.091 ± 1.984	0.968

CHAPTER SEVEN

Peptidoglycan Compositional Analysis of *Enterococcus faecalis* by Stable Isotope Labeling by Amino Acids in Cell Culture

Abstract

Peptidoglycan (PG) is a major component of the cell wall in Gram-positive bacteria, where it functions as both a protective barrier against the extracellular environment and a scaffold for the attachment of proteins and polymers essential for growth and division, microbial pathogenesis, and antibiotic resistance. Therefore accurate quantification of the changes in PG composition by mass spectrometry would provide valuable insight into bacterial cellular functions and their responses to the external stimuli. However, because of the complex mixture of muropeptide fragments that result from various chemical modifications to the PG-repeat subunits, compositional analysis of PG remains challenging and time consuming. Here we use stable isotope labeling by amino acids in cell culture (SILAC) to characterize the changes in the PG composition of *Enterococcus faecalis* associated with the biofilm formation by growing bacteria in defined medium containing L-[$^{13}C_6$, $^{2}D_9$, $^{15}N_2$]Lys and compare them against the bacteria from unlabeled media. As most muropeptide fragments contain multiple Lys, isotopic distributions of the labeled species are highly dependent on the isotopic enrichment and the label incorporation efficiency. We demonstrate how these factors can be accounted for in order to provide accurate quantification of PG composition changes in *E. faecalis*, as we determined the isotopic enrichment for labeled Lys to be 98.33% ± 0.05% and the label incorporation rate to be 83.23% ± 1.16%. SILAC analysis shows

that PG from *E. faecalis* attached to the plastic plate wells has higher oligomerization and shorter peptide stems in their composition.

Introduction

Approximately 50 nm thick, the cell wall of *Enterococcus faecalis*, Gram-positive bacteria, serves as the physical barrier against the hostile environmental conditions while providing the platform for bacteria to anchor macromolecules that interact with the outside (Figure 7.1a).[16, 114] Peptidoglycan (PG) is the primary component of the cell wall, where PG-repeat units polymerize to form a complex biopolymer. Each of the PG-repeat unit in *E. faecalis* consists of a disaccharide (GlcNAc-MurNAc), pentapeptide stem (L-Ala-D-iso-Glu-L-Lys-D-Ala-D-Ala) attached to MurNAc, and bridge structure (L-Ala-L-Ala) attached to the ε-nitrogen of L-Lys in the pentapeptide PG stem (Figure 7.1c).[106] The PG-repeat units are first polymerized by the extension of disaccharide to form the glycan chain. Then the glycan chains are interconnected with cross-links that covalently link two neighboring glycan chains with a peptide bond between the *N*-terminus of L-Ala from the bridge to the *C*-terminus of penultimate D-Ala from the acceptor stem with the terminal D-Ala (5^{th} amino acid) being removed during the link formation.[115, 159] The assembled PG units form a lattice structure that encompasses each bacteria to function as the cell wall, the boundary between bacteria and the external environment (Figure 7.1b).[18, 20] As a component of the cell wall of a live organism, PG changes in response to various external stimuli through chemical modifications.[14, 101, 116, 123] Built layer by layer from the part closest to the cell, these sugar-links and cross-links impart upon the cell wall its mechanical strength.[147] The degree of cross-linking itself has been known to be altered by factors that directly affect the cell wall.[22] Terminal D-Ala-D-Ala from the

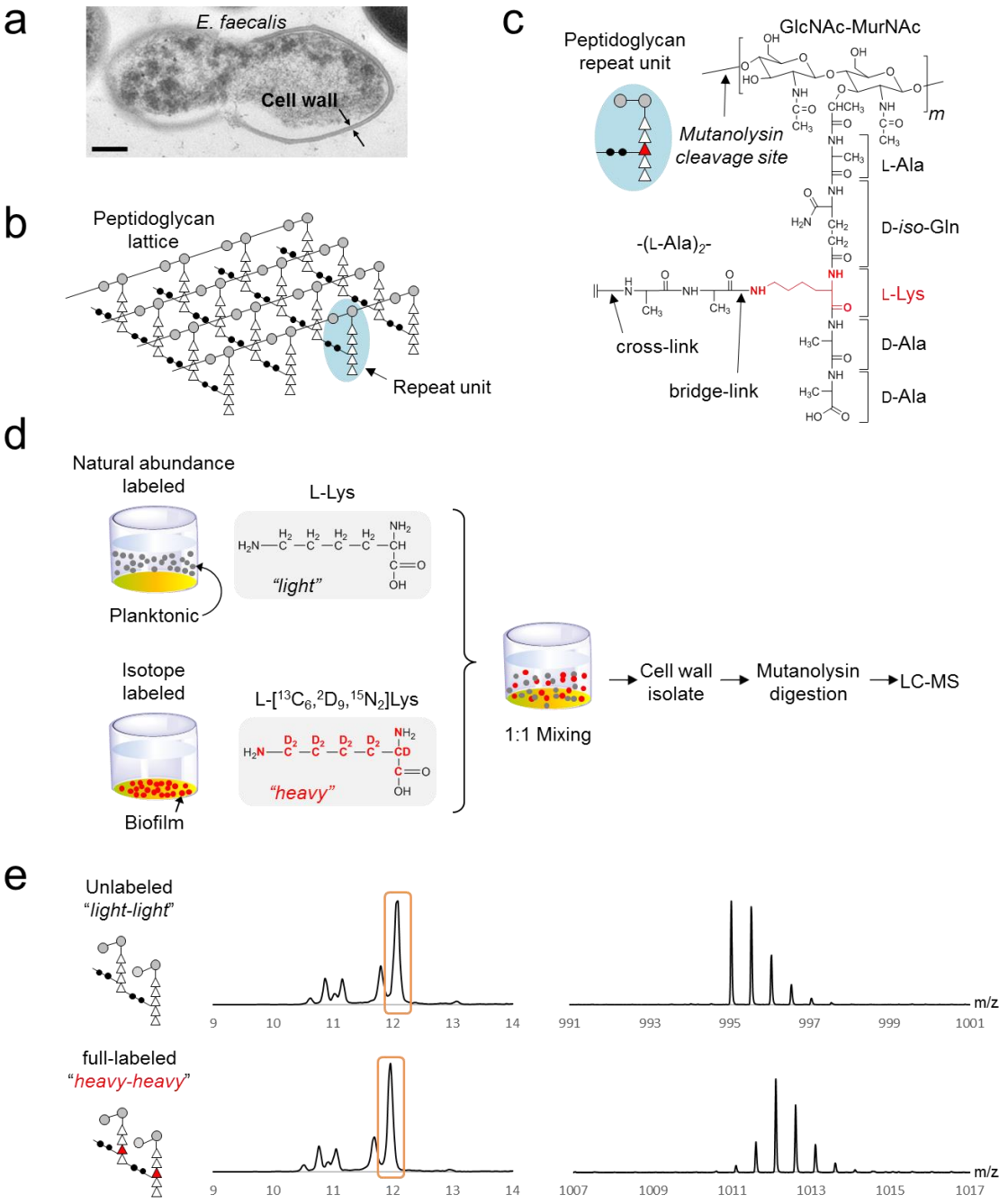

Figure 7.1: *E. faecalis* cell wall and SILAC. (a) TEM image of *E. faecalis* shows a thick, well-defined cell wall. (b) Schematic representation of *E. faecalis* cell wall with repeating PG subunits shows how a lattice structure is formed through links between PG subunits. (c) Each PG subunit is composed of GlcNAc-MurNAc disaccharide, pentapeptide stem, and cross-link bridge. The Lysine labeled in this study is shown in red. (d) Workflow for SILAC of PG in this study involved harvesting the unlabeled planktonic bacteria and labeled bacteria physically attached to the plate. After 1:1 mixing, the cell wall was isolated from rest of the bacteria and digested with mutanolysin to generate PG fragments for LC-MS. (e) XIC and mass spectra for unlabeled and labeled PG dimers show nearly identical XICs but a distinctly different isotopic distribution for the labeled fragment.

peptide stem can be edited by the bacteria in response to external stimulus,[160] and O-acetylation of NAM and N-deacetylation of NAG can change the disaccharides and alter the way bacteria interacts with their environment.[32, 161]

PG composition analysis can shed important insights into understanding the fundamental ways bacteria interacts with their environment. Unfortunately, PG analysis is not amenable to most biochemical techniques and spectroscopic methods due to PG's heterogeneity, size, complexity, and insolubility.[18] While solid-state NMR can provide compositional analysis on global scale, the results are in the scale of whole organisms and not on individual variations to the PG themselves. In contrast, LC-MS analysis of the enzymatically digested cell wall fragments offers a way for detailed analysis of PG and chemical modifications associated with it.[26, 31-33, 162] Mutanolysin is an *N*-acetylmuramidase which cleaves the $\beta_{1\text{-}4}$ glycosidic linkage of the glycan chain, and mutanolysin digestion of PG leaves intact PG-repeat units bound through cross-links as a whole.[163] As N-deacetylation of NAG nor O-acetylation of NAM affect the mutanolysin digestion, resulting PG fragments also preserve the PG subunit modifications. This ability to discern and quantify variations in the PG also makes LC-MS analysis difficult, as accurate identification and quantification requires a way to account for the staggering complexity and diversity arising from these chemical modification of PG-repeat units.[33] Nevertheless, the LC-MS analysis remains the most accurate method to provide insights into the chemical diversity with the ability to discern various modifications necessary for characterizing changes to the PG under varying conditions.

Stable isotope labeling with amino acids in cell culture (SILAC) utilizes near complete level of isotope labeled amino acid incorporation, which is achieved by

providing cells with isotope-labeled essential amino acids.[164-165] Hence SILAC has been successfully used for quantitative proteome and metabolome analyses in cell cultures.[166-169] But in the case of bacterial or autotrophic organisms, SILAC is less frequently used as the exogenous isotope labeled amino acid is not taken up and/or has low incorporation efficiency due to the organism's endogenous amino acid biosynthesis that provides unlabeled amino acids that compete with the labeled amino acid for incorporation.[170-171] Nonetheless if a way to correct for the incomplete incorporation could be devised, it would make the study of these organisms with SILAC more accessible. In this study of PG composition analysis of *E. faecalis* by SILAC, we selected L-[$^{13}C_6$, $^{2}D_9$, $^{15}N_2$]Lys for labeling as it is found only once per PG-repeat unit with mass increase of 17 Da (Figure 7.1d). In addition, Lys has the highest incorporation efficiency of all amino acids in PG-repeat unit, approximately twice that of D-Ala as bacteria preferentially uses exogenous Lys over synthesizing it *de novo* and burdening the limited nitrogen resource pool.[172] Nonetheless, the endogenous Lys biosynthesis still occurs and lowers the labeled Lys incorporation. In addition to the label dilution, relatively high number of Lys with less than 100% isotopic enrichment in oligomeric muropeptide significantly alters the isotopic mass distribution from that of the natural abundance fragments. To make the one-to-one comparison between labeled and unlabeled fragments through SILAC, it is necessary to account for this difference in the isotopic distribution that affects the abundance of ions with a particular m/z value (Figure 7.1e). Thus, accurate quantification of PG composition by SILAC must account for both the different isotopic distribution patterns that inevitably arise due to the size and makeup of the muropeptides and the incomplete incorporation of labeled amino acids that depresses the observed amounts of labeled

fragments. In this study, we show a way to correct for these two factors from the MS data of PG by considering both as probabilistic events, and apply these corrections into the SILAC experiment of PG from two *E. faecalis* populations that have segregated themselves into two separate locations within the same culture.

Experimental Section

Bacterial Biofilm Growth and Isotope Labeling

An overnight starter culture of *Enterococcus faecalis* (ATCC 29212) grown in brain-heat infusion medium was added as 1% (v/v) inoculum to the wells of cell culture treated polystyrene plates with six wells (Corning® Costar®), where each well contained 4 mL of Enterococcal Defined Media (EDM). EDM was modified for SILAC labeling by substituting the natural abundance L-Lys (Light) with L-[$^{13}C_6$, $^{2}D_9$, $^{15}N_2$]Lys (Heavy). The isotopic enrichment ranges for the labeled Lys provided by the vendor (Cambridge Isotopes) was 96-99%. The formulation for EDM is described on Supplementary Table 7.S1.

Following 24 hr growth at 37 °C with 80 rpm shaking, free floating planktonic cells were harvested from the wells containing EDM with natural abundance L-Lys using pipette. Sessile cells physically attached to the plate in the wells containing EDM supplemented with L-[$^{13}C_6$, $^{2}D_9$, $^{15}N_2$]Lys were separated from planktonic cells by removing suspended cells, then washing the wells twice with 4 mL of cold phosphate buffered saline (PBS) to remove any remaining planktonic cells.. Then the sessile cells were collected by physically scraping the cells attached to the polystyrene surface. Harvested cells were washed with PBS and then placed in a boiling water bath for 30 min

to inactivate autolysins. The planktonic and sessile cells were vigorously resuspended by mechanical means in PBS to equal optical density of 0.60 at 600 nm, then planktonic cells grown in natural abundance L-Lys containing EDM and sessile cells from isotope labeled EDM were combined in equal volume (1:1; v/v).

Cell Wall Isolation and Mutanolysin Digestion

The cells were divided equally into multiple microcentrifuge tubes with each containing approximately 400 µL (0.65 g) of 0.5 mm glass beads. Cells were disrupted using a bead beater (Disruptor Genie, Scientific Industries) for 8 cycles of 1 min disruption and 1 min rest. Beads were separated from disrupted cells using Steriflip 20 µm nylon net vacuum filter (EMD Millipore). Disrupted cells were washed once in PBS, boiled in 2% sodium dodecyl sulfate solution for 30 min, then washed 5 times with deionized water to remove sodium dodecyl sulfate. Resulting isolated cell walls were suspended in 20 mM Tris pH 8.0 buffer, and 200 µg of DNase (Sigma-Aldrich) added prior to 24 hr of incubation at 37°C and 180 RPM shaking. This incubation was followed by addition of 300 µg of trypsin (Sigma-Aldrich) for additional 24 hr of digestion. Isolated cell walls were then digested with 100 units of mutanolysin (Sigma-Aldrich) for 24 hr at room temperature, then additional 100 units were added for 24 hr of further digestion. Undigested cell walls were removed by using 30 kDa molecular weight cutoff filters by centrifuging the digest mixture at 14800 RPM. Soluble muropeptide fragments were reduced using 10 mg of sodium borohydride in 1 mL 0.5 M borate buffer pH 9.0 at room temperature for 30 min. Reduction was quenched by adding 120 µL of 85% phosphoric acid, and the samples were frozen and lyophilized.

LC-MS Analysis

Digested cell wall fragments (20-40 mg) in 500 μL of 20 mM Tris pH 8.0 buffer were diluted 1:10 in methanol with 0.1% formic acid. Waters Synapt G2 High Definition Mass Spectrometer (HDMS) with Time-of-Flight (TOF) mass analyzer and Waters C18 ACUITY Ultra Performance Liquid Chromatography (UPLC) were used to analyze the peptidoglycan digest mixture. Chromatographic separation was carried out on Waters nanoACQUITY C18 reverse-phase column (75 μm X 100 mm, 1.7 μm beads with 130 Å pore size) with nanoACQUITY C18 trap column (180 μm X 20 mm, 5 μm beads with 100 Å pore size). First, 1 μL of the sample from a 5 μL sample loop was injected to the column under isocratic condition of 99% buffer A (99.8% anhydrous methanol with 0.1% formic acid) and 1 % buffer B (100% acetonitrile) over 5 min. After the sample injection, a linear gradient to 50% buffer B was applied for 60 min for separation. The column was subsequently regenerated under isocratic condition with 85% buffer B for 5 min, a linear gradient to 98% buffer A for 1 minute, then isocratic at 98% buffer A for 23 min. The flow rate was kept constant (0.6 μL/min) throughout the analysis. Resulting eluents were analyzed by Waters Synapt G2 HDMS-TOF mass analyzer operating in positive ion mode with the fragments ionized through electrospray ionization (ESI) with spray voltage of 35 V and capillary voltage of 3.5 kV. The mass analyzer was optimized for the ions in the m/z range of 100-2000, with Fibrinopeptide B (Glu-Fib) as the standard lock mass for calibration.

Data Analysis

MassLynx Mass Spectrometry Software (Waters) was used to obtain m/z and peak intensity values from the LC-MS data. The difference between observed and

calculated masses needed to be less than 20 ppm for ions to be identified as positive matches. Exact masses for the PG library generated with an in-house MATLAB (MathWorks) program utilized values calculated from the Molecular Mass Calculator on the Biological Magnetic Resonance Data Bank (www.bmrb.wisc.edu). Calculations for the isotopic distributions of both the natural abundance and L-[$^{13}C_6$, $^{2}D_9$, $^{15}N_2$]Lys labeled PG at various isotopic enrichments were carried out using MATLAB

Results

Isotopic Enrichment Determination and Correction

SILAC of PG oligomers by definition involves the presence of multiple isotopically labeled amino acids in each PG fragment, as peptidoglycan is built up from identical subunits with the same amino acids. In this study, the amino acid labeling was done through Lysine, which is present once per each subunit. However, even with high isotopic enrichment of atoms being labeled, the total number of labeled atoms in an oligomeric fragment increases to the point the isotopic distribution that deviate from the natural abundance arising from partially enriched amino acid becomes a factor. The probability of a fragment (P) having n number of enriched atoms can be expressed in a following equation (Equation 1):

$$P_n = E^{(\mathrm{as}-u)}(1-E)^u \quad (1)$$

where E is the enrichment rate of atoms to be labeled, a is the number of labeled atoms per amino acid, s is the number of oligomeric subunits, and u is the number of atoms left unenriched through the enrichment process. Therefore, the binomial probability distribution can be used to express the distribution of labeled atoms in a PG fragment

given the enrichment rate, and combining this probability distribution with the isotopic distribution calculated for natural abundance isotopes with MATLAB gives the distribution pattern expected for peptidoglycan fragments of certain oligomeric size and chemical composition with the enrichment rate E.

While a possible range of enrichment rate for the labeled Lysine was provided by the supplier, metabolism of labeled Lysine in the bacteria could introduce partially labeled Lysine in to the cell and potentially lower the enrichment rate seen in the PG fragments. To account for this possibility, isotopic distribution observed from a peptidoglycan fragment with clear, strong peaks in the mass spectra was used to calculate the isotopic enrichment of Lysine observed in the PG. The fragment chosen was a dimer with 8 Ala and no acetylation number changes, as it was found to be especially abundant with clear peaks in the distribution (Figure 7.2a). To determine the accurate enrichment rate of the labeled Lysine in the sample, a series of calculated isotopic distributions were first generated using in-house MATLAB program that utilized the Equation 1, then the calculated intensities from each distribution were normalized into probabilities using the following equation (Equation 2)

$$P(I_k) = \frac{I_k}{\sum I} \quad (2)$$

where $P(I_k)$ is the intensity of the k-th peak in terms of probability, I_k is the observed intensity of the peak at the k-th position, and k is the position of the peak in the distribution. The observed distribution was also normalized to convert intensities into probabilities, and the observed distribution was matched against calculated distributions by minimizing the sum of squared differences of probabilities. The best matched

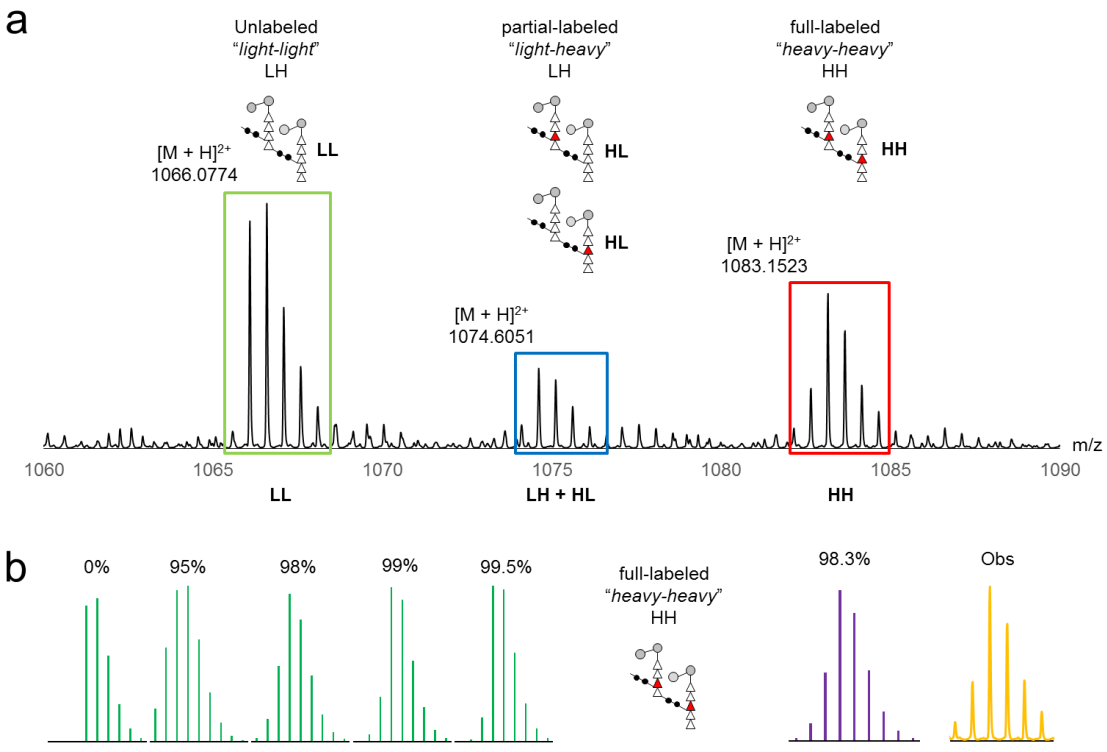

Figure 7.2: Label isotopic enrichment determination. (a) Mass spectrum of a dimeric PG after the sample mixing shows three distinct states for the label incorporation: no labels (green), one label (blue), and two labels (red) incorporated. Isotopic distributions differ based on the number of labels incorporated. Schematic representations of the dimer with labels are shown above the spectrum. (b) Calculated isotopic distributions for various levels of enrichment (green) were matched against the observed distribution for the dimers with two labels incorporated (yellow) by least square fitting. Isotopic distribution for the enrichment rate determined (98.33% ± 0.05%, n = 3) is shown in purple.

enrichment rate from the calculated distribution was determined (98.33% ± 0.05% 95% confidence interval, n = 3), and this rate was used for all subsequent isotopic enrichment corrections (Figure 7.2b).

As isotopic distributions of the PG fragments with labeled Lysine differed from the one with natural abundance Lysine, these distributions were collapsed into single peaks in order to accurately compare the peak intensity of labeled and unlabeled fragments in order to avoid the base peak intensity depression that arises from higher dispersal of the distribution in the labeled sample. As the isotopic distribution

normalized to probabilities for each fragment could be generated using in-house MATLAB program, simply dividing the base peak intensity by the probability for the base peak accounted for the distribution dispersal and allowed for determining the true peak intensity from the observed one (Figure 7.3a).

Label Incorporation Correction

Isotopic labeling using amino acids in bacteria can pose challenges as these bacteria can meet all their amino acids needs by endogenously synthesizing them *de novo*. This self-sufficiency allows bacteria to not exclusively rely on the provided labeled amino acid for growth, leading to lower than 100% incorporation rate of labels. This incomplete incorporation of the label results with two problems in accurately quantifying the peak spectral intensities of these PG fragments: partial incorporation leads to lowering of fully labeled PG's peak intensities, and completely unlabeled PG would be present even in the sample from bacteria grown in enriched media and increase the peak intensities from the unlabeled culture (Figure 7.2c).

These two issues were addressed by estimating the incorporation rate from partially labeled peaks in the observed spectrum. Like isotopic enrichment, label incorporation can also be treated as events with a fixed probability of success. As the addition of Lysine occurs to individual subunits during their *de novo* biosynthesis prior to any modifications, it can be safely assumed that all PG fragments would have the same label incorporation rate regardless of their modifications that take place after biosynthesis. Thus, to calculate the label incorporation efficiency, isotopic distributions of peaks for a dimer with 0, 1, and 2 labeled Lysine incorporated were combined using the isotopic enrichment determined in the previous section. For the labeled sample, the

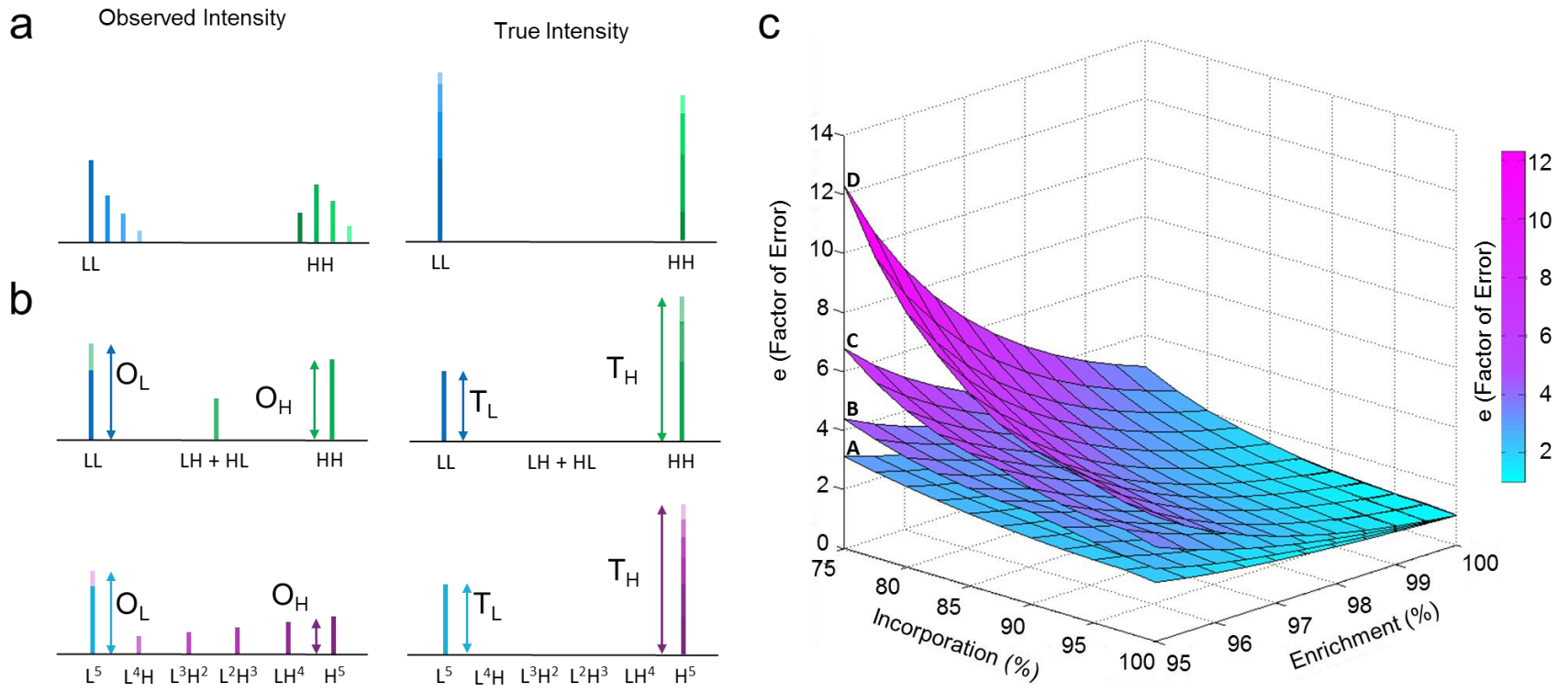

Figure 7.3: Label enrichment and incorporation corrections. (a) Isotopic distribution correction converts observed peak intensities into a monoisotopic peak intensity equivalent, removing the bias from incomplete label enrichment. (b) Label incorporation correction gives the true peak intensities that would result from 100% label incorporation by calculating the true fully labeled peak intensity using the incorporation rate determined. (c) Factor of error represents the amount of correction necessary to account for partial enrichment and incomplete incorporation. The four surfaces show the factor of error plotted for dimers (A), trimers (B), tetramers (C), and pentamers (D).

probability of having number of Lysine incorporated (P) is as follows (Equation 3)

$$P(c) = r^c(1-r)^{n-c} \quad (3)$$

where r is the incorporation rate and n is the number of PG subunits in a fragment. These calculated probabilities directly correspond to the observed peak intensities that have been compensated for the isotopic distribution normalized as probabilities. As probabilities that represent fragments with full, partial, and no label incorporation must sum to 1, knowing the peak intensities of fully and partially labeled PG allows the determination of unlabeled PG as well. Furthermore, binomial coefficient of order n can be used to describe the probabilities arising from various combinations of labeled and unlabeled amino acids in oligomers of size n. Thus the incorporation rate r can be calculated from the observed dimers (83.30 ± 1.16%, n = 3). Once the incorporation rate has been calculated, the intensity of a peak with 100% label incorporation can be calculated solely from the intensity of fragments with all labeled Lysine, a process akin to collapsing all the peaks arising from the probability distribution into a single peak (Figure 7.3b).

The amount of correction necessary to compensate for lower than complete isotopic enrichment and label incorporation can grow rapidly as the oligomeric size of fragments increases. Partial and zero label incorporation lead to underestimating the amounts of fragments that should have been labeled fully and overestimating the amount of zero-labeled fragments from the unlabeled sample, which results with the ratio of $\frac{labeled}{unlabeled}$ to be lower than the actual value. Figure 7.3c graphs the factor of error, the amount by which the observed SILAC ratio must be multiplied to account for both enrichment and incorporation inefficiencies, as a function of enrichment and

incorporation percentages for the PG oligomers of increasing size with the same modifications. For the values determined in this experiment (98.33 ± 0.05% enrichment and 83.23 ± 1.16% incorporation), the factor of error for a dimer with only two labeled Lysine is already 1.602. The factor of error increases rapidly as both percentages decrease, with the correction necessary for observed SILAC ratio of a pentameric oligomer reaching a factor of 12 for 95% enrichment and 75% incorporation.

SILAC Results for E. faecalis Peptidoglycan

By applying both corrections described in previous sections, we were able to compare the PG composition differences between mobile bacteria suspended in the media and sessile bacteria attached to the walls of culture plates by using the SILAC ratios between two samples. Three distinct modifications of PG were examined in this study: the degree of cross-linking driven polymerization, number of Alanine present in the unlinked cross-linking bridge and the D-Ala-D-Ala stem ending on the terminal PG subunit, the overall acetylation number of the fragments. Identification and accurate quantification of these peaks required aid from isotopic distribution patterns calculated in the correction step. All the fragments with labeled Lysine incorporated had isotopic distributions that markedly differed from their counterparts produced under natural isotopic abundance condition. This difference was especially evident in larger fragments with multiple Lysine (Figure 7.4c and d), where determination of the m/z value of fully enriched and labeled PG fragment was crucial for m/z value-driven matching of the fragments. Once the m/z targets have been determined, an in-house MATLAB program for m/z library generation and matching previously composed was used to identify both the labeled and unlabeled peaks. While the chromatographic retention time was not

crucial for the identification of PG fragments as the cell wall isolation purified the PG and m/z values were used to identify individual PG, retention time differences observed nonetheless demonstrated structural differences within a group of fragments that varied from each other through a single type of modification such as polymerization (Figure 7.4b).

While changes to the degree of polymerization with their large mass changes were readily observable and quantifiable through SILAC, covalent modifications that directly changed the PG subunits themselves could also be analyzed. One of these modifications was the change to the acetylation state of PG through an increase by O-acetylation of NAM or a decrease by N-deacetylation of NAG (Figure 7.5a). As PG fragments were categorized according to their overall acetylation numbers and not the location of their acetylation changes, this approach allowed a snapshot of fluctuations in the overall acetylation state of PG for a population of bacteria (Figure 7.5b). Through the use of a reverse phase column, changes to the hydrophobicity of PG through the addition or removal of acetyl groups manifested themselves as large changes in the retention time (Figure 7.5c). These shifts were large enough to cause overlaps between these PG that differed from one another through polymerization and with acetylation in the total ion chromatogram, thus highlighting the necessity of using extracted ion chromatograms and m/z value matching for identifying and quantifying these PG fragments instead of the traditional UV absorbance method. Examples of these PG fragments with a varying number of acetylation are shown for both unlabeled and labeled samples (Figure 7.5d and e). The SILAC ratio change analysis could also be expanded to the number of Alanine in the terminal PG subunit as well. Modifications to both terminal D-Ala in the peptide

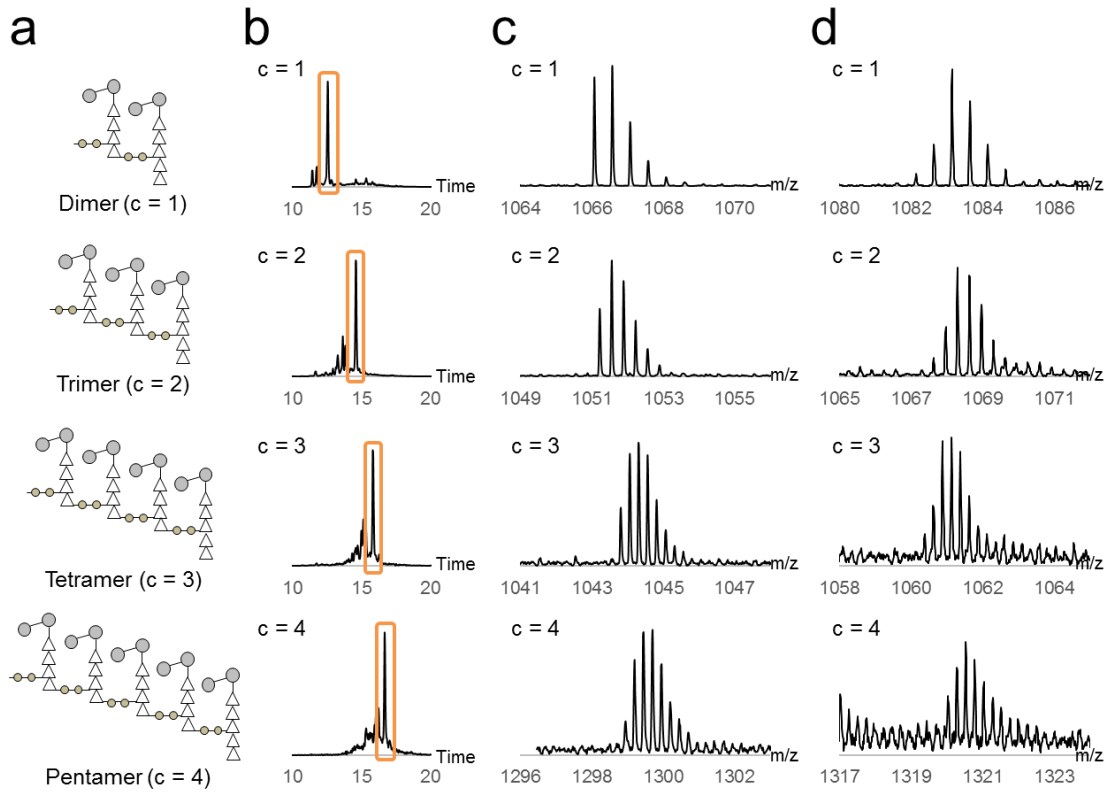

Figure 7.4: Cross-linking of PG. (a) Schematic representations for PG fragments with the number of cross-links ranging from 1 to 4 are listed. (b) XICs, and mass spectra of the unlabeled (c) and fully labeled (d) PG fragments with the cross-link number that corresponds to (a) are shown.

stem and two L-Ala in the unlinked cross-linking bridge that resulted in lower Alanine number in the fragment could be identified and quantified (Figure 7.6a). Like the acetylation number, the alanylation number were analyzed through extracted ion chromatograms and spectra (Figure 7.6b, c, and d).

After the peak intensities of PG fragments for both the unlabeled and labeled samples were corrected, changes to the amounts of PG fragments with varying combinations of modifications arising from the differences in the bacterial population location could be determined and tabulated through SILAC ratios (Figure 7.7a). By averaging the SILAC ratios of PG fragments grouped according to their modifications,

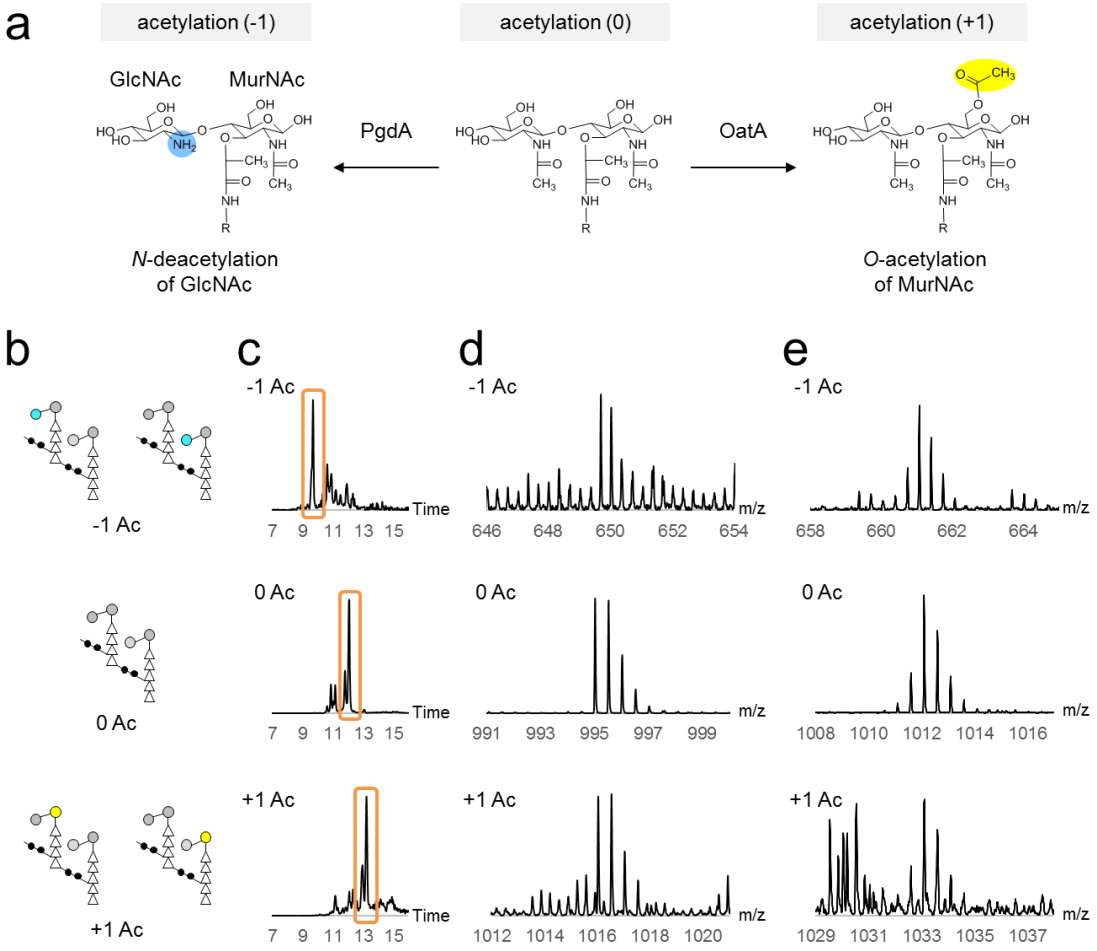

Figure 7.5: Acetylation state of PG. (a) Unmodified PG subunit (middle) can be N-deacetylated on GlcNAc by PgdA (left) and O-acetylated on MurNAc by OatA (right). (b) Schematic representations for PG dimers with acetylation states ranging from -1 to 1 are listed. (c) XICs, and mass spectra of the unlabeled (d) and fully labeled (e) PG fragments with the acetylation state that corresponds to (b) are shown.

the effect bacterial mobility and location have on the PG composition was able to be quantified. Averaged ratios for various modifications are listed in Supplementary Table 7.S2. Of particular note was the prevalence for highly cross-linked pentameric oligomers in the sessile phase (Log_2 SILAC ratio of 0.188 ± 0.101) (Figure 7.7b), which indicates a slower rate of PG biosynthesis and turnover for *E. faecalis* attached to the inorganic surface. Change to the peptide stem length was also noticeable, as PG with little or no

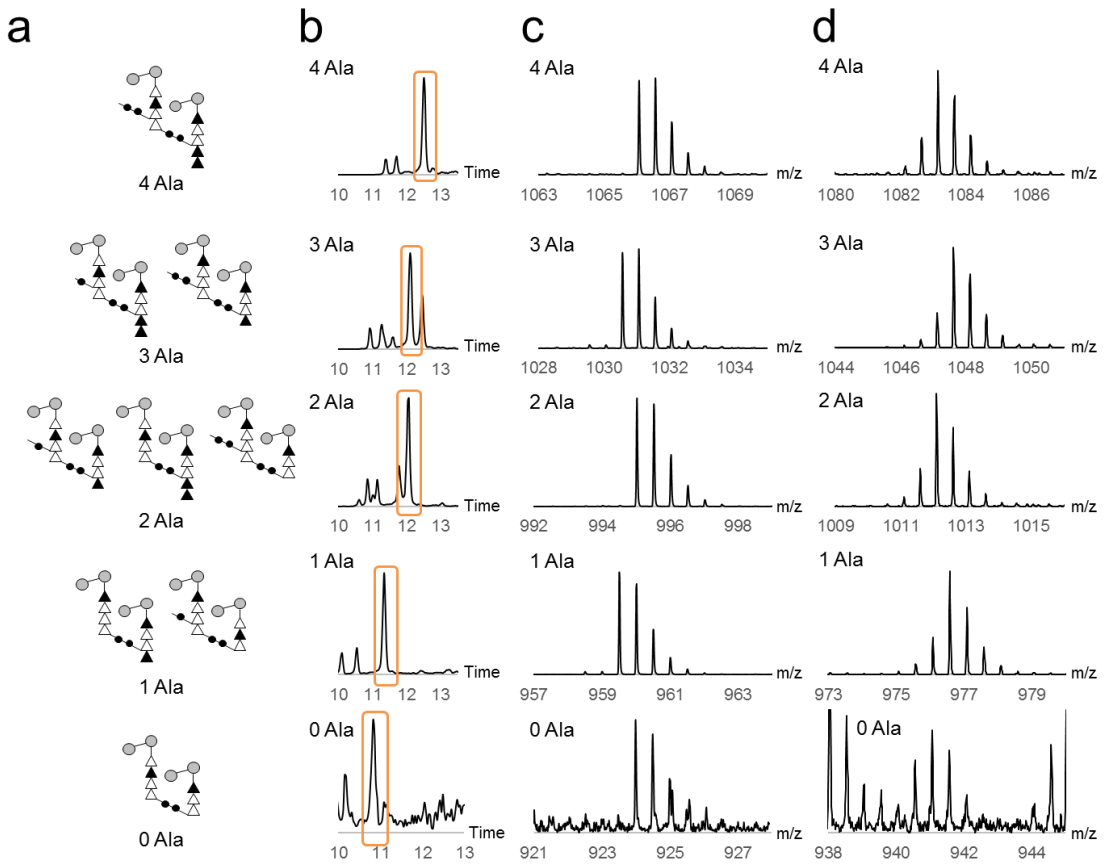

Figure 7.6: Number of terminal D-Ala and cross-linking L-Ala. (a) Schematic representations for PG dimers with varying numbers of D-Ala in the terminal PG subunit's peptide stem and L-Ala in the unlinked cross-linker bridge show different combinations of stem and bridge lengths that result in the alanylation number. (b) XICs, and mass spectra of the unlabeled (c) and fully labeled (d) PG fragments with the alanylation number that corresponds to (a) are shown.

editing of the peptide stem with 4 or 5 Alanine were found in higher amounts for the mobile phase (Figure 7.7c). An exception could be found for those PGs missing both the D-Ala-D-Ala stem ending and a cross-linking bridge, which were found in the mobile phase. These may be the result of bacteria utilizing these fully edited PG stems as markers to preclude any further cross-linking of PG, which is in agreement with the highly cross-linked species being found in the sessile phase. Prevalence of O-acetylation in the mobile phase would increase the hydrophobicity of the bacterial cell wall and allow them to be repelled from the charged surface of the tissue culture treated plates, whereas

N-deacetylation found in the sessile phase would attract the bacteria to the plates and aid in the attachment (Figure 7.7d).

Discussion

The bacterial cell wall is intricately involved in the way bacteria interacts with their environment and analysis of its composition offers insights into bacterial adaptation to different situations.[173-174] In this study, we demonstrate that mass spectrometry, through the application of SILAC, allows for monitoring of small details in the changes to the cell wall beyond the reach of traditional biochemical methods to be examined. Classification and analysis of the PG composition are most often performed on the species level where fundamentally all of the PG being compared have distinct interspecies differences in their chemical structures. We show that through comparing the SILAC ratios even the spatial differences in the PG composition between two populations of the same bacterial strain with identical growth condition can be identified and quantified. While this study focused on general trends in the PG composition change, this method also enables different approaches to examine the PG. For example, application of principal component analysis (PCA) to the list of PG fragments with variations and SILAC ratios may allow typing of the bacterial populations according to both its spatial and temporal properties. This ability to add both the spatial and temporal dimension to the analysis of bacterial population behavior allows an additional approach to investigate clinically relevant phenomena by pathogens that manifest at the population-level such as biofilm formation. Especially amenable for analysis through SILAC of the PG composition would be clinically-relevant Gram-positive pathogens with abundant PG

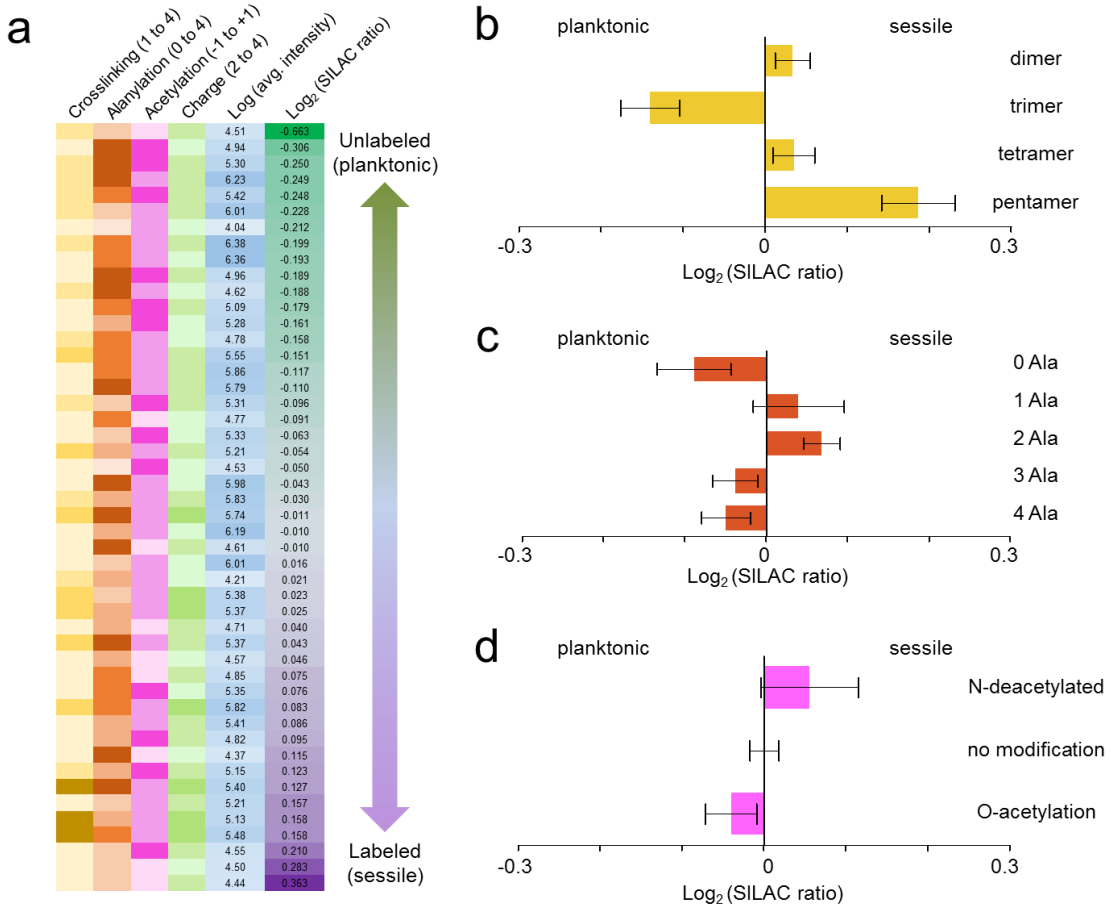

Figure 7.7: Profile of peptidoglycan SILAC pairs. (a) Ratios of intensities for PG SILAC pairs are listed. Darker shades indicate a higher number of cross-links (yellow), alanylation number (brown), acetylation state (pink), and fragment charge state (green). Average intensities of each SILAC pair (n = 3) are shown (blue). Ratios of corresponding SILAC pairs are listed (far right). (b, c, d) Average $\log_2$ SILAC ratio for species with different (b) number of cross-links, (c) alanylation number, and (d) acetylation state. Error bars represent SEM (n = 3)

in their cell walls such as *Staphylococcus aureus*, *Streptococcus pneumoniae*, and *Enterococcus faecium*.

Corrections utilized in this study could also be used in different biological systems to broaden the scope of questions SILAC can answer. The ability to account for partial enrichment of labels allows for experiments to be performed with amino acid that are both high in the number of labeled isotopes and low in the enrichment rate without either factors causing a bias in the SILAC ratios. Determining the incorporation rate of

amino acid labels opens up the possibility of directly comparing abundances of peptides or other biopolymers without the near complete labeling required in SILAC experiments. Both corrections can also be applied to accurately quantify relative amounts of ions with multiple amino acids of different enrichment and incorporation. These corrections would also simplify SILAC experiments to be done on biological systems with endogenous amino acid production, such as bacteria or plants, as well as animal cells with non-essential amino acid labeling. Application of these corrections would enable SILAC to quantitate minute changes in the amounts of analytes that otherwise would have been overlooked in the bias introduced by lower than assumed enrichment and incorporation. This would make possible to answer by SILAC biological questions previously deemed inaccessible for the technique.

Supplementary Table 7.S1: Formulation for Enterococcus Defined Media.

K_2HPO_4	4.3 g	Adenine	5 mg
KH_2PO_4	4.0 g	Uracil	5 mg
$(NH_4)_2SO_4$	1 g	Cytosine	5 mg
EDTA	1 mg	Guanine	5 mg
Boric Acid	0.1 mg	Xanthine	5 mg
Biotin	0.1 mg	L-Aspartic Acid	100 mg
Folic Acid	0.2 mg	L-Cysteine	100 mg
Thiamine HCl	2 mg	L-Tryptophan	100 mg
Calcium pantothenate	2 mg	L-Proline	100 mg
Pyridoxine HCl	20 mg	L-Isoleucine	100 mg
Niacin (Nicotinic acid)	2 mg	L-Leucine	100 mg
Riboflavin	2 mg	L-Valine	100 mg
Inositol	1 mg	L-Phenylalanine	100 mg
P-aminobenzoic acid	0.05 mg	L-Arganine	100 mg
Cyanobalamin	0.01 mg	L-Threonine	100 mg
$NiAc_2$ 4H2O	0.1 mg	L-Histidine	100 mg
$(NH_4)_6Mo_7O_{24}$ $4H_2O$	0.2 mg	L-Serine	100 mg
$MgSO_4$ $7H_2O$	30 mg	L-Methionine	100 mg
$MnSO_4$ H_2O	10 mg	L-Asparagine	100 mg
$CuSO_4$ $5H_2O$	1 mg	L-Alanine	100 mg
$ZnSO_4$ H_2O	1 mg	Glycine	100 mg
NaCl	10 mg	L-Glutamic Acid	100 mg
$CaCl_2$ $2H_2O$	1 mg	L-Glutamine	100 mg
$FeSO_4$ $7H_2O$	10 mg	L-Tyrosine	100 mg
D-Glucose	10 g	L-Lysine (labeled or unlabeld)	100 mg

Supplementary Table 7.S2: Table of SILAC ratios.

(a) Cross-linking number

	Mean SILAC ratio	95% CI
Dimer	0.034	0.043
Trimer	-0.140	0.073
Tetramer	0.035	0.053
Pentamer	0.186	0.101

(n = 3)

(b) Alanylation number

	Mean SILAC ratio	95% CI
0 Ala	-0.089	0.111
1 Ala	0.040	0.114
2 Ala	0.069	0.046
3 Ala	-0.038	0.056
4 Ala	-0.049	0.061

(n = 3)

(c) Acetylation number

	Mean SILAC ratio	95% CI
-1 Ac	0.056	0.121
0 Ac	0.001	0.035
+1 Ac	-0.040	0.063

(n = 3)

CHAPTER EIGHT

Conclusion

Studies presented in this dissertation highlight the progress made in examining and analyzing peptidoglycan composition in the cell wall of Gram-positive bacteria *Staphylococcus aureus* and *Enterococcus faecalis*. The ability to survey the overall chemical composition of peptidoglycan with liquid chromatography-mass spectrometry, when supplemented with the accurate quantification of specific components of the peptidoglycan through solid-state NMR, provides much clearer picture of Gram-positive bacterial cell wall than ever before.[33] These studies demonstrate the power of analytical methods outlined in the introduction, that with current techniques and instruments even the spatial and temporal identification of bacteria can be achieved through looking at peptidoglycan. Technological advances in ionization and separation techniques for liquid chromatography-mass spectrometry and polarization enhancement for solid-state NMR could one day allow these methods to be used in clinical setting for aiding physicians in not just diagnosis, but also in treatment specialized for the progression of an infection and pathogen behavior.[175-177]

Further experiments currently being undertaken emphasize this ability to detect finer changes to the peptidoglycan composition, and they include studying biofilm formation and bacterial mobility, response to antibiotics, and effects of other cell wall macromolecules on the peptidoglycan composition. Methods highlighted in preceding chapters are being applied to questions that were once unanswerable by examination of

peptidoglycan, such as bacterial colony formation on different physical support and true cost to the bacteria from antibiotic resistance in terms of population-level changes to survival fitness. These experiments promise to shed light into intricate details in the way bacteria interact with both their environment and other bacteria as a community. Yet further challenges remain on elucidating the structure of cell wall at the molecular level. Results from the studies performed hint at some level of organization on the secondary structure level, where amino acids and sugars from the peptidoglycan subunits connect to each other.[17-18, 56, 72, 84] The fact that certain parts of the peptidoglycan composition changes are correlated hint this possibility. Clearly, there is a point at which well-ordered structures at the molecular level experience decoherence and cease to depend on adjacent cell wall regions for their structure and become random.

Answering such questions would require different approaches. Solid-state NMR techniques are well suited for accurately determining the chemical structure on the molecular level. Mass spectrometry gives the localized connectivity at the fragment level, but as it can be seen from the studies in this dissertation the scope of this method is still restricted to the secondary structural level. While electron microscopy has the potential to analyze tertiary structure, it is unclear that the rules governing the transition from order to disorder can be determined by a series of electrographs that only show the surface level of the cell wall.[174, 178-179] Peptidoglycan structure most likely exists in both ordered and disordered states depending on the circumstances the bacteria experience.

Computer simulations of the peptidoglycan organization may offer a way that bridges the molecular level analysis of solid-state NMR and mass spectrometry with the cellular level overview of electron microscopy. There have been studies that attempted to

simulate the physical properties of the cell wall from materials science perspective to explain remarkable tensile strength of the cell wall.[180-183] But simulations could also offer testable predictions on the chemical structure and composition of peptidoglycan that can be examined by solid-state NMR and mass spectrometry, and larger scale simulations could approximate the structural randomness seen on electron microscopy studies.[184] They will need to incorporate both the randomness and directed modifications to the peptidoglycan, which would allow them to simulate structures that have both order at the local level and disorder at the global level. Three testable predictions would arise from these simulations: at the molecular level in terms of distant constraints between various parts of peptidoglycan, at the compositional level reflecting the cross-linking, sugar-linking, and covalent modifications to the subunits, and at the structural level on the emergence of disordered nature of the cell wall.

There remain many questions on the cell wall of Gram-positive bacteria. Studies presented in this dissertation offer insights into the cell wall; properties that have been previously out of reach for traditional biochemical methods. It is this candidate's hope that the reader comes away from this dissertation convinced that the cell wall and peptidoglycan are not intractable problems beyond the reach of current investigative techniques. Further examination of these pathogens' cell wall will not only offer clinically relevant conclusions to help the treatment of infections caused by these bacteria, but promise to further advance analytical methods to investigate these questions.

BIBLIOGRAPHY

1. Rogers, H. J.; Perkins, H. R. *Cell Walls and Membranes*; E & F.N. Spon Ltd.: London, 1968.

2. *Surface Carbohydrates of the Prokaryotic Cell*; Sutherland, I. Ed.; Academic Press: London, 1977.

3. Neidhardt, F. C.; Ingraham, J. L.; Schaechter, M. *Physiology of the Bacterial Cell: A Molecular Approach*; Sinauer Associates, Inc.: Sunderland, MA, 1990.

4. Silhavy, T. J.; Kahne, D.; Walker, S. The Bacterial Cell Envelope. *Cold Spring Harb. Perspect. Biol.* **2010**, *2(5)*, a000414.

5. Cotter, P. D.; Hill, C. Surviving the Acid Test: Responses of Gram-Positive Bacteria to Low pH. *Microbiol. Mol. Biol. Rev.* **2003**, *67(3)*: 429-453.

6. Tong, S. Y. C.; Davis, J. S.; Eichenberger, E.; Holland, T. L.; Fowler, V. G. *Staphylococcus aureus* Infections: Epidemiology, Pathophysiology, Clinical Manifestations, and Management. *Clin. Microbiol. Rev.* **2015**, *28(3)*: 603-661.

7. Glaser, P.; Martins-Simoës, P.; Villain, A.; Barbier, M.; Tristan, A.; Bouchier, C.; Ma, L.; Bes, M.; Laurent, F.; Guillemot, D.; Wirth, T.; Vandenesch, F. Demography and Intercontinental Spread of the USA300 Community-Acquired Methicillin-Resistant *Staphylococcus aureus* Lineage. *mBio* **2016**, *7(1)*: e02183-15

8. Vollmer, W.; Blanot, D.; De Pedro, M. A. Peptidoglycan Structure and Architecture. *FEMS Microbiol. Rev.* **2008**, *32(2)*: 149-167.

9. Glauner, B. Separation and Quantification of Muropeptides with High-Performance Liquid Chromatography. *Anal. Biochem.* **1988**, *172(2)*: 451-64.

10. Cabeen, M. T.; Jacobs-Wagner, C. Bacterial Cell Shape. *Nature Rev. Microbiol.* **2005**, *3*, 610-610.

11. Malanovic, N.; Lohner, K. Gram-Positive Bacterial Cell Envelopes: The Impact on the Activity of Antimicrobial Peptides. *BBA-Rev. Biomembranes* **2016**, *1858(5)*: 936-946.

12. Work, E. The Mucopeptides of Bacterial Cell Walls. *J. Gen. Microbiol.* **1961**, *25*, 167-189.

13. Beeby, M.; Gumbart, J. C.; Roux, B.; Jensen, G. J. Architecture and Assembly of the Gram-Positive Cell Wall. *Mol. Microbiol.* **2013**, *88(4)*: 664-672.

14. Vollmer, W. Structural Variation in the Glycan Strands of Bacterial Peptidoglycan. *FEMS Microbiol. Rev.* **2008**, *32(2)*: 287-306.

15. Sharif, S.; Kim, S. J.; Labischinski, H.; Chen, J.; Shaefer, J. Uniformity of Glycyl Bridge Lengths in the Mature Cell Walls of Fem Mutants of Methicillin-Resistant *Staphylococcus aureus. J. Bacteriol.* **2013**, *195(7)*: 1421-1427.

16. Tong, G.; Pan, Y.; Dong, H.; Pryor, R.; Wilson, G. E.; Shaefer, J. Structure and Dynamics of Pentaglycyl Bridges in the Cell Walls of *Staphylococcus aureus* by ^{13}C-^{15}R REDOR NMR. *Biochemistry* **1997**, *36(32)*: 9859-9866.

17. Kim, S. J.; Singh, M.; Sharif, S.; Shaefer, J. Cross-Link Formation and Peptidoglycan Lattice Assembly in the FemA Mutant of *Staphylococcus aureus. Biochemistry* **2014**, *53(9)*: 1420-1427.

18. Kim, S. J.; Chang, J.; Singh, M. Peptidoglycan Architecture of Gram-Positive Bacteria by Solid-state NMR. *BBA-Rev. Biomembranes* **2015**, *1848(1B)*: 350-362.

19. Zuber, B.; Haenni, M.; Ribeiro, T.; Minnig, K.; Lopes, F.; Moreillon, P.; Dubochet, J. Granular Layer in the Periplasmic Space of Gram-Positive Bacteria and Fine Structures of *Enterococcus gallinarium* and *Streptococcus gordonii* Septa Revealed by Cryo-Electron Microscopy of Vitreous Sections. *J. Bacteriol.* **2006**, *188(18)*: 6652-6660.

20. Kim, S. J.; Cegelski, L.; Preobrazhenskaya, M.; Shaefer, J. Structures of *Staphylococcus aureus* Cell-Wall Complexes with Vancomycin, Eremomycin, and Chloroeremomycin Derivatives by ^{13}C{^{19}F} and ^{15}N{^{19}F} Rotational-Echo Double Resonance. *Biochemistry* **2006**, *45(16)*: 5235-5250.

21. Kim, S. J.; Cegelski, L.; Studelska, D. R.; O'Connor, R. D.; Mehta, A. K.; Shaefer, J. Rotational-Echo Double Resonance Characterization of Vancomycin Binding Sites in *Staphylococcus aureus. Biochemistry* **2002**, *41(22)*: 6967-6977.

22. Singh, M.; Chang, J.; Coffman, L.; Kim, S. J.; Solid-State NMR Characterization of Amphomycin Effects on Peptidoglycan and Wall Teichoic Acid Biosynthesis in *Staphylococcus aureus. Sci. Rep.* **2017**, *6*: 31757.

23. O'Conner, R. D.; Singh, M.; Chang, J.; Kim, S. J.; VanNieuwenhze, M.; Schaefer, J. Dual Mode of Action for Plusbacin A3 in *Staphylococcus aureus. J. Phys. Chem.* **2017**, *121(7)*: 1499-1505.

24. Kim, S. J.; Singh, M.; Sharif, S.; Schaefer, J. Desleucyl-Oritavancin with a Damaged D-Ala-D-Ala Binding Site Inhibits the Transpeptidation Step of Cell-Wall Biosynthesis in Whole Cells of *Staphylococcus aureus. Biochemistry* **2017**, *56(10)*: 1529-1535.

25. Chang, J.; Zhou, H.; Preobrazhenskaya, M.; Tao, P.; Kim, S. J. The Carboxyl-Terminus of Eremomycin Binding to the Non-D-Ala-D-Ala Segment of the Peptidoglycan Pentapeptide Stem. *Biochemistry* **2016**, *55(24)*: 3383-3391.

26. Patti, G. J.; Chen, J.; Shaefer, J.; Gross, M. L. Characterization of Structural Variations in the Peptidoglycan of Vancomycin-Susceptible *Enterococcus faecium:* Understanding Glycopeptide-Antibiotic Binding Sites Using Mass Spectrometry. *J. Am. Soc. Mass. Spectrom.* **2008**, *19(10)*:1467-1475.

27. Patti, G. J.; Chen, J.; Gross, M. L. A Method Revealing Bacterial Cell-Wall Architecture by Time-Dependent Isotope Labeling and Quantitative Liquid Chromatograph/Mass Spectrometry. *Anal. Chem.* **2009**, *81(7)*: 2437-2445.

28. Kühner, D.; Stahl, M.; Demircioglu, D. D.; Bertsche, U. From Cells to Muropeptide Structures in 24 h: Peptidoglycan Mapping by UPLC-MS. *Sci. Rep.* **2014**, *4*: 7494.

29. Severin, A.; Wu, S. W.; Tabei, K.; Tomasz, A. Penicillin-Binding Protein 2 is Essential for Expression of High-Level Vancomycin Resistance and Cell Wall Synthesis in Vancomycin-Resistant *Staphylococcus aureus* Carrying the Enterococcal *vanA* Gene Complex. *Antimicrob. Agents Chemother.* **2004**, *48(12)*: 4566-4573.

30. Pinho, M. G.; Filipe, S. R.; de Lencastre, H.; Tomasz, A. Complementation of the Essential Peptidoglycan Transpeptidase Function of Penicillin-Binding Protein 2 (PBP2) by the Drug Resistance Protein PBP2A in *Staphylococcus aureus*. *J. Bacteriol.* **2001**, *183(22)*: 6525-6531.

31. Bern, M.; Beniston, R.; Mesnage, S. Towards an Automated Analysis of Bacterial Peptidoglycan Structure. *Anal. Bioanal. Chem.* **2017**, *409(2)*: 551-560.

32. Chang, J. D.; Foster, E. E.; Wallace, A. G.; Kim, S. J. Peptidoglycan O-acetylation Increases in Response to Vancomycin Treatment in Vancomycin-Resistant *Enterococcus faecalis. Sci. Rep.* **2017**, *7:* 46500.

33. Chang, J. D.; Foster, E. E.; Yang, H.; Kim, S. J. Quantification of the D-Ala-D-Lac-Terminated Peptidoglycan Structure in Vancomycin-Resistant *Enterococcus faecalis* Using a Combined Solid-State Nuclear Magnetic Resonance and Mass Spectrometry Analysis. *Biochemistry* **2017**, *56(4)*: 612-622.

34. Lowy, F. D. *Staphylococcus aureus* Infections. *N. Engl. J. Med.* **1998**, *339*: 520-532.

35. Arias, C. A.; Murray, B. E. The Rise of Enterococcus: Beyond Vancomycin Resistance. *Nat. Rev. Microbiol.* **2012**, *10*: 266-278.

36. Chatterjee, S. S.; Otto, M. Improved Understanding of Factors Driving Methicillin-Resistant *Staphylococcus aureus* Epidemic Waves. *Clin. Epidemiol.* **2013**, *5*: 205-217.

37. Monecke, S.; Coombs, G.; Shore, A. C.; Coleman, D. C.; Akpaka, P. Borg, M.; Chow, H.; Ip, M.; Jatzwauk, L.; Jonas, D.; Kadlec, K.; Kearns, A.; Laurent, F.; O'Brien, F. G.; Pearson, J.; Ruppelt, A.; Schwarz, S.; Scicluna, E.; Slickers, P.; Tan, H.-L.; Weber, S.; Ehricht, R. A Field Guide to Pandemic, Epidemic and Sporadic Clones of Methicillin-Resistant *Staphylococcus aureus.* Planet, P. J. Ed. *PLoS One* **2011**, *6(4)*: e17936.

38. Matsuhashi, M.; Dietrich, C. P.; Strominger, J. L. Incorporation of Glycine into the Cell Wall Glycopeptide in *Staphylococcus aureus:* Role of sRNA and Lipid Intermediates. *Proc. Natl. Acad. Sci.* **1965**, *54(2)*: 587-594.

39. Barna, J. C. J.; Williams, D. H. The Structure and Mode of Action of Glycopeptide Antibiotics of the Vancomycin Group. *Ann. Rev. Microbiol.* **1984**, *38*: 339-57.

40. Nieto, M.; Perkins, H. R. Physiochemical Properties of Vancomycin and Iodovancomycin and their Complexes with Diacetyl-L-Lysyl-D-Alanyl-D-Alanine. *Biochem. J.* **1971**, *123(5)*: 773-787.

41. Ong, S.-E.; Blagoev, B.; Kratchmarova, I.; Kristensen, D. B.; Steen, H.; Pandey, A.; Mann, M. Stable Isotope Labeling by Amino Acids in Cell Culture, SILAC, as a Simple and Accurate Approach to Expression Proteomics. *Mol. Cell. Proteomics* **2002**, *1*: 376-386.

42. Ong, S.-E.; Mann, M. A Practical Recipe for Stable Isotope Labeling by Amino Acids in Cell Culture (SILAC). *Nat. Protoc.* **2007**, *1(6)*: 2650-2660.

43. Yuet, K. P.; Tirrell, D. A. Chemical Tools for Temporally and Spatially Resolved Mass Spectrometry-Based Proteomics. *Ann. Biomed. Eng.* **2014**, *42(2)*: 299-311.

44. Fernández-Fernández, M.; Rodríguez-González, P.; García Alonso, J. I. A Simplified Calculation Procedure for Mass Isoptomer Distribution Analysis (MIDA) Based on Multiple Linear Regression. *J. Mass Spectrom.* **2016**, *51(10)*: 980-987.

45. Goff, D. Antimicrobial Efficacy Review. *Infect. Dis. Sp. Ed.* **2002**, *5*, 31-34.

46. Nagarajan, R. *Glycopeptide Antibiotics*; Marcel Dekker: New York, NY, 1994.

47. Nicolaou, K. C.; Cho, S. Y.; Hughes, R.; Winssinger, N.; Smethurst, C.; Labischinski, H.; Endermann, R. Solid- and Solution-Phase Synthesis of Vancomycin and Vancomycin Analogues with Activity Against Vancomycin-Resistant Bacteria. *Chemistry* **2001**, *7(17)*: 3798-823.

48. Loll, P. J.; Axelsen, P. H. The Structural Biology of Molecular Recognition by Vancomycin. *Annu. Rev. Biophys. Struct.* **2000**, *29*, 265-289.

49. Cegelski, L.; Kim, S. J.; Hing, A. W.; Studelska, D. R.; O'Connor, R. D.; Mehta, A. K.; Schaefer, J. Rotational-Echo Double Resonance Characterization of the Effects of Vancomycin on Cell Wall Synthesis in *Staphylococcus aureus. Biochemistry* **2002**, *41*, 13053-13058.

50. Hammes, W. P.; Neuhaus, F. C. On the Mechanism of Action of Vancomycin: Inhibition of Peptidoglycan Synthesis in *Gaffkya homari. Antimicrob. Agents Chemother.* **1974**, *6*, 722-728.

51. Rao, J.; Colton, I. J.; Whitesides, G. M. Using Capillary Electrophoresis to Study the Electrostatic Interaction Involved in the Association of D-Ala-D-Ala with Vancomycin. *J. Am. Chem. Soc.* **1997**, *119*, 9336-9340.

52. Nitatani, Y.; Kikuchi, T.; Kakoi, K.; Hanamaki, S.; Fujisawa, I.; Aoki, K. Crystal Structures of the Complexes Between Vancomycin and Cell-Wall Precursor Analogs. *J. Mol. Biol.* **2009**, *385*, 1422-1432.

53. Prowse, W. G.; Kline, A. D.; Skelton, M. A.; Loncharich, R. J. Conformation of A82846B, a Glycopeptide Antibiotic, Complexed with Its Cell Wall Fragment: an Asymmetric Homodimer Determined Using NMR Spectroscopy. *Biochemistry* **1995**, *34*, 9632-9644.

54. Nagarajan, R. Structure-Activity Relationships of Vancomycin-Type Glycopeptide Antibiotics. *J. Antibiot.* **1993,** *46*, 1181-1195.

55. Kim, S. J.; Singh, M.; Schaefer, J. Oritavancin Binds to Isolated Protoplast Membranes but Not Intact Protoplasts of *Staphylococcus aureus. J. Mol. Biol.* **2009**, *391*, 414-425.

56. Kim, S. J.; Schaefer, J. Hydrophobic Side-Chain Length Determines Activity and Conformational Heterogeneity of a Vancomycin Derivative Bound to the Cell Wall of *Staphylococcus aureus*. *Biochemistry* **2008**, *47*, 10155-10161.

57. Kim, S. J.; Matsuoka, S.; Patti, G. J.; Schaefer, J. Vancomycin Derivative with Damaged D-Ala-D-Ala Binding Cleft Binds to Cross-Linked Peptidoglycan in the Cell Wall of *Staphylococcus aureus*. *Biochemistry* **2008**, *47*, 3822-3831.

58. Olsufyeva, E. N.; Berdnikova, T. F.; Miroshnikova, O. V.; Reznikova, M. I.; Preobrazhenskaya, M. N. Chemical Modification of Antibiotic Eremomycin at the Asparagine Side Chain. *J. Antibiot.* **1999**, *52*, 319-342.

59. Cooper, R. D.; Snyder, N. J.; Zweifel, M. J.; Staszak, M. A.; Wilkie, S. C.; Nicas, T. I.; Mullen, D. L.; Butler, T. F.; Rodriguez, M. J.; Huff, B. E.; Thompson, R. C. Reductive Alkylation of Glycopeptide Antibiotics: Synthesis and Antibacterial Activity. *J. Antibiot.* **1996**, *49*, 575-581.

60. Nicas, T. I.; Mullen, D. L.; Flokowitsch, J. E.; Preston, D. A.; Snyder, N. J.; Zweifel, M. J.; Wilkie, S. C.; Rodriguez, M. J.; Thompson, R. C.; Cooper, R. D. Semisynthetic Glycopeptide Antibiotics Derived from LY264826 Active Against Vancomycin-Resistant Enterococci. *Antimicrob. Agents Chemother.* **1996**, *40*, 2194-2199.

61. Malabarba, A.; Nicas, T. I.; Thompson, R. C. Structural Modification of Glycopeptide Antibiotics. *Med. Res. Rev.* **1997**, *17*, 69-137.

62. Rodriguez, M. J.; Snyder, N. J.; Zweifel, M. J.; Wilkie, S. C.; Stack, D. R.; Cooper, R. D.; Nicas, T. I.; Mullen, D. L.; Butler, T. F.; Thompson, R. C. Novel glycopeptide Antibiotics: N-Alkylated Derivatives Active Against Vancomycin-Resistant Enterococci. *J. Antibiot.* **1998**, *51*, 560-569.

63. Miroshnikova, O. V.; Printsevskaya, S. S.; Olsufyeva, E. N.; Pavlov, A. Y.; Nilius, A.; Hensey-Rudloff, D.; Preobrazhenskaya, M. N. Structure-Activity Relationships in the Series of Eremomycin Carboxamides. *J. Antibiot.* **2000**, *53*, 286-293.

64. Gullion, T.; Schaefer, J. Detection of Weak Heteronuclear Diploar Coupling by Rotational-Echo Double Resonance Nuclear Magnetic Resonance. *Adv. Magn. Reson.* **1989**, *13*, 57-83.

65. Gullion, T.; Schaefer, J. Rotational-Echo Double Resosnance NMR. *J. Magn. Reson.* **1989**, *81*, 196-200.

66. Solov'eva, S. E.; Printsevskaya, S. S.; Olsufyeva, E. N.; Batta, G.; Preobrazhenskaya, M. N. New Derivatives of Eremomycin Containing ^{15}N or F Atoms for NMR Study. *Russ. J. Bioorg. Chem+* **2008**, *34*, 747-754.

67. Kim, S. J.; Preobrazhenskaya, M. N.; Scheafer, J. *Characterization of Staphylococcus aureus Peptidoglycan Tertiary Structure Using Glycopeptide as Prove by Solid-State NMR*, Proceedings of Interscience Conference on Antimicrobial Agents and Chemotherapy, 2008; American Society for Microbiology, Washington D.C. F2-2073.

68. Gullion, T.; Baker, D. B.; Conradi, M. S. New, Compensated Carr-Purcell Sequences. *J. Magn. Reson.* **1990**, *89*, 479-484.

69. Mueller, K. T.; Jarvie, T. P.; Aurentz, D. J.; Roberts, B. W. The REDOR Transform: Direct Calculation of Internuclear Couplings from Dipolar-Dephasing NMR Data. *Chem. Phys. Lett.* **1995**, *242*, 535-542.

70. De la Caillerie, J.-B. d. E.; Fretigny, C. Analysis of the REDOR Signal and Inversion. *J. Magn. Reson.* **1998**, *133*, 273-280.

71. Vanommeslaeghe, K.; MacKerell, A. D. Automation of the CHARMM General Force Field (CGenFF) I: Bond Perception and Atom Typing. *J. Chem. Inf. Model* **2012**, *52*, 3144-3154.

72. Kim, S. J.; Singh, M.; Preobrazhenskaya, M.; Scheafer, J. *Staphylococcus aureus* Peptidoglycan Stem Packing by Rotational-Echo Double Resonance NMR Spectroscopy. *Biochemistry* **2013**, *52*, 3651-3659.

73. Cegelski, L.; Stueber, D.; Mehta, A. K.; Kulp, D. W.; Axelsen, P. H.; Schaefer, J. Conformational and Quantitative Characterization of Oritavancin-Peptidoglycan Complexes in Whole Cells of *Staphylococcus aureus* by *in vivo* ^{13}C and ^{15}N Labeling. *J. Mol. Biol.* **2006**, *357*, 1253-126.

74. Schäfer, M.; Schneider, T. R.; Sheldrick, G. M. Crystal Structure of Vancomycin. *Structure* **1996**, *4*, 1509-1515.

75. Loll, P. J.; Bevivino, A. E.; Korty, B. D.; Axelsen, P. H. Simultaneous Recognition of a Caboxylate-Containing Ligand and an Intramolecular Aurrogate Ligand in the Crystal Structure of an Asymmetric Vancomycin Dimer. *J. Am. Chem. Soc.* **1997**, *119*, 1516-1522.

76. Sharman, G. J.; Try, A. C.; Dancer, R. J.; Cho, Y. R.; Staroske, T.; Bardsley, B.; Maguire, A. J.; Cooper, M. A.; O'Brien, D. P.; Williams, D. H. The Roles of Dimerization and Membrane Anchoring in Activity of Glycopeptide Antibiotics Against Vancomycin-Resistant Bacteria. *J. Am. Chem. Soc.* **1997**, *119*, 12041-12047.

77. Allen, N. E.; LeTourneau, D. L.; Hobbs, J. N. The Role of Hydrophobic Side Chains as Determinants of Antibacterial Activity of Semisynthetic Glycopeptide Antibiotics. *J. Antibiot.* **1997**, *50*, 677-684.

78. Beauregard, D. A.; Williams, D. H.; Gwynn, M. N.; Knowles, D. J. Dimerization and Membrane Anchors in Extracellular Targeting of Vancomycin Group Antibiotics. *Antimicrob. Agents Chemother.* **1995**, *39*, 781-785.

79. Kim, S. J.; Tanaka, K. S.; Dietrich, E.; Rafai Far, A.; Schaefer, J. Locations of the Hydrophobic Side Chains of Lipoglycopeptides Bound to the Peptidoglycan of *Staphylococcus aureus. Biochemistry* **2013**, *52*, 3405-3414.

80. Printsevskaya, S. S.; Pavolv, A. Y.; Olsufyeva, E. N.; Mirchink, E. P.; Isakova, E. B.; Reznikova, M. I.; Goldman, R. C.; Branstrom, A. A.; Baizman, E. R.; Longley, C. B.; Sztaricskai, F.; Batta, G.; Preobrazhenskaya, M. N. Synthesis and Mode of Action of Hydrophobic Derivatives of the Glycopeptide Antibiotic Eremomycin and des-(N-methly-D-leucyl)Eremomycin Against Glycopeptide-Sensitive and -Resistant Bacteria. *J. Med. Chem.* **2002**, *45*, 1340-1347.

81. Harris, C. M.; Kopecka, H.; Harris, T. M. The Stabilization of Vancomycin by Peptidoglycan Analogs. *J. Antibioc.* **1985**, *38*, 51-57.

82. Arias, C. A.; Murray, B. E. The Rise of the Enterococcus: Beyond Vancomycin Resistance. *Nat. Rev. Microbiol.* **2012**, *10*¸ 266-278.

83. Cetinkaya, Y.; Falk, P.; Mayhall, C. G. Vancomycin-Resistant Enterococci. *Clin. Microbiol. Rev.* **2000**, *13*, 686-707.

84. Singh, M.; Kim, S. J.; Sharif, S.; Preobrazhenskaya, M.; Schaefer, J. REDOR Constraints on the Peptidoglycan Lattice Architecture of *Staphylococcus aureus* and its FemA Mutant. *Biochim. Biophys. Acta.* **2015**, *1848*, 363-368.

85. Bouhss, A.; Josseaume, N.; Allanic, D.; Crouvoisier, M.; Gutmann, L.; Mainardi, J. L.; Mengin-Lecreulx, D.; van Heijenoor, J.; Arthur, M. Identification of the UDP-MurNAc-Pentapeptide:L-Alanine Ligase for Synthesis of Branched Peptidoglycan Precursors in *Enterococcus faecalis*. *J. Bacteriol.* **2001**, *183*, 5122-5127.

86. van Heijenoort, J. Formation of the Glycan Chains in the Synthesis of Bacterial Peptidoglycan. *Glycobiology* **2001**, *11*, 25R-36R.

87. Arthur, M.; Molinas, C.; Bugg, T. D.; Wright, G. D.; Walsh, C. T.; Courvalin, P. Evidence for *in vivo* Incorporation of D-Lactate into Peptidoglycan Precursors of Vancomycin-Resistant Enterococci. *Antimicrob. Agents Chemother.* **1992**, *36*, 876-869.

88. Billot-Klein, D.; Gutmann, L.; Collatz, E.; van Heijenoort, J. Analysis of Peptidoglycan Precursors in Vancomycin-Resistant Enterococci. *Antimicrob. Agents Chemother.* **1992**, *36*, 1487-1490.

89. Walsh, C. T.; Fisher, S. L.; Park, I. S.; Prahalad, M.; Wu, Z. Bacterial Resistance to Vancomycin: Five Genes and One Missing Hydrogen Bond Tells the Story. *Chem. Biol.* **1996**, *3*, 21-28.

90. Bugg, T. D.; Wright, G. D.; Dutka-Malen, S.; Arthur, M.; Courvalin, P.; Walsh, C. T. Molecular Basis for Vancomycin Resistance in *Enterococcus faecium* BM4147: Biosynthesis of a Depsipeptide Peptidoglycan Precursor by Vancomycin Resistance Proteins VanH and VanA. *Biochemistry* **1991**, *30*, 10408-10415.

91. Derlot, E.; Courvalin, P. Mechanisms and Implications of Glycopeptide Resistance in Enterococci. *Am. J. Med.* **1991**, *91*, 82S-85S.

92. Patel, R.; Uhl, J. R.; Kohner, P.; Hopkins, M. K.; Cockerill, F. R. Multiplex PCR Detection of *vanA, vanB, vanC-1* and *vanC-2/3* Genes in Enterococci. *J. Clin. Microbiol.* **1997**, *35*, 703-707.

93. Leclercq, R.; Derlot, E.; Duval, J.; Courvalin, P. Plasmid-Mediated Resistance to Vancomycin and Teicoplanin in *Enterococcus faecium*. *N. Engl. J. Med.* **1988**, *319*, 157-161.

94. Evers, S.; Courvalin, P. Regulation of *VanB*-Type Vancomycin Resistance Gene Expression by the VanS(B)-VanR(B) Two-Component Regulatory System in *Enterococcus faecalis* V583. *J. Bacteriol.* **1996**, *178*, 1302-1309.

95. Arthur, M.; Molinas, C.; Dutka-Malen, S.; Courvalin, P. Structural Relationship Between the Vancomycin Resistance Protein VanH and 2-Hydroxycarboxylic Acid Dehydrogenases. *Gene* **1991**, *103*, 133-134.

96. Evers, S.; Reynolds, P. E.; Courvalin, P. Sequence of the *vanB* and *ddl* Genes Encoding D-Alanine:D-Lactate and D-Alanine:D-Alanine Ligases in Vancomycin-Resistant *Enterococcus faecalis* V583. *Gene* **1994**, *140*, 97-102.

97. Reynolds, P. E.; Depardieu, F.; Dutka-Malen, S.; Arthur, M.; Courvalin, P. Glycopeptide Resistance Mediated by Enterococcal Transposon *Tn1546* Requires Productino of VanX for Hydrolysis of D-Alanyl-D-Alanine. *Mol. Microbiol.* **1994**, *13*, 1065-1070.

98. Arthur, M.; Depardieu, F.; Snaith, H. A.; Reynolds, P. E.; Courvalin, P. Contribution of VanY D,D-Carboxypeptidase to Glycopeptide Resistance in *Enterococcus faecalis* by Hydrolysis of Peptidoglycan Precursors. *Antimicrob. Agents Chemother.* **1994**, *38*, 1899-1903.

99. Wright, G. D.; Molinas, C.; Arthur, M.; Courvalin, P.; Walsh, C. T. Characterization of VanY, a D,D-Carboxypeptidase from Vancomycin-Resistant *Enterococcus faecium* BM4147. *Antimicrob. Agents Chemother.* **1992**, *36*, 1514-1518.

100. Handwerger, S.; Pucci, M. J.; Volk, K. J.; Liu, J.; Lee, M. S. The Cytoplasmic Peptidoglycan Precursor of Vancomycin-Resistant *Enterococcus faecalis*Terminates in Lactate. *J. Bacteriol.* **1992**, *174*, 5982-5984.

101. Gutmann, L.; Billot-Klein, D.; al-Obeid, S.; Klare, I.; Francoual, S.; Collatz, E.; van Heijenoort, J. Inducible Carboxypeptidase Activity in Vancomycin-Resistant Enterococci. *Antimicrob. Agents Chemother.* **1992**, *36*, 77-80.

102. de Jonge, B. L.; Handwerger, S.; Gage, D. Altered Peptidoglycan Composition in Vancomycin-Resistant *Enterococcus faecalis*. *Antimicrob. Agents Chemother.* **1996**, *40*, 863-869.

103. Billot-Klein, D.; Shlaes, D.; Bryant, D.; Bell, D.; van Heijenoort, J.; Gutmann, L. Peptidoglycan Structure of *Enterococcus faecium* Expressing Vancomycin Resistance of the *VanB* Type. *Biochem. J.* **1996**, *313*, 711-715.

104. Severin, A.; Tabei, K.; Tenover, F.; Chung, M.; Clarke, N.; Tomasz, A. High Level Oxacillin and Vancomycin Resistance and Altered Cell Wall Composition in *Staphylococcus aufeus* Carrying the Staphylococcal *mecA* and the Enterococcal *vanA* Gene Complex. *J. Biol. Chem.* **2004**, *279*, 3398-3407.

105. Munch, D.; Engels, I.; Muller, A.; Reder-Christ, K.; Falkenstein-Paul, H.; Bierbaum, G.; Grein, F.; Bendas, G.; Sahl, H. G.; Schneider, T. Structural Variations of the Cell Wall Precursor Lipid II and Their Influence on Binding and Activity of the Lipoglycopeptide Antibiotic Oritavancin. *Antimicrob. Agents Chemother.* **2015**, *59*, 772-781.

106. Bouhss, A.; Josseaume, N.; Severin, A.; Tabei, K.; Hugonnet, J. E.; Shlaes, D.; Mengin-Lecreulx, D.; van Heijenoort, J.; Arthur, M. Synthesis of the L-Alanyl-L-Alanine Cross-Bridge of *Enterococcus faecalis* Peptidoglycan. *J. Biol. Chem.* **2002**, *277*, 45935-45941.

107. Patti, G. J.; Kim, S. J.; Schaefer, J. Characterization of the Peptidoglycan of Vancomycin-Susceptible *Enterococcus faecium*. *Biochemistry* **2008**, *47*, 479-484.

108. McDowell, L. M.; Schmidt, A.; Cohen, E. R.; Studelska, D. R.; Schaefer, J. Structural Constraints on the Ternary Complex of 5-Enolpyruvylshikimate-3-Phosphate Synthase from Rotational-Echo Double Resonance NMR. *J. Mol. Biol.* **1996**, *256*, 160-171.

109. Kim, S. J.; Cegelski, L.; Stueber, D.; Singh, M.; Dietrich, E.; Tanaka, K. S.; Parr, T. R.; Far, A. R.; Schaefer, J. Oritavancin Exhibits Dual Mode of Action to Inhibit Cell-Wall Biosynthesis in *Staphylococcus aureus*. *J. Mol. Biol.* **2008**, *377*, 281-293.

110. Deborde, C.; Boyaval, P. Interactions Between Pyruvate and Lactate Metabolism in *Propionibacterium freudenreichii subsp. shermanii*: *in vivo* (13)C Nuclear Magnetic Resonance Studies. *Appl. Environ. Microbiol.* **2000**, *66*, 2012-2020.

111. Leblanc, D. In *The Prokaryotes: a Handbook on the Biology of Bacteria, 3rd edition*; Dworkin, M., Falkow, S., Rosenberg, E., Schleifer, K.-H., Stckenbrandt, E., Eds.; Springer: New York, 2006; 1-6.

112. van Heijenoort, J. Recent Advances in the Formation of the Bacterial Peptidoglycan Monomer Unit. *Nat. Prod. Rep.* **2001**, *18*, 503-519.

113. Gunetileke, K. G.; Anwar, R. A. Biosynthesis of Uridine Diphospho-N-Acetylmuramic Acid. II. Purification and Properties of Pyruvate-Uridine Diphospho-N-Acetylglucosamine Transferase and Characterization of Uridine Diphospho-N-Acetylenolpyruvylglucosamine. *J. Biol. Chem.* **1968**, *243*, 5770-5778.

114. Giesbrecht, P.; Kersten, T.; Maidhof, H.; Wecke, J. Staphylococcal Cell Wall: Morphogenesis and Fatal Variations in the Presence of Penicillin. *Microbiol. Mol. Biol. Rev.* **1998**, *62*, 1371-1414.

115. Typas, A.; Banzhaf, M.; Gross, C. A.; Vollmer, W. From the Regulation of Peptidoglycan Synthesis to Bacterial Growth and Morphology. *Nat. Rev. Microbiol.* **2012**, *10*, 123-136.

116. Tran, T. T.; Panesso, D.; Mishra, N. N.; Mileykovskaya, E.; Guan, Z.; Munita, J. M.; Reyes, J.; Diaz, L.; Weinstock, G. M.; Murray, B. E.; Shamoo, Y.; Dowhan, W.; Bayer, A. S.; Arias, C. A. Daptomycin-Resistant *Enterococcus faecalis* Diverts the Antibiotic Molecule from the Division Septum and Remodels Cell Membrane Phospholipids. *mBio* **2013**, *4*, e00281-13.

117. Courvalin, P. Vancomycin Resistance in Gram-Positive Cocci. *Clin. Infect. Dis.* **2006**, *42*, S25-S34.

118. Munita, J. M.; Bayer, A. S.; Arias, C. A. Evolving Resistance Among Gram-Positive Pathogens. *Clin. Infect. Dis.* **2015**, *61*, S48-S57.

119. Allen, N. E.; LeTourneau, D. L.; Hobbs, J. N. Molecular Interactions of a Semisynthetic Glycopeptide Antibiotic with D-Alanyl-D-Alanine and D-Alanyl-D-Lactate Residues. *Antimicrob. Agents Chemother.* **1997**, *41*, 66-71.

120. Gold, H. S. Vancomycin-Resistant Enterococci: Mechanisms and Clinical Observations. *Clin. Infect. Dis.* **2001**, *33*, 210-219.

121. Hébert, L.; Courtin, P.; Torelli, R.; Sanguinetti, M.; Chapot-Chartier, M. P.; Auffray, Y.; Benachour, A. *Enterococcus faecalis* Constitutes an Unusual Bacterial Model in Lysozyme Resistance. *Infect. Immun.* **2007**, *75(11)*: 5390-8.

122. Moynihan, P. J.; Clarke, A. J. O-Acetylated Peptidoglycan: Controlling the Activity of Bacterial Autolysins and Lytic Enzymes of Innate Immune Systems. *Int. J. Biochem. Cell Biol.* **2011**, *43*, 1655-1659.

123. Moynihan, P. J.; Sychantha, D.; Clarke, A. J. Chemical Biology of Peptidoglycan Acetylation and Deacetylation. *Bioorg. Chem.* **2014**, *55*, 44-50.

124. Bussiere, D. E.; Pratt, S.; Katz, L.; Severin, J. M.; Holzman, T.; Park, C. H. The Structure of VanX Reveals a Novel Amino-Dipeptidase Involved in Mediating Transposon-Based Vancomycin Resistance. *Mol. Cell* **1998**, *2*, 75-84.

125. Pfeffer, J. M.; Strating, H.; Weadge, J. T.; Clarke, A. J. Peptidoglycan O-Acetylation and Autolysin Profile of *Enterococcus faecalis* in the Viable but Nonculturable State. *J. Bacteriol.* **2006**, *188*, 902-908.

126. Emirian, A.; Fromentin, S.; Eckert, C.; Chau, F.; Dubost, L.; Delepierre, M.; Gutmann, L.; Arthur, M.; Mesnage, S. Impact of Peptidoglycan O-Acetylation on Autolytic Activities of the *Enterococcus faecalis* N-Acetylglucosaminidase AtlA and N-Acetylmuramidase AtlB. *FEBS Lett.* **2009**, *583(18)*: 3033-8.

127. Uhlemann, A.-C.; Otto, M.; Lowy, F. D.; DeLeo, F. R. Evolution of Community- and Healthcare-Associated Methicillin Resistant *Staphylococcus aureus. Infect. Genet. Evol.* **2014**, *21*: 563-574.

128. Knox, J.; Uhlemann, A.-C.; Lowy, F. D. *Staphylococcus aureus* Infections: Transmission Within Households and the Community. *Trends. Microbiol.* **2016**, *23(7)*: 437-444.

129. Sievert, D. M.; Rudrik, J. T.; Patel, J. B.; McDonald, L. C.; Wilkins, M. J.; Hageman, J. C. Vancomycin-Resistant *Staphylococcus aureus* in the United States, 2002-2006. *Clin. Infect. Dis.* **2008**, *46(5)*: 668-74.

130. Chang, S.; Sievert, D. M.; Hageman, J. C.; Boulton, M. L.; Tenover, F. C.; Pouch Downes, F.; Shah, S.; Rudrik, J. T.; Rupp, G. R.; Brown, W. J.; Cardo, D.; Fridkin, S. K. Infection with Vancomycin-Resistant *Staphylococcus aureus* Containing the *vanA* Resistance Gene. *N. Engl. J. Med.* **2003**, *348*: 1342-1347.

131. Périchon, B.; Courvalin, P. VanA-Type Vancomycin-Resistant *Staphylococcus aureus. Antimicrob. Agents Chemother.* **2009**, *53(11)*: 4580-4587.

132. Limbago, B. M.; Kallen, A. J.; Zhu, W.; Eggers, P.; McDougal, L. K.; Albrecht, V. S. Report of the 13th Vancomycin-Resistant *Staphylococcus aureus* Isolate from the United States. *J. Clin. Microbiol.* **2014**, *52(3)*: 998-1002.

133. Chambers, H. F.; DeLeo, F. R. Waves of Resistance: *Staphylococcus aureus* in the Antibiotic Era. *Nat. Rev. Microbiol.* **2009**, *7(9)*: 629-641.

134. Centers for Disease Control and Prevention (CDC). Notifiable Disease and Mortality Table. *MMWR Morb. Mortal. Wkly. Rep.* **2017**, *66(11)*: ND202-221.

135. Kos, V. N.; Desjardins, C. A.; Griggs, A.; Cerqueira, G.; Van Tonder, A.; Holden, M. T.; Godfrey, P.; Palmer, K. L.; Bodi, K.; Mongodin, E. F.; Wortman, J.; Feldgarden, M.; Lawley, T.; Gill, S. R.; Haas, B. J.; Birren, B.; Gilmore, M. S. Comparative Genomics of Vancomycin-Resistant *Staphylococcus aureus* Strains and Their Positions Within the Clade Most Commonly Associated with Methicillin-Resistant *S. aureus* Hospital-Acquired Infections in the United States. *mBio* **2012**, *3(3)*: e00112-12.

136. Clark, N. C.; Weigel, L. M.; Patel, J. B.; Tenover, F. C. Comparison of *Tn1546*-Like Elements in Vancomycin-Resistant *Staphylococcus aureus* Isolates from Michigan and Pennsylvania. *Antimicrob. Agents Chemother.* **2005**, *49(1)*: 470-472.

137. Rossi, F.; Diaz, L.; Wollam, A.; Panesso, D.; Zhou, Y.; Rincon, S.; Narechania, A.; Xing, G.; Di Gioia, T.; Doi, A.; Tran, T. T.; Reyes, J.; Munita, J. M.; Carvajal, L. P.; Hernandez-Roldan, A.; Brandão, D.; van der Heijden, I. M.; Murray, B. E.; Planet, P. J.; Weinstock, G. M.; Arias, C. A. Transferable Vancomycin Resistance in a Community-Associated MRSA Lineage. *N. Engl. J. Med.* **2014**, *370(16)*: 1524-1531.

138. Kobayashi, S. D.; Musser, J. M.; DeLeo, F. R. Genomic Analysis of the Emergence of Vancomycin-Resistant *Staphylococcus aureus*. *mBio* **2012**, *3(4)*: e00170-12.

139. Gardete, S.; Tomasz, A. Mechanisms of Vancomycin Resistance in *Staphylococcus aureus*. *J. Clin. Invest.* **2014**, *124(7)*: 2836-2840.

140. Arthur, M.; Reynolds, P.; Courvalin, P. Glycopeptide Resistance in Enterococci. *Trends. Microbiol.* **1996**, *4(10)*: 401-407.

141. Eliopoulos, G. M.; Gold, H. S. Vancomycin-Resistant Enterococci: Mechanisms and Clinical Observations. *Clin. Infect. Dis.* **2001**, *33(2)*: 210-219.

142. Foucault, M.-L.; Courvalin, P.; Grillot-Courvalin, C. Fitness Cost of VanA-Type Vancomycin Resistance in Methicillin-Resistant *Staphylococcus aureus*. *Antimicrob. Agents Chemother.* **2009**, *53(6)*: 2354-2359.

143. Périchon, B.; Courvalin, P. Synergism Between β-Lactams and Glycopeptides Against VanA-Type Methicillin-Resistant *Staphylococcus aureus* and Heterologous Expression of the *vanA* Operon. *Antimicrob. Agents Chmother.* **2006**, *50(11)*: 3622-3630.

144. Fox, P. M.; Lampen, R. J.; Stumpf, K. S.; Archer, G. L.; Climo, M. W. Successful Therapy of Experimental Endocarditis Caused by Vancomycin-Resistant *taphylococcus aureus* With a Combination of Vancomycin and β-Lactam Antibiotics. *Antimicrob. Agents Chemother.* **2006**, *50(9)*: 2951-2956.

145. Werth, B. J.; Vidaillac, C.; Murray, K. P.; Newton, K. L.; Sakoulas, G.; Nonejuie, P.; Pogliano, J.; Rybak, M. J. Novel Combination of Vancomycin Plus Ceftaroline or Oxacillin Against Methicillin-Resistant Vancomycin-Intermediate *Staphylococcus aureus* (VISA) and Heterogeneous VISA. *Antimicrob. Agents Chemother.* **2013**, *57(5)*: 2376-2379.

146. Bera, A.; Biswas, R.; Herbert, S.; Götz, F. The Presence of Peptidoglycan O-Acetyltransferase in Various Staphylococcal Species Correlates With Lysozyme Resistance and Pathogenicity. *Infect. Immun.* **2006**, *74(8)*: 4598-4604.

147. Lovering, A. L.; Safadi, S. S.; Strynadka, N. C. J. Structural Perspective of Peptidoglycan Biosynthesis and Assembly. *Annu. Rev. Biochem.* **2012**, *81*: 451-478.

148. de Jonge, B.; Tomasz, A. Abnormal Peptidoglycan Produced in a Methicillin-Resistant Strain of *Staphylococcus aureus* Grown in the Presence of Methicillin: Functional Role for Penicillin-Binding Protein 2A in Cell Wall Synthesis. A*ntimicrob. Agents Chemother.* **1993**, *37*: 342-346.

149. Ton-That, H.; Labischinski, H.; Berger-Bächi, B.; Schneewind, O. Anchor Structure of Staphylococcal Surface Proteins III. Role of the FemA, FemB, and FemX Factors in Anchoring Surface Proteins to the Bacterial Cell Wall. *J. Biol. Chem.* **1998**, *273*: 29143-29149.

150. Belley, A.; Arhin, F. F.; Sarmiento, I.; Deng, H.; Rose, W.; Moeck, G. Pharmacodynamics of a Simulated Single 1200-milligram Dose of Oritavancin in an *in vitro* Pharmacokinetic / Pharmacodynamic Model of Methicillin-Resistant S*taphylococcus aureus* Infection. *Antimicrob. Agents Chemother.* **2013**, *57*: 205-211.

151. Arhin, F. F.; Sarmiento, I.; Moeck, G. Oritavancin Retains Bactericidal Activity *in vitro* Against Standard and High Inocula of Heterogeneous Vancomycin-Intermediate *Staphylococcus aureus* (hVISA). *Int. J. Antimicrob. Agents* **2013**, *41*: 397-398.

152. Arhin, F. F.; Sarmiento, I.; Parr, T. R.; Moeck, G. Activity of Oritavancin and Comparators *in vitro* Against Standard and High Inocula of *Staphylococcus aureus*. *Int. J. Antimicrob. Agents* **2012**, *39*: 159-162.

153. Westwell, M. S.; Bardsley, B.; Dancer, R. J.; Try, A. C.; Williams, D. H. Cooperativity in Ligand Binding Expressed at a Model Cell Membrane by the Vancomycin Group Antibiotics. *Chem. Commun.* **1996**, 580-590.

154. Williams, D. H. The Glycopeptide Story – How to Kill the Deadly 'Superbugs'. *Nat. Prod. Rep.* **1996**, *13*: 469-477.

155. Mehta, A. K.; Cegelski, L.; O'Connor, R. D.; Schaefer, J. REDOR With a Relative Full-Echo Reference. *J. Magn. Reson.* **2003**, *163*: 182-187.

156. Clarke, A. J.; Dupont, C. O-Acetylated Peptidoglycan: its Occurrence, Pathobiological Significance, and Biosynthesis. *Can. J. Microbiol.* **1992**, *38*: 85-91.

157. Ge, M.; Chen, Z.; Onishi, H. R.; Kohler, J.; Silver, L. L.; Kerns, R.; Fukuzawa, S.; Thompson, C.; Kahne, D. Vancomycin Derivatives that Inhibit Peptidoglycan Biosynthesis Without Binding D-Ala-D-Ala. *Science* **1999**, *284*: 507-511.

158. Munch, D.; Sahl, H. G. Structural Variations of the Cell Wall Precursor Lipid II in Gram-Positive Bacteria – Impact on Binding and Efficacy of Antimicrobial Peptides. *Biochim. Biophys. Acta* **2015**, *1848*: 3062-3071.

159. Boneca, I.; Huang, Z.-H.; Gage, D.; Tomasz, A. Characterization of *Staphylococcus aureus* Cell Wall Glycan Strands, Evidence for a New β-N-Acetylglucosaminidase Activity. *J. Biol. Chem.* **2000**, *275*: 9910-9918.

160. Meziane-Cherif, D.; Stogios, P. J.; Evdokimova, E.; Savchenko, A.; Courvalin, P. Structural Basis for the Evolution of Vancomycin Resistance D,D-Peptidases. *Proc. Natl. Acad. Sci.* **2014**, *111*: 5872-5877.

161. Benachour, A.; Ladjouzi, R.; Le Jeune, A.; Hebert, L.; Thorpe, S.; Courtin, P.; Chapot-Chartier, M.-P.; Prajsnar, T.; Foster, S.; Mesnage, S. The Lysozyme-Induced Peptidoglycan N-Acetylglucosamine Deacetylase PgdA (EF1843) Is Required for *Enterococcus faecalis* Virulence. *J. Bacteriol.* **2012**, *194*: 6066-6073.

162. Figueiredo, T.; Sobral, R.; Ludovice, A.; de Almeida, J.; Bui, N.; Vollmer, W.; de Lencastre, H.; Tomasz, A. Identification of Genetic Determinants and Enzymes Involved with the Amidation of Glutamic Acid Residues in the Peptidoglycan of *Staphylococcus aureus. PLoS Pathog.* **2012**, *8*: e1002508.

163. Sieradzki, K.; Tomasz, A. Inhibition of Cell Wall Turnover and Autolysis by Vancomycin in a Highly Vancomycin-Resistant Mutant of *Staphylococcus aureus*. *J. Bacteriol.* **1997**, *179*: 2557-66.

164. Ong, S.-E.; Blagoev, B.; Kratchmarova, I.; Krisetensen, D.; Steen, H.; Pandey, A.; Mann, M. Stable Isotope Labeling by Amino Acids in Cell Culture, SILAC, as a Simple and Accurate Approach to Expression Proteomics. *Mol. Cell. Proteomics* **2002**, *1*: 376-386.

165. Mann, M.; Kulak, N. A.; Nagaraj, N.; Cox, J. The Coming Age of Complete, Accurate, and Ubiquitous Proteoms. *Mol. Cell* **2013**, *49*: 583-590.

166. Dietrich, D. C.; Link, A. J.; Graumann, J.; Tirrell, D.; Schumann, E. Selective Identification of Newly Synthesized Proteins in Mammalian Cells Using Bioorthogonal Noncanonical Amino Acid Tagging (BONCAT). *Proc. Natl. Acad. Sci.* **2006**, *103*: 9482-9487.

167. Hilger, M.; Mann, M. Triple SILAC to Determine Stimulus Specific Interactions in the Wnt Pathway. *J. Proteome Res.* **2012**, *12*: 982-994.

168. Aebersold, R.; Mann, M. Mass-Spectrometric Exploration of Proteome Structure and Function. *Nature* **2016**, *537*: 347-355.

169. MacLeod, A. K.; Fallon, P. G.; Sharp, S.; Henderson, C. J.; Wolf, C. R.; Huang, J. T. An Enhanced *in vivo* Stable Isotope Labeling by Amino Acids in Cell Culture (SILAC) Model for Quantification of Drug Metabolism Enzymes. *Mol. Cell. Proteomics* **2015**, *14*: 750-760.

170. Frölich, F.; Christiano, R.; Walther, T. C. Native SILAC: Metabolic Labeling of Proteins in Prototroph Microorganisms Based on Lysine Synthesis Regulation. *Mol. Cell. Proteomics* **2013**, *12(7)*: 1995-2005.

171. Phillips, N. J.; Steichen, C. T.; Schilling, B.; Post, D. M. B.; Niles, R. K.; Bair, T. B.; Falsetta, M. L.; Apicella, M. A.; Gibson, B. W. Proteomic Analysis of *Neisseria gonorrhea* Biofilm Shows Shift to Anaerobic Respiration and Changes in Nutrient Transport and Outermembrane Proteins. *PLoS One* **2012**, *7*: e38303.

172. Patti, G. J.; Kim, S. J.; Yu, T. Y.; Dietrich, E.; Tanaka, K. S.; Parr, T. R.; Far, A. R.; Schaefer, J. Vancomycin and Oritavancin Have Different Modes of Action in *Enterococcus faecium. J. Mol. Biol.* **2009**, *392(5)*: 1178-91.

173. Navarre, W.; Schneewind, O. Surface Proteins of Gram-Positive Bacteria and Mechanisms of Their Targeting to the Cell Wall Envelope. *Microbiol. Mol. Biol. Rev.* **1999**, *63(1)*: 174-229.

174. Tocheva, E. I.; López-Garrido, J.; Hughes, H. V.; Fredlund, J.; Kuru, E.; VanNieuwenhze, M. S.; Brun, Y. V.; Pogliano, K.; Jensen, G. J. Peptidoglycan Transformations During *Bacillus subtilis* Sporulation. *Mol. Microbiol.* **2013**, *88*: 673-686.

175. Cheng, K.; Chui, H.; Domish, L.; Hernandez, D.; Wang, G. Recent Development of Mass Spectrometry and Proteomics Applications in Identification and Typing of Bacteria. *Proteomics Clin. Appl.* **2016**, *10(4)*: 346-357.

176. Ni, Q. Z.; Daviso, E.; Can, T. V.; Markhasin, E.; Jawla, S. K.; Swager, T. M.; Temkin, R. J.; Herzfield, J.; Griffin, R. G. High Frequency Dynamic Nuclear Polarization. *Acc. Chem. Res.* **2013**, *46(9)*: 1933-1941.

177. Yamamoto, K.; Caporini, M. A.; Im, S.-C.; Waskell, L.; Ramamoorthy, A. Cellular Solid-State NMR Investigation of a Membrane Protein Using Dynamic Nuclear Polarization. *Biochim. Biophys. Acta* **2015**, *1848(0)*: 342-349.

178. Matias, V. R.; Beveridge, T. J. Cryo-Electron Microscopy Reveals Native Polymeric Cell Wall Structure in *Bacillus subtilis* 168 and the Existence of a Periplasmic Space. *Mol. Microbiol.* **2005**, *56(1)*: 240-51.

179. Tocheva, E. I.; Matson, E. G.; Morris, D. M.; Moussavi, F.; Leadbetter, J. R.; Jensen, G. J. Peptidoglycan Remodeling and Conversion of an Inner Membrane into an Outer Membrane During Sporulation. *Cell* **2011**, *146(5)*: 799-812.

180. Renner, L. D.; Eswaramoorthy, P.; Ramamurthi, K. S.; Weibel, D. B. Studying Biomolecule Localization by Engineering Bacterial Cell Wall Curvature. *PLoS One* **2013**, *8(12)*: e84143.

181. Gumbart, J. C.; Beeby, M.; Jensen, G. J.; Roux, B. *Escherichia coli* Peptidoglycan Structure and Mechanics as Predicted by Atomic-Scale Simulations. *PLoS Comput. Biol.* **2014**, *10(2)*: e1003475.

182. Nguyen, L. T.; Gumbart, J. C.; Beeby, M.; Jensen, G. J. Coarse-Grained Simulations of Bacterial Cell Wall Growth Reveal that Local Coordination Alone Can be Sufficient to Maintain Rod Shape. *Proc. Natl. Acad. Sci.* **2015**, *112(28)*: E3689-E3698.

183. Misra, G.; Rojas, E. R.; Gopinathan, A.; Huang, K. C. Mechanical Consequences of Cell-Wall Turnover in the Elongation of a Gram-Positive Bacterium. *Biophys. J.* **2013**, *104(11)*: 2342-2352.

184. Milne, J. L. S.; Subramaniam, S. Cryo-Electron Tomography of Bacteria: Progress, Challenges, and Future Prospects. *Nature Rev. Microbiol.* **2009**, *7*: 666-675.